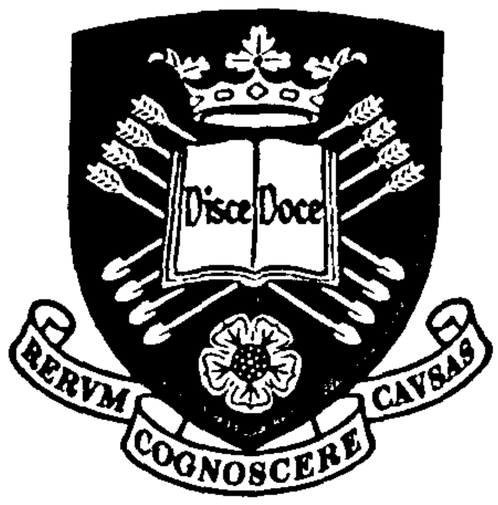

The University Of Sheffield.

Application of x-ray microtomography to the description of single granules

by

Daniel Barrera-Medrano

Department of Chemical and Process Engineering
Particle Products Group

Supervisors

Prof. M.J. Hounslow

Prof. A.D. Salman

A dissertation submitted in partial fulfilment of the requirements for the degree of Doctor of Philosophy in Chemical Engineering

March, 2007

Blank Page

ABSTRACT

The performance of agglomerated products is determined by their composition and structure [1]. For a given product, composition is usually fixed and the structure of the agglomerates is determined by the way they are manufactured. In this work, a commercial X-ray tomography (XRT) system was used in order to investigate the structure of individual agglomerates and how it is affected by different parameters during the granulation process.

Qualitative analysis of cross-sectional images for different granulation systems show typical structures for different granulation methods (ranging from the opened structure of fluidised bed granules to the more compact high-shear granules). It is also shown that granules from the same batch can have different structures due to the coexistence of different granulation mechanisms during the granulation process.

Further studies were carried out for high-shear melt granulation using calcium carbonate and polyethylene glycol as a model system. A method was developed to analyze XRT data in terms of radial profiles of greyscale intensity within the granules in order to provide information on their internal structure. Different process and formulation parameters were studied using this method alongside qualitative analysis of the images and dissolution/strength information.

An increasing radial consolidation was observed in all cases. Higher impeller speed and longer granulation time increased the overall consolidation in the granules tested, resulting in stronger and slower to dissolve granules. The effect of formulation parameters was not clear in the radial profiles (XRT scans do not show clear structural differences due to resolution/ composition issues); but the effect was clear in the performance indicators: increasing primary particle size, binder molecular weight and binder to solid ratio resulting in stronger/more difficult to dissolve granules.

ACKNOWLEDGEMENTS

This project would not have been possible without the support of many people. They are far too many to thank individually, but I would like to thank a few that stand out for their encouragement, advice and understanding.

Firstly I would like to thank my supervisors Prof. Mike Hounslow and Prof. Agba Salman for their supervision, motivation and support during my PhD. Many thanks go to Dr. Gavin Reynolds for his tireless assistance all throughout my work. Also thanks to Dr. Judith Bonsall from Unilever R&D Port Sunlight for allowing the use of their X-ray tomography system.

Secondly, thanks to all the members of the Particle Products Group with whom I have shared my time in Sheffield. Their help has made this project possible and for that I am forever grateful.

I would also like to thank all the people I have met during this time and that have made it memorable. Ally, David, Bram, Joe, Ian, Bob, people at Tapton and Crooksmoore Rd., Kelly & Co., and all of you out there now frowning because you cannot see your name printed here. Thanks to you all, thank you very much indeed.

Thanks also to Carlos and Dani, and all my friends from Spain, for making me feel always welcome even when being away.

Special thanks go to my family. Without them I just would not be. I love them, and to them I dedicate this work. They inspire me, they support me and they are always there for me. Mum, Dad, Natalia, Picky; I love you always.

CONTENTS

LIST OF TABLES

LIST OF FIGURES

LIST OF SYMBOLS

XRT	X-ray tomography
SEM	Scanning electron microscopy
MRI	Magnetic resonance imaging
DEM	Discrete element modelling
PEG	Polyethylene glycol
LAS	Linear alkyl benzene sulfonic (acid)
HPC	Hydroxypropyl cellulose
$\underline{x}_{i,j,k}$	Position vector corresponding to spatial coordinates *(i,j,k)*
$g_{i,j,k}$	Greyscale intensity at spatial coordinates *(i,j,k)*
$r_{i,j,k}$	Scalar defining radial distance from centre of mass to spatial coordinates *(i,j,k)*
m_i	Element of mass at a distance r_i of the centre of mass
$\underline{\tilde{x}}$	Centre of mass of an agglomerate
$\tilde{x}_x$	x-coordinate of the centre of mass
$\tilde{x}_y$	y-coordinate of the centre of mass
$\tilde{x}_z$	z-coordinate of the centre of mass
r_n	Radial distance to the centre of mass of bin *n*
g_n	Mean greyscale intensity in bin *n*
s	Radius of gyration
ϕ	Flux density of x-rays normal to surface of agglomerate
L/S	Liquid to solid ratio
I	Impeller speed
C	Chopper speed
rpm	Revolutions per minute
t_{90}	Dissolution time (time taken for 90% of one gram of granules to dissolve)

1

INTRODUCTION

1.1 INTRODUCTION

1.1.1 Particulate systems

Particulate systems are all around us. They range from systems that are readily present in nature (such as sand dunes or pebble beaches) to manufactured daily consumer products such as instant coffee granules or pharmaceutical tablets. These systems are constituted of particles with sizes spanning over several orders of magnitude in size, from rocks to the submicron particles in a pharmaceutical tablet [2].

In industry, particle technology is a science of growing importance, as the functionality of products is required to be strongly specific in order to accommodate the growing demands of a competitive world. In the home, people demand in domestic life, our painkillers to act quickly, but also to taste inoffensive; want our coffee granules to dissolve instantly but not to break up in the jar; detergent tablets that not only clean our clothes but make them smell great and iron easy. Whilst in industry silos need to discharge quickly to speed up production in addition the dust levels must be minimized, caking has to be avoided, homogeneity in pharmaceutical tablets is crucial, etc. These are only a few examples of how particulate systems play a crucial role in day to day life and also human economy.

In industry approximately 75% of manufacturing processes involve fine particles at some point [3]. Manufactured materials that are particulate in nature cover a broad range of possibilities, from low-cost materials such as construction sands or agricultural grains to high-value particulates manufactured with a very specific function as is the case of the pharmaceutical or the fine chemical industry. As a result, particle technology is of importance in the majority of processes in the chemical, food and pharmaceutical industries as almost all of their products are in a powder form. It is estimated in [4] that up to 60% of the products in the chemical industry are manufactured as particulates, and a further 20% use powder as ingredients, whereby the value of these products accounts for up to US$1 trillion in the United States alone.

Proper design and handling of these fine particles are key to making a process successful. Careful attention to particle characteristics during the design and operation of a facility can significantly improve environmental performance and increase profitability by improving product yield and reducing waste as pointed out in [3]. However, the behaviour of particulate solids differs greatly from that of liquids or gases. Firstly, liquid or gases can be considered a continuum, whereas particulate solids are not. A good example on how different it is dealing with particulate solids than with liquids is explained in [5], showing that for an engineer a liquid, such as ethanol, is significant on its own, the formula of ethanol can be deduced from its name as can its properties and conversely this collection of properties define ethanol. When it comes to particulate solids things are more complicated with other factors such as size distribution, flowability or hardness playing a fundamental role in the description of the material.

For all the reasons described above it is clearly important to gain an understanding on how the different processes that particulate solids are subjected to, can affect their behaviour.

1.1.2 Granulation and thesis motivation

When dealing with small particulate solids it is useful to aggregate them together in order to form larger entities, granules. Granulation can be defined as the process of agglomerating particles together into larger, semi-permanent aggregates (granules) in which the original particles can still be distinguished [6]. This work refers to wet granulation, in which the agglomeration of the particulate products is achieved by using a liquid binder in order to form interparticulate bonds [4].

Granulation can be seen as an example of particle design, by which the properties of the granules are controlled by a combination of formulation and process parameters [4]. Formulation parameters include all variables related to the original particulate material and the liquid binder used, for example particle size distribution of the start materials, type of binder or binder to solid ratios; whereas process parameters refer to all variables related to the equipment used to carry out the granulation process as well as the operation parameters used such as mixing time, intensity of mixing or operating temperature.

The type of properties achieved by means of granulation include for example [1, 6]:

- Elimination of dust handling hazards or product losses.
- Improved product appearance.
- Reduced caking or lump formation by improving flowability.
- Increased bulk density for storage.
- Creation of non-segregating blends.
- Control of solubility.

Some examples of products prepared utilising granulation can be seen in [1] such as fine chemicals like dyestuffs, food both for humans and animals or household products like detergents amongst other types of product.

Granulation can also be used in order to obtain functionalized products, for example in pharmaceutical applications active powders can be contained within a binder matrix that would only dissolve when in contact with the right kind of environment.

Particulate products and particulate processes can be studied at different length scales: macro, meso and microscale. Some examples can be seen in Table 1.1.

Table 1.1. Particle products and processes: Scales of view (adapted from [7])

Scales	Particulate processes	Particulate products
Macro view	Production of granular alumina (Al_2O_3) from bauxite ore (Bayer Process)	Definition of the product (density, appearance, purity, etc.)
Meso view	Study of the individual unit operations involved (grinding, dissolution, calcinations, etc.)	Particle size distribution
Micro view	Primary processes (e.g. what is the time needed for the dissolution of a 10 μm crystal when the rate is governed by mass transfer)	How does the particle look like, what is its surface area, is it porous, etc.

For wet granulation it is evident that the properties exhibited by the granules (whether as a tablet or as a group of individual granules) will be affected by the structure of the granules, and that this structure is determined by the granulation process. There is a lack of understanding on how the manufacturing process affects the structure of individual granules even though these structures are responsible for the properties exhibited by the final product. Research has traditionally focused on trying to relate formulation/process parameters to the properties exhibited by the products, but usually the effect of these parameters on the structure is overlooked.

This thesis aims to gain an understanding of the relationships between the process and the properties by looking at the structure of granules, which

originates from the manufacturing process and which is responsible for the properties exhibited by them.

To achieve this, the effect of different variables on the structure of the manufactured granules was studied using x-ray tomography, which allows a physical insight of the constituents of the granules. For a series of both process and formulation parameters, the insight into the granular structure was coupled with the properties exhibited by those granules (dissolution and strength), in collaboration with on-going research by other members of the Particle Products Group at the University of Sheffield, Chemical & Process Engineering.

1.2 THESIS OVERVIEW

After this short introduction (Chapter 1) a review of relevant literature is made (Chapter 2). Chapter 3 outlines the experimental methodologies used for this work. Chapter 4 presents the results obtained and analyses them qualitatively. In Chapter 5 a method to carry out quantitative analysis is developed and applied on a series of high-shear melt granulation experiments in Chapter 6. Chapter 7 outlines the main conclusions extracted from this work, and Chapter 8 suggests different possibilities to take this work further.

2

LITERATURE REVIEW

2.1 INTRODUCTION TO GRANULATION

In this work, the definition for granulation will be that of wet granulation: the process of agglomerating fine powder (primary particles) together in the presence of a liquid binder in order to obtain a smaller number of larger particles (granules). At any instant during the granulation process a granule will be made up of the original primary particles, binder, entrapped air and/or fragments of other granules that coalesce forming one agglomerate. The terms granule and agglomerate will be used indistinctively in this work.

The benefits of this size enlargement process in industrial applications have been outlined in the introduction and are explained in further details in [6].

2.1.1 Methods for granulation

Different methods can be used in wet granulation processes. There are four main types and the selection of the process depends on factors such as desired properties in the product (such as bulk density of granule size) as well as size and process limitations (such as inability to handle very viscous binders). Table 2.1 compares the strengths and weaknesses of these processes.

Table 2.1. Comparison of the granulation capabilities of different types of granulation processes (source [1])

	Low shear mechanical mixers	High shear mechanical mixers	Fluidised bed granulators	Steam rewetting (instantising)
Fine/cohesive feed powders	-	+++	-	++
Coarse feed powders	+	-	+	-
High viscosity binders	+	+++	-	N/A
Low density <1mm granules	+	-	+	+++
Dense <1mm spherical granules	-	+	-	-
Dense 1-10 mm size spherical granules	+++	-	-	N/A

Examples of the different types of mixers can be found in [1] and are as follows:

- Low shear mixers: the powder is lifted mechanically but flows under gravity (e.g. rotating drum mixers).
- High shear mixers: the material is mixed by means of a fast rotating impeller impacting and shearing the material within the mixing bowl (e.g. high shear mixers).
- Fluidised bed granulators: the movement of particles is induced by a gas stream and at any time the proportion of liquid binder in the mixer needs to be kept low enough to avoid defluidisation.
- Steam re-wetting: applicable to highly soluble solids that are dispersed in air and contacted with water vapour in a drying tower to create low density granules.

In this project the experiments are carried out using high-shear mixers. A detailed description of a high-shear mixer, including design, scale up and process

parameters can be found in [8]. The high-shear mixer used in this work is described in Chapter 3.

In high shear granulation the primary particles are added to the mixing bowl and the liquid binder can be added by three different methods [9]:

- Poured onto the surface of the powder bed (pour-on)
- Sprayed onto the surface of the powder (spray-in)
- Added as solid binder flakes to the powder bed (melt-in).

The method of binder addition will affect the way the granulation occurs and the properties of the granules. Also in [9] it is reported that binder distribution within agglomerates is initially size dependant although tending to a uniform distribution with long granulation times.

More details about the high shear mixer and the experimental protocol used for the experiments in this work can be found in the experimental chapter.

2.1.2 Mechanisms of granulation

The first research in granulation took place about 50 years ago using sand in drum granulators [10]. Since then the knowledge and understanding of the process has increased considerably. In 1973 Sastry and Fuerstenau proposed a theory to explain the mechanisms involved in granulation [11]. It was a rather complex explanation that included several competing mechanisms, the distinction between those depending on the cut size established to differentiate between granules and non-granulated materials (Figure 2.1).

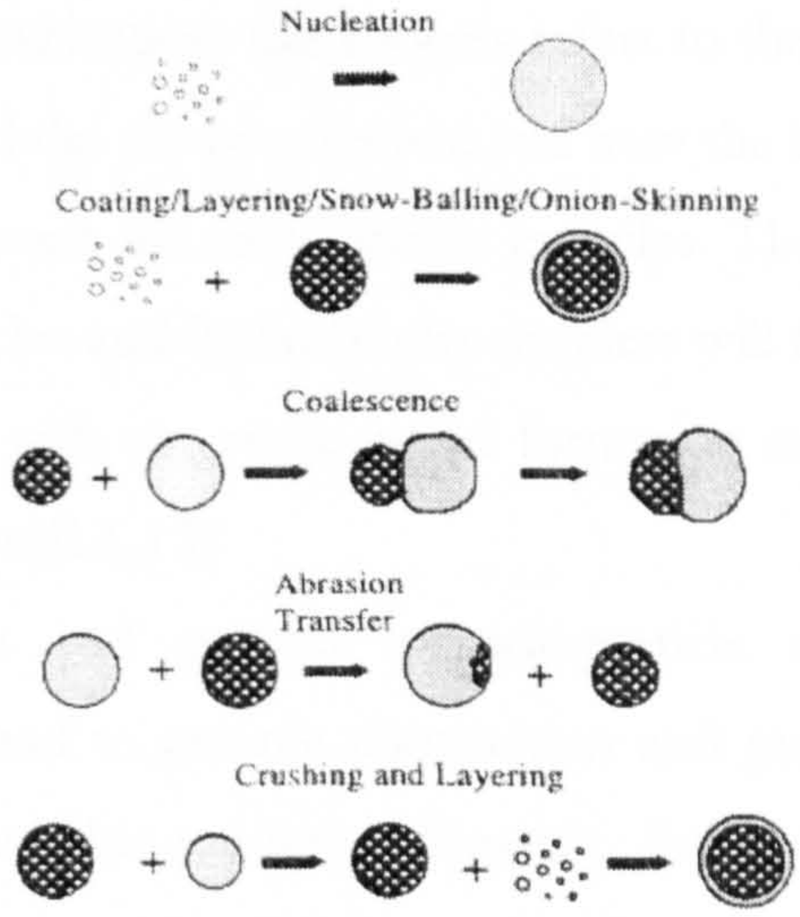

Figure 2.1. Traditional granulation mechanisms (source [4]).

Some of those mechanisms can be considered as cases of coalescence or breakage, and Ennis and Litster in 1997 explained granulation as a combination of three rate processes: wetting and nucleation, consolidation and coalescence, and attrition and breakage [6] (Figure 2.2).

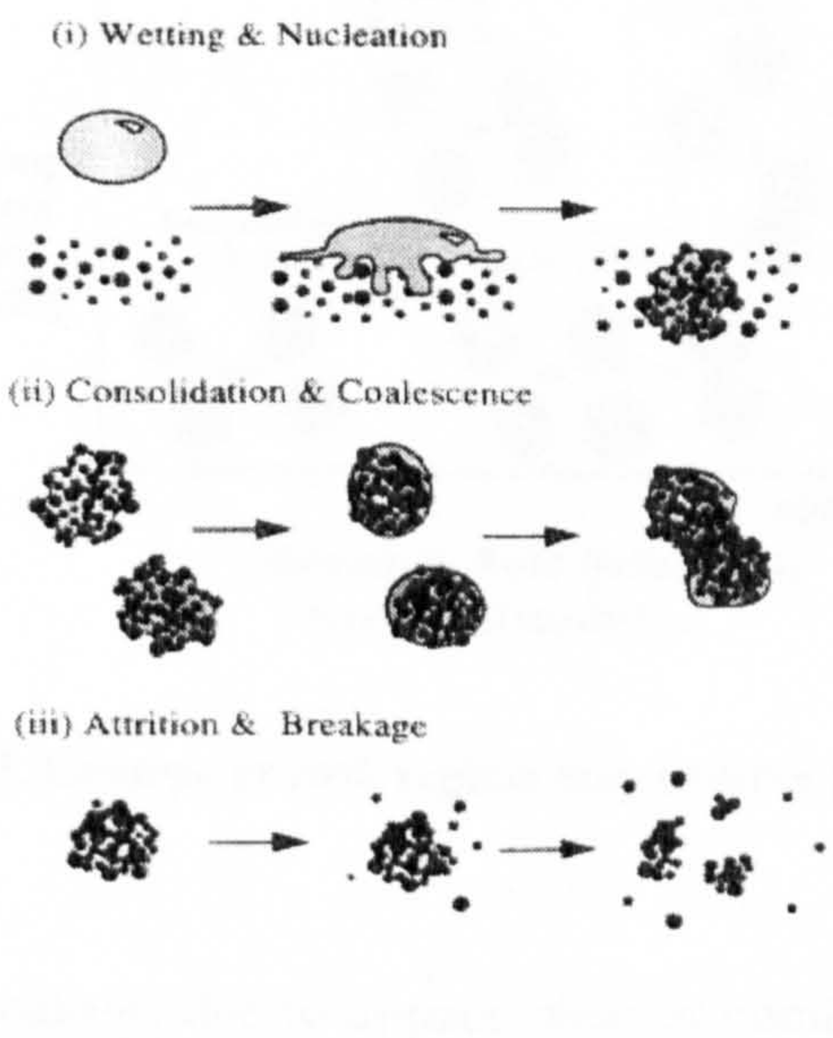

Figure 2.2. "Modern" approach to granulation (source [4]).

A detailed description and importance of each of the three rate processes can be found in [4]. Briefly:

- Wetting and nucleation: this process refers to the initial contact between the binder and the dry powder bed and how the binder distributes within this bed to create the initial nuclei granules. The relative sizes between primary particles and liquid binder droplets will influence the nucleation mechanisms, with two main nuclei formation mechanisms (distribution and immersion)[12, 13].
- Consolidation and growth: particle-particle and particle-equipment interactions lead to granule compaction and growth. Different authors have described this process differently. For example Vonk *et al.* [14] propose a destructive nucleating growth mechanism by which growth occurs after initial nuclei are broken down and further densified. Iveson and Litster [15] introduced a growth regime map showing the dominating granule growth mechanism as a function of granule deformation (given by the Stokes deformation number).

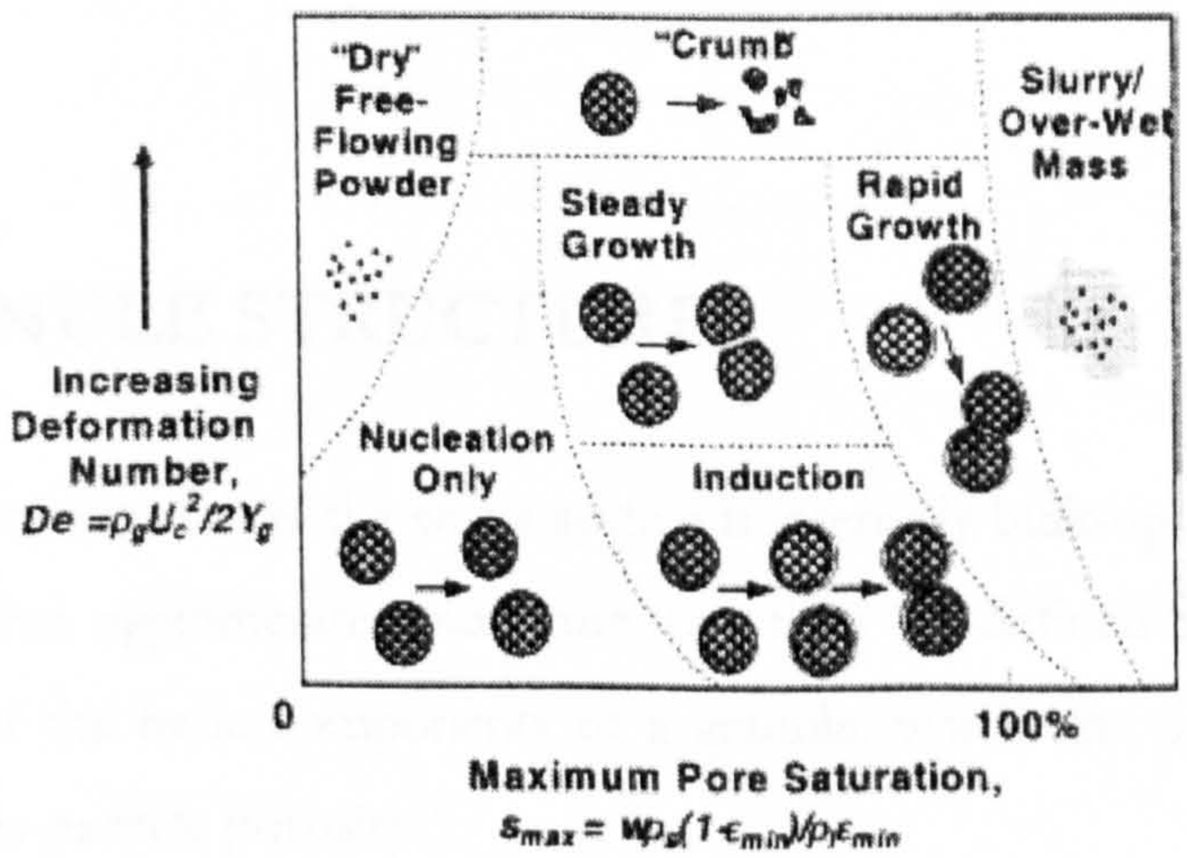

Figure 2.3. Granule growth regime map (source [15]).

- Attrition and breakage: due to impact, wear or compaction in the mixer or during further product handling. Different breakage/attrition mechanisms are reported in the literature, classified according to the effect of the damage on the agglomerates, or on the type of forces that cause this damage (for example in [16]).

2.1.3 Final considerations

Even though granulation has been the subject of research for almost 60 years, the discipline is currently extremely active with much research being conducted at a fast pace. Industrial interest in granulation has also gradually grown in the last decades with virtually every product that appears as a powder undergoing a granulation step to benefit from the improved product characteristics it offers.

The granulation mechanisms are not well understood. However extensive research in the field has allowed a better understanding of the different variables that affect the process. The future of granulation will go through the understanding of the granulation mechanisms at the different length scales so that granulation processes can be designed to obtain specific product properties. It is there that this work focuses: on trying to understand the effect that different granulations conditions have in the structure on single granules and how this structure may show in the properties they exhibit.

2.2 GRANULE STRUCTURE

The term structure describes the way a system is internally built-up from its basic components. For agglomerates, structure can then be defined as the spatial arrangement of the basic components of a granule, which are: primary solids, binder and intra-particle porosity.

Scale information should also be given alongside structural information. In this case, macro-structure would refer to the powder bed or the tablet structure, meso-structure to internal agglomerate structure and micro-structure would describe the structure of the basic components. To quantify structure the following must be known [17]:

- Amount of each component: quantified by its phase volume.

- Size of the defined phases, which can be calculated using chord length distributions.
- Distribution of the phases throughout the system, describing the granule homogeneity.

These characteristics can quantify the structure of an isotropic, spatially unlimited structure. They do not account for the granule's shape, outer morphology or radial concentration gradients.

2.2.1 Importance of granule structure

The structure of an agglomerate is a key factor in determining the final properties of the product, whether as independent agglomerates or tablets. The performance of agglomerated products is determined by their composition, structure and the way they have been manufactured [6]. For a given product, composition is usually fixed and the structure of the agglomerates is determined by the way they are formed. It is therefore very important to understand how the structural characteristics of an agglomerate are going to affect its properties as well as how the manufacturing method is going to affect the structure achieved by the agglomerate. This way it would be possible to build links between manufacturing and final product properties that will encompass the structuring of agglomerates from the beginning of their processing in order to obtain a desired product performance. Early work (1966) shows how the granulation methods have a direct effect on the properties exhibited by the final product, but does not relate this effect to the granule structure [18].

Knowing how to measure and describe the internal structure of agglomerates would also allow its incorporation into fundamental modelling of granulation [19] allowing the use of structural characteristics in simulation tools, physical models or to predict structure dependant granule behaviour [17] .

Properties of granulated material are determined by its composition, size distribution, shape and internal structure [17]. The composition is fixed usually

by chemical requirements to achieve certain properties of the product. The size distribution is usually chosen to meet criteria such as appearance, dust content and bulk density targets. Therefore it is the agglomerate morphology, shape and structure that ultimately determine the properties of the granule. Although this statement is mostly applicable in a pharmaceutical environment (in non-pharmaceutical environments there is more freedom to change parameters, use different additives to modify certain properties, etc.), it highlights the importance of granule structure.

The granule structure will determine important properties such as the intergranular bonding during compression (important for tabletting), breakage or dissolution rates of the product.

The intergranular bonding behaviour during compression is described in [20] as are the resulting tablets properties and structure [20, 21]. Previous work [22, 23] described four types of structure depending on the manufacturing process of the granules (Figure 2.4). These models are summarized in

Table 2.2 and show different types of intergranular bonding during the compression of the granules to form tablets (Figure 2.5):

- For pre-compressed granules (roller compacted granule) the binder particles are present as discrete particles within the granules and little intergranular bonding occurs during tabletting (bonds are only formed between solid particles), leading to the formation of low strength tablets.
- The opposite occurs in the case of spray dried granules. The high concentration of the binder at the surface creates large areas of intergranular binder to binder contact, even at low tabletting pressure.
- For wet-massed granules, the granules make contact between binder and binder, binder and crystals and the crystals themselves. The area of intergranular binder bonding is smaller, resulting in tablets weaker than those produced from spray dried granules.
- Spray-coated granules are characterized by the presence of a surface layer of binder (Figure 2.4 and Figure 2.6).

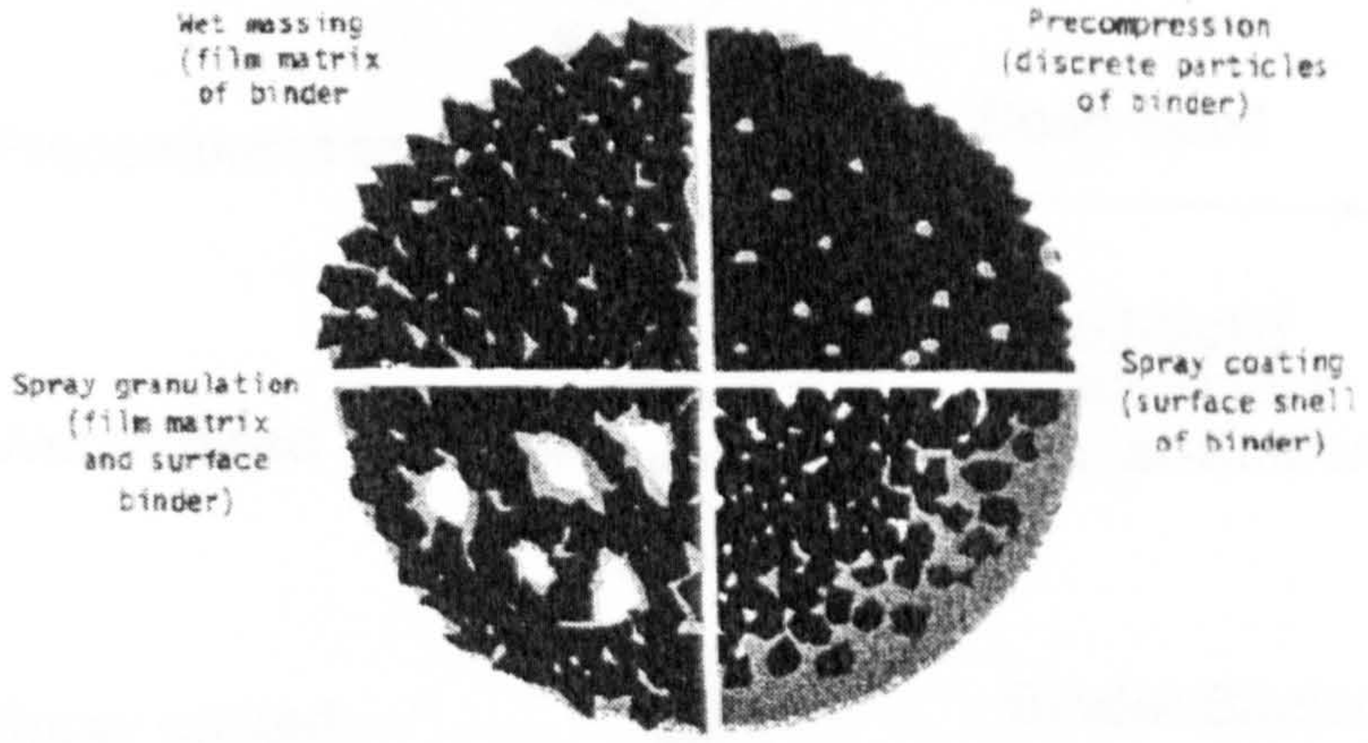

Figure 2.4. Structure of granules prepared by different process methods (modified from [23]).

The term "spray drying" and "spray granulation" are used as synonyms in this early work and the structures reported for this type of agglomerates (see Figure 2.4) correspond to the typical opened structure of fluidised bed granules (as we will see in Chapter 4).

Table 2.2 was modified in order to accommodate the term "fluidised bed granulation" alongside the properties typical of agglomerates obtained this way.

Table 2.2. Characteristics of granules prepared by different processes (modified from [23])

Granulation process	Granule property				
	State of binder in granules	Concentration of binder at surface	Granule density	Bulk density	Main bonding mechanisms (during tabletting)
Pre-compression	Discrete particles or particle fragments	Very low	Very high	Very High	Particle fusion+ Particle interlocking++ Plastic deformation
Wet massing	Film matrix	Low	High	High	Binder cohesion Interparticulate bonding*
Fluidised bed granulation	Film matrix	Moderate	Low	Low	Binder cohesion Interparticulate bonding*
Spray coating	Surface shell	High	High/low	High/low	Binder cohesion Interparticulate bonding*

\+ Cold melting during compression
++ Particle fracture during compression
* Precipitation of partially dissolved solid during compression

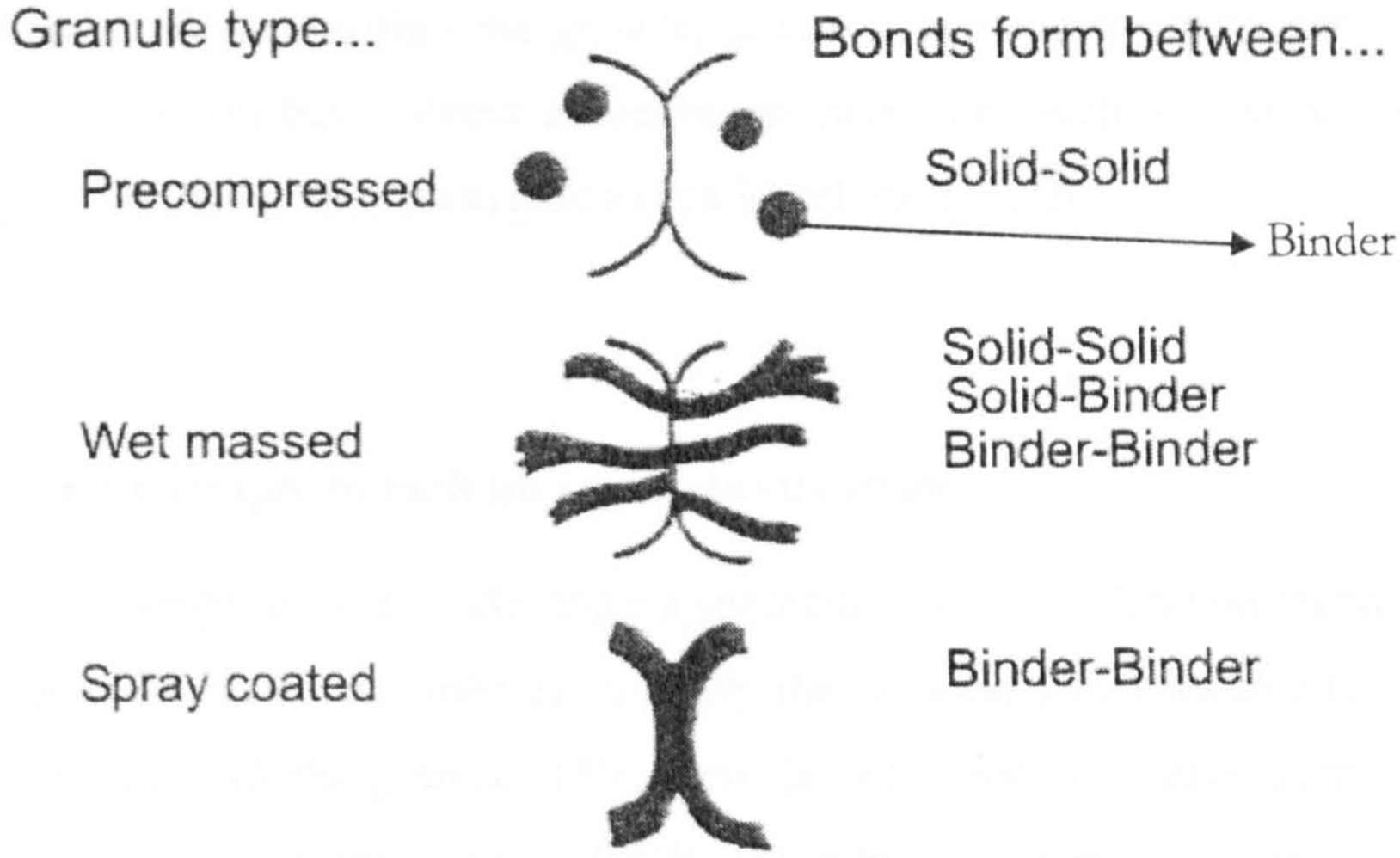

Figure 2.5 Schematic representation of granule structure and intergranular bonding during compression (modified from [20]).

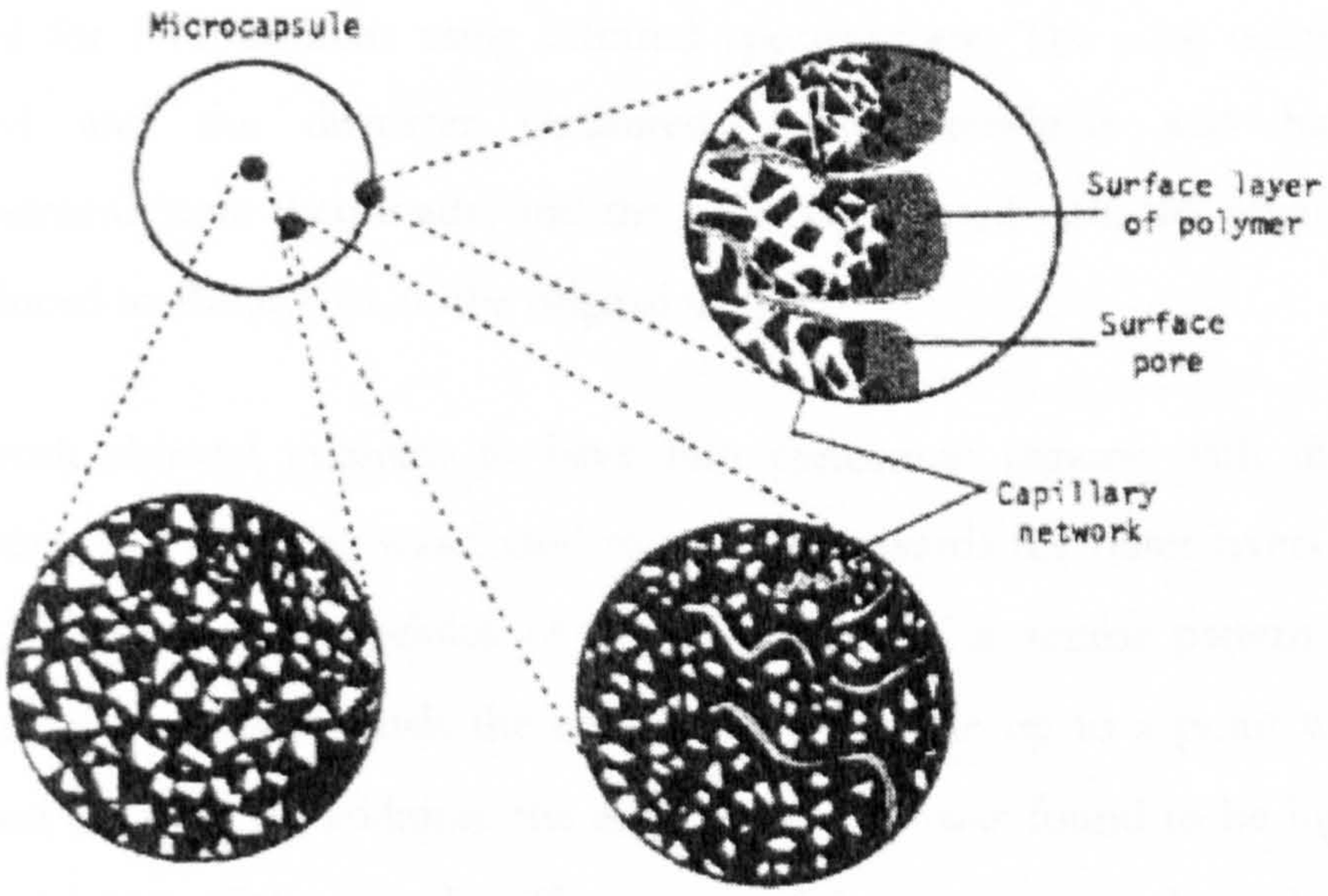

Figure 2.6. Internal structure of a typical spray coated powder (source [23]).

More recent work shows the importance of structural characteristics on the properties shown by agglomerates, such as breakage [1, 24] or the behaviour of granules under stress [25]. The void fraction, as well as the size and spatial

distribution of pores within the granule, is also a key characteristic since the presence of pores has a direct influence on properties such as wet and dry strength, dissolution and disintegration in a liquid medium [26].

2.2.2 First attempts to look into granule structure

The first attempt to look inside single agglomerates used an abrasion technique combined with chemical analysis to study the position and concentration of binder throughout the granules [27]. Granules of magnesium carbonate were created using polyvinylpyrrolidone (PVP) as binding agent by wet massing. The distribution of binder within the granule and its effect on local strength as drying occurred was studied by calculating the radial distribution of binding agent at different stages during the drying process.

In order to do this, an attrition method previously described in [28] and [29] was used; a method by which the outer layers of the specimens were removed and analysed for PVP content using infrared spectroscopy. The core weight was recorded and the diameter measured. Elastic modulus and hardness measurements were then made, and the process repeated until the core weight was reduced to about 10% of the original weight.

This work showed granules to have two concentric regions with different properties. The hardness was found to increase towards the outer layers of the granule. The Young's modulus of elasticity followed a similar pattern to the hardness, decreasing towards the centre of the granule up to a point where it remained constant. In addition, the amount of PVP was found to be higher in the outer layers of the granules. The extent of these properties depends on the drying profile the samples are subjected to.

With regards to pharmaceutical composition, non-uniform distribution of binder within agglomerates can be coupled to misdistribution of the active component. Therefore, any attrition during storage or further processing can cause fines with a composition different from the bulk, resulting in lower product quality.

Optical techniques were also developed [30] to determine the distribution of polyvinylpyrrolidone (PVP) binder in fluidized bed dried granules, by labelling the binder with a fluorescent material and assessing its position within the granules by light microscopy. They used fluorescein isothiocyanate (FIC) to label the binder and make it fluoresce when excited by light.

Following this, a mixture of the labelled PVP and normal PVP was created to achieve suitable fluorescence, and this mixture then used to granulate powder mixtures in a fluidized bed. Sample granules were taken and observed using a fluorescence microscope. Sample granules were also embedded in wax and cut into 20 μm thick sections with a microtome. The sections were also inspected with a fluorescence microscope and they report that the distribution of PVP within the granules could be seen perfectly. Unfortunately, no quantitative results are given in their work about how the binder distributes within the agglomerates, only the method is explained.

2.2.3 Solvent extraction methods

Seager et al. [22] initially tried to study the structure of agglomerated material as related to the manufacturing process and final product conditions. Previous work from the same authors [23] had suggested that properties of granules are governed by the distribution of the binding agent within them, which is in turn determined by the method of manufacture. A solvent extraction method was then developed [22] to study the position of the binder within granules prepared by three different methods (roller compaction, wet massing and spray drying) and relate the product structure with the production process mechanism (Figure 2.7).

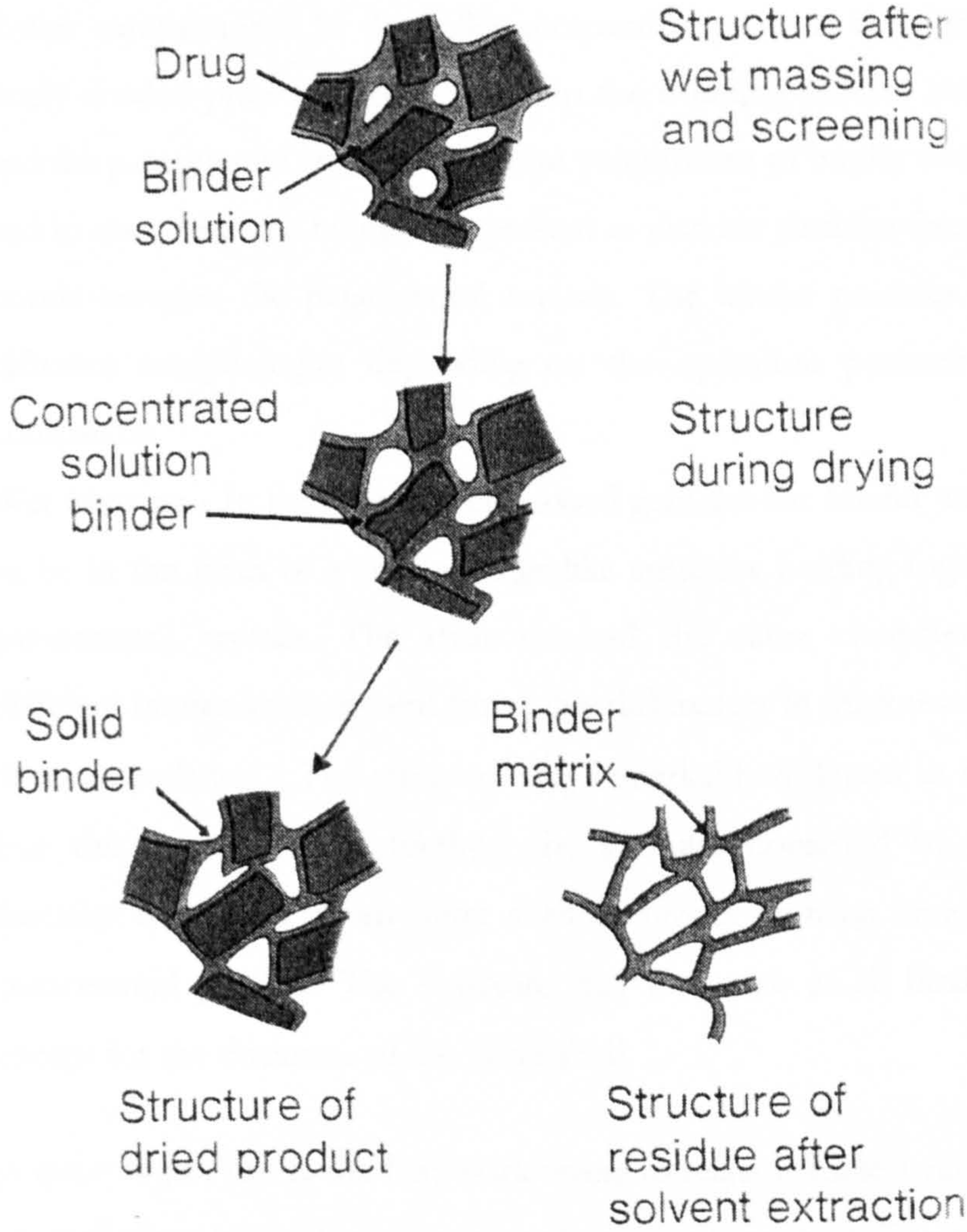

Figure 2.7. Schematic diagram of the mechanisms of the solvent extraction method for binder matrix formation (source [22]).

In order to study the structure by a solvent extraction technique an appropriate combination of drug and binder was chosen with different properties of solubility. The system chosen was paracetamol with a hydrolysed gelatine binder. The solvent used consisted of 60/40 (v/v) chloroform and ethanol. The paracetamol readily dissolves in this mixture and the gelatine binder is not affected. Therefore the paracetamol is dissolved and washed away and the binder is kept intact.

After the extraction process, the binder residue was observed using SEM. As expected, different structures were seen for the different manufacturing techniques:

- Roller compaction - In the roller-compaction process, the binder was finely divided prior to addition to help the bonding process between it and the paracetamol crystals. Different proportions of binder were tested and in every case the binder was present as discrete particles forming the bonds between the paracetamol crystals. The binder particles showed different morphologies depending on the operation pressure of the compactor.
- Wet Massing - In the case of wet-massed granules the binder was found to be in the form of a solid sponge-like structure holding together the paracetamol crystals. The structure had the same characteristics at different binder levels, except for visible differences in thickness.
- Spray-granulation - The structure was remarkably different in this case. For this manufacturing method the granules consisted of spherical particles composed of an outer shell of binder with an inner core of paracetamol powder. The structure was the same at all binder levels except for the thickness of the outer shell.

Although quite vague, this is the first work trying to relate granule structure with process manufacture, introducing the solvent extraction method. Three different kinds of structure for the different ways of manufacturing the granules were described: wet-massed granules showed the binder distributed throughout the agglomerates in a sponge-like matrix, spray-dried granules showed the binder concentrated as a shell at the surface of a sphere, and pre-compressed granules where the binder was present as discrete particles embedded in the agglomerates which were formed largely from interparticulate bonds between the paracetamol crystals (Figure 2.8).

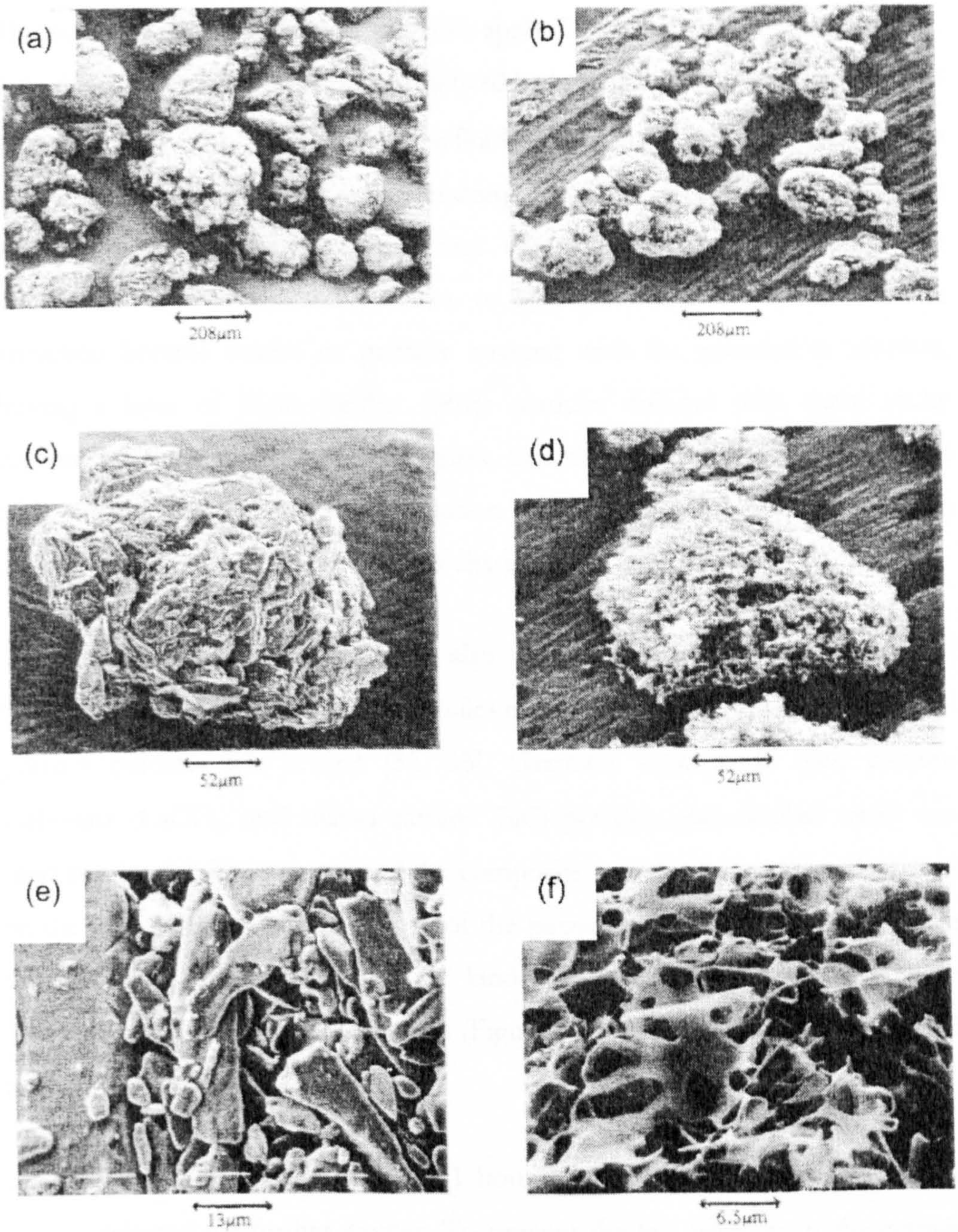

Figure 2.8. SEM photographs of the binder extraction methods (source [6]): (a) view of wet massed granules; (b) view of the state of the binder after solvent extraction process; (c) wet massed granule; (d) wet massed granule after solvent extraction process; (e) surface appearance of wet massed granule; (f) surface appearance of wet massed granule after solvent extraction method.

This method led onto investigations focused on the effect of the structural characteristics of granules on their bonding and tabletting properties [20, 21].

The solvent extraction method was also applied to fluidized bed granules [31]. Two different size ranges from the fluidized bed granules (250-500 and 500-1000 μm) were analysed to discover that the fluidized bed granules had a more porous structure than wet-massed ones, resulting from the random nature of the agglomeration/fluidization process and the absence of shear during the fluidization. Individual solid particles or aggregates formed by electrostatic attraction became coated or partially covered with the granulation solution, leaving a layer of sticky binder. Other particles collided with these sticky crystals/agglomerates forming aggregates, that then themselves became coated with further deposits of binder solution and this process continued as the aggregates grew into granules, giving a characteristic open structure.

The solvent extraction technique was also used to dissolve the agglomerates and then describe the structure of the granules in terms of the size distribution of the primary particles left behind [32, 33]. Granules were made with calcium carbonate ($CaCO_3$) and silicon carbide (SiC) powder, and distilled water was used as a binder. The structure of the composite granules formed was discussed on the basis of the size distributions of the silicon carbide particles contained in the granule, dividing them into six kinds of structure models, which were affected by the granulation conditions (Figure 2.9 and Figure 2.10). The method is described below:

- The granules were dried for 1 hour at 120 °C and different sieve sizes selected for further studies. To prevent the SiC particles in the granule from being affected by further physical/chemical treatment they were solidified by heating the granules for 1 h at 1000 °C. These are named *a-granules.*
- To separate the SiC particles from the granule, the $CaCO_3$ was dissolved with a HCl solution. The SiC agglomerates are named *b-agglomerates.*
- Further treatment applied attempted to break up clusters of SiC that had been formed during the treatments by using EDTA·2Na in order to break bonds due to the presence of calcium silicate (Ca_2SiO_4) which might be produced by heating the granule composed of SiC and $CaCO_3$.

The solution added did not have any effect on agglomerates of pure SiC that had been formed in the granulation process. These SiC agglomerates contained in the b-granules are named *c-agglomerates.*

	a-1	a-2	a-3	a-4	a-5	a-6
(a) Image of composite a-granule [D_p] (mm)	 D_p =1.128	 1.005	 1.005	 1.046	 0.147	 0.160
(b) Image of SiC b-agglomerates [$\bar{d}_{pb}$] (mm)	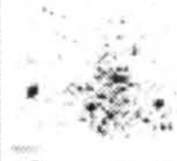 $\bar{d}_{pb}$ =0.088	 0.692	 0.763	 1.036	 0.146	0
(c) Image of SiC c-agglomerates [$\bar{d}_{pc}$] (mm)	 $\bar{d}_{pc}$ =0.078	 0.641	 0.068	 0.062	 0.146	0
(d)Particle size characteristics	$D_p \gg \bar{d}_{pb}$ $\bar{d}_{pb} = \bar{d}_{pc}$	$D_p > \bar{d}_{pb}$ $\bar{d}_{pb} = \bar{d}_{pc}$	$D_p > \bar{d}_{pb}$ $\bar{d}_{pb} \gg \bar{d}_{pc}$	$D_p = \bar{d}_{pb}$ $\bar{d}_{pb} \gg \bar{d}_{pc}$	$D_p = \bar{d}_{pb}$ $= \bar{d}_{pc}$	$D_p \gg \bar{d}_{pb}$ $\bar{d}_{pb} = \bar{d}_{pc}$

Figure 2.9. Typical morphology of composite granules observed by electron probe micro-analyser (source [33]).

The structure of the binary composite granules made of $CaCO_3$ and SiC powders is discussed in terms of the size distributions of SiC agglomerates (c-agglomerates) contained in the granules. They grouped the structure into three classes (A, B and C) according to the characteristics of the dispersion of SiC agglomerates in a single granule. Each of these groups was further divided into two-subgroups according to the mean diameters of the *a, b* and *c-granules* (sizes D_p, d_{pb} and d_{pc} respectively).

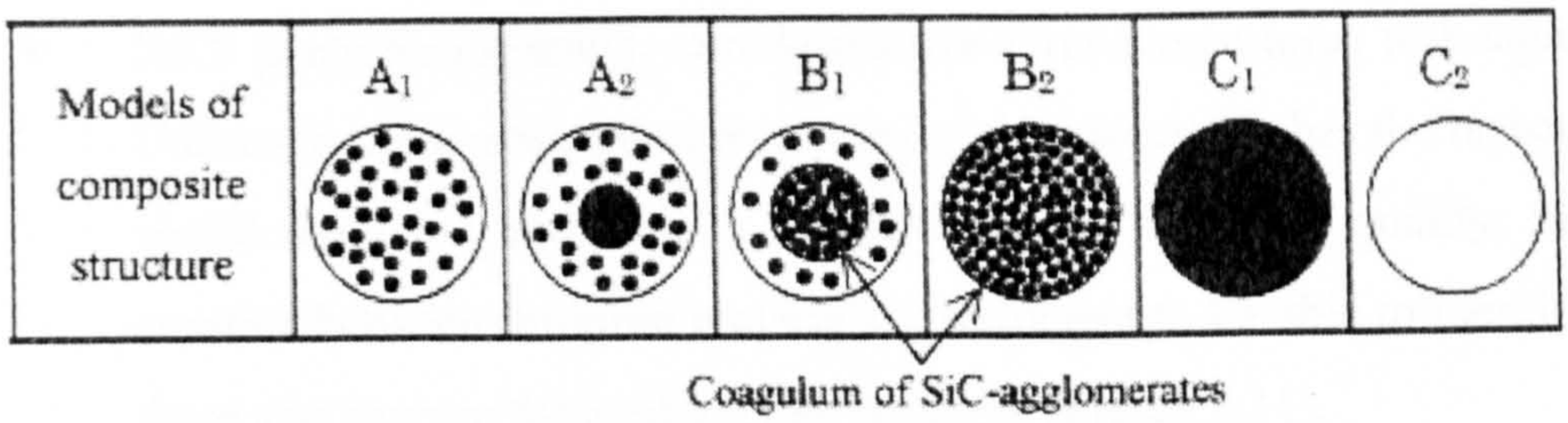

Figure 2.10. Analysis of composite granules composed of the binary mixture of $CaCO_3$ and SiC powders using image analyser and estimated composite structure models of a granule. In the models, the white part denotes the $CaCO_3$ component and the black denotes and agglomerate of SiC particles (source [33]).

2.2.4 Imaging techniques

Following the definition of structure as the spatial arrangement of the basic components of a granule [17], a technique capable of measuring it should give the spatial arrangement inside the granule either in two or three dimensions. Some of the techniques that can provide this kind of information are (from [17]):

- SEM (scanning electron microscopy): standard tool to image microstructures. It has a high spatial resolution and good material contrast, therefore allowing the identification of different phases present in a granule. It is only a two-dimensional technique therefore in order to image internal structures they have to be exposed, requiring slicing of the specimen to be analysed. An example of the application of SEM in characterizing agglomerate morphology can be seen in [34].
- IR (infrared) microscopy: in this case infrared signal can be used for material identification. It presents the same disadvantages as SEM, and its spatial resolution is much lower.
- MRI (magnetic resonance imaging): non-destructive three-dimensional technique. Uses nuclear magnetic resonance properties of the material. High spatial resolution but it cannot be easily used with any specimen.

- XRT (x-ray tomography): non-destructive three-dimensional technique. Utilizes the x-ray absorption properties of the material. It has the highest spatial resolution and if the x-ray source is of sufficient quality, the contrast between different materials is sufficient to be able to identify them and analyze the agglomerate structure (Figure 2.11).

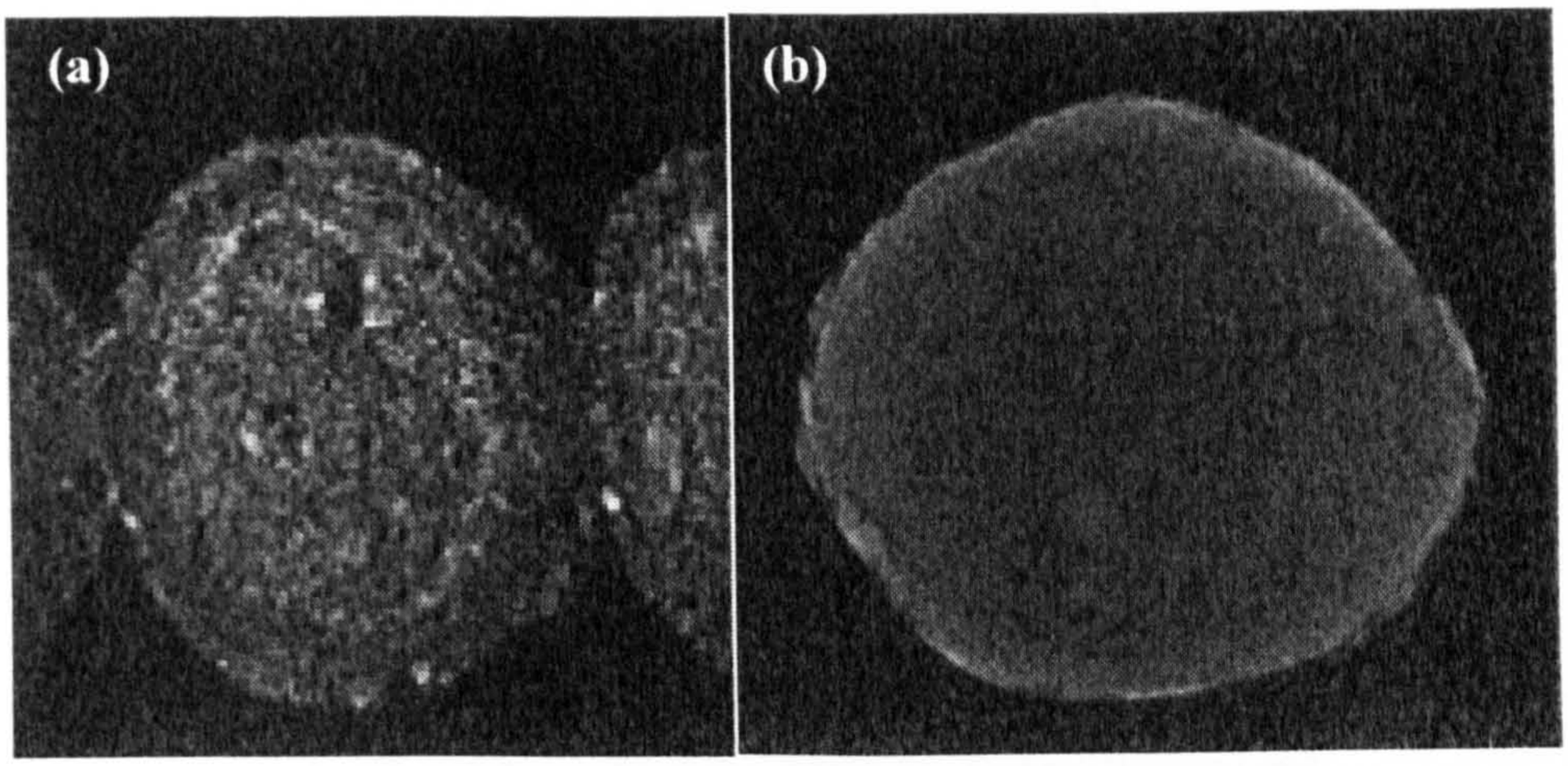

Figure 2.11 Comparison of MRI and XRT images of single granules. (a) Cross section through a single granule using MRI, nominal resolution 35 x 35 x 50 μm (source [35]); (b) cross section through a single granule using XRT, nominal resolution 4.25 x 4.25 x 4.25 μm.

2.2.5 Quantification of granule structure from imaging techniques

A segmentation step is necessary in order to quantify granular structure from images, signifying that each point in the image has to be classified as part of one of the defined phases [17].

In the segmentation process the main area of uncertainty arises when partial voxeling happens (Figure 2.12). This effect happens when two or more phases occur in a single voxel. When only one phase is present in a voxel the signal intensity will be characteristic of that phase, but when more than one phase is present the signal will be a combination of the contributions of the different

phases. The quantitative limitations imposed by the partial voxeling effect have been subject to study in fields like medical imaging, and different mathematical approaches have been used in order to quantify and correct for this problem (for example [36]). Most research into this topic has been done in the field of medical imaging using MRI as the technique.

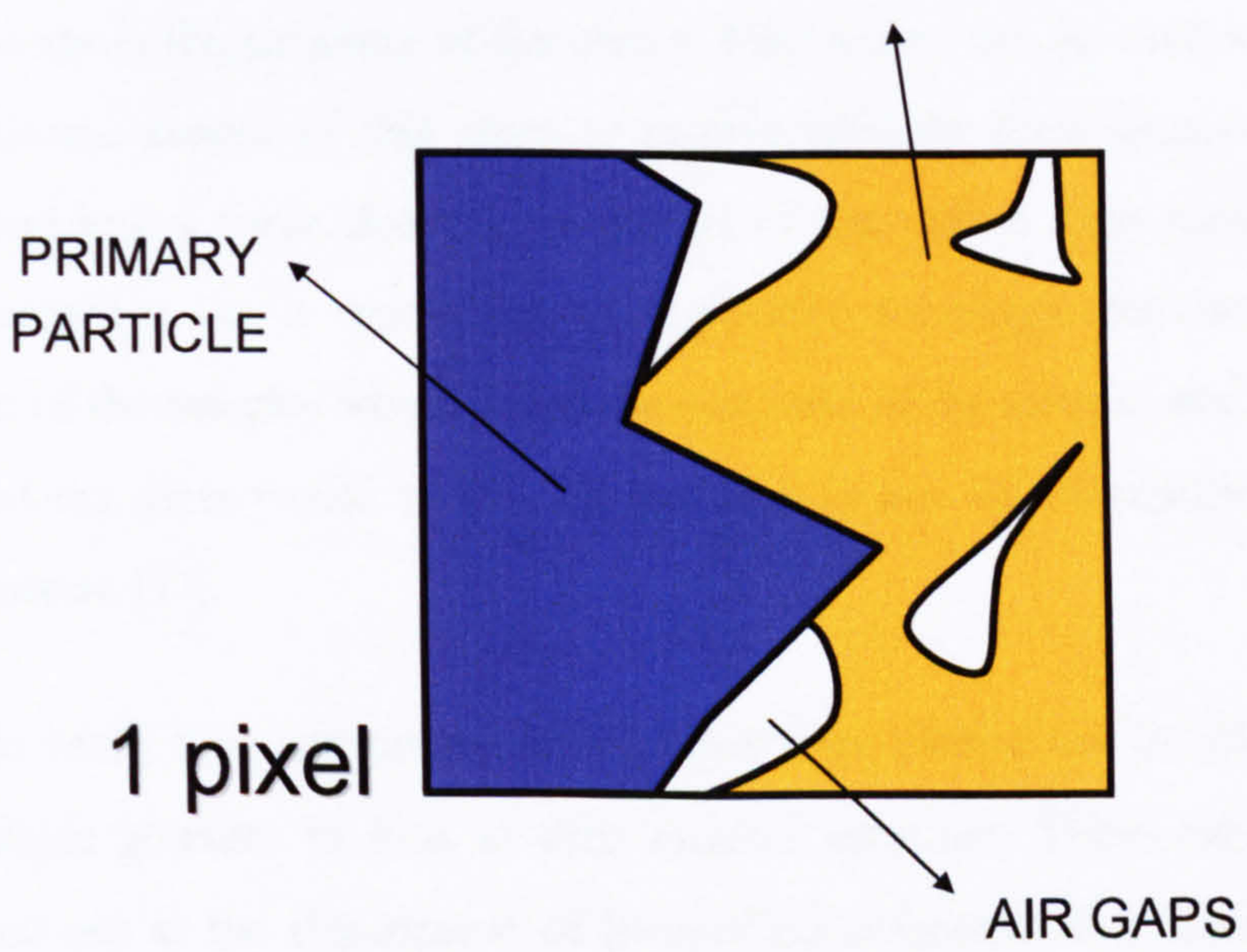

Figure 2.12. Schematic representation of partial voxeling: it occurs when more than one component occurs in the same voxel. The intensity of the voxel depends on the proportions of the components present.

A set of five key descriptors in order to quantify granule structure are also proposed in [17] using imaging techniques as the basis for this analysis and include the amounts of the phase volumes, their sizes and a homogeneity measurement.

2.3 X-RAY COMPUTED MICROTOMOGRAPHY

2.3.1 Introduction

Optical or electron microscopes can provide very detailed information about the surface of a sample. However, the information they provide is only two dimensional and it is not always possible to transform it into three dimensional information about the structure of the object. Microscopy can be used to obtain two dimensional images of thin slices of sample whereby these images can be reconstructed into a three dimensional model of the object. This method not only is destructive but it would not be applicable for single granules as the preparation of the samples would affect the structure of the sample, and also the thickness of the slices would be too big and lead to loss of information of the sample structure [37].

In order to verify this, microtomy experiments were carried out to obtain thin slices of single granules to look at their internal structure. These experiments were carried out at the department of Biomedical Science at the University of Sheffield due to their background on using the technique on medical and biological applications. The samples were embedded in wax and slices 5 μm thick were cut. However, it was clearly seen using an optical microscope that the structure of the granules had been modified due to the action of the blade (Figure 2.13).

Another method to study the structure of the granules needed to be found. It has to be non-destructive in order to preserve granule structure and accurate enough in order to analyze single granules. X-ray microtomography was deemed a suitable method due its resolution, non-destructive nature and ability to deal with samples without prior preparation. Furthermore access to X-ray tomography was granted by Unilever.

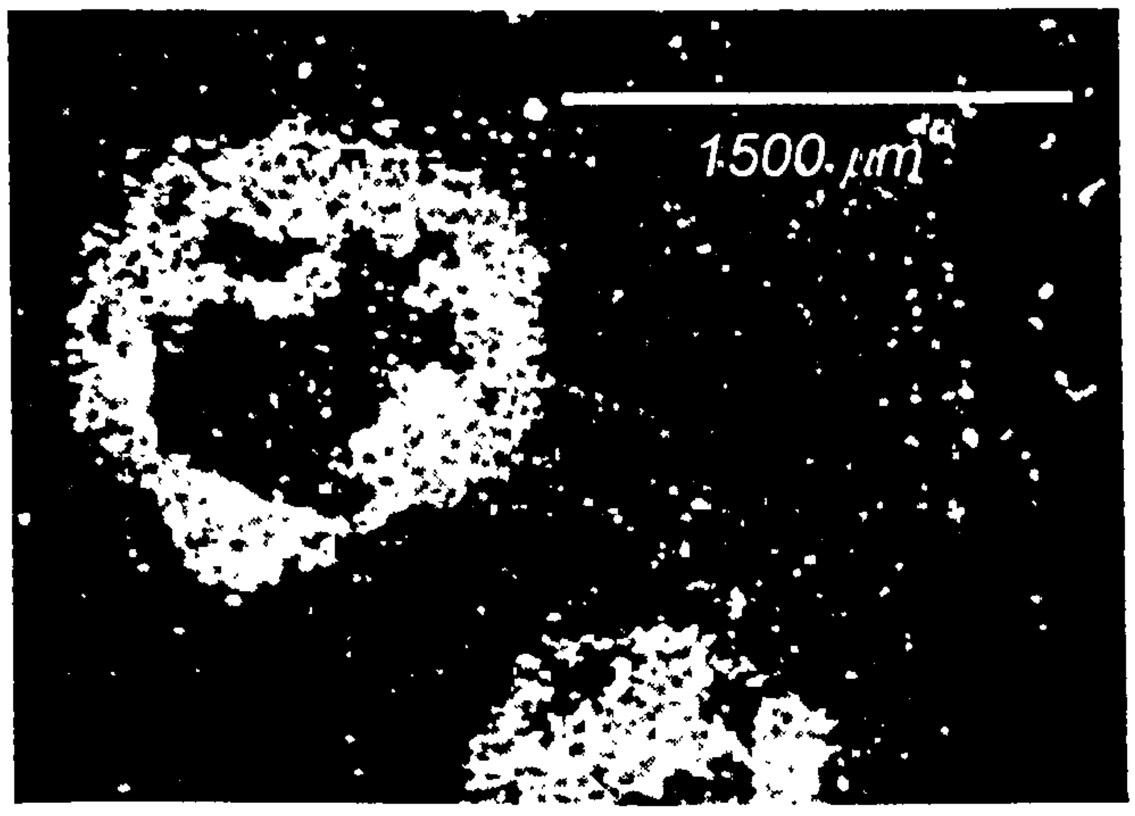

Figure 2.13. Microscopy image of a slice through a single granule using a microtome.

Standard X-ray images are two dimensional shadow images of complete three-dimensional structures in which the depth information is lost as they only show an integration of the absorption properties of the material along one axis. X-ray tomography uses series of shadow images of the sample obtained at different angles in order to reconstruct the internal structure samples. As an example consider an object with only one point of significant absorption. An x-ray beam is fired through the object creating a two dimensional shadow image of the absorption point with a one dimensional shadow line corresponding to the absorption point within the object. This shadow line is detected and all possible location points of absorption are marked along this line in a computer. The object is then rotated, and another shadow image taken. This process is repeated. With each new rotation a new line of possible object positions is added to the reconstruction area. This operation is called "back projection" and after several rotations the position of the absorption point within the object can be localised. By increasing the number of shadow projections the position becomes more defined [37]. This is illustrated in Figure 2.14.

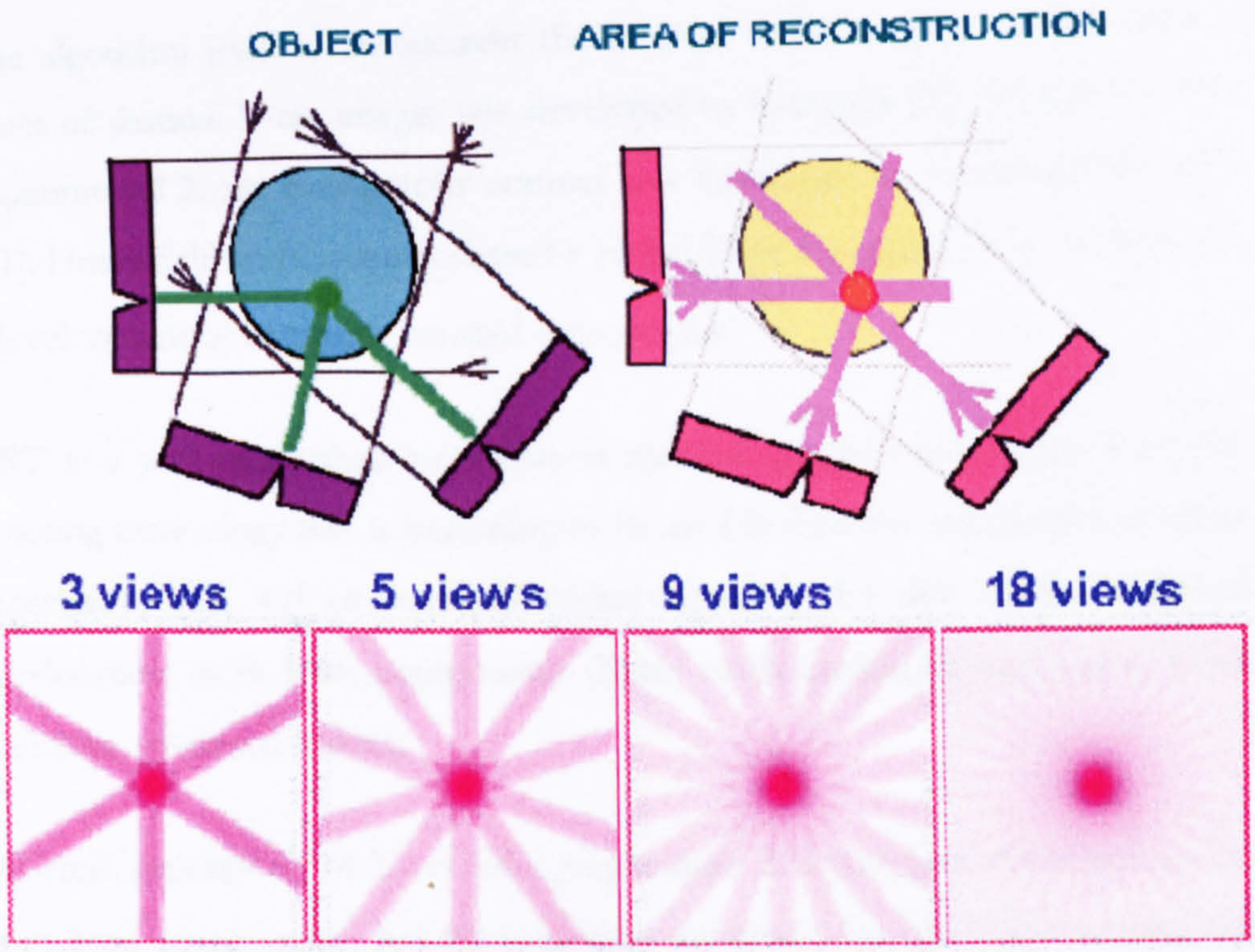

Figure 2.14. Diagram showing the location of an absorption point within an object using back-projection and effect of the number of rotations (source [37]).

Real objects can be understood as many of absorption points and hence be analyzed with this technique. The object is represented as a number of separate absorption voxels, with the linear attenuation for a given x-ray beam corresponding to the sum of the absorption of all the voxels inside this beam. This way, two dimensional slices can be obtained using one dimensional shadow lines from different angles and the three dimensional structure of an object can be obtained by layering the two dimensional slices on top of each other.

XRT then generates images of different cutting planes of the material non-destructively, and three dimensional maps of density and elemental distributions can potentially be obtained with high resolution and short scanning time. By implementing a mathematical algorithm, XRT creates cross-sectional images of the internal structure of a sample from measurement and analysis of penetrating radiation directed through the sample [38].

The algorithm used to reconstruct the internal structure of a sample from a series of shadow X-ray images was developed by Cormack [39, 40] and the first experimental X-ray tomography scanner was developed by Hounsfield in 1972 [41]. Hounsfield and Cormack shared a Nobel Prize for medicine in 1979 for the "development of computer assisted tomography".

XRT is a well established technique in medical imagery, but is also a rapidly evolving technology that is beginning to be used in different applications such as geosciences [42, 43] or materials technology [44, 45] due to the technical development of its basic components (X-ray configuration, X-ray source, X-ray detectors, specimen holder).

Different generations of X-ray tomographs have different geometries and layout of its basic components, but the principles on which they are based remains the same and is depicted in Figure 2.15. Any XRT system consists of two parts [38]:

- A physical measuring technique (x-ray source, detector, specimen holder), that generates and stores the two dimensional shadow images of the sample at different angles.
- A mathematical reconstruction algorithm that creates cross-sectional images of the internal structure of a sample from measurement and analysis of the shadow images.

Several reconstruction algorithms have been developed. One of the most common is the cone-beam reconstruction algorithm developed by Feldkamp *et al.* [46]. Other common algorithms are the fan-beam or the spiral scan. A comparison and critical analysis of different reconstruction algorithms (fan-beam, cone-beam, spiral scan) has been made by Sasov [47].

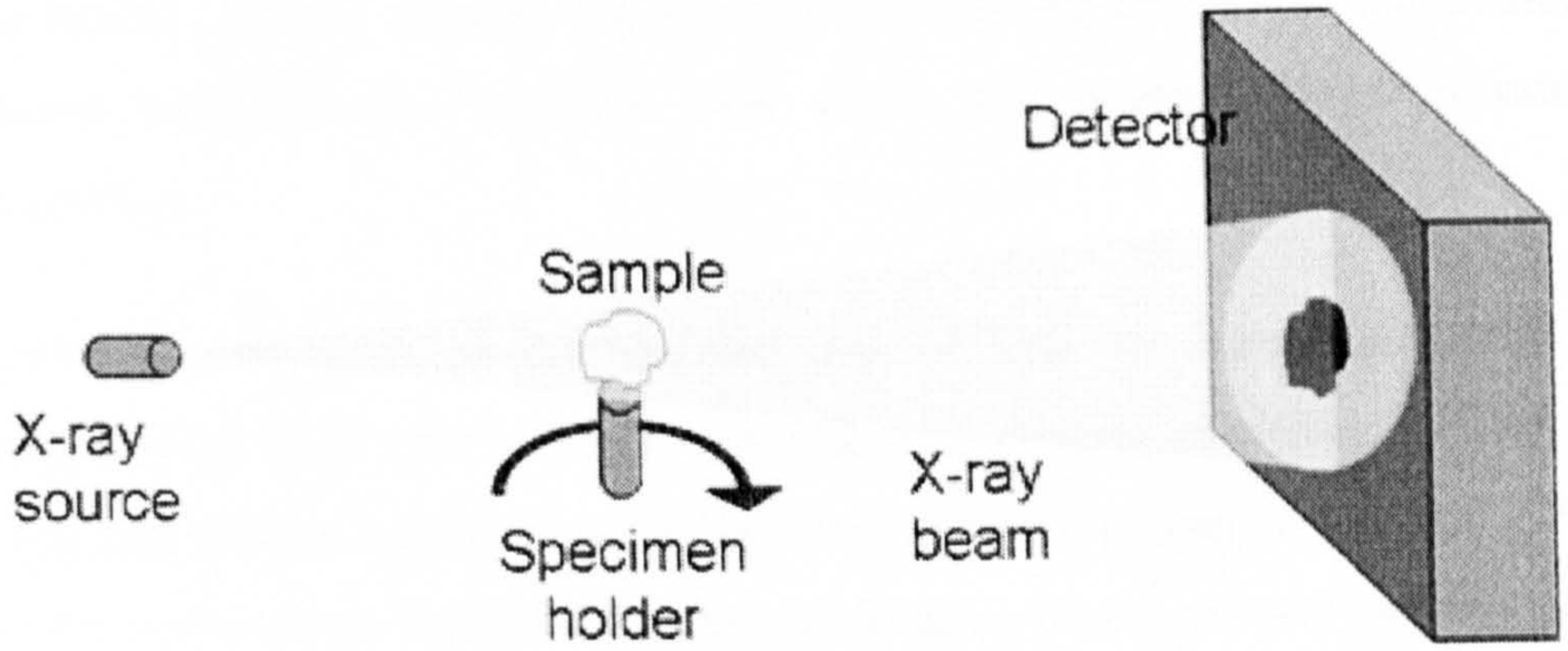

Figure 2.15. Schematic of the typical X-ray tomography set-up.

The main advantages of XRT over other imaging techniques is that it allows for a non-destructive, three-dimensional evaluation of the internal structure of objects, with a continuously increasing special resolution as its physical components develop.

A more detailed description of each of the different components and details in how the technique can be used can be seen in [38], [48] or [49].

2.3.2 Applications in Powder Technology

Due to its origin outside powder technology, its applications in this area are only starting to be explored, but the potential of the technique is immense due to the optimisation of the most appropriate scanning configuration, suitable X-ray sources and detectors, X-ray energy, calibration and hence minimization of the artefacts created by the technique.

A very interesting application of XRT to particle technology is reported in [50] that uses XRT to characterize the internal structure of agglomerates. Two "test" granules were created with two different binders and two different primary powders, by dropping a single droplet of binder onto a bed of powder. XRT showed different structures: loosely packed for non-cohesive powders that let

the binder disperse through the powder surrounding the nuclei and densely packed with cohesive powders with which the nuclei contract towards themselves.

Further investigations on the potential uses of XRT to characterize granular structure that were used as an input for discrete element modelling (DEM) to verify and validate existing models [51]. A model granule was created and XRT used to characterize the three-dimensional location of the primary particles and their respective diameters (Figure 2.16 and Figure 2.17). Simulations of a spherical-shaped granule produced within the DEM code were compared to those of the XRT characterized granule, showing different behaviour between the two different agglomerates, due only to structural and shape differences.

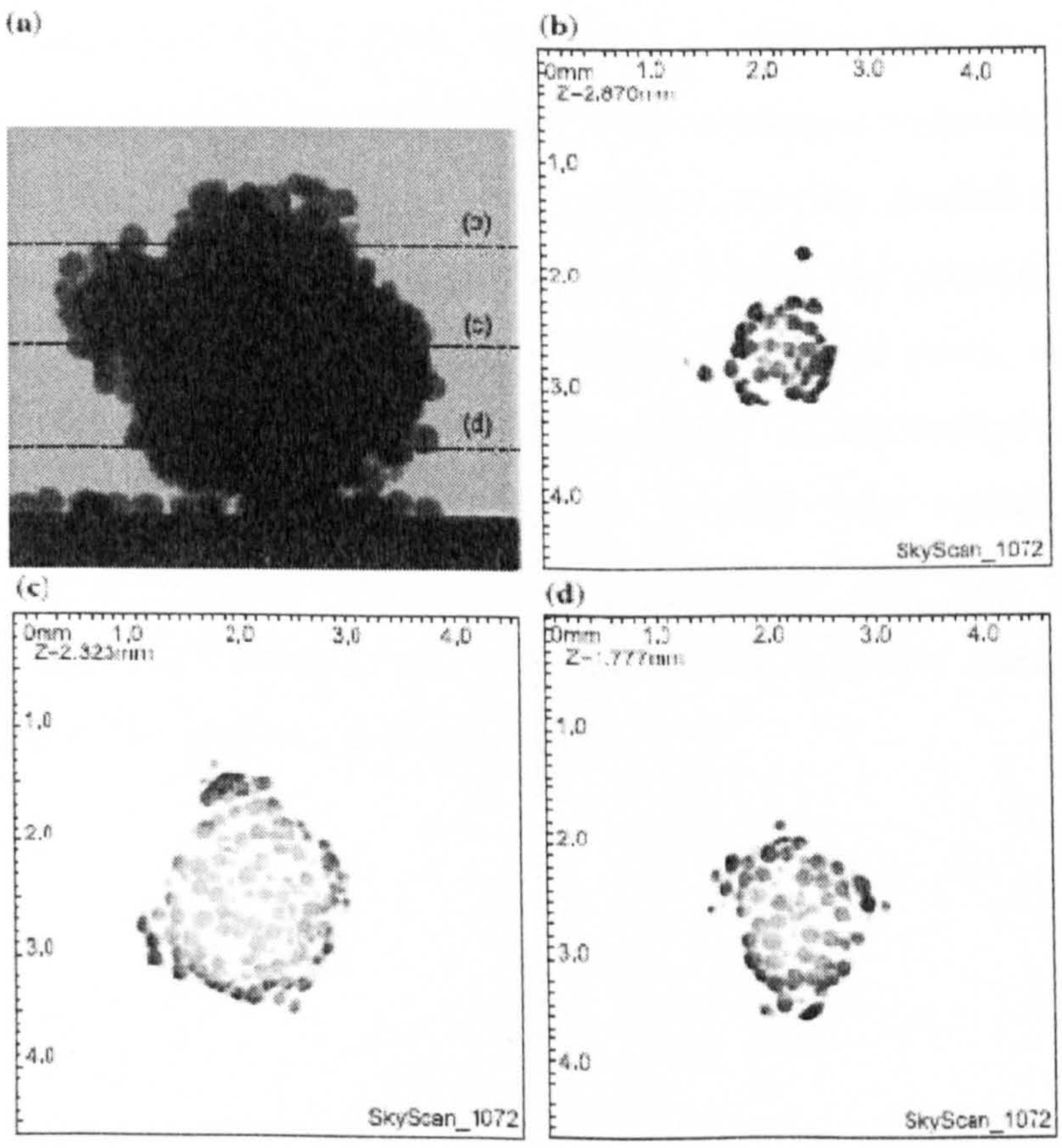

Figure 2.16. X-ray microtomographs of model granule. (a) Side view, (b) to (d) cross sections at different heights (source [51]).

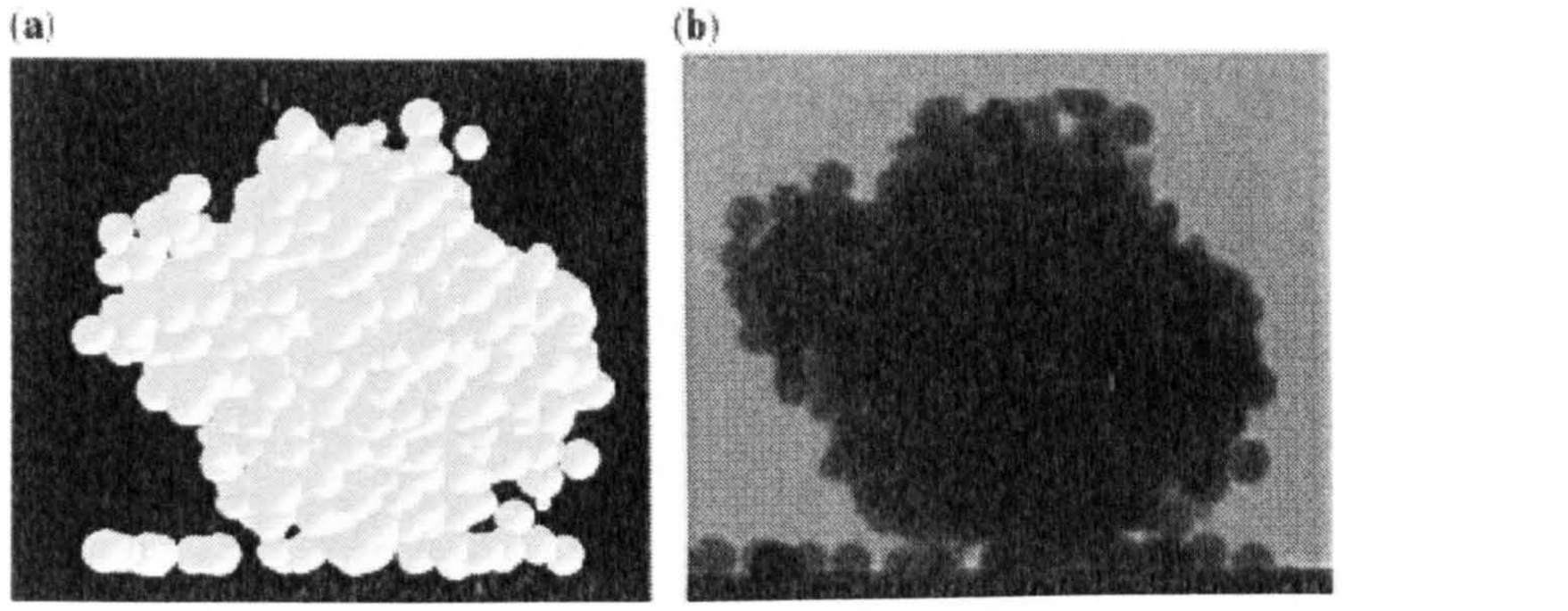

Figure 2.17. Model granule. (a) DEM reconstruction based on XRT characterization, (b) original x-ray image of granule (source [51]).

XRT has also been used to calculate the total porosity, pore size distribution and geometric structure of pores in pharmaceutical granules and compare the results to data obtained with more conventional methods such as mercury porosimetry and gas adsorption [26]. Results showed that XRT is less precise in the determination of total porosity than the more conventional methods, but on the other hand the main advantage of XRT is that it provides detailed information about the true pore geometry and distribution within the granules in a non-destructive manner. It also accounts for internal occluded pores, although its resolution can not yet resolve narrow pore channels. In this work the granule is considered as a two-component system: air and solid matter, with no differentiation between binder and primary particles. This way, the images resulting form XRT analysis had to be transformed to binary ones, hence the need to find a threshold value (Figure 2.18).

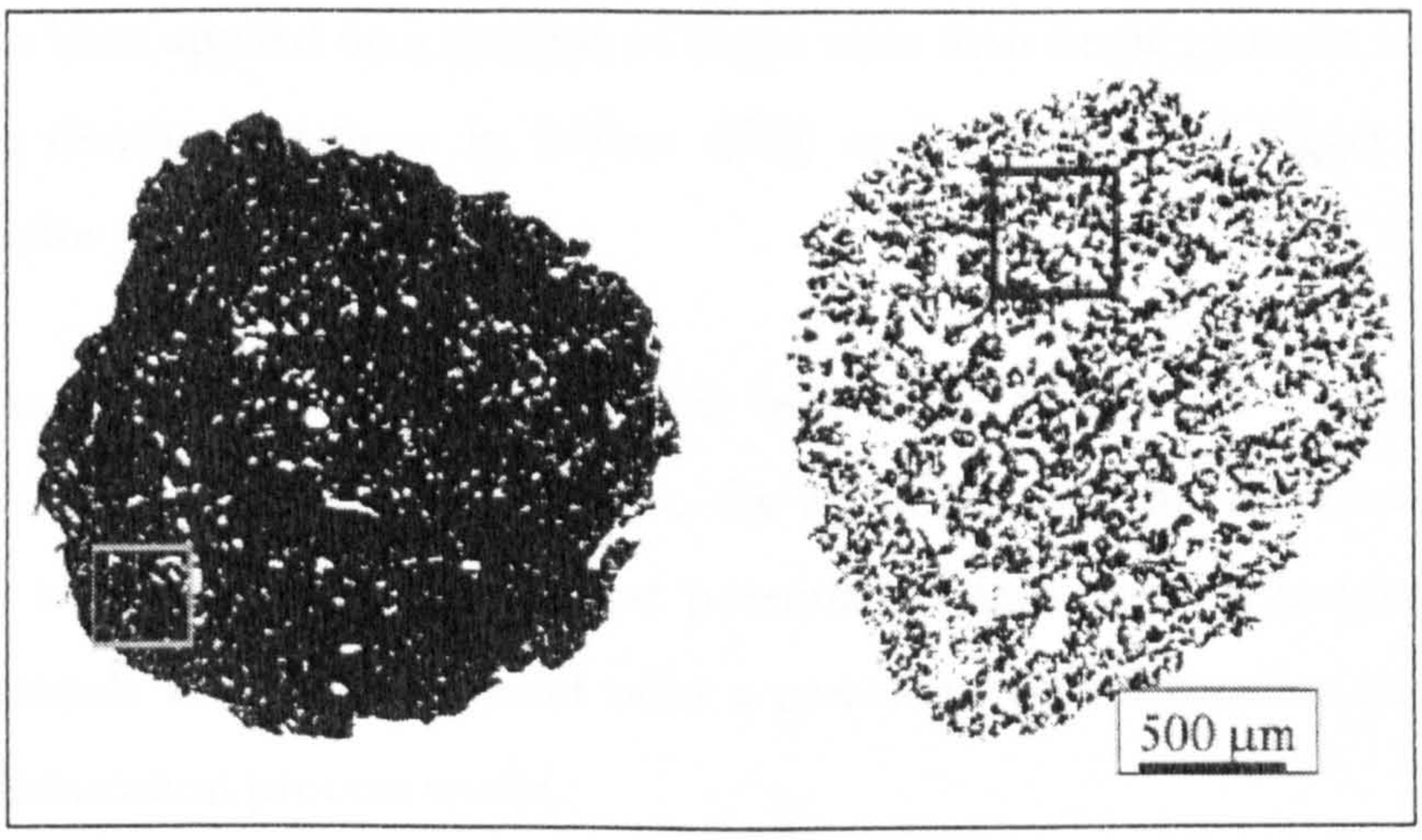

Figure 2.18. Reconstructed cross-section images from XRT analysis of two different granules done under different granulation conditions, showing the difference in structure (source [26]).

The effect of the amount of binder in the structure and behaviour of granules under stress has also been studied using XRT [25]. For this analysis the cross-sections provided by the XRT analysis of the samples had to be transformed into binary images by choosing a threshold value. As before, this transforms the sample in a two-component system: air and solid, without differentiating between solid and binder (Figure 2.19).

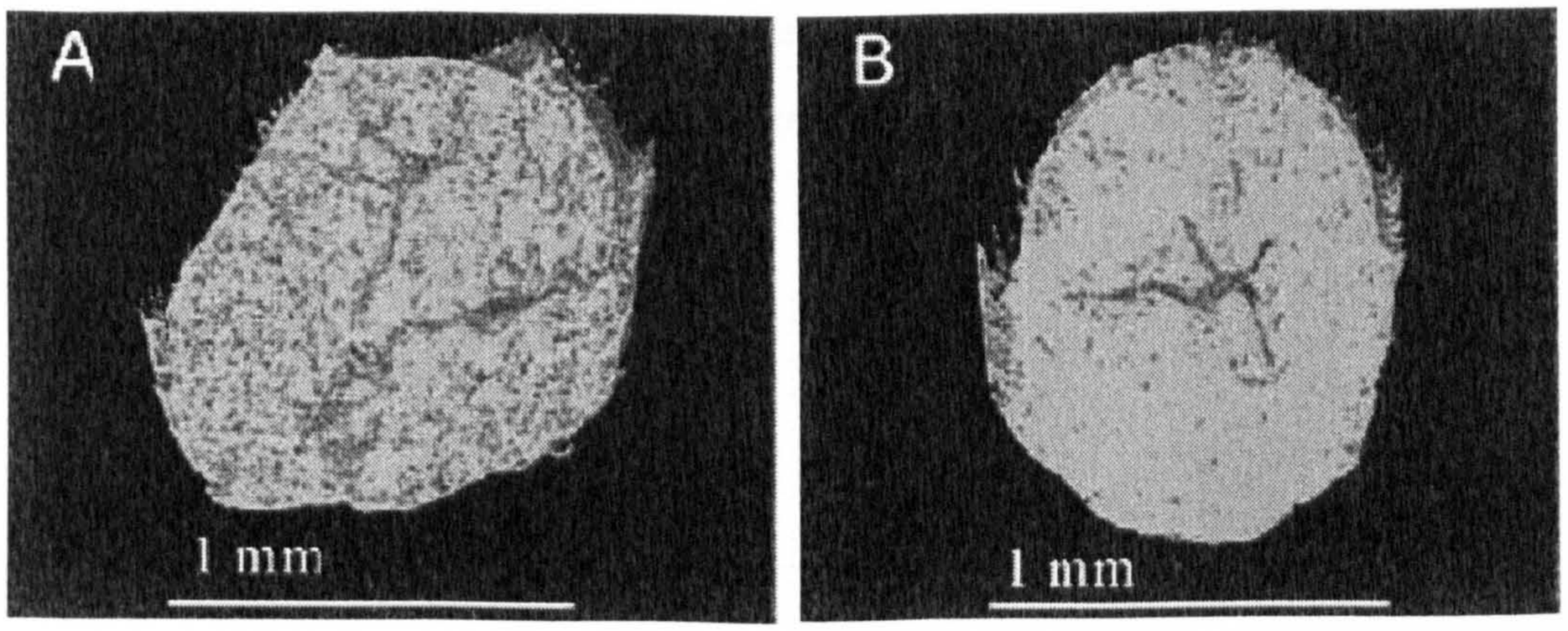

Figure 2.19. Reconstructed cross-section images from XRT analysis of granules at two different granulation times: (a) 180 seconds, (b) 900 seconds (source [25]).

XRT has been applied on a systems of larger scale than single granules such as to measure density variations in tablets ([52]) and on an even bigger scale to characterize powder mixing ([53]).

As it can be seen, not much work has been done using XRT to resolve the structure of single granules. However, the application of this technique to the powder technology area offers great potential to gain physical insight on the single granule scale, which would offer a great deal of information about how the agglomeration process works.

With the increasing availability of high-quality x-ray sources (synchrotron radiation) and the development of the physical instruments that compose an XRT scanner (detectors, specimen holders, x-ray sources and computing power) this non-destructive technique has the potential to become an extremely useful tool in power technology, allowing the resolution of each individual phase within single agglomerates.

The linear attenuation coefficient of the materials plays a key role in being able to identify different phases within an agglomerate using X-ray tomography. The bigger the difference in the linear attenuation coefficient, the better the contrast that can be obtained between the different phases. The linear attenuation coefficient for the different materials depends on the voltage applied to the x-ray source; hence the XRT scan can be tuned in order to obtain the best results. Figure 2.20 illustrates the different linear attenuation coefficients as a function of voltage for some materials commonly used in granulation.

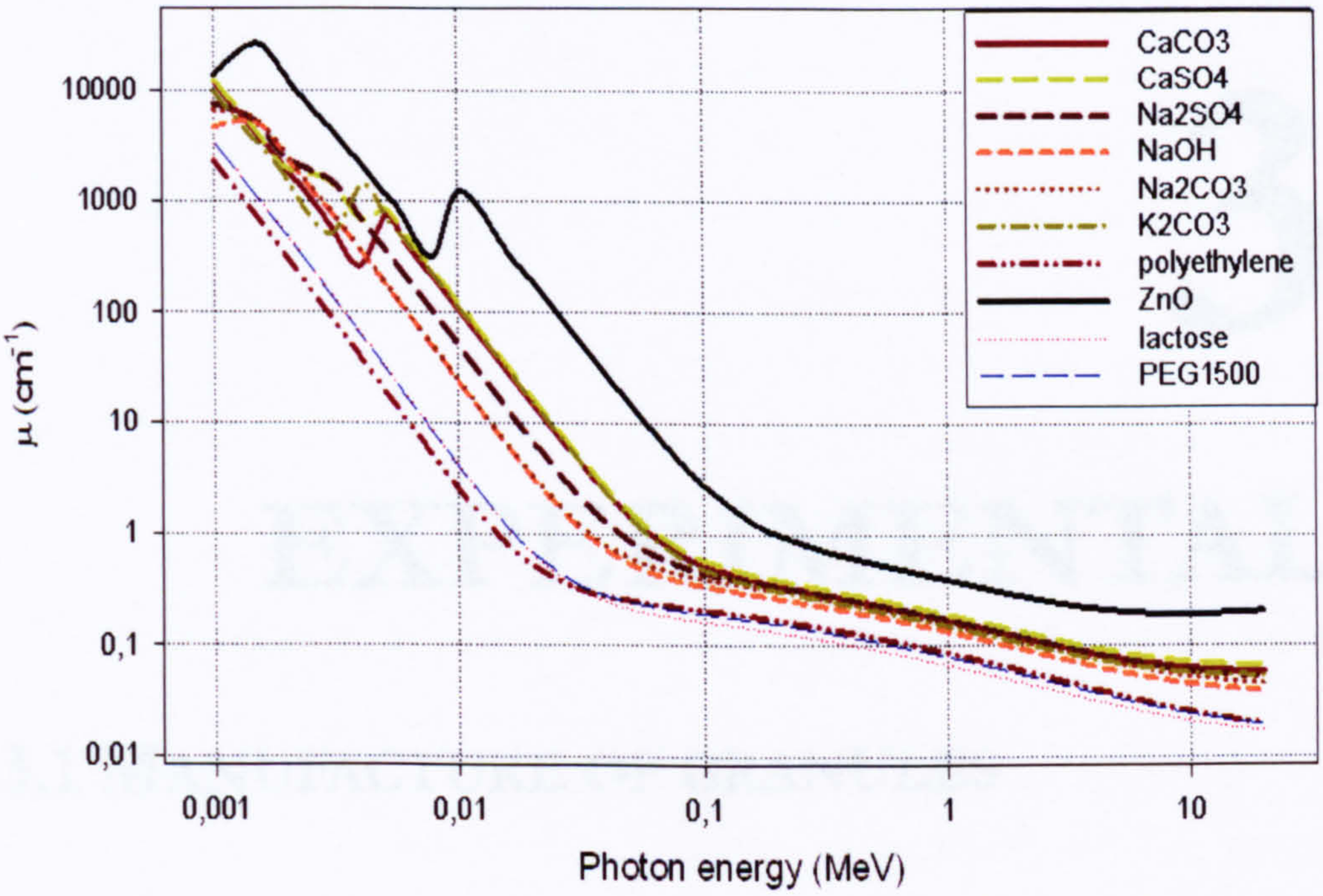

Figure 2.20. Linear attenuation coefficient for some common materials in granulation.

2.3.3 Introduction of the current work

This thesis will apply X-ray tomography in order to identify how different formulation/process parameters affect the structure of agglomerates. As part of this work a new methodology to extract information from XRT analysis on agglomerates (in the form of radial greyscale profiles) will be developed.

3

EXPERIMENTAL

3.1 MANUFACTURE OF GRANULES

3.1.1 Materials used

Unless otherwise stated granules were produced from Durcal (an industrial form of comminuted calcium carbonate, $CaCO_3$) as primary particles and polyethylene glycol flakes (PEG) as a binder.

Polyethylene glycols are polymers with the general formula $H(OCH_2CH_2)_nOH$ where n indicates the degree of polymerisation. They can be found with different molecular weights, giving them different characteristics such as melting points or viscosity.

Different types of PEGs are characterized by a number indicating their molecular weight, for example PEG1500 has an average molecular weight of 1500 Daltons (in general: PEG-N has an average molecular weight of N Daltons). Different types of PEG will have different properties and appearance. For example PEG200, 300, 400 and 600 are clear viscous liquids; PEG1000 is semi-solid at room temperature and higher molecular weight PEGs are solid at ambient temperature. They melt at temperatures ranging from 40°C to 60°C. PEGs are water soluble with the solubility being higher the lower the molecular weight [8]. The grading of PEG used in the experiments is PEG1500 (when other grades of PEG are used it will be specified) in the form of flakes (see

Figure 3.1). The size distribution of the PEG1500 flakes was obtained by image analysis using a Camsizer; an example is given in Figure 3.2. Calculating this size distribution is not trivial. Camsizer calculates the sizes from analysis of the projected areas of the sample analyzed. This is not very accurate in this case due to the flake-shaped nature of the PEG1500. However sieving would also be inaccurate due to the same reason. A better method to size this type of material was not found, so the results obtained with the Camsizer are here presented.

PEG1500 has an average molecular weight of 1500 Daltons and a melting point of approximately 45°C. Viscosities of different grade PEGs can be seen in Figure 3.3.

Durcal also has different gradings; referring to its particle size, for example Durcal 40 (D40) has an x_{50} size of approximately 23 μm (volume basis). Other grades of Durcal are defined in Table 3.1 (from [54]). The true density of this material is 2730 kg/m^3 ([54]).

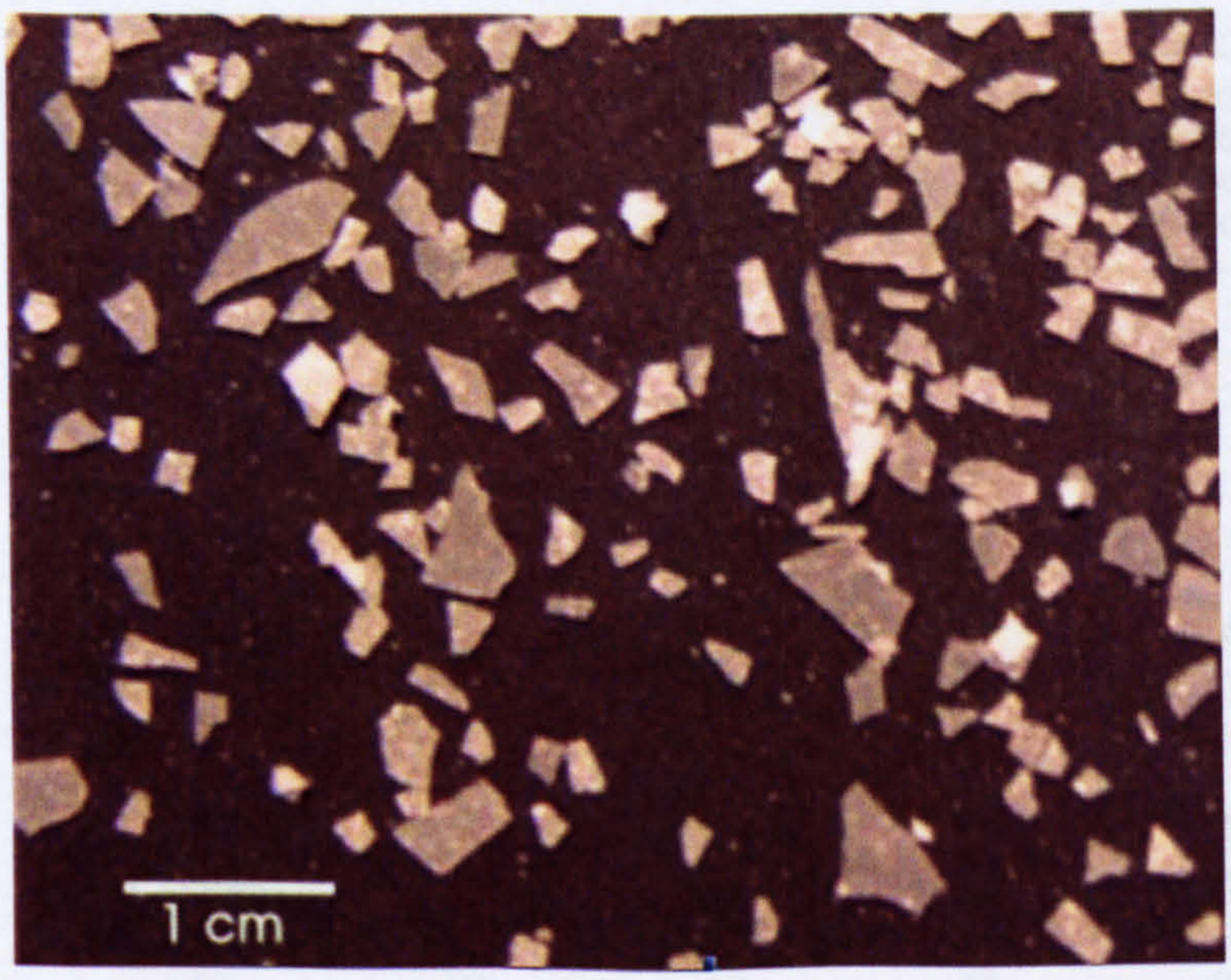

Figure 3.1. Appearance of PEG1500 flakes.

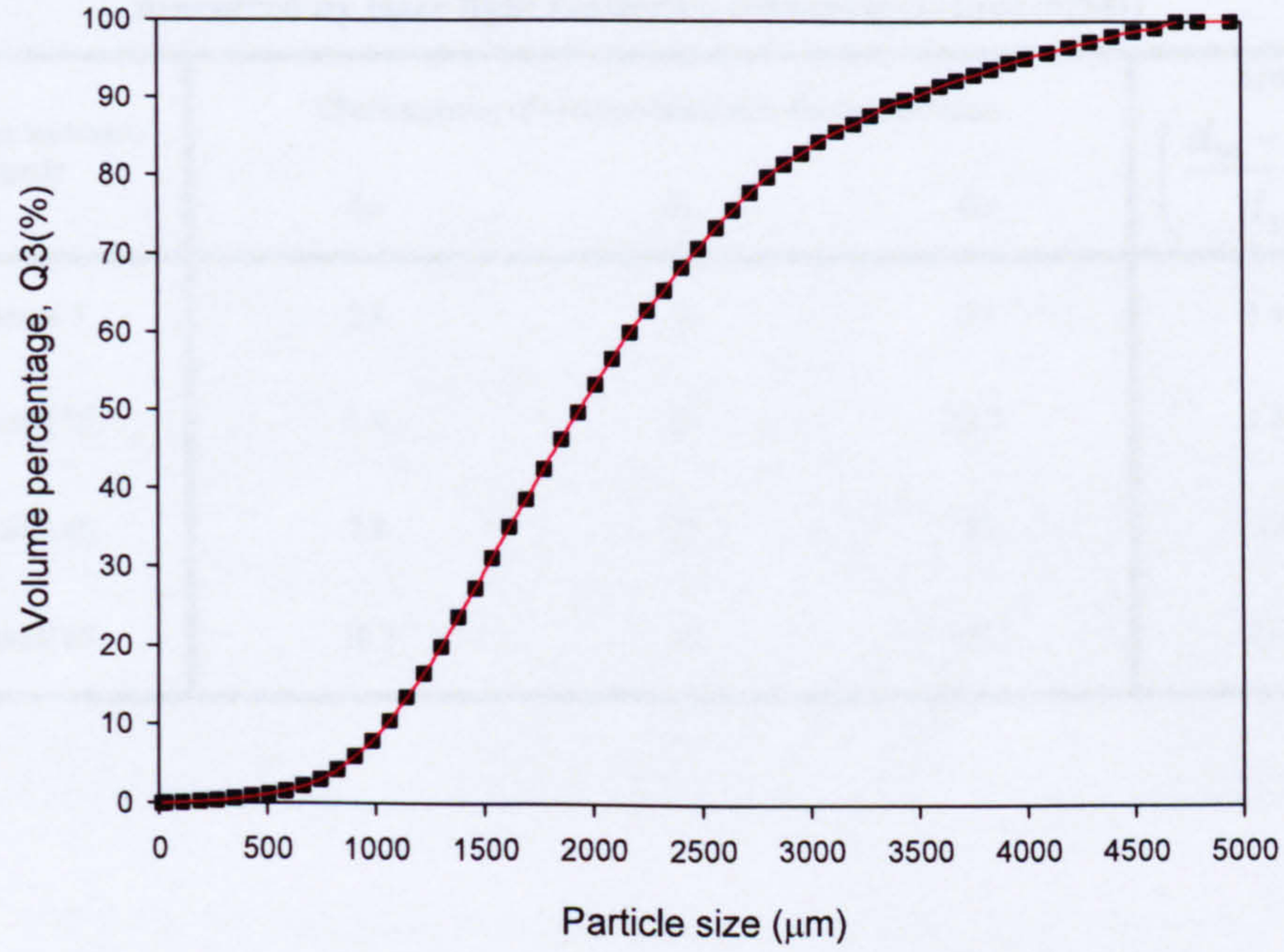

Figure 3.2. Size distribution from image analysis of the PEG1500 flakes used as binder. Obtained using a Camsizer®.

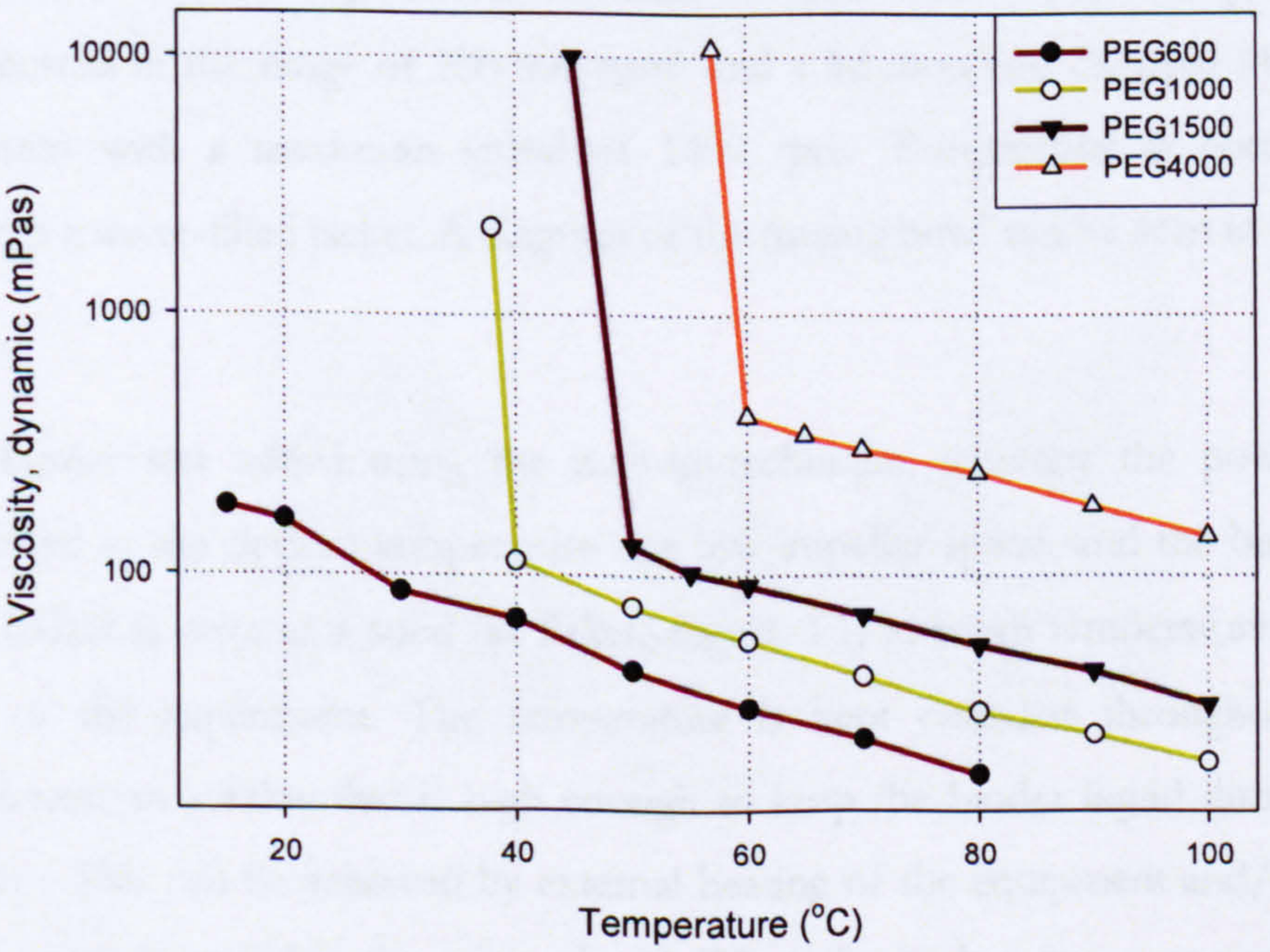

Figure 3.3. Viscosities of different grades of PEG at different temperatures.

Table 3.1. Characteristic size distribution of the calcium carbonate (Durcal) grades as measured by laser light scattering (Sympatec) (source[54])

Calcium carbonate grade	Characteristics of volume-based size distribution (μm)			Span $\left(\frac{d_{90}-d_{10}}{d_{50}}\right)$
	d_{10}	d_{50}	d_{90}	
Durcal 5	2.8	6	23	3.36
Durcal 15	5.9	15	52.7	3.25
Durcal 40	7.8	23	86	3.4
Durcal 65	10.2	35	103.3	2.66

3.1.2 Granulation experiments – Melt agglomeration

The granules used in the experiments were manufactured in a Zanchetta Roto Junior laboratory scale mixer supplied by Romaco, Italy (Figure 3.4), with a capacity of 10 litres and a bowl diameter of 30 cm. The unit contains a vertically mounted three-blade impeller with a maximum speed of 800 rpm (the speed can be adjusted in the range of 100-800 rpm) and a lid-mounted chopper (45 mm diameter) with a maximum speed of 1400 rpm. Temperature is controlled through a water-filled jacket. A diagram of the mixing bowl can be seen in Figure 3.5.

The binder was added using the melt-in technique, whereby the powder is preheated to the desired temperature at a low impeller speed, and the binder is then added at once as a solid (as flakes, Figure 3.1) at room temperature at the start of the experiment. The temperature is kept constant throughout the experiment to a value that is high enough to keep the binder liquid during the process. This can be achieved by external heating of the equipment and/or due to frictional heat within the mixing bowl. When the agglomerates are cooled to ambient temperature they form dry agglomerates due to solidification of the binder.

The impeller speed and a chopper speed are selected and kept constant throughout the experiment.

Figure 3.4. Zanchetta Roto Junior laboratory scale mixer used in the experiments: (a) overall view; (b) top view of the mixing bowl with the three-bladed impeller.

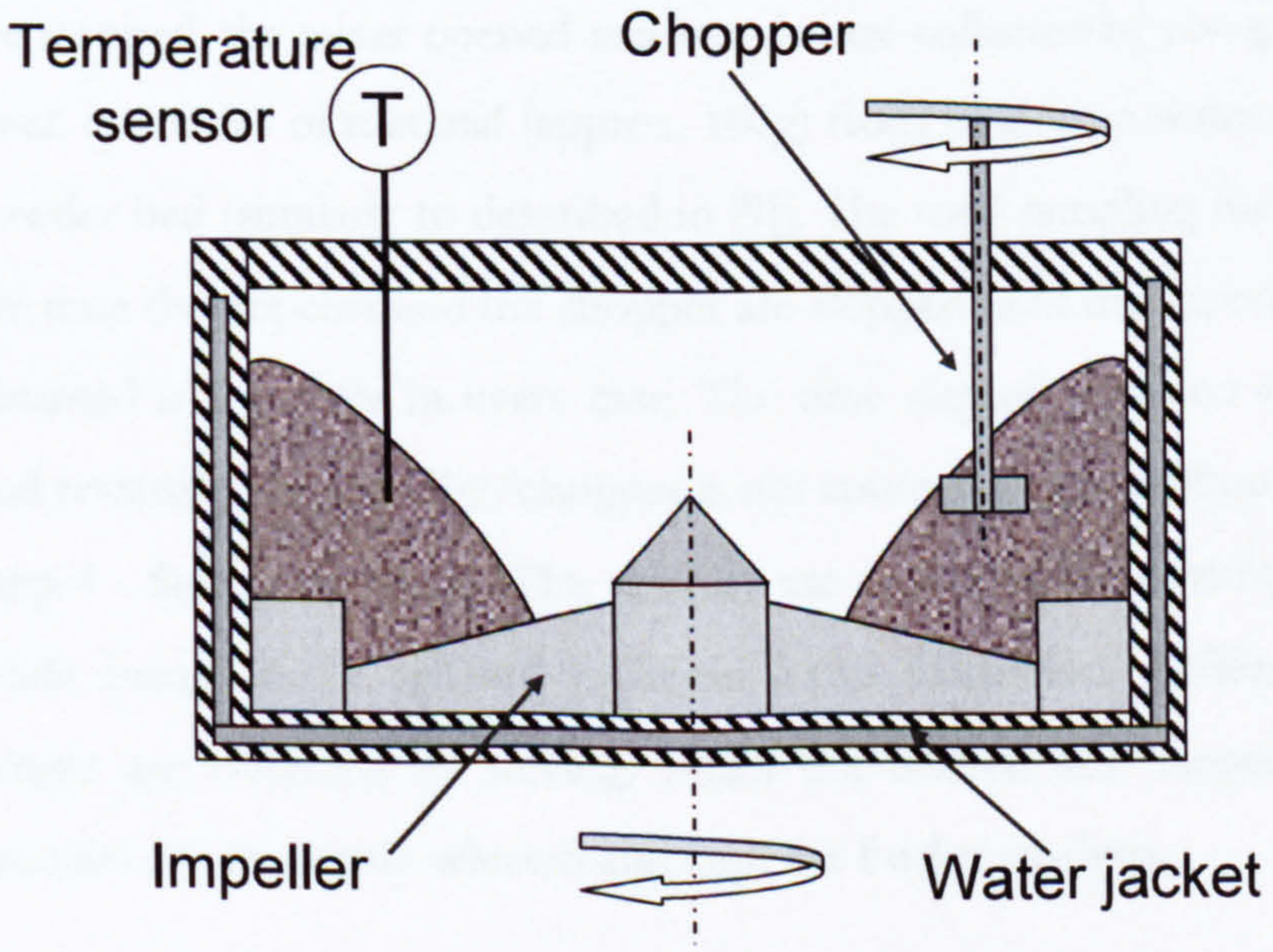

Figure 3.5. Schematic representation of the mixing bowl in a high-shear granulator, showing the water jacket used to control the temperature, the temperature sensor and both the impeller and the chopper.

This melt-in experimental approach is used as a model for wet granulation, in which the binder is a liquid during the process. Samples are taken by stopping the mixer and sampling material from different locations in the bed. The samples require gentle agitation during cooling to avoid the granules agglomerating into large 'lumps'. Different size fractions are obtained by sieving the cooled samples. Single granules are then randomly selected from within the size fractions of interest. A description of the standard experimental procedure is found below:

- Step 1 - Addition and pre-warming of the dry powder: 2 kg of dry powder (Durcal) are added to the Roto Junior mixer. The impeller speed is set to a low value (100 rpm) and the powder is preheated to the operation temperature.
- Step 2 - Addition of the binder: For a binder-to-solid ratio (L/S) of 0.13, 260 g of binder flakes are added to the mixer with the impeller switched off. The amount of binder is changed if different L/S values are required. After addition the mixer is closed and the mixing process started. This is taken as time zero in the experiment.
- Step 3 - Sampling: At a specific granulation time the impeller/chopper are stopped, the mixer opened and samples are collected by scooping out small quantities of material (approx. 100g) from random positions in the powder bed (similarly to described in [9]). The total sampling time, from the time the impeller and the chopper are stopped until the experiment is resumed is 1 minute in every case. The time elapsed between stopping and restarting the impeller/chopper is not counted as granulation time.
- Step 4 - Sample handling. The samples are cooled to room temperature while being gently agitated to avoid lump formation. Different size ranges are obtained by sieving. From the desired size ranges, single granules are randomly selected and kept for further analysis.

Melt agglomeration offers a series of benefits when compared to other agglomeration methods. It avoids the drying phase of the product and also the liquid addition phase as the binder is added as a solid. This makes it advantageous when dealing with, for example, toxic solvents. On the other hand

a main disadvantage of the method is that it is not suitable when dealing with heat sensitive materials due to the high temperatures required during the process[8].

3.1.3 Why single granules

The experimental approach thus extracts individual granules from a whole batch (Figure 3.6). The purpose of this analysis at a single granule scale is to understand the micro-scale properties of the agglomerates so that then can be applied in the description of the macro-scale properties of the final product (such as dissolution or strength). Also, the physical insight that X-ray tomography provides at such small scale could be applied to the modelling of the relationships observed, as distributions of primary particles and binder within a granule (and not only the amount of each phase) could potentially be considered when trying to develop models that describe granulation ([19]).

By looking at single granule structure it is expected to gain a better understanding of the mechanisms that take place during the granulation process determining the internal granule structure, which will then determine the way the agglomerates behave. Optical images of single granules (obtained with a stereo microscope Discovery V12 from Zeiss) were also used to complement the structural information obtained via X-ray tomography.

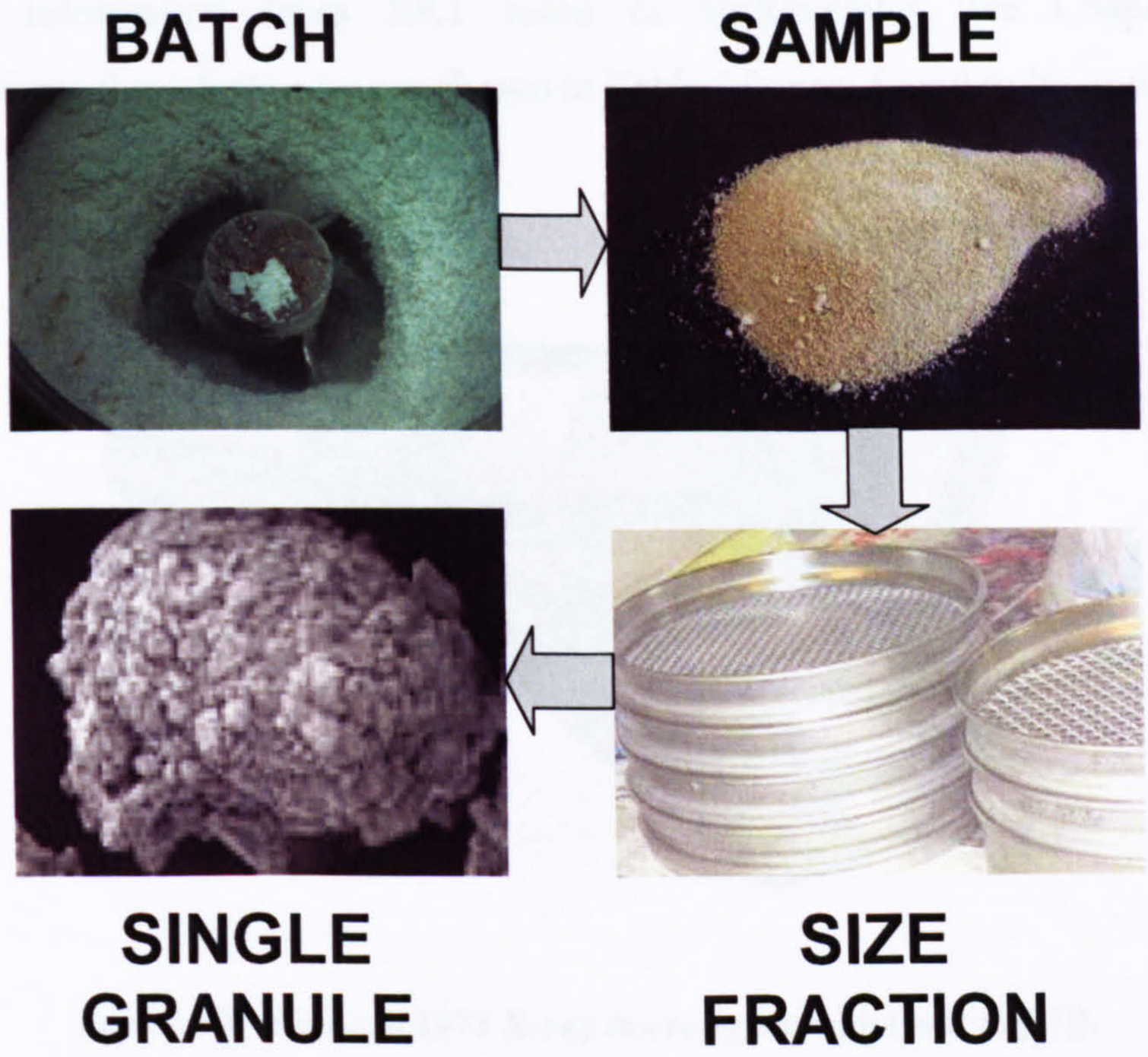

Figure 3.6. Experimental approach: a random sample is taken from a whole batch, the desired size fractions are separated by sieving and finally single granules are randomly picked from the size ranges of choice.

3.2 X-RAY TOMOGRAPHY OF SAMPLES

Single granules are selected and scanned using a commercial desktop XRT system (SkyScan 1072 X-ray Microtomograph, Figure 3.7).

XRT uses a set of two-dimensional shadow X-ray images of an object to reconstruct its three dimensional structure using a mathematical algorithm. In these experiments approximately 200 images are used. The number can be increased by reducing the increment angle or increasing the scan rotation angle, but this would require longer scanning and reconstruction times. Different settings (values for frame averaging, scan rotation and increment angle) were tested on agglomerates in order to see their effect on the method developed to

extract information from XRT scans of agglomerates (see Chapter 5). Considering these facts, settings shown in Table 3.2 were found to be optimum.

Figure 3.7. SkyScan 1072 X-ray microtomograph (source [37]).

Table 3.2. Experimental settings for the SkyScan 1072 Microtomograph.

Magnification	90 ×
Pixel size (μm/pixel)	3.26
Scan Rotation Angle (°)	180
Increment Angle (°)	0.9
Frame Averaging	On (2)

An example of a shadow X-ray image and three cross-sections at different cutting planes of the granule can be seen in Figure 3.8.

For all the scans the magnification was chosen so that the sample always stayed within the field of view of the detector. By doing so there are always some x-rays that do not go through the object at all, only through air, and can be used as a basis for further calibrations. The reconstructed results are calculated as an array of float point pixels due to the unknown density range in the investigated object.

This array of radiation intensities needs to be transformed to an image. Two peaks usually appear in the histogram of intensities recorded. One corresponds to the attenuation of air and the other one to the material under study. SkyScan software transforms any intensity range into a 256 greyscale image. As a result, in the cross-sections obtained white will correspond to air, and different shades or grey will reflect areas of different densities inside the object. The transformation is linear so that greyscale value is proportional to x-ray attenuation.

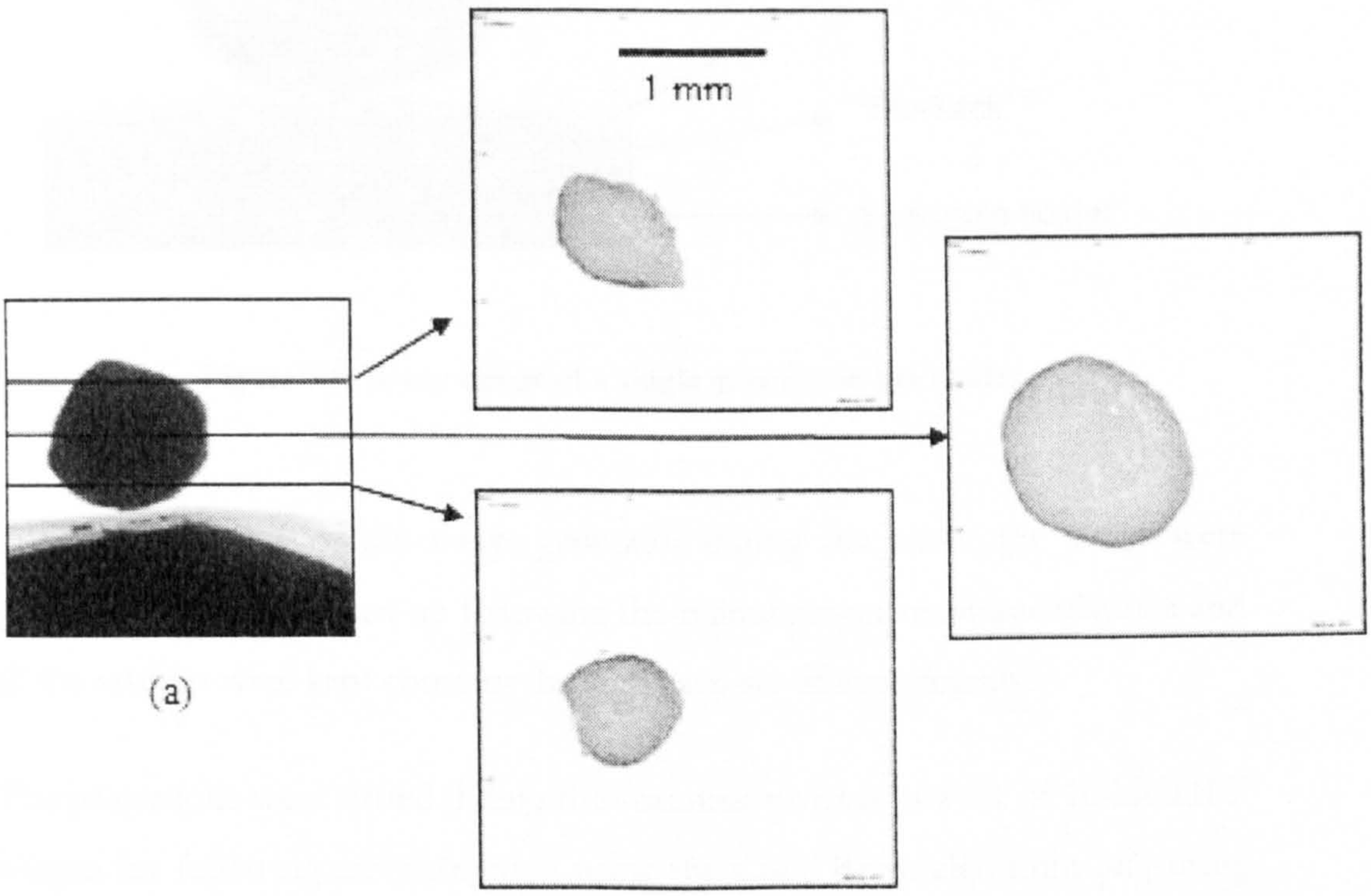

Figure 3.8. Shadow image (a) of a single granule with three reconstructed slices through it at different cutting planes. The light areas correspond to materials that attenuate x-rays less (white corresponding to the background air), the darker areas correspond to more attenuating materials.

For each of the experiments an individual granule was placed on the specimen holder, using "Blu-Tack"® (adhesive paste) and/or adhesive tape to fix the granule to the holder (Figure 3.9). The "Blu-Tack"® acts as support for the adhesive tape that would have the sticky surface in contact with the granule. The smallest of the specimen holders provided (4 mm diameter) was used as it allows maximum magnification. Once the sample was in the scanning chamber, the holder was adjusted in terms of height and distance to the x-ray source to

achieve the optimum imaging conditions using a micromanipulator controlled using the provided scanning software.

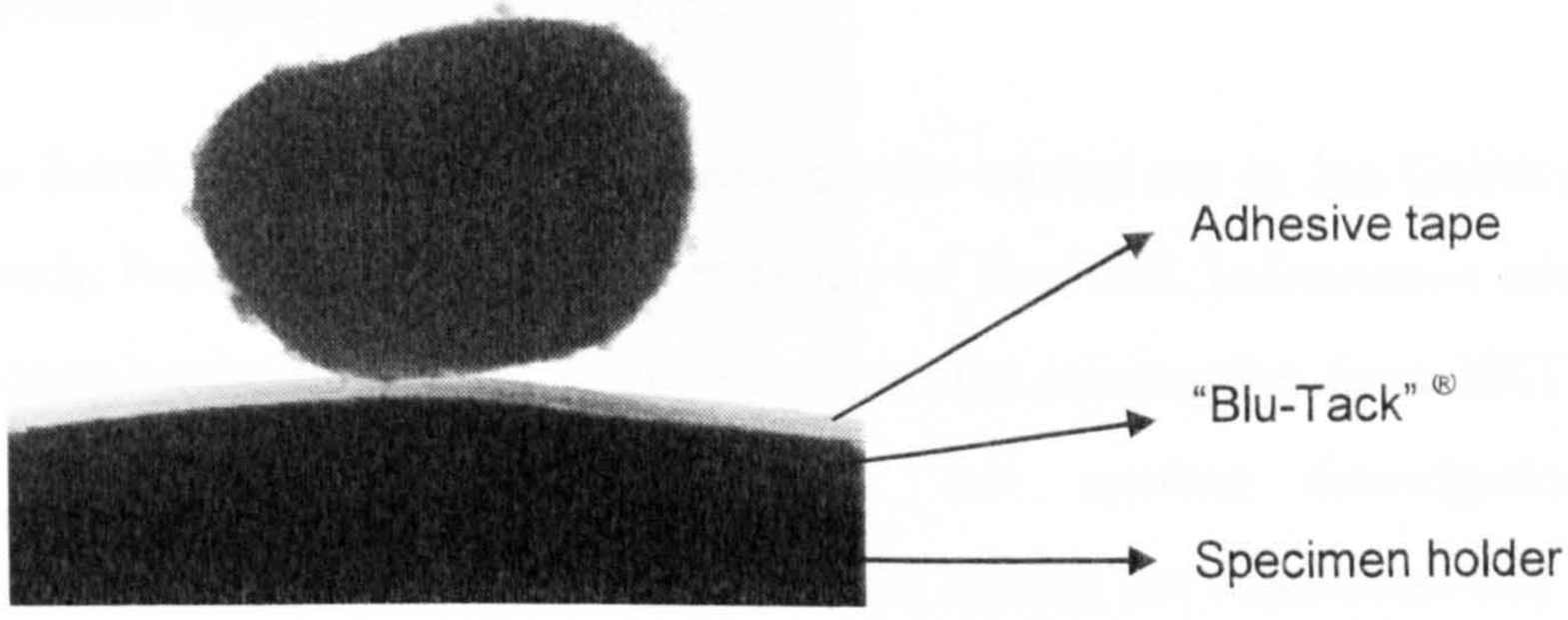

Figure 3.9. X-ray image of a single granule on the holder.

To ensure stability of the x-rays generator during the scans, the x-rays were "aged" at the system start-up following the manufacturer recommendations and all the settings were kept constant through each set of experiments.

The projections were stored during the scanning process as a set of 16-bit TIFF images for following reconstruction using the Cone Beam algorithm [46] using the software provided by the manufacturer.

3.3 STRENGTH AND DISSOLUTION

For some of the samples, measurements of granule strength and dissolution rates were carried out in order to try and interpret these properties of the product by looking at the physical insight of the granules that X-ray microtomography allows.

Dissolution and strength are key properties of granulated materials. For example strength plays a very important role in terms of transport, handling and storage of the granulated material, and dissolution is a key parameter when it comes to drug delivery, detergents or the food industry. It is also known that there is a trade-off between these properties, with strong granules usually having long dissolution times, and vice versa [55].

The dissolution/strength measurements were carried out by Ian Gabbott, at the Particle Products Group at the University of Sheffield. Information was shared to complement his investigations with structural information from XRT analysis of single granules and to enrich this current investigation with dissolution/strength data. The methods for testing the dissolution and strength are summarized below.

3.3.1 Granule strength measurement [55]

Compression tests have widely been used to characterize granule properties. In this situation, the granules were compressed diametrically using a universal mechanical tester (Zwick/Roell). This method is the most widely reported for granule strength measurement. The sample granules are compressed between two smooth stainless steel platens. The upper platen was driven at a constant speed of 1 mm/min while the bottom platen remains stationary. The load displacement behaviour is recorded by a PC. The load cell and displacement measurements are accurate to 0.001 N and 0.23 μm respectively.

For each case the value given as failure load is the average of 20 single granule compression tests.

3.3.2 Granule dissolution [55]

The dissolution rate of the granules is measured by calculating the time taken for 90% of one gram of granules of the size of interest to dissolve. The extent of dissolution is determined by measuring the change in conductivity of 600 ml of distilled water. The test is carried out at a constant temperature of 20°C and with a magnetic stirrer set at 600 rpm.

3.4 PROCESS/FORMULATION PARAMETERS

Wet granulation in a high-shear mixer is caused by the interaction of several variables that can affect the quality of a product obtained. Those factors can be split in two different groups:

- Process variables: related to the equipment that is used to carry out the agglomeration and the way it is used. For example impeller speed, presence or not of a chopper and its speed, granulator load, temperature or binder addition method.
- Formulation variables: related to the materials used for the agglomeration. For example, type of primary particles, type of binder, size distribution of primary particles or ratio of binder to primary particles.

Many studies try to relate these variables to the qualities exhibited by the product, ranging from its shape [56], breakage characteristics [57] or size distribution and porosity [13]. The aim of all these studies is to improve the understanding of the granulation process in order to be able to control the product quality.

Unfortunately even though the structure of the granules determines the way they behave, relationships between process/formulation parameters and properties

have been studied (as explained above) with a lack of understanding on how these process/formulation parameters affect the structure of those granules.

By using x-ray tomography the aim of this research is to understand the product properties by looking at the internal structure of the granules, and at the process/formulation parameters that generated it.

Different single granules, obtained from batches manufactured under different granulation conditions, covering a broad range of process/formulation parameters have been scanned using X-ray microtomography in order to highlight their very different structures.

A series of varied structures obtained in very different granulation conditions (ranging from fluidised bed granulation to high-shear granulation) will be presented in the next chapter. Also a more detailed study on some process and formulation parameters in high-shear mixers will be reviewed in this work.

4

RESULTS: QUALITATIVE ANALYSIS

4.1 Different granule structures

The structure of agglomerates is affected by both process and formulation parameters. For the tomographic scanning of the samples, the granule composition plays a very important role. This is because different materials interact differently with the x- ray radiation, i.e. certain combinations of binder/primary particles will show their structure better than others using XRT.

A series of samples manufactured from different materials and under different granulation conditions were scanned in order to gain a physical insight of different internal structures for single granules. Even though x-ray tomography produces a stack of adjacent images of cross-sections through the sample only the central cross-sections will be shown here as it is the most representative.

The total number of images per scan depends on the size of the granule and the resolution at which the scan is carried out, for example a 1.5 mm granule on the z-axis scanned at a resolution of 5 μm/pixel will generate 300 cross-sectional

images. A complete stack of images belonging to a single granule are included in Appendix B as an example.

The images of the cross-sections of samples were obtained using the software provided with the scanner Data Viewer for MicroCT ver. 1.0, SkyScan, Belgium © 2004.

4.1.1 High-shear granulation / Fluidized-bed granulation

A good example of how process parameters affect the structure of agglomerates is the difference between high-shear and fluidised bed granules. The mechanisms underlying both types of granulation are fundamentally dissimilar hence creating very different structures that will result in different product properties. Figure 4.1 and Figure 4.2 show the typical structures of granules made under high-shear conditions and in fluidized beds. High shear granulation agglomerates are typically compact and rounded whereas fluidized bed granules tend to be a much more opened structure. High shear granules are characterised by high density and low porosity values, whereas fluidised bed granules are of lower density and higher porosity. For example, for the same starting materials and amounts, high shear granules have been reported to have a bulk density of around 2.5 times the bulk density of fluidised bed granules [58].

Figure 4.1 shows three cross sectional images of a typical granule made in a high-shear mixer. The granule was made using calcium carbonate as primary powder and polyethylene glycol (PEG1500) as binder, following the melt-in technique. Figure 4.2 shows three cross sections of a typical fluidized bed granule made using glass ballotini as primary particles bound by spraying polyethylene glycol in a fluidized bed. It can be appreciated that the structure is much more porous compared with that shown by the high shear granule.

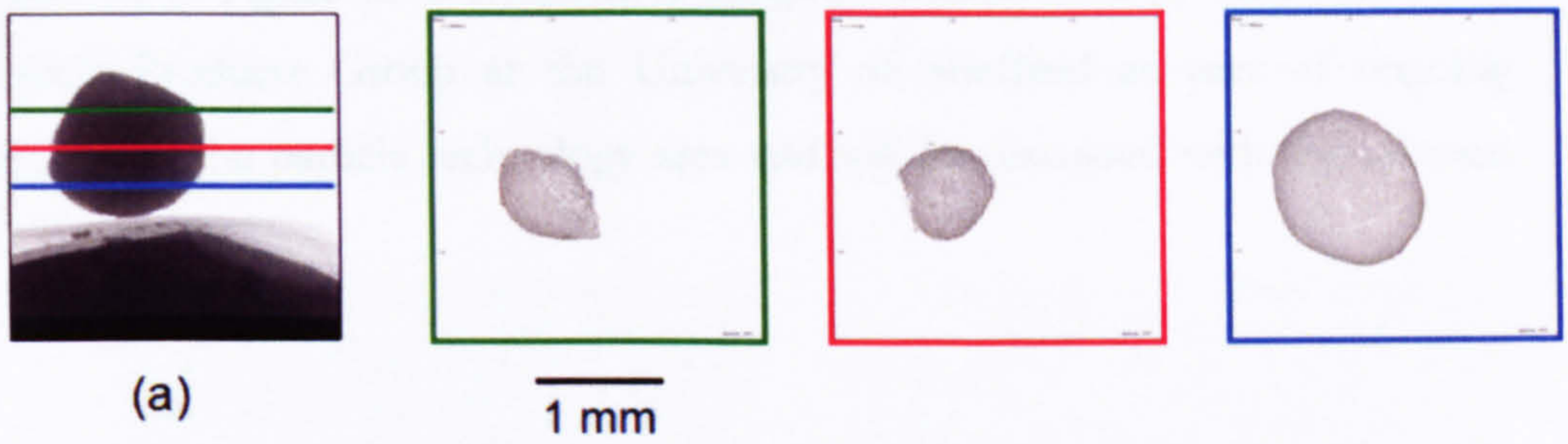

Figure 4.1. Example of three cross sections through a typical high-shear granule made of $CaCO_3$ and polyethylene glycol (PEG). An x-ray shadow image of the corresponding granule is shown in (a).

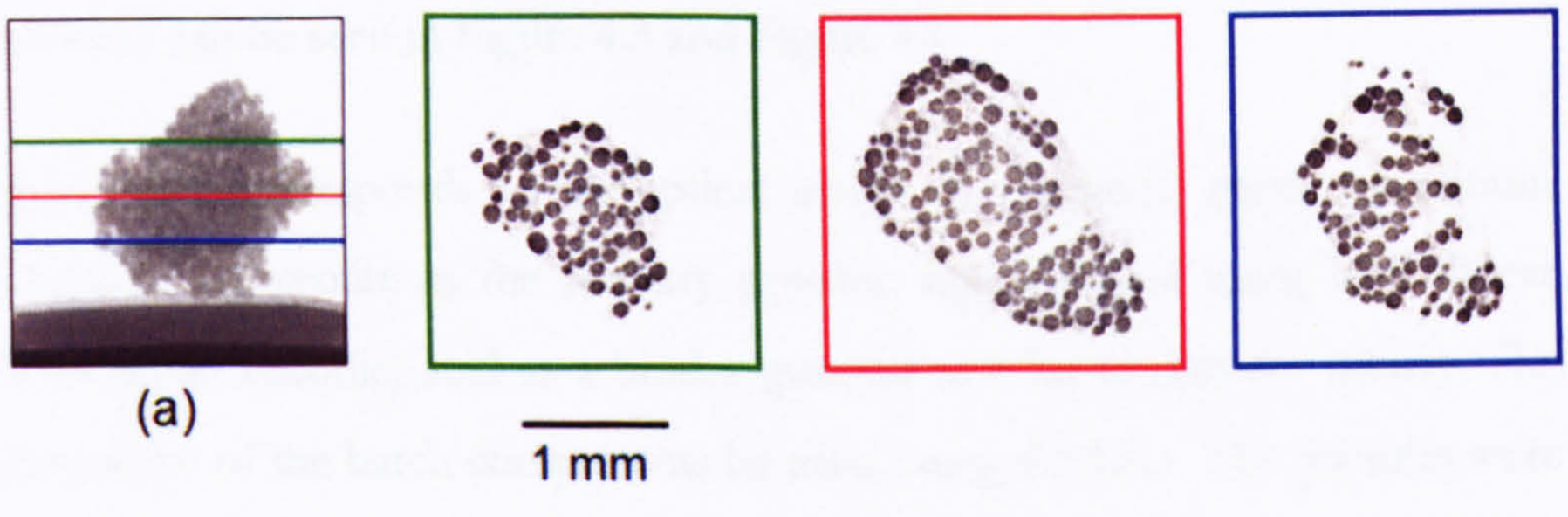

Figure 4.2. Example of three cross sections through a typical fluidised-bed granule made of glass ballotini and PEG. The corresponding x-ray shadow image is shown in (a).

4.1.2 Other granulation conditions and materials

High shear and fluidised bed granulation illustrate two extreme cases of possible structures. In order to visualize the structures from a wide variety of other granulation conditions and materials, particles obtained from different granulation systems studied by the Particle Products Group at the University of Sheffield were scanned. Optical images of the samples obtained with a microscope (stereo microscope Discovery V12, from Zeiss) are also included here so that external appearance and the internal structure, as revealed by x-ray tomography, can be compared.

Figure 4.3 to Figure 4.8 correspond to samples manufactured by members of the Particle Products Group at the University of Sheffield as part of ongoing research in the particle technology area and will be discussed with the relevant XRT scan.

High shear granulation plus fluidised bed granulation

This first example shows a combination of high-shear and fluidized bed granulation. Granules are manufactured in a high-shear mixer and then fed into a fluidized bed where more binder is added for further granulation. The resulting structures can be seen in Figure 4.3 and Figure 4.4.

Figure 4.3-a corresponds to an optical image of a granule made of calcium carbonate and zeolite as the primary powder, agglomerated using LAS (linear alkylbenzene sulfonic) acid as a binder (poured as a liquid into the mixer). The proportions of the batch components by mass being 4.5:1.6:1. The granules were manufactured in a modified food mixer, as a model for a small scale high-shear granulator, and taken after 2.5 minutes of granulation time. These granules were then added as solid feed to a fluidised bed as "seed" granules and granulated for a further 5 minutes by spraying extra LAS.

Figure 4.3-b corresponds to an optical image of a granule taken after the fluidisation process.

Figure 4.3-c and d are the corresponding x-ray tomography central cross sections of the granules shown in Figure 4.3-a and b respectively.

The XRT images show that the fluidized bed granules are composed of "seeds" stuck together by the extra added binder. The internal structures of the "seed" granules that make up the fluidized bed agglomerate still show a remarkable likeness to the internal structure of the high shear granules they came from.

The external appearance of the high shear agglomerate presents a much smoother surface when compared to the fluidized bed granule, in which the "seeds" that make up the granules are clearly visible.

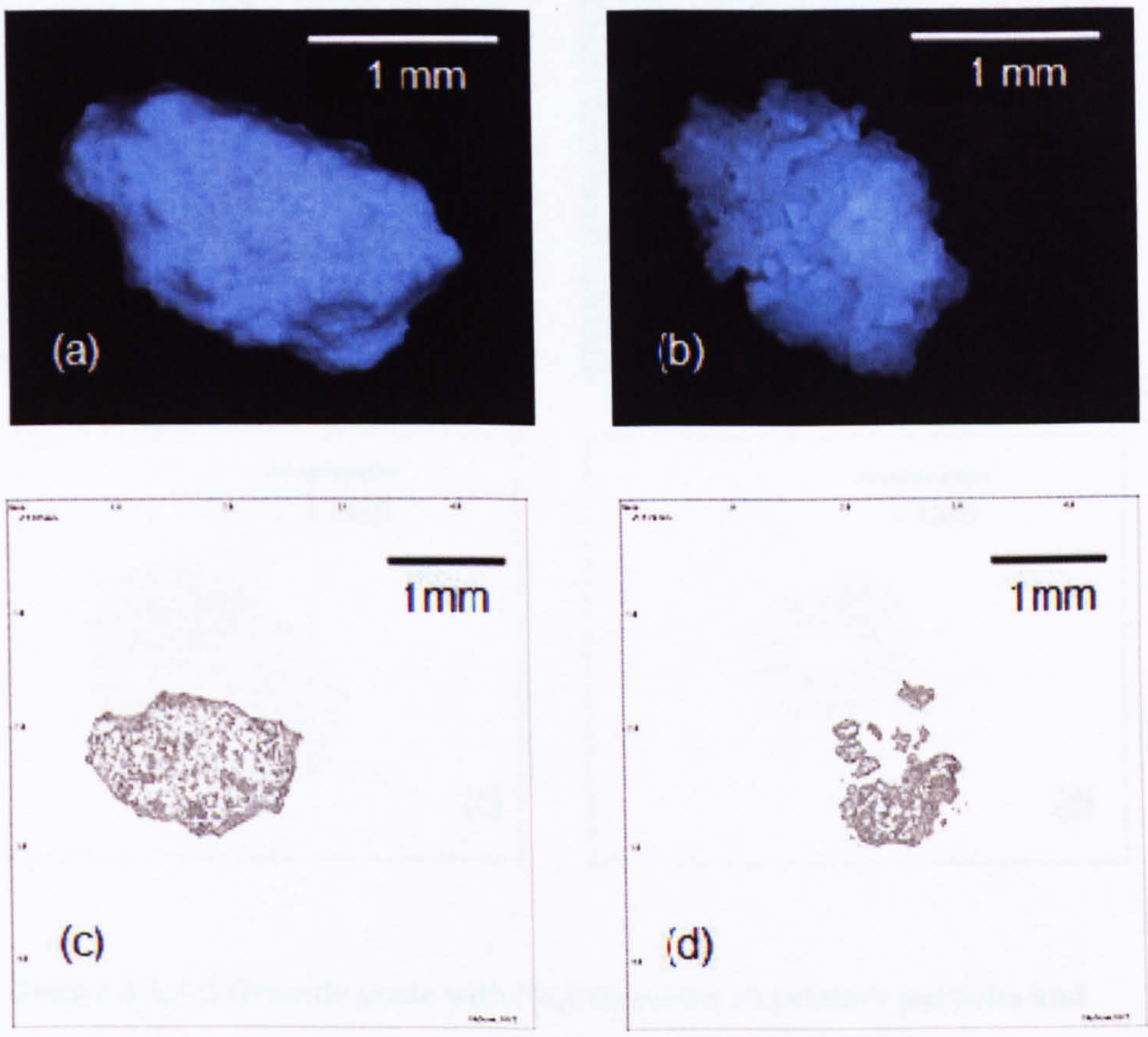

Figure 4.3 (a) Granule made of $CaCO_3$/zeolite as primary particles and LAS acid as a binder (63:23:14) in a food mixer after 2.5 minutes of mixing time; (b) fluidized bed granule using granules manufactured as (a) as seeds and agglomerated by spraying LAS acid for a period of 5 minutes; (c) and (d) corresponding x-ray tomography cross sections.

Figure 4.4 illustrates a similar example but in this case the high shear granules are manufactured with sodium carbonate and zeolite as primary particles and LAS acid as a binder (1.73:2:1). After 5 minutes of granulation time they where added to a fluidized bed and further agglomerated by spraying extra LAS acid for an extra 5 minutes. Optical images are shown in Figure 4.4-a and b and corresponding x-ray tomography central cross sections in Figure 4.4-c and d.

The "seed" granules that make up the fluidised granules can be seen both optically (on the surface of the granule) and in the x-ray cross sections.

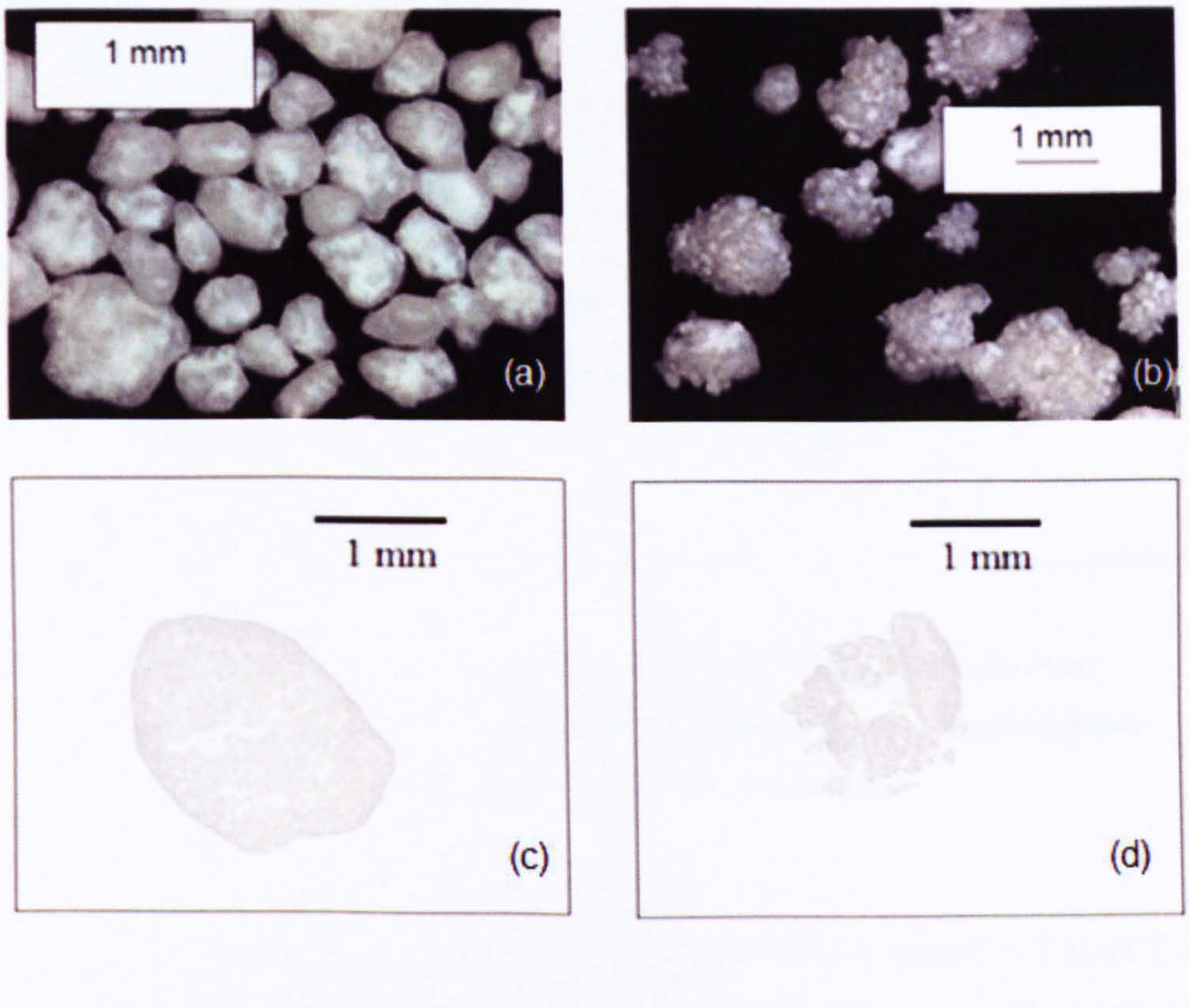

Figure 4.4. (a) Granule made with Na_2CO_3/zeolite as primary particles and LAS acid as a binder (1.73:2:1) in a high-shear mixer after 5 minutes of granulation time; (b) fluidised bed granules using granules manufactured as (a) as seeds agglomerated by spraying LAS acid for a further 5 minutes; (c) and (d) corresponding x-ray tomography cross sections.

"Cored" high-shear granule

Figure 4.5-a illustrates a melt-in high-shear mixer granule taken early on the granulation process (2 minutes). Calcium carbonate was used as primary particles (Durcal 40) and PEG1500 as binder. The binder was added as a solid flake to the mixer following the melt-in procedure. The shear was kept to a low level with an impeller speed of 300 rpm and the sample was taken after only 2 minutes of

granulation time. X-ray tomography allows the visualization of a PEG1500 core inside the granule.

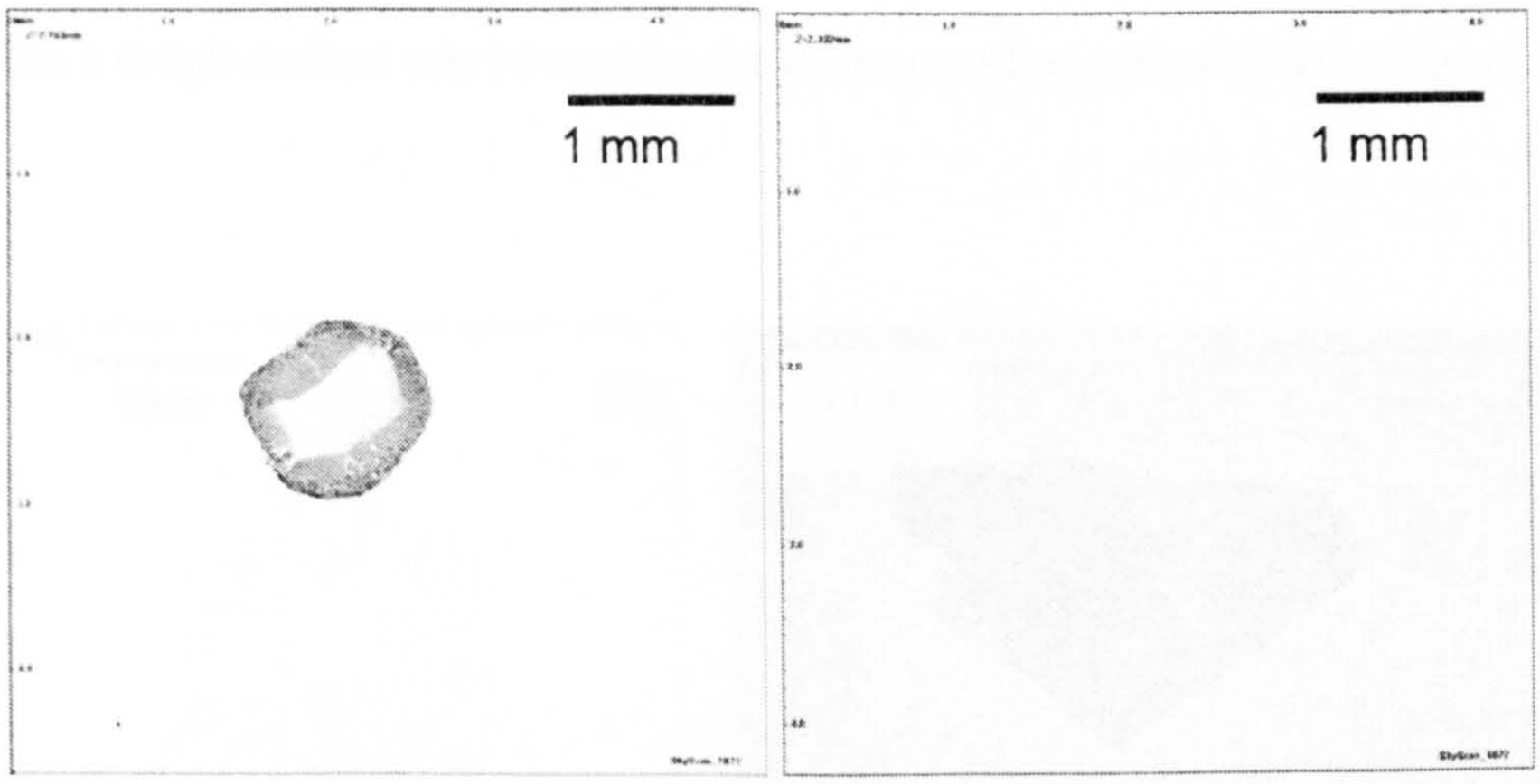

Figure 4.5. (a) Central cross section of a $CaCO_3$/PEG1500 high-shear granule showing a binder core; (b) PEG1500 flake similar to those added as solid binder in the melt-in experiments.

An x-ray tomography cross section of a PEG1500 flake is shown in Figure 4.5-b. Comparing both images it can be seen that the PEG1500 core in the high shear granule still keeps a flake-like shape due the combination of low shear and low granulation time. It is indicated that one of the effects of prolonged granulation time and higher shear is squeezing the melting core towards the outside of the granule as the primary powder particles push in towards the centre of the granule due to the shear forces present in the mixer.

"Binderless" granule

Figure 4.6 illustrates the case of "binderless" granules, manufactured in a high-shear mixer using polystyrene particles as primary particles (mean diameter approximately 0.5 μm). Water was used as a binder in the high-shear mixer to agglomerate the polystyrene particles, but the granules were then dried to evaporate the water and create a "binderless" granule. The detailed procedure on

how the granules are manufacture can be found in [59]. In the x-ray tomography cross-section of the granule (Figure 4.6-a) internal porosity can be seen within the granule. The external appearance of the granule, round in shape and with quite a rough surface can be seen in the corresponding optical image (Figure 4.6-b).

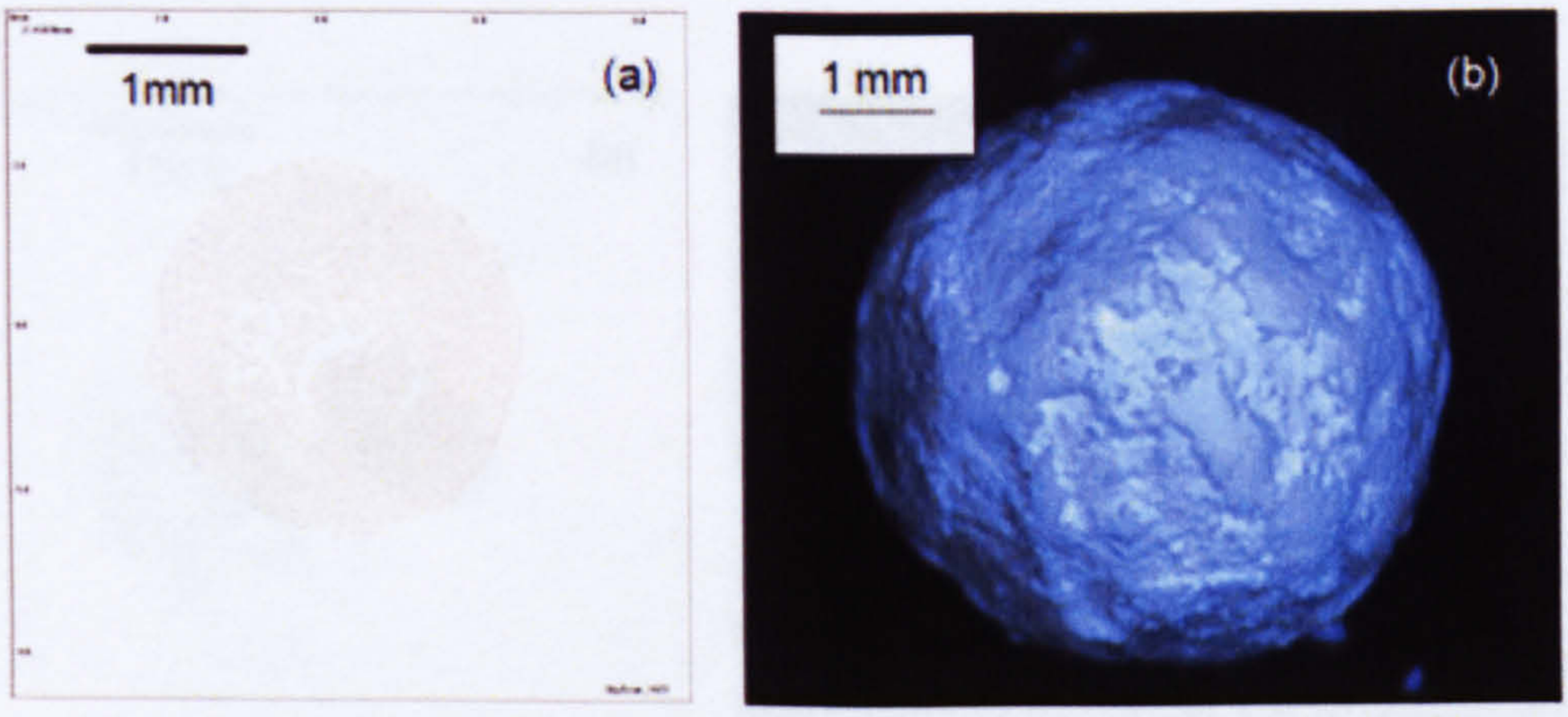

Figure 4.6. (a) Central cross section through a binderless granule made up with polystyrene particles in a high-shear mixer. (b) Image of the same granule shown in (a) obtained with an optical microscope.

Different granule structures within the same batch

The next two examples (Figure 4.7 and Figure 4.8) illustrate how even within the batch, different granule structures can be found due to the different agglomeration mechanisms that coexist in any given experiment [60].

Figure 4.7 correspond to granules manufactured in a high shear mixer using lactose and starch as primary particles (2.18:1) and a solution of HPC (Hydroxy Propyl Cellulose) in water as binder (1:6.25). The binder was poured into the mixing bowl. The binder to solid ratio was 0.15 and the samples were taken after 11 minutes of granulation time. In the x-ray cross sections (Figure 4.7-a) the granule on the right hand side has the structure of a dense, rounded granule,

typically found in high-shear granulation. The left hand side image shows an open and irregular structure and seems that it is a product of the agglomeration of debris from the breakage of granules in the mixer, stuck together with extra binder available in the bowl. The external appearance of the granules is also remarkably different as can be seen in the optical micrograph of the granules (Figure 4.7-b).

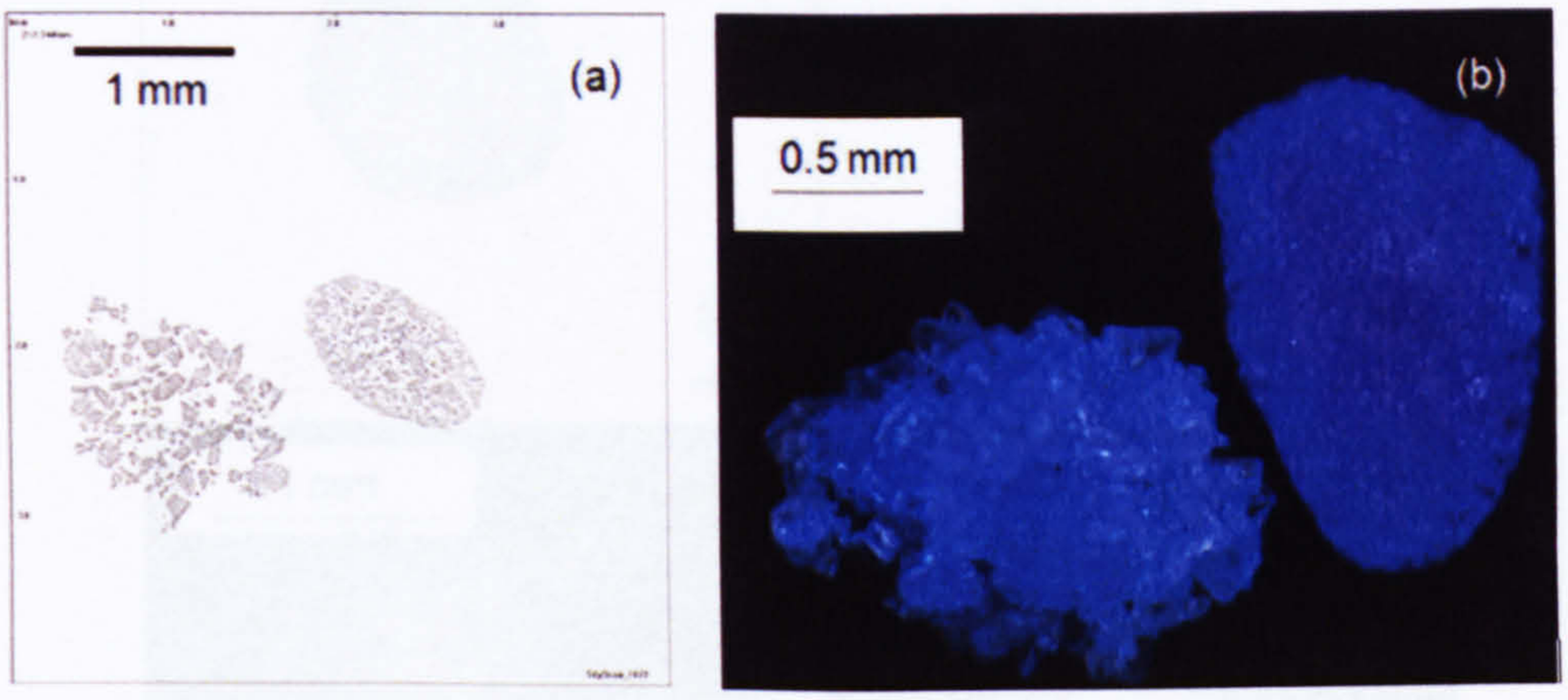

Figure 4.7. (a) Central cross sections of two granules made from a mixture of lactose and starch as primary particles and a solution of HPC in water as binder, taken from the same batch and sieve class after 11 minutes of granulation time; (b) optical microscope image of the same two granules.

Another example of different structures obtained from the same batch is given in Figure 4.8. In this occasion, the granules were manufactured in a high shear mixer using calcium carbonate (Durcal 40) as the primary particles and a mixture of PEG1500 and HPC as a binder, with a binder to solid ratio of 0.13. The impeller speed was set to 300 rpm and the chopper to 1400 rpm, and the granules taken after 10 minutes of granulation time.

The XRT cross sections (Figure 4.8-a and b) of the two samples show very different structures. The granule on the left is round and compacted, whereas the one on the right shows an opened structure due to the agglomeration of debris

within the mixing bowl. The appearance of the granules is also different, from a smooth surface to a rough surface in which the fragments that make up the granule can be clearly distinguished (Figure 4.8-c and d).

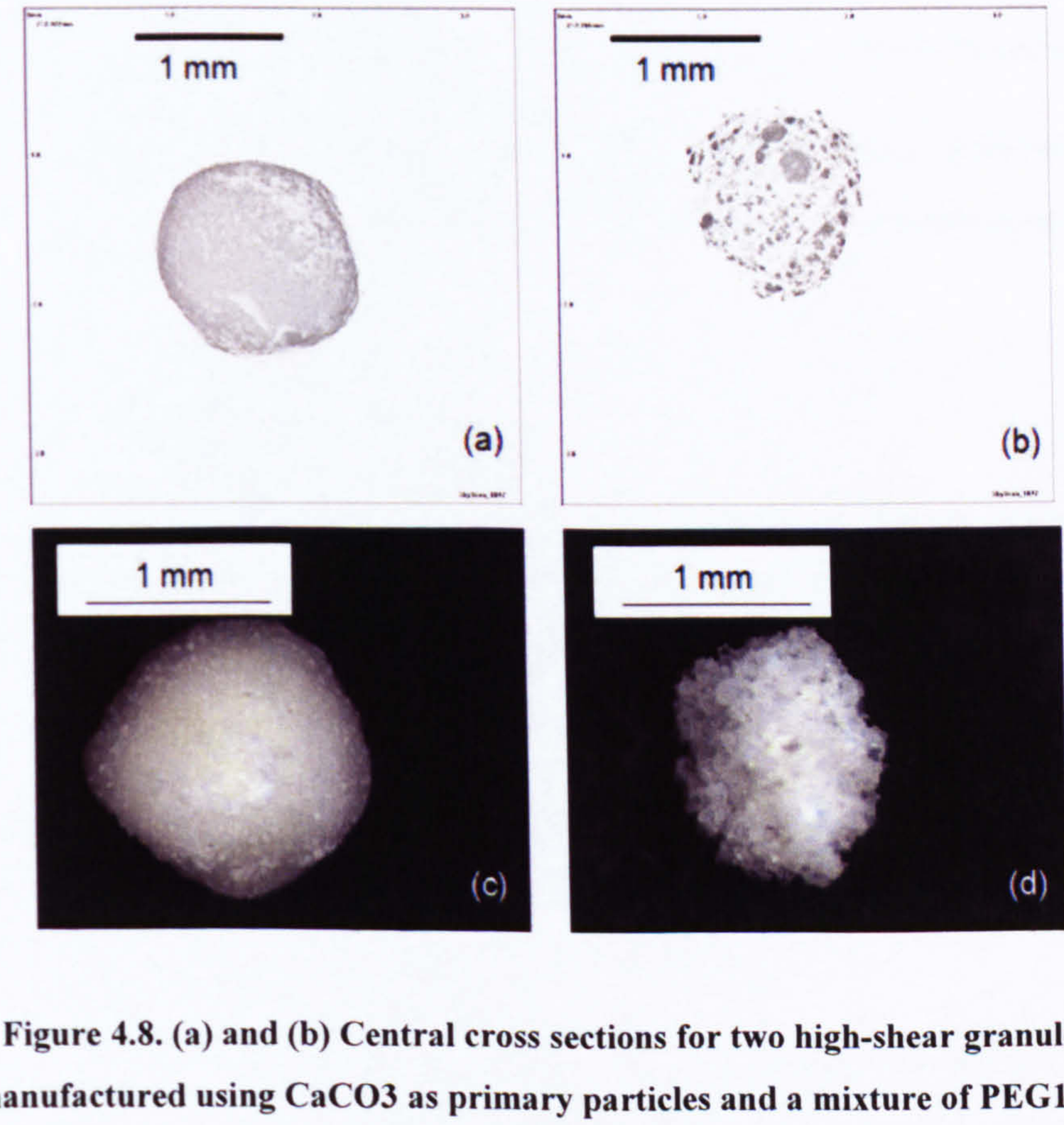

Figure 4.8. (a) and (b) Central cross sections for two high-shear granules manufactured using CaCO3 as primary particles and a mixture of PEG1500 and HPC as binder taken from the same batch and sieve class after 10 minutes of granulation time; (c) optical microscope image of the granule shown in (a); (d) optical image of the granule shown in (b).

Effect of temperature

The effect of temperature on the internal structure of high shear agglomerates made with calcium carbonate (Durcal40) as primary particles and PEG1500 as binder (following the melt-in technique) is illustrated in Figure 4.9 and Figure 4.10. Two experiments were carried out using the same conditions but at two different temperature settings (60 and 80°C) to study the effect of temperature in

the initial stages of the agglomeration process. The process and formulation parameters used are summarized in Table 4.1. The effect was expected to be significant in the resulting agglomerate structure, as it will affect the melting speed of the binder flakes. .

Table 4.1. Process and formulation parameters for the temperature effect experiments.

Process parameters	
Binder addition method	Melt-in
Impeller speed (rpm)	200
Chopper speed (rpm)	1400
Granulation time (min)	2
Temperature (°C)	60, 80
Granule size for analysis (μm)	1000-1400
Formulation parameters	
Primary particles (S)	Durcal40 (2000 g)
Binder (L)	PEG1500 (260 g)
Binder to solid ratio (L/S)	0.13

Figure 4.9 shows the external appearance of the granules manufactured at the different operating temperatures. The external appearance of the granules appears to differ in shape and colour:

- The granules manufactured at the lowest temperature have a more flake-like shape, resembling the shape of the initial binder flakes added to the mixer (Figure 4.9-a).
- The external colour of the granules manufactured at the highest temperature is darker (Figure 4.9-b).

The calcium carbonate used in the experiments is a fine white powder. The agglomerates taken from the batch manufactured at the highest temperature show a yellow-like external colour indicating that in this case, the powder has been more wetted with the binder than in the agglomerates at the lowest

temperature. The change in external colour of agglomerates has been noticed in different experiments, and was attributed to a better distribution of the binder within the agglomerate [61].

The observations in colour and shape indicate that, as expected, the increase of temperature helps to melt the binder flakes faster and improves the distribution of the binder within the mixer. However, from these images little is know about the internal structure of the agglomerates.

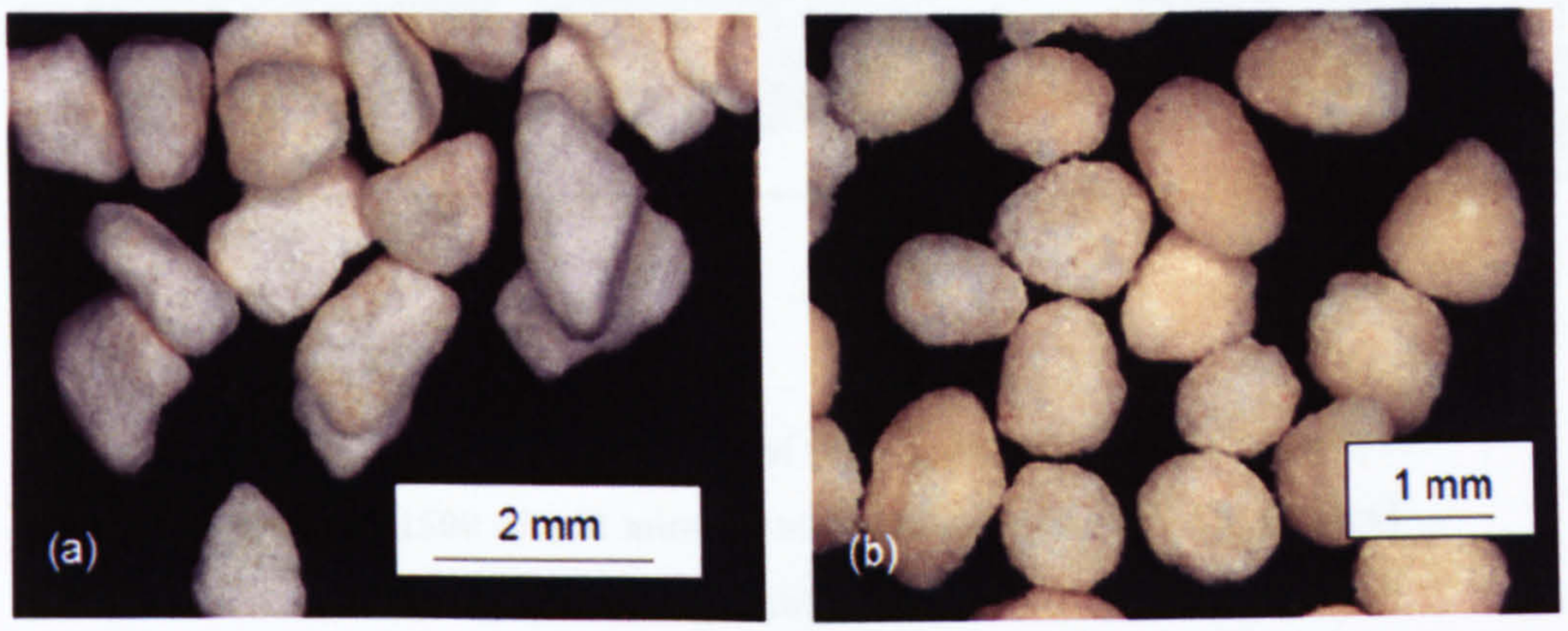

Figure 4.9. Optical images of high shear agglomerates manufactured with $CaCO_3$ and PEG1500 with the same process/formulation parameters except the temperature: (a) 60°C; (b) 80°C.

Figure 4.10 shows the x-ray tomography central cross sections of six granules. The top row (a) corresponds to granules manufactured at the lower temperature (60°C) and the bottom row (b) to granules manufactured at the higher temperature of 80°C. The structural characteristics of the two types of agglomerates are completely different. The granules obtained at the lower operating temperature show internal PEG cores. The temperature increase speeds up the melting of the binder and therefore no core is visible when granulating at 80°C. This structural difference, which will have a big effect on the product properties, is not visible with a visual analysis of the granules but is obvious when using XRT.

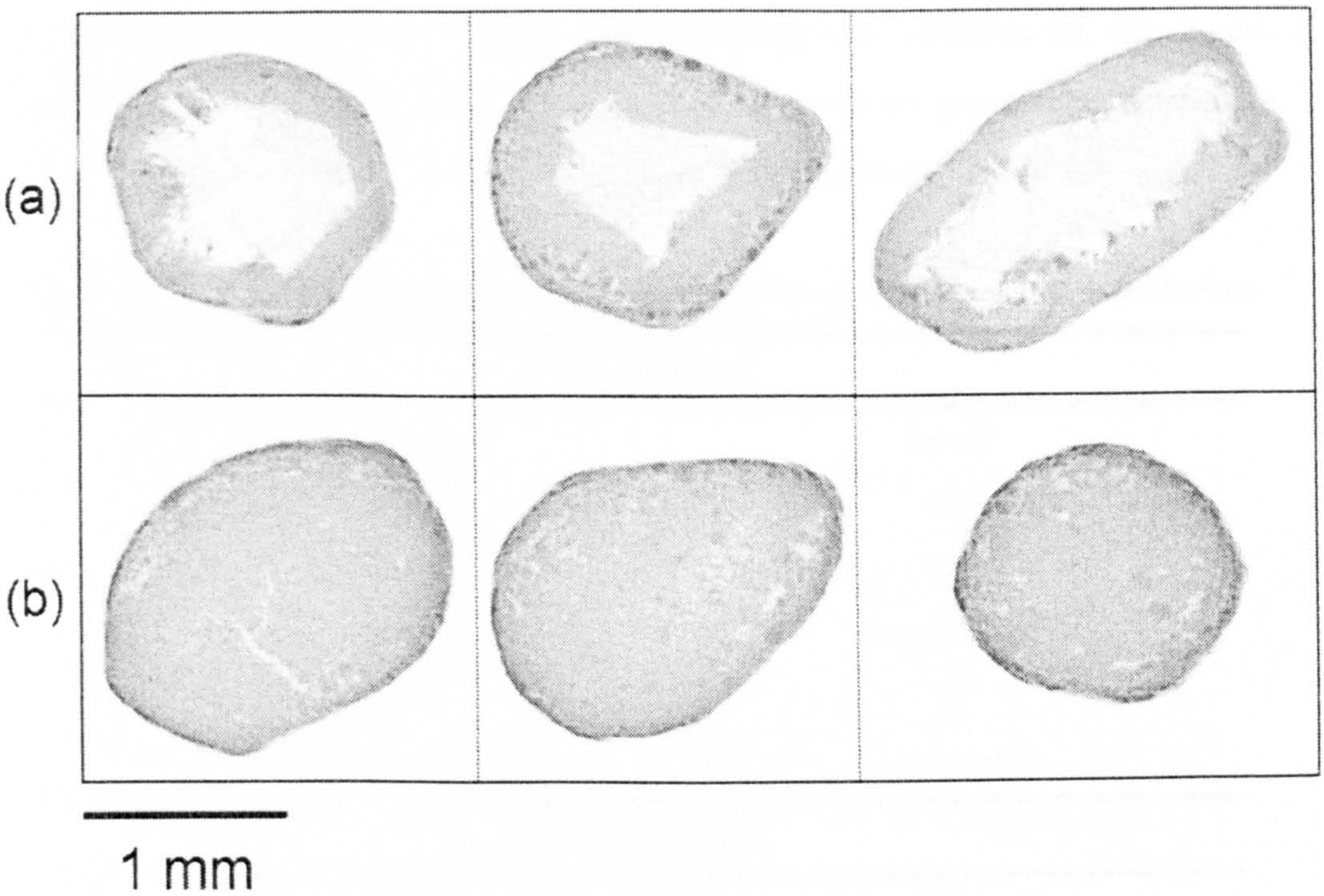

Figure 4.10. (a) Central cross sections of three high shear granules made of $CaCO_3$ and PEG1500 after 2 minutes of granulation at 60°C. (b) Central cross sections of three high shear granules made of $CaCO_3$ and PEG1500 after 2 minutes of granulation time at 80°C.

Effect of granulation time

The structure of agglomerates will change during the granulation process due to the impacts that granules undergo with other granules and/or equipment surface. The changes occur at a faster rate at the beginning of the granulation process, then tend to stabilize [4]. Also, the amount of massing time will influence the capacity of the poured binder to distribute within the powder bed due to the mixing action of the impeller in the bowl.

The granules were made with a mixture of lactose and starch as primary powder and a solution of HPC in water as binder. The two solids were pre-mixed in a high-shear mixer before adding the binder by pouring. The total amount of binder was added over approximately 30 seconds with the impeller running, and

the granulation time was started after finalizing the addition of the liquid. Samples were taken after 5, 10, 15, 30 and 60 seconds of granulation time. The process and formulation parameters used are summarized in Table 4.2

Table 4.2. Process and formulation parameters for the granulation time experiments.

Process parameters	
Binder addition method	Pour-on
Impeller speed (rpm)	350
Chopper speed (rpm)	N/A
Granulation time (seconds)	5, 10, 15, 30, 60
Temperature (°C)	18
Granule size for analysis (μm)	1000-1180
Formulation parameters	
Primary particles (S)	Lactose 200M (1500 g) + Starch (690 g)
Binder (L)	HPC/water (0.16)
Binder to solid ratio (L/S)	0.15

Figure 4.11 and Figure 4.12 illustrate the effect of granulation time on the structure of high shear agglomerates.

Figure 4.11 shows sample granules for different granulation times. Their colouring is due to the addition of a red dye (Erythrosine) to the liquid binder (as part of another on going research in the Particle Products Group).

The surface of the first three samples (Figure 4.11-a to c) is rough with groups of particles protruding. The colouring of these samples is not homogeneous, and some areas do not seem to be covered by the binder at all (indicated by a lack of colour). On the other hand, in the longer granulation time (Figure 4.11-d and e) the surface of samples is much smoother and the colouring is more homogeneous.

Figure 4.12 shows the XRT central cross sections corresponding to the granules shown in Figure 4.11. Similar to the external optical images the cross sections for

the first three granulation times show no significant differences, all of them having rough edges and a similar internal structure (Figure 4.12 a-c). For the longer granulation times, the edges appear to be much more rounded and there is a closer packing of the primary particles within the agglomerates (Figure 4.12 d and e).

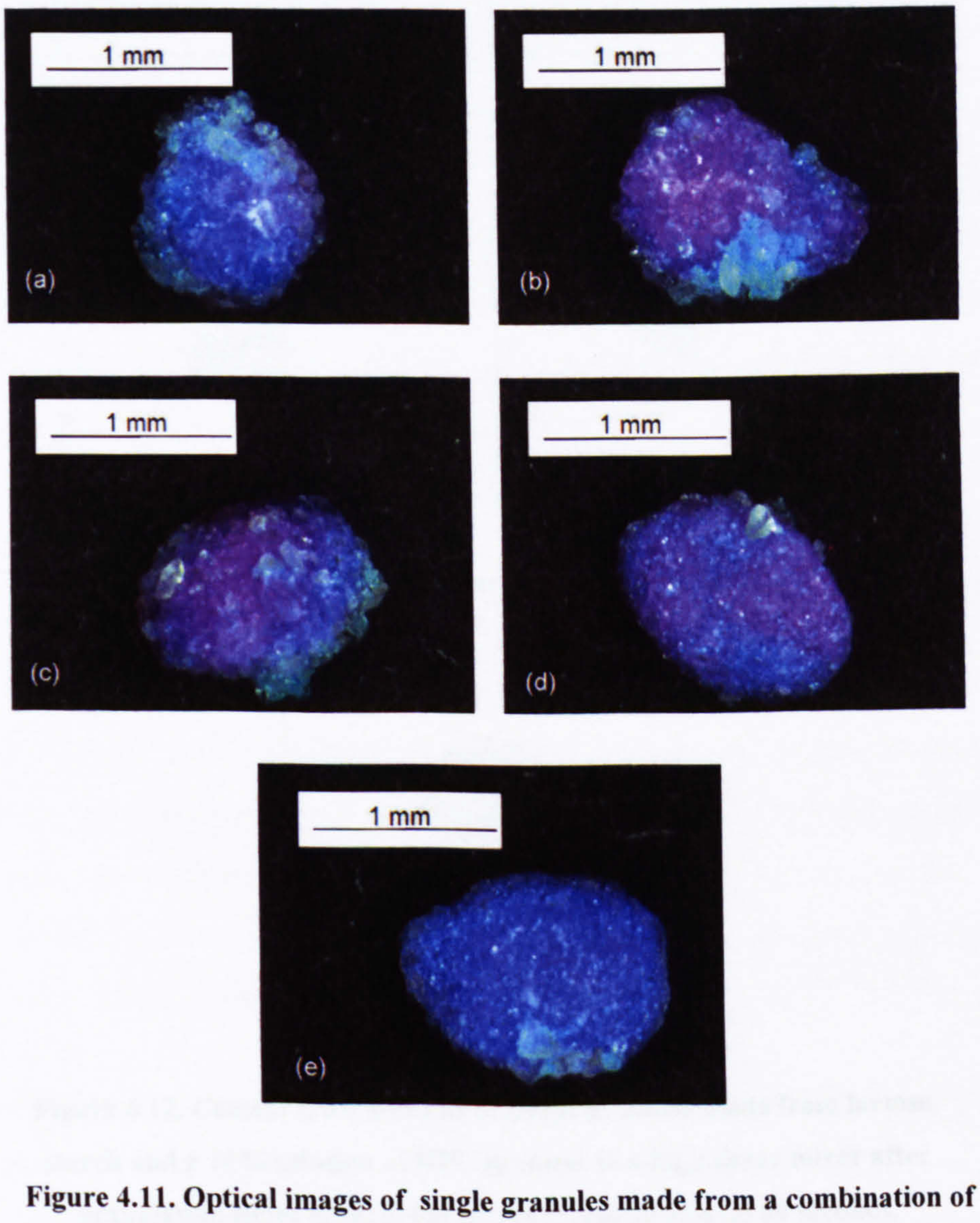

Figure 4.11. Optical images of single granules made from a combination of lactose, starch and a 16% solution of HPC in water in a high shear mixer after granulation times of (a) 5, (b) 10, (c) 15, (d) 30 and (e) 60 seconds.

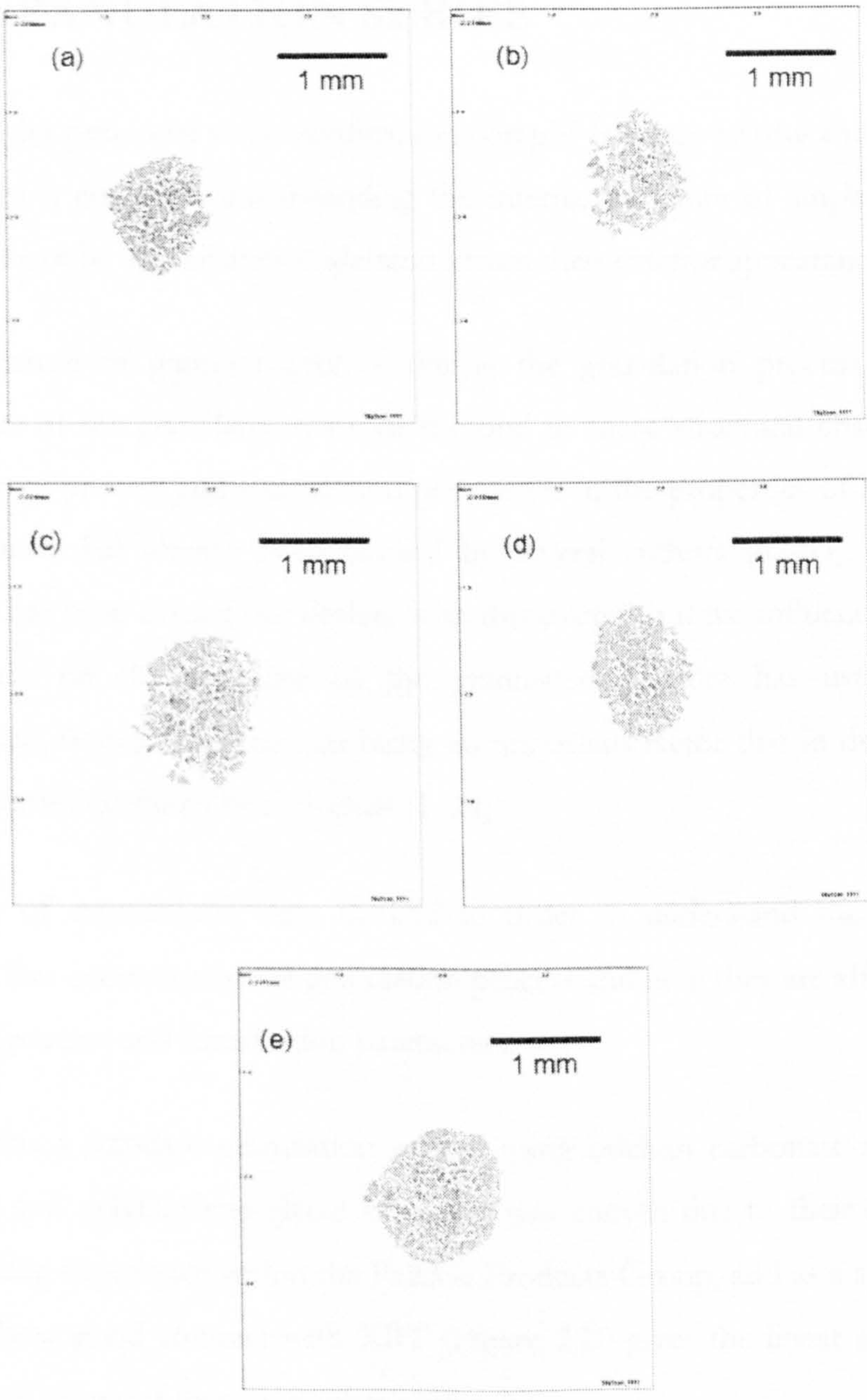

Figure 4.12. Central cross sections of single granules made from lactose, starch and a 16% solution of HPC in water in a high shear mixer after granulation times of (a) 5, (b) 10, (c) 15, (d) 30 and (e) 60 seconds.

4.2 GRANULATION SERIES

The samples presented so far confirm tomography is a very helpful and powerful tool when it comes to understanding the internal structure of single granules, which cannot be immediately understood from their exterior appearance.

The structure of granules evolves during the granulation process, and the properties of the granulated material respond to these structural changes. The influence of process and formulation parameters in the properties of high-shear agglomerates has already been studied by several authors [62-64]. Extensive research has been carried out dealing with this matter, but the influence of these parameters on the structure of the granulated product has usually been overlooked, despite the structure being an important factor that in determining the properties exhibited by a product [1, 24].

A series of experiments were devised in order to understand the structural changes that occur during the granulation process and how they are affected by a series of process and formulation parameters.

To do this a standard granulation system using calcium carbonate as primary particles and polyethylene glycol as binder was chosen due to their availability and existing experience within the Particle Products Group, and as a system that would show good contrast with XRT (Figure 2.20 gives the linear attenuation coefficient values of these and other materials).

Impeller speed and granulation time (as process parameters); and primary particle size, binder viscosity and binder to solid ratio (as formulation parameters) were chosen as the parameters to study as they are known to have a big effect on granule properties and they are expected to create the bigger structural changes in the granules.

The results of these experiments will be illustrated as "granulation series". Each one of the series shows the effect of one of the process/formulation parameters on the structure of the agglomerates. A qualitative study of the series is given in

this chapter, and a qualitative analysis is carried out in Chapter 6 after the development of a suitable method to do so in Chapter 5.

For each of the granulation series, only a very limited amount of samples was studied. This was due mainly to time limitations related to the scanning of single granules. Scanning a whole batch of granules one by one, although ideal, was unrealistic. Therefore, the conclusions drawn from the limited amount of single granules studied are not claimed to be representative for the whole batch. However, and as seen before in this chapter, two typical structures were present in the granulation batches carried out: smooth more spherical granules (product of consolidation), and rougher more irregular granules (from the coalescence of debris/material within the mixer). Only single granules of the "consolidation type" were scanned, since this type was prevalent in the size range studied for the experiments hereby presented. It was assumed that the structures within the two types of granules would be consistent in a batch.

4.2.1 Granulation time at low shear

To study the effect that granulation time has on the structure of the granules, a batch was carried out at low shear (impeller speed of 200 rpm) with the experimental conditions detailed in Table 4.3.

Samples were taken after 2, 4, 6, 10 and 15 minutes of granulation time. The sampled material was sieved into different size fractions and 5 single granules for each granulation time were randomly selected from the 1000-1180 μm size range. These were then scanned using a SkyScan 1072 micro-CT system with the experimental settings already described.

Table 4.3. Experimental settings for the granulation time experiments.

Process parameters	
Binder addition method	Melt-in
Impeller speed (rpm)	200
Chopper speed (rpm)	1400
Granulation time (min)	2, 4, 6, 10, 15
Temperature (°C)	60
Granule size (μm)	1000-1180
Formulation parameters	
Primary particles (S)	Durcal40 (2000 g)
Binder (L)	PEG1500 (260 g)
Binder to solid ratio (L/S)	0.13

Optical images of samples taken at different granulation times can be seen in Figure 4.13., with the respective tomographic central cross sections for the samples in Figure 4.14.

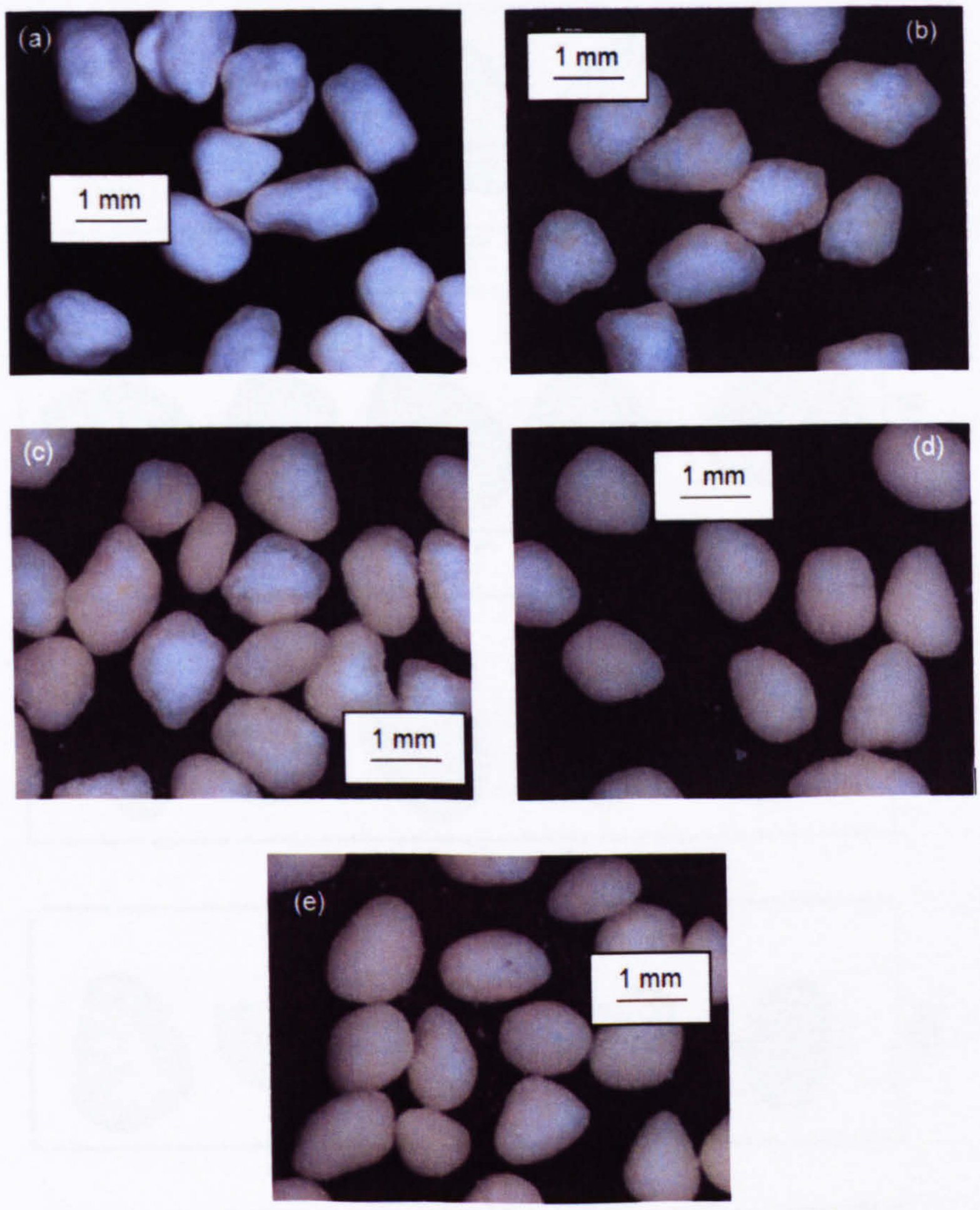

Figure 4.13. Optical images of granules at different granulation times: (a) 2, (b) 4, (c) 6, (d) 10 and (e) 15 minutes. All the samples are in the size range 1000-1180 μm.

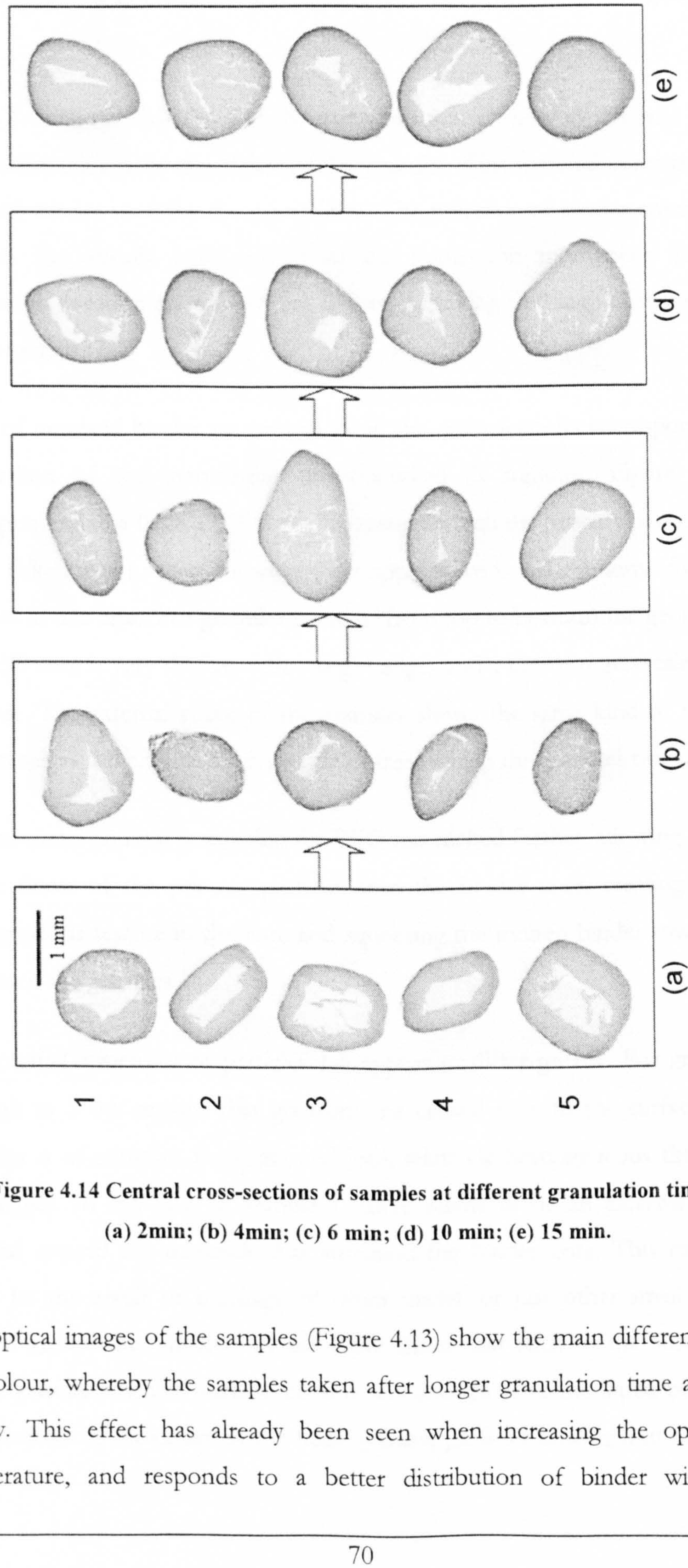

Figure 4.14 Central cross-sections of samples at different granulation times: (a) 2min; (b) 4min; (c) 6 min; (d) 10 min; (e) 15 min.

The optical images of the samples (Figure 4.13) show the main difference to be the colour, whereby the samples taken after longer granulation time are more yellow. This effect has already been seen when increasing the operational temperature, and responds to a better distribution of binder within the

agglomerate. The granules show less flake-like shapes with increased granulation times.

Figure 4.14 shows that most of the samples scanned show an internal core of low density material in the centre of the granule. This material corresponds to the PEG binder used for the granulation. The presence of binder cores within granules has already been related to the immersion mechanism for melt granulation, creating granules with a shape resembling the original shape of the binder particles [65].

Areas of unmixed binder are present in all the cross-sections corresponding to the earliest of the granulation times studied (2 minutes, Figure 4.14-a), corresponding to a flake of PEG binder around which the primary particles stick as the flake starts to melt. However, the appearance is not the same for all the granules at this time. For granules 2 and 4 (from top to bottom) the geometry of the PEG core is very similar, with straight edges and a uniform greyscale around the core. The external shape of the granules shows the same kind of flake-like appearance as the original binder particles from which the granules originated.

For granules 3 and 5 it seems that the PEG has melted further, allowing the flow of the finest of the primary particles into the binder core, creating a more homogeneous texture in the core and squeezing the molten binder towards the surface of the granules.

The internal structures of particles 1-5 appear to differ greatly. For granules 2 through to 5 the regions that go from the central core to the surface of the granules is of constant thickness and look relatively homogeneous throughout the images. In the case of granule 1, there seems to be an external layer of material around the materials that surround the binder core. This extra layer could be the result of breakage of other nuclei, or just other small granules formed around the smallest of the PEG flakes that stick to the surface of a bigger granule when its surface became wet enough after the liquid binder was squeezed out of the centre by the finest primary particles flowing into the flake.

After 4 minutes of granulation time (Figure 4.14-b), the situation has changed substantially when compared to 2 minutes of granulation time (Figure 4.14-a). Granules 1, 3 and 4 (from top to bottom) still show the presence of an inner core of binder, but it has already lost the flake-like shape due to the increasing amount of fine particles that have penetrated it, squeezing the material towards the surface. Whereas granules 2 and 5 the binder core is no longer present; instead it is replaced by the finest of the primary particles, with unmixed regions rich in binder towards the surface of the granule. No proof of breakage is evident to this time, as all granules have an intact core of binder, or have that space occupied by primary particles.

After 6 minutes of granulation time (Figure 4.14-c) the situation is very similar to that for 4 minutes. The size of the binder cores has decreased due to penetration of primary particles and it no longer retains the flake-like shape. The molten PEG is squeezed towards the surface of the granules where it allows for the collection of other primary particles or smaller nuclei. In the case of granule 2 (from top to bottom) the core has completely disappeared suggesting that more primary particles have occupied the unmixed areas where binder presence was observed.

For granulation times of 10 and 15 minutes (Figure 4.14-d and 3-e) the situation has not significantly changed.

It can be concluded that nucleation happens around the binder flakes, and that as granulation time increases, the size of the binder core decreases due to penetration of primary particles which squeeze the molten material towards the surface of the granule allowing further growth. However, even after a granulation time of 15 minutes the core is still present in some of the samples. This is due to the low impeller speed used in the experiments. When the impeller speed is increased the binder core disappears at lower granulation times.

4.2.2 Impeller speed series

To study the effect that the impeller speed has on the structure of the granules, four batches were carried out with the experimental conditions detailed in Table 4.4. Each of them with a different impeller speed. In every case, sampling took place after 10 minutes of granulation time. The sampled material was sieved into different size fractions and 3 single granules were randomly selected from the 1000-1400 μm size range. They were then scanned using a SkyScan 1072 micro-CT system with the experimental settings already described.

Optical images of samples obtained at different impeller speeds can be seen in Figure 4.15 and compared to the XRT central cross-sections of the samples in Figure 4.16.

Table 4.4. Experimental settings for the impeller speed experiments.

Process parameters	
Binder addition method	Melt-in
Impeller speed (rpm)	200, 400, 600, 800
Chopper speed (rpm)	1400
Granulation time (min)	10
Temperature (°C)	60
Granule size (μm)	1000-1400
Formulation parameters	
Primary particles (S)	Durcal40 (2000 g)
Binder (L)	PEG1500 (260 g)
Binder to solid ratio (L/S)	0.13

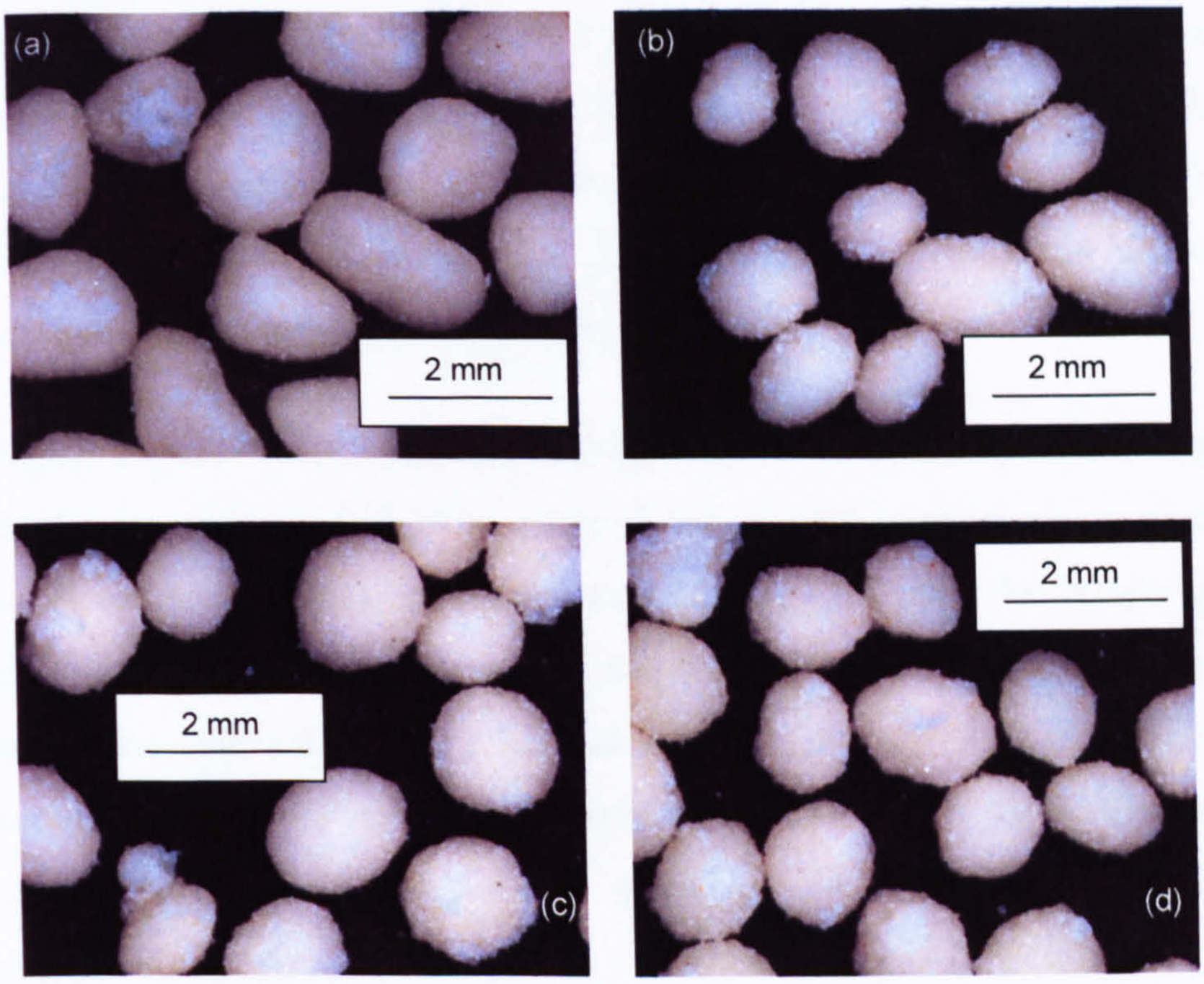

Figure 4.15. Optical images of granules manufactured at different impeller speeds: (a) 200 rpm, (b) 400 rpm, (c) 600 rpm and (d) 800 rpm. All the samples are taken after 10 minutes of granulation time and are in the size range 1000-1400 μm.

The optical images of granules obtained using different impeller speeds only show the shape to differ (Figure 4.15). Granules obtained under low shear conditions appear to be more elongated. As impeller speed is increased the granules tend to become more spherical due to the effect of the increased shear forces in the mixing bowl.

This can be explained by looking at the internal structure of the particles using XRT. The samples corresponding to the lower impeller speed (Figure 4.16-a, 200 rpm) show the presence of a core of binder. The regions close to this binder core show homogenous greyscale values, which could correspond to the finer primary particles that have been squeezed in by the shearing forces in the mixer. Towards the edge of the granules the images show unmixed areas richer in binder.

When the impeller speed is increased to 400 rpm (Figure 4.16-b) the core of binder decreases in size. In the case of granules 1 and 3 no core can be distinguished. Instead its space has been occupied by primary particles. In the case of granule 2, the core seems to be in its last stages before all the molten material is squeezed towards the surface of the granule.

For higher impeller speeds (600 and 800 rpm) the core of binder is no longer visible (Figure 4.16-c and d). The image shows more homogeneous greyscale intensities, without big regions of unmixed binder. However, the images get lighter towards the centre of the samples indicating some areas of binder are still present at the higher impeller speed tested. With regards to the shape of the granules, an increase in impeller speed causes a much rounder shape. This was expected, as by increasing the impeller speed the shear that the granules are subjected to also increases.

The impeller speed has a greater impact than granulation time. The increased shear accelerates the densification of the granules due to increased forces in the mixing bowl that intensify the collisions between granules and between granules and equipment, squeezing the cores of binder and making the disappear. For impeller speeds over 400 rpm binder cores within the granules are no longer present after 10 minutes of granulation time. A rounding effect is also clearly observed as the impeller speed increases, making more compact spherical-shaped granules (Figure 4.16).

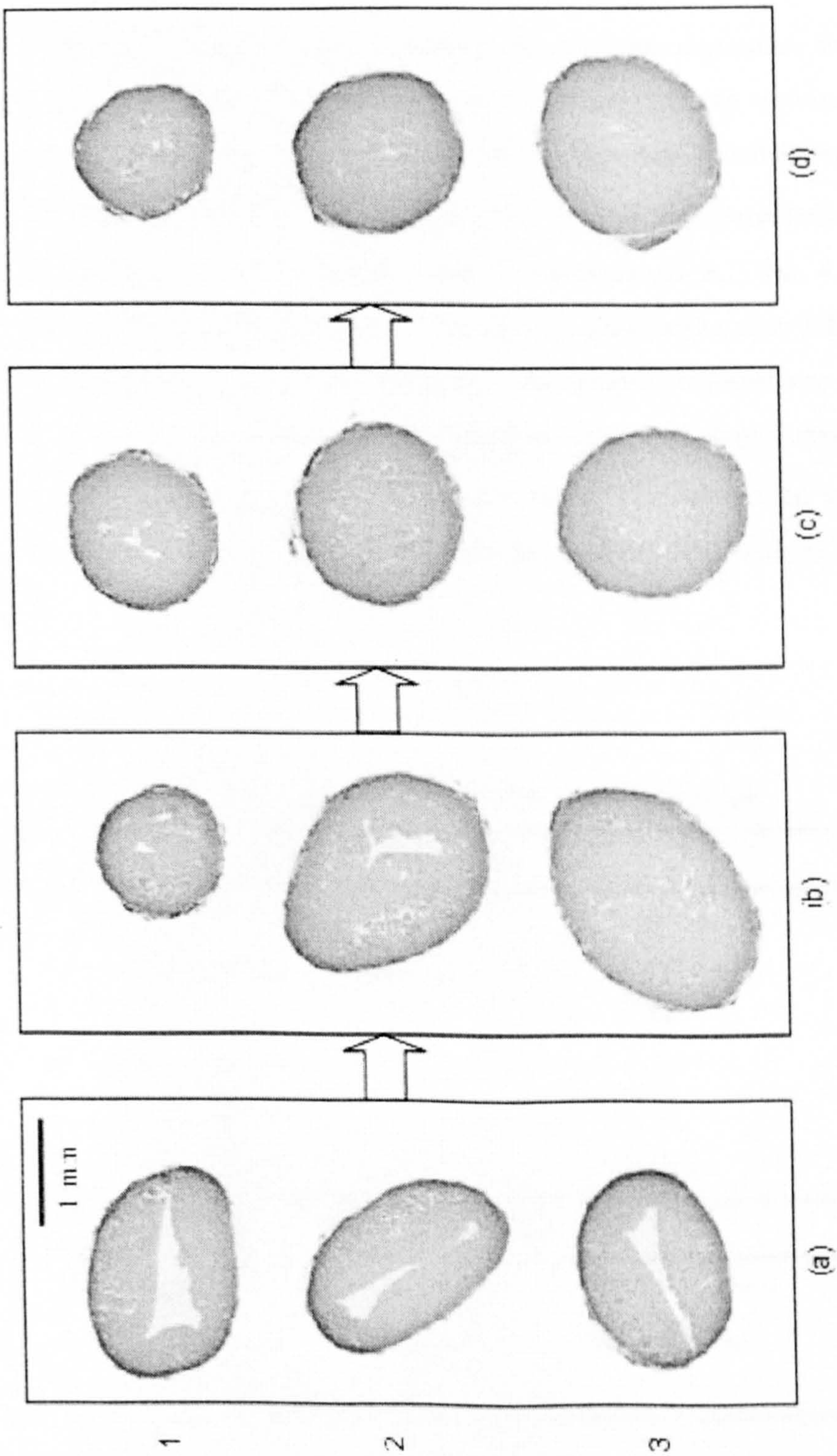

Figure 4.16. Central cross-sections of samples at different impeller speeds, taken after 10 minutes of granulation time: (a) 200 rpm; (b) 400 rpm; (c) 600 rpm; (d) 800 rpm.

4.2.3 Primary particle size

The effect that the primary particle size has on the structure of granules was also studied. Three batches using a different grade of Durcal (calcium carbonate) as primary particles: Durcal 5, 15 and 40, with d50 (volume size distribution) of 6, 15 and 23 μm respectively, were studied. The rest of the formulation and process parameters were kept constant and are summarized in Table 4.5. For each batch samples were taken after 10 minutes of granulation time following the sampling procedure previously described. The sampled material was sieved into different size fractions and 2 single granules from each batch time were randomly selected from the 1000-1400 μm size range. They were then scanned using a SkyScan 1072 micro-CT system with the experimental settings already described.

Table 4.5. Experimental settings for the Durcal size series.

Process parameters	
Binder addition method	Melt-in
Impeller speed (rpm)	400
Chopper speed (rpm)	1400
Granulation time (min)	10
Temperature (°C)	60
Granule size (μm)	1000-1400
Formulation parameters	
Primary particles (S)	Durcal 5/15/40 (2000 g)
Binder (L)	PEG1500 (260 g)
Binder to solid ratio (L/S)	0.13

Optical images of samples with different primary particle sizes can be seen in Figure 4.17 with the respective XRT central cross sections in Figure 4.18.

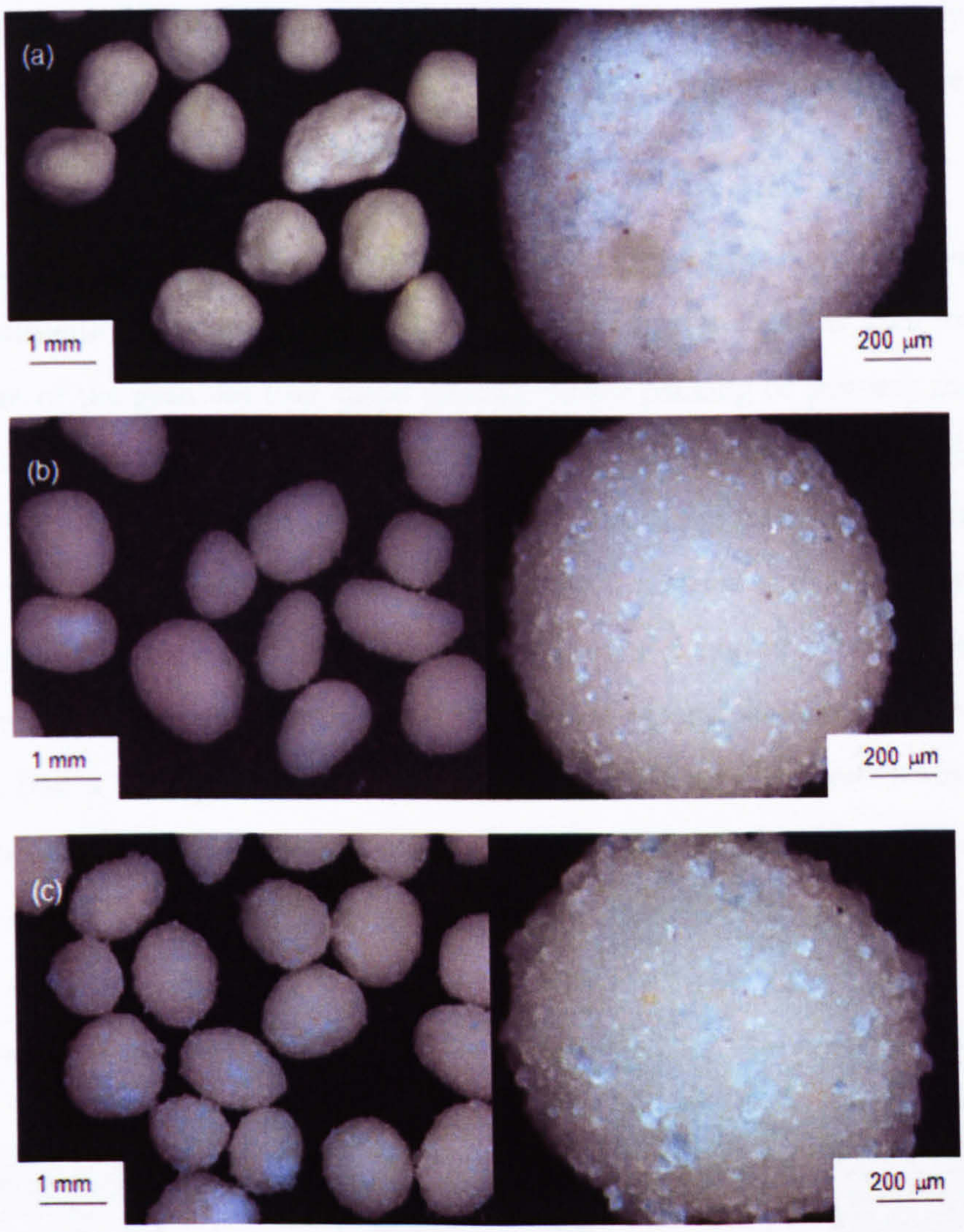

Figure 4.17. Optical images of granules manufactured with different sizes of $CaCO_3$ as primary particles: (a) Durcal 5; (b) Durcal 15 and (c) Durcal 40, alongside detailed images of their surface characteristics.

From the optical images of the samples it can be see that the granules manufactured with the smallest of the Durcal grades (Durcal 5, Figure 4.17-a) show a more fine-powdery surface, looking slightly dryer that the others. Durcal 15 and 40 have very similar surface characteristics.

The cross-sections of the scanned granules also do not demonstrate many differences either between the Durcal 15 and 40 samples, other than a slightly higher surface roughness corresponding to the samples with the biggest primary

particle size (Figure 4.18-c) that could also be seen from the optical analysis of the granules. Unmixed areas are present in all the samples manufacture with Durcal 15 and 40.

In the case of the granules manufactured with Durcal 5 (Figure 4.18-a) the internal structure seems more compact. However there is a darker area towards the centre of the granules that could indicate closer packing of primary particles in that area. This could be due to the finer size of the primary particles, allowing them to penetrate easier in the binder flakes as they melt, squeezing it completely towards the outside of the granule, and creating a nucleus that allows layers or more material to stick into it. Externally, the Durcal 5 granules looked and felt (to the tact) completely different than the Durcal 15 and 40 granules. Durcal 5 granules had a very powdery and weak appearance and crumbled really easily under the minimum pressure. It was very difficult to handle them individually without feeling the external layers of the granule "peel away".

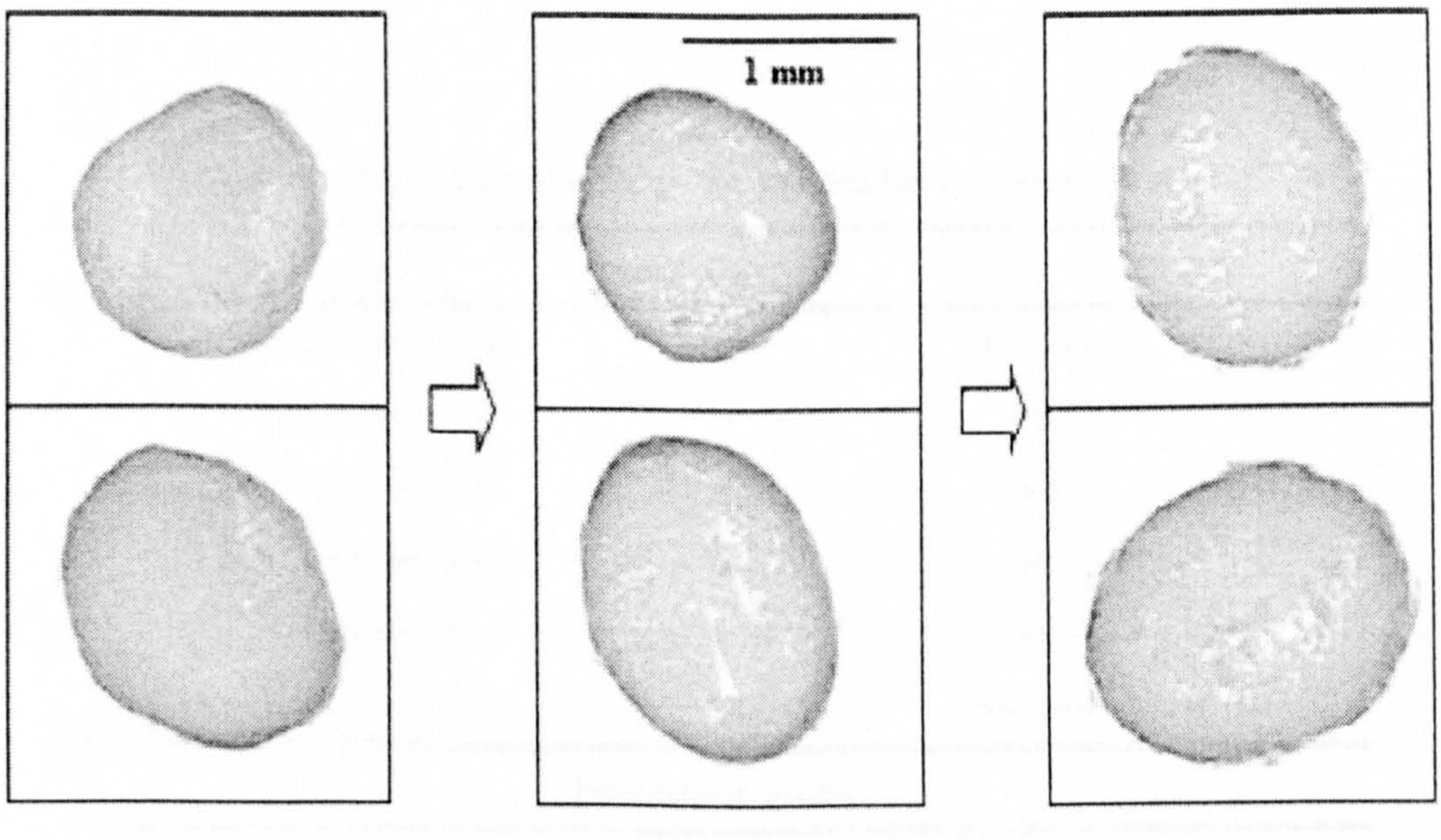

Figure 4.18. Central cross-sections of samples made with different sizes of $CaCO_3$ as primary particles: (a) Durcal 5; (b) Durcal 15 and (c) Durcal 40.

4.2.4 Binder molecular weight

To study the effect of the binder molecular weight on the granule structure, the experimental procedure described in Chapter 3 had to be modified. Four different grades of PEG were used as binders ranging from PEG600 to PEG20000. PEG600 is liquid at room temperature, and therefore melt-in granulation could not be used. In order to maintain experimental conditions as constant as possible (with the binder viscosity being the only variable) the other binders tested (PEG 1500, 6000 and 20000) that are solid are room temperature were melted, and the binder addition method for the experiments was pour-on (binder is poured as a liquid on top of the powder bed and granulation time started). Experimental settings are summarized in Table 4.6. For each batch, samples were taken after 10 minutes of granulation time and 2 single granules from each batch time were randomly selected from the 1000-1400 μm size range. They were then scanned using a SkyScan 1072 micro-CT system with the experimental settings already described.

Table 4.6. Experimental settings for the binder viscosity size series.

Process parameters	
Binder addition method	Pour-on
Impeller speed (rpm)	400
Chopper speed (rpm)	1400
Granulation time (min)	10
Temperature (°C)	60
Granule size (μm)	1000-1400
Formulation parameters	
Primary particles (S)	Durcal 40 (2000 g)
Binder (L)	PEG600/1500/6000/20000 (260 g)
Binder to solid ratio (L/S)	0.13

Optical images of samples with different binders can be seen in Figure 4.19. The central cross sections for all the samples scanned can be seen in Figure 4.20.

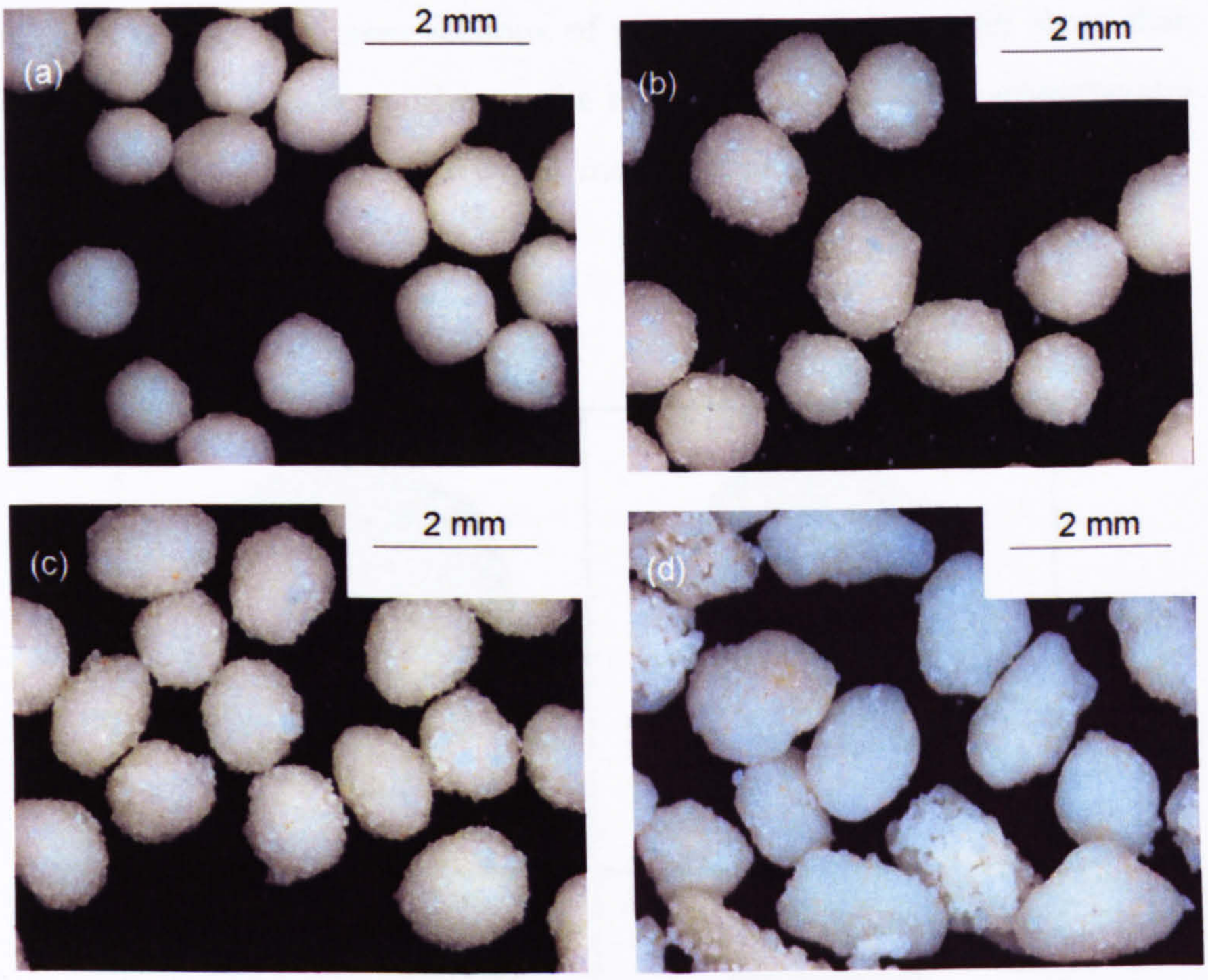

Figure 4.19. Optical images of granules manufactured with PEG binders of different molecular weight: (a) PEG600, (b) PEG1500, (c) PEG6000 and (d) PEG20000.

From the optical images it can be seen that the granules manufactured using the binder with the lowest molecular weight (PEG600, Figure 4.19-a) have the most spherical shape and smoothest surface. The higher the molecular weight of the binder, the rougher the surface is and the more irregular the shape of the agglomerates becomes.

The surface of the agglomerates with the highest molecular weight binder (PEG20000, Figure 4.19-d) is covered with what seems to unconsolidated material from the mixing bowl. This indicates that the higher molecular weight binders create stronger bonds between particles in the mixing bowl as they can

solidify at the operating temperature of the process. Also the granules are strong enough not to have their shape altered (rounding effect due to shear in the mixing bowl) as much as granules manufactured with a lower viscosity binder.

The x-ray tomography cross sections of the samples (Figure 4.20) show that, unlike shape and surface roughness, the internal structure of the agglomerates does not seem to be too affected by the molecular weight of the binder.

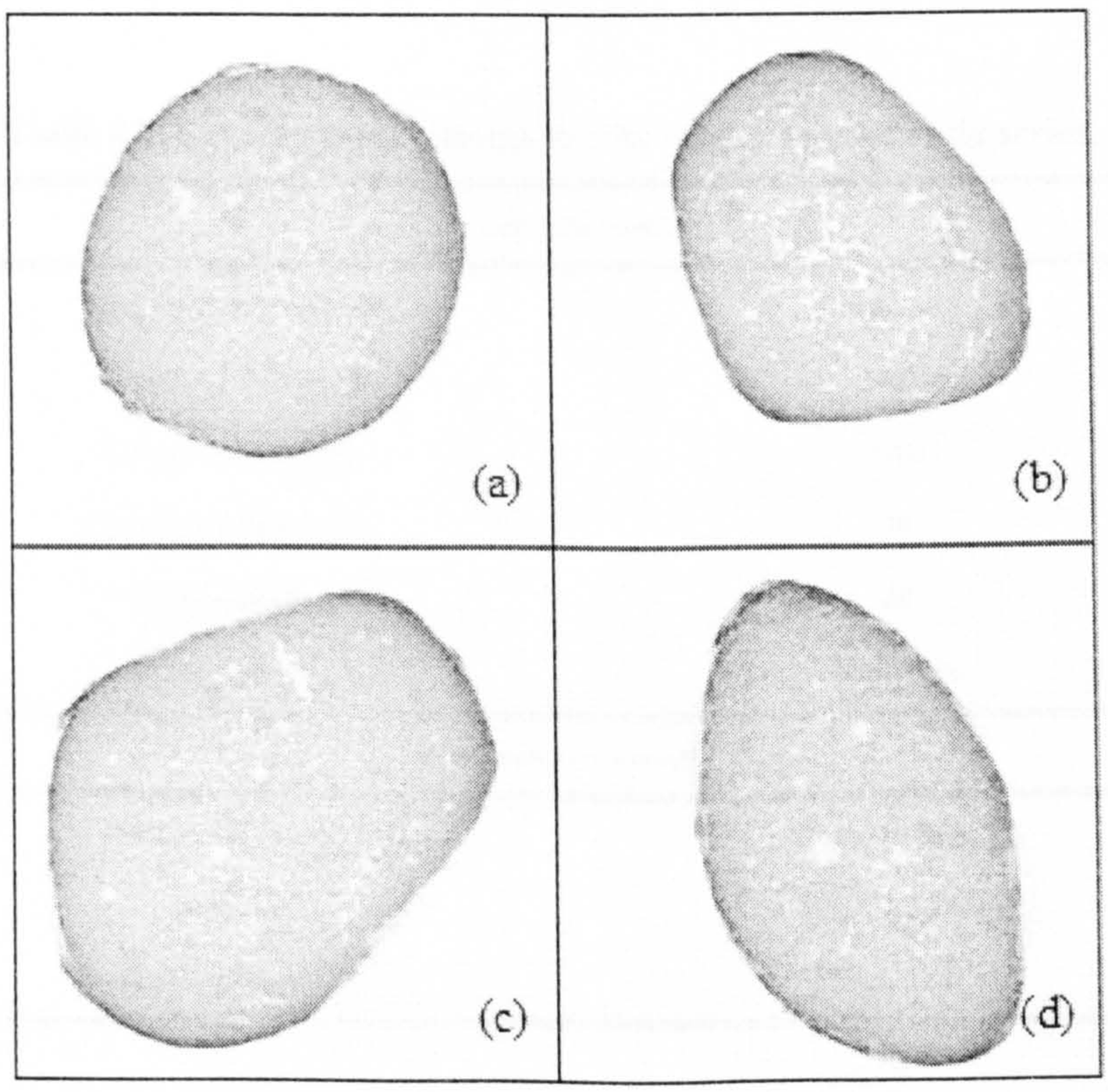

Figure 4.20. Central cross-sections of samples made with different grades of PEG as binder: (a) PEG600; (b) PEG1500; (c) PEG6000 and (d) PEG20000.

4.2.5 Binder to solid ratio

To study the effect of the binder to solid ratio two batches were made using different amounts of binder. The experimental settings for these experiments are detailed in Table 4.7. Liquid to solid ratios of 0.1 and 0.16 were chosen. For each batch, samples were taken after 10 minutes of granulation time and 2 single granules from each batch time were randomly selected from the 1000-1400 μm size range. They were then scanned using a SkyScan 1072 micro-CT system with the experimental settings already described.

Table 4.7. Experimental settings for the binder to solid ratio series.

Process parameters	
Binder addition method	Melt-in
Impeller speed (rpm)	400
Chopper speed (rpm)	1400
Granulation time (min)	10
Temperature (°C)	60
Granule size (μm)	1000-1400
Formulation parameters	
Primary particles (S)	Durcal 40 (2000 g)
Binder (L)	PEG1500 (260 g)
Binder to solid ratio (L/S)	0.1, 0.16

Optical images of samples with different liquid to solid ratios can be seen in Figure 4.21 with the respective XRT cross sections in Figure 4.22.

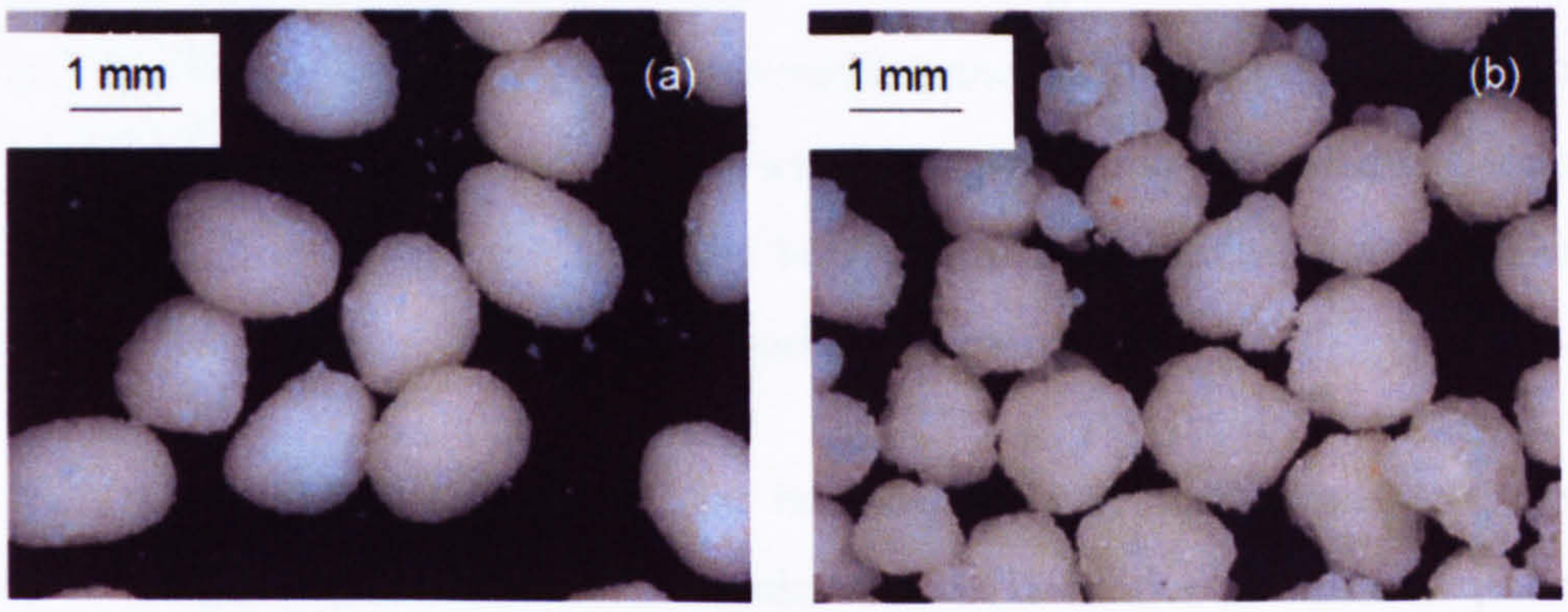

Figure 4.21. Optical images of granules manufactured with different amounts of binder to solid ratios: (a) 0.1 and (b) 0.16.

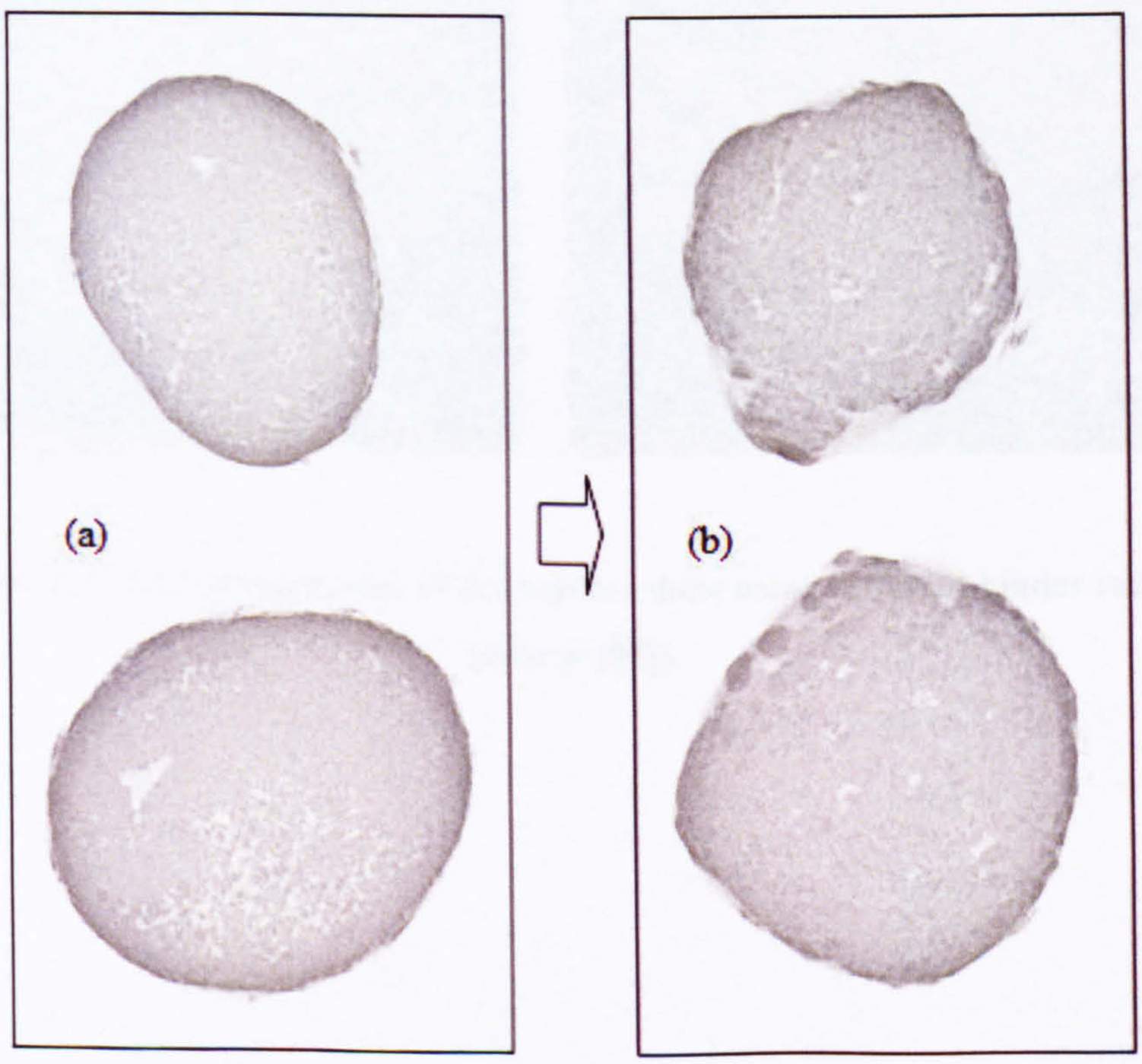

Figure 4.22. Central cross sections images of granules manufactured with different amounts of binder to solid ratios: (a) 0.1 and (b) 0.16.

The appearance of the granules is quite different (Figure 4.21). Granules made with 10% binder have a much smoother surface and shape. This is confirmed by the XRT cross sections (Figure 4.22) with the overall internal structure being similar, but the agglomerates from the batch with more binder appear uneven and show areas of unmixed binder around the edges.

In addition to the appearance of the batches, the way they granulate is also different (Figure 4.23). The batch made with 16% binder granulated quickly forming large agglomerates after 10 minutes of granulation time, while the batch made with 10% binder remained powdery , with plenty of fines [55].

Figure 4.23. Representation of the batches done using different binder ratios (source [55]).

5

ANALYSIS OF XRT DATA

How to go one step forward in the way we can extract information from tomographic analysis of single granules. Not only can we look at the images of the cross sections that represent the true internal structure of the granules, but we can transform all that information into radial greyscale profiles within the granules.

5.1 METHOD DEVELOPMENT

XRT analysis on single granules provides a vast amount of data that comes in the form of a stack of adjacent cross-sectional images, showing the internal microstructure of the sample. As part of this work it was intended to develop a way of analyzing these images so that information about granule structure can be extracted.

The raw data can be understood as a group of spatial coordinates (position vectors $\underline{x}_{i,j,k} = (i,j,k)$) with an associated greyscale intensity value, $g_{i,j,k}$ (Figure 5.1). This intensity value provides information on the material attenuation coefficient which is function of the material density.

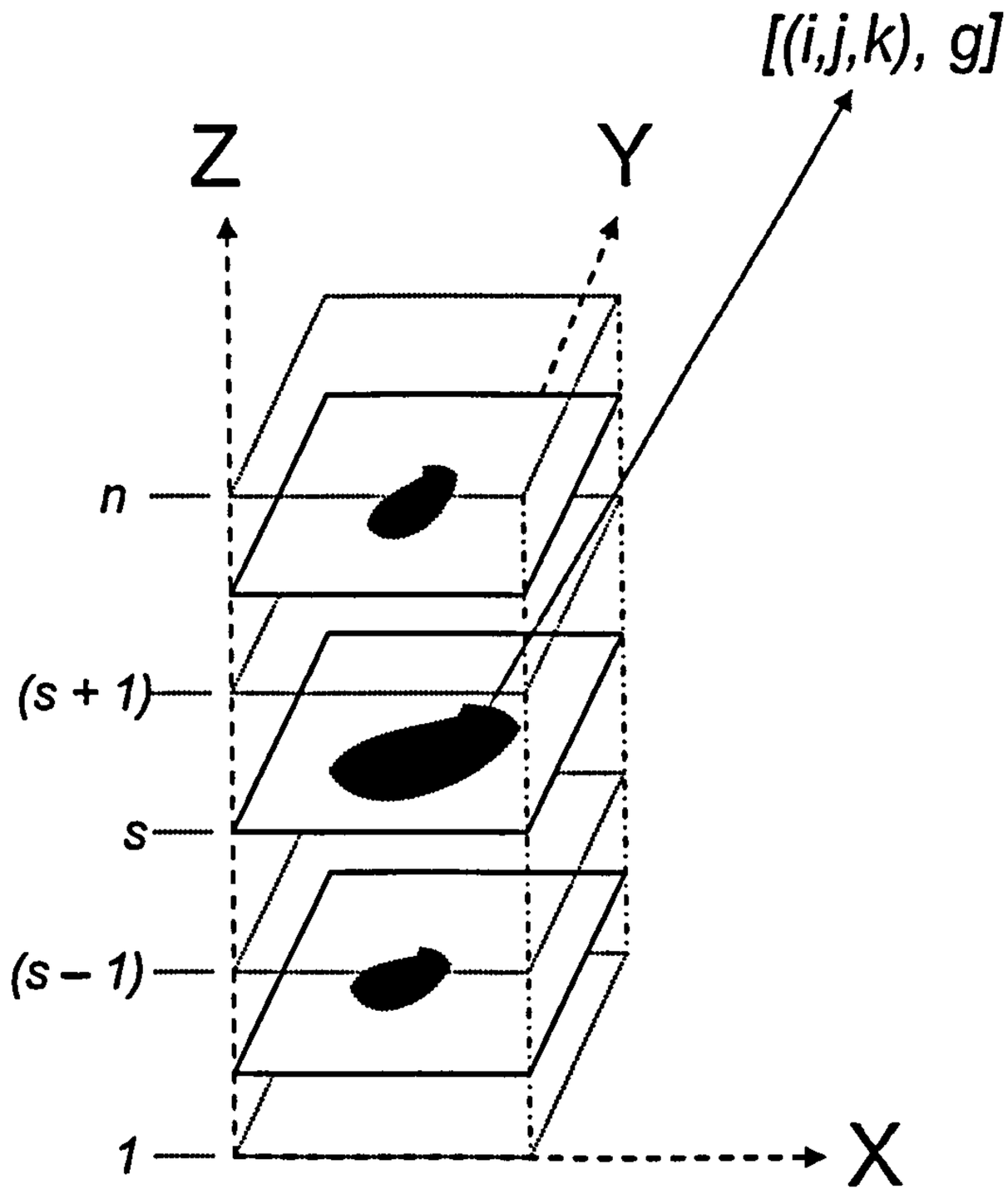

Figure 5.1. Schematic representation of a stack of images after XRT scanning and reconstruction. The granule is represented by a stack of adjacent cross-sectional slices, each of them showing the internal structure of the granule.

A new method was required to interpret this data in the form of radial distributions of greyscale intensities in the granule as an indication of structure; hence a new way of describing the output images from XRT analysis was developed.

To calculate the radial intensity distribution the first step is to find the centre of mass of the particle, $\underline{\tilde{x}}$. This is calculated by averaging the greyscale and the coordinates for every pixel within the granule for each of the cross-sections obtained after XRT.

$$\sum g_{i,j,k}\left(\underline{x}_{i,j,k} - \underline{\tilde{x}}\right) = 0 \qquad (1)$$

Once the centre of mass is known, the next step involves finding a scalar defining the position of all the granule pixels referred to it.

$$r_{i,j,k} = \left| \underline{x}_{i,j,k} - \underline{\tilde{x}} \right| \tag{2}$$

The following set of equations describes how to calculate the x-coordinate of the centre of mass of the granule by averaging the greyscale and the coordinates of every pixel describing the granule:

$$\sum_{i,j,k} g_{i,j,k} \left(\underline{x}_i - \tilde{x}_x \right) = 0 \tag{3}$$

$$\sum_{i,j,k} g \underline{x}_i - \tilde{x}_x \sum_{i,j,k} g = 0 \tag{4}$$

$$\tilde{x}_x = \frac{\sum_{i,j,k} g_{i,j,k} \underline{x}_i}{\sum_{i,j,k} g_{i,j,k}} \tag{5}$$

Equations 3 to 5 outline the operations done to calculate the x-coordinate of the centre of mass. The y and z-coordinates are calculated using analogous equations.

The centre of mass can then be described as:

$$\underline{\tilde{x}} = \frac{\sum_{i,j,k} g_{i,j,k} \underline{x}}{\sum_{i,j,k} g_{i,j,k}} \tag{6}$$

The scalar (distance) defining the position of all the granule pixels referred to the position of centre of mass can be calculated as follows:

$$r_{i,j,k} = \sqrt{\left(x_i - \tilde{x}_x\right)^2 + \left(x_j - \tilde{x}_y\right)^2 + \left(x_k - \tilde{x}_z\right)^2} \tag{7}$$

All the pixels in the stack of adjacent cross-sectional images representing the internal structure of the granule are now in the form of pairs of data: [greyscale intensity, radial distance to the centre of mass] as illustrated in Figure 5.2.

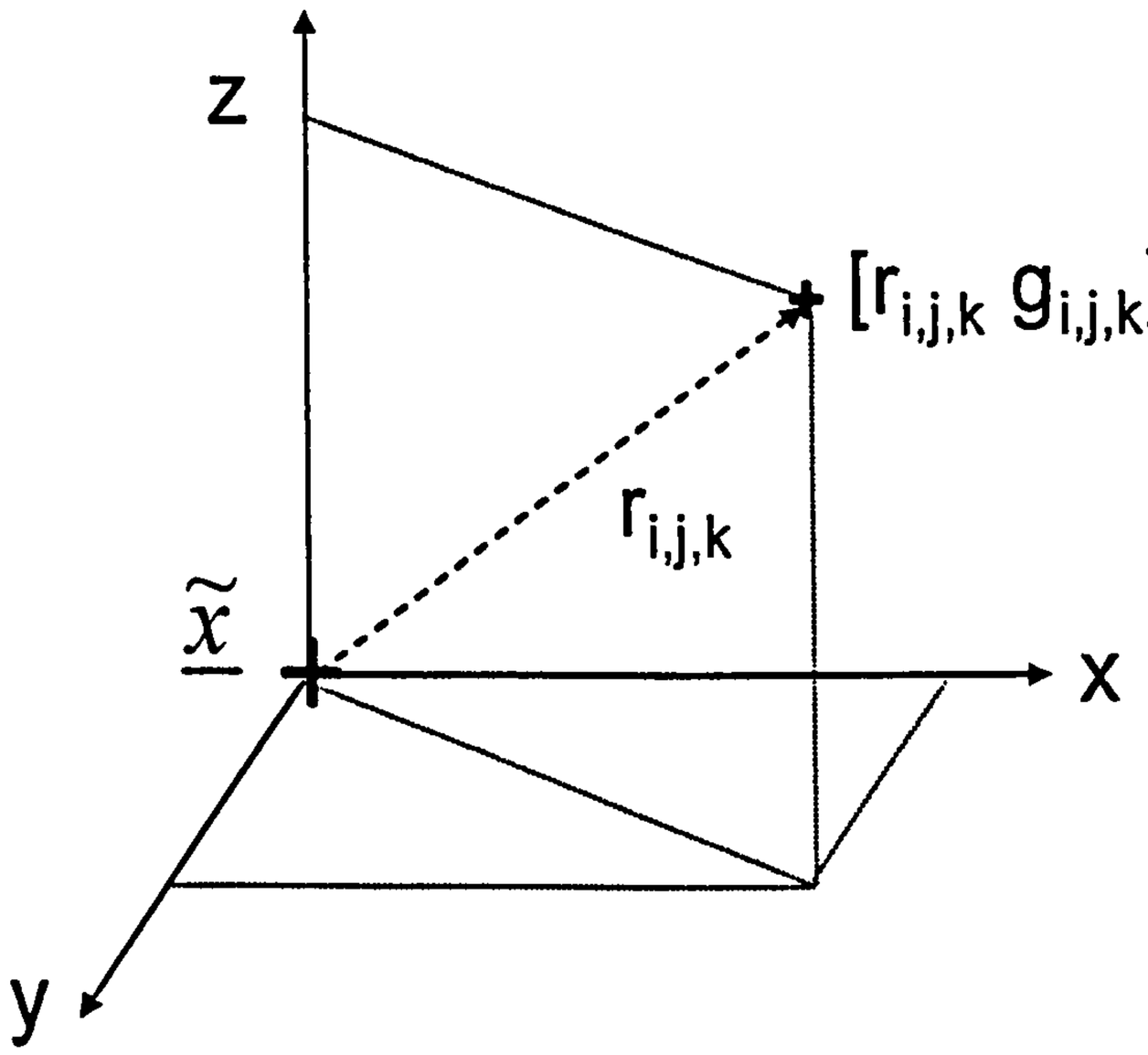

Figure 5.2. Each of the pixels in the cross-sectional slices representing the granule is now represented by the pair $[r_{i,j,k}, g_{i,j,k}]$.

Once the scalar is known, the data is binned by radius and all the information required to define each of the bins is calculated. Results can then be analyzed in the form of radial distributions of greyscales in the single granules.

The binning of the data consists on dividing the radial distance from the centre of mass in regular intervals, creating a series of concentric spherical shells around the calculated centre of mass or the granule. The average greyscale value of all the pixels included in each bin is calculated and assigned to a radial distance corresponding to the middle point of the bin.

5.1.1 Masking

The reconstructed two dimensional slices show the internal microstructure of the granule but not all the pixels of those images belong to the granule itself, as the cross section of the granule depicted in each slice does not completely fill the field of view. The background corresponds to air which does not attenuate the x-rays.

Although precautions are taken by making flat field corrections and using random movement for the scans, the resulting cross sections show artefacts that create noise in the images, hence the background is not completely homogeneous. This causes some of the pixels outside the granule to have a value different from zero. In order not to include these pixels in the calculations for the centre of mass, or any further calculations, a masking procedure was included as part of the algorithm. Its aim is to identify pixels within the granule boundary.

The masking procedure is based on tolerance. Given an image and a pixel coordinate it isolates all neighbouring pixels with values within a present tolerance. The optimum level of tolerance was adjusted manually by checking individual slices (from top, bottom and middle section of the granule) to make the main body of the granule be included in the mask and not the noise pixels.

Figure 5.3 shows a cross-section of a granule and the corresponding mask created by the programme; including also a schematic representation of the binning procedure in 2D (the real process is a three-dimensional process).

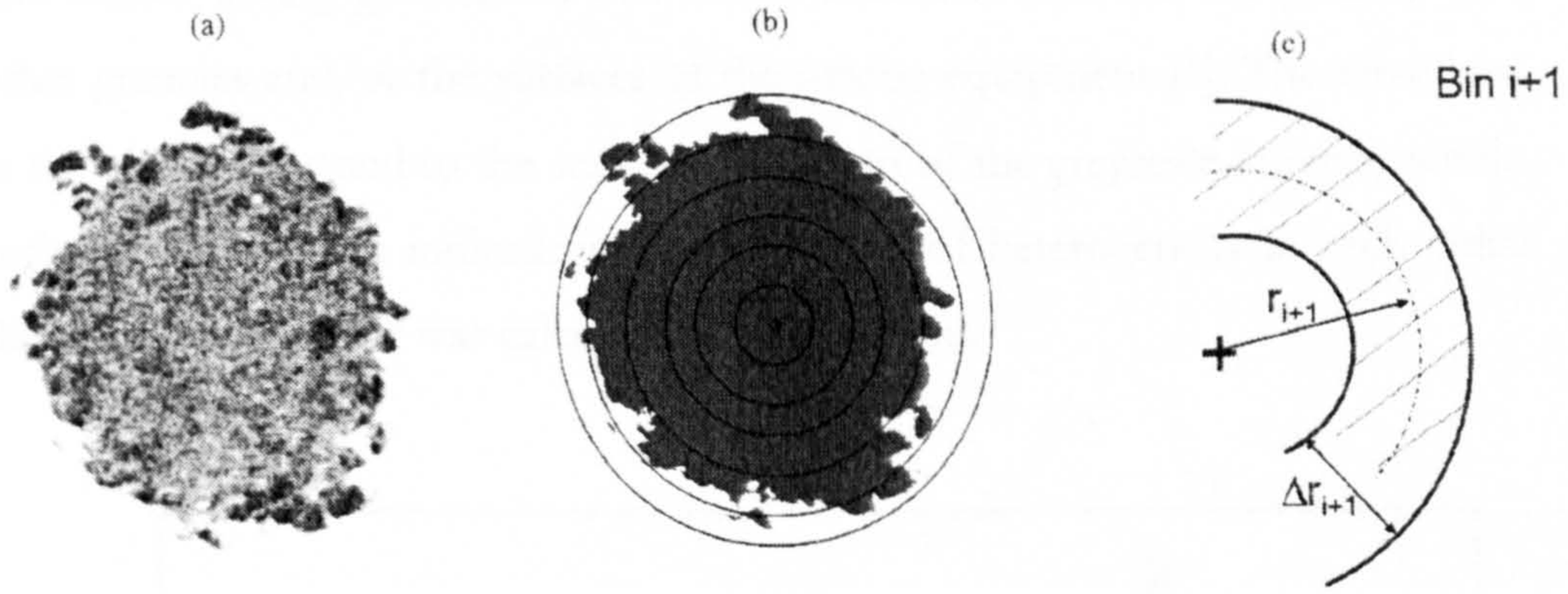

Figure 5.3. Masking procedure to select only the pixels belonging to the granule: (a) XRT image of a cross-section through the granule; (b) mask over that section (only the pixels in the black area will be included in further operations) with a schematic representation of the bins (c) schematic of the binning procedure (bin *i +1*, with width Δr_{i+1} and radial distance r_{i+1}).

5.1.2 Radial profiles

All the calculations for the centre of mass and radial profiles data are done using a purpose written Matlab code. With the results obtained the radial distribution of greyscales for each granule can be plotted.

In these profiles the vertical axis, labelled *g*, shows the average greyscale value of each bin. It falls between 0 and 255. Higher greyscale values correspond to a higher absorption of the x-rays and hence denser materials. The lower the greyscale value the less dense the material, with 0 corresponding to air. The horizontal axis, labelled *r*, shows the radial distance from the centre of each bin to the centre of mass of the particle, hence $r = 0$ corresponds to the calculated centre of mass of the granule.

An example of a radial profile obtained with this method can be seen in Figure 5.4. The edge of the granule is located at a radial distance of just over 900 μm when the profile drops to a value of zero, corresponding to the background air. In order to detect the exact edges of the granule the masking procedure was required. The profile shows increasing consolidation from the centre of mass of the granule towards the edge, which would agree with the consolidation process

that occurs during granulation due to the collisions between the granule with other granules and/or the surfaces of the mixing equipment [4]. The error bars in the plot correspond to the standard deviation of the greyscale intensity within each bin and give an indication about the level of heterogeneity in each radial skin. The graph below was calculated using 500 bins.

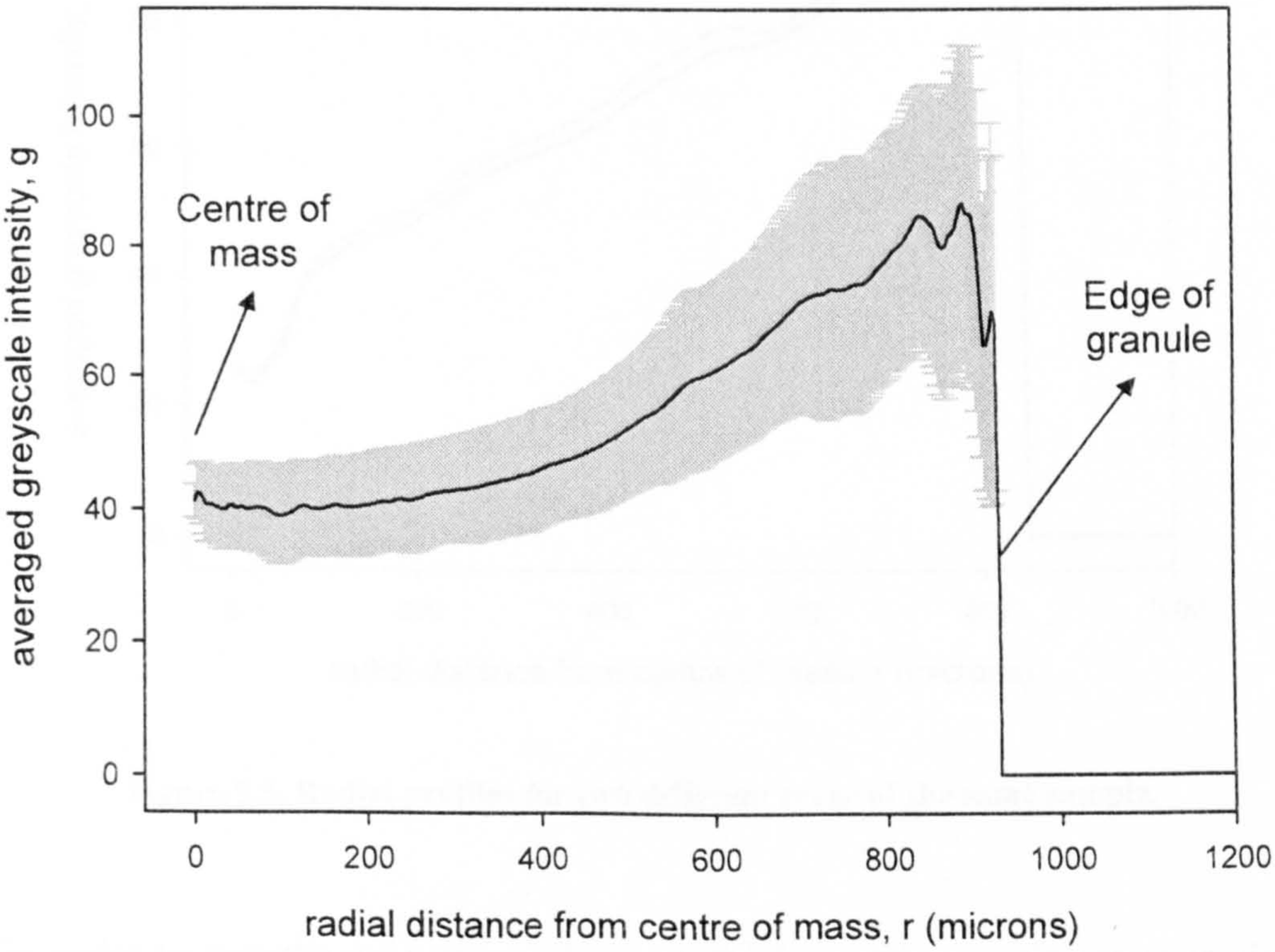

Figure 5.4. Example of radial profile. The y axis shows the greyscale intensity value with increasing values corresponding to more absorbent materials. The x axis shows the radial distance to the calculated centre of mass of the particle. The grey bars correspond to calculated standard deviation in each of the bins.

5.1.3 Validation of the method

The repeatability of the scans was tested by scanning the same sample twice under the same experimental settings, but with a different position of the sample on the specimen holder. Calculations of the centre of mass and the radial profiles were carried out independently for both scans.

The results obtained are shown in Figure 5.5 indicating good agreement, proving the independence of sample orientation and the repeatability of the scan.

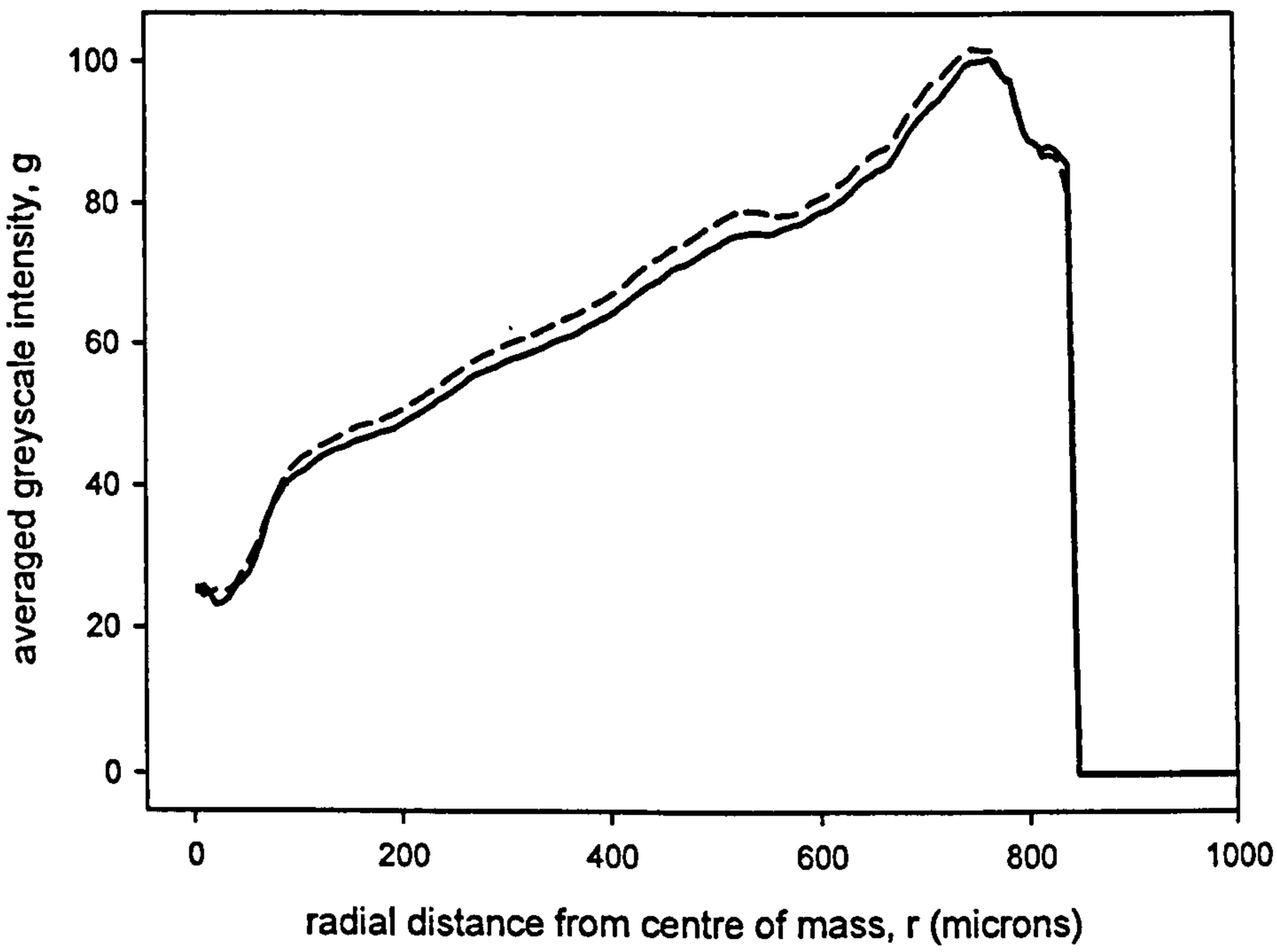

Figure 5.5. Radial profiles for two different scans of the same sample.

In order to test the robustness of the method against possible errors in the calculation of the centre of mass and their effect in further analysis, the following test was devised. The centre of mass and radial greyscale profile were calculated for a given sample. The radial profile was then re-calculated for induced perturbations in the coordinates of the centre of mass. The perturbations were made in each and all of the three spatial coordinates, ranging from 1 to 10% of the radius of gyration (s) of the sample.

The radius of gyration is a parameter characterizing the size of a body of any shape. For a rigid particle consisting of mass elements of mass m_i, each located at a distance r_i from the centre of mass, the radius of gyration, s, is defined as the square root of the mass-average of r_i^2 for all the mass elements,

$$s = \left(\frac{\sum_i m_i r_i^2}{\sum_i m_i} \right)^{1/2} \tag{8}$$

If we approximate that the greyscale intensity shown in the cross sections is proportional to the material density, and given that the volume of the individual voxels that make up the granule is constant throughout the sample, the radius of gyration can be calculated as,

$$s \approx \left(\frac{\sum_i g_i r_i^2}{\sum_i g_i} \right)^{1/2} \tag{9}$$

For a sphere of constant density the radius of gyration is $\sqrt{15}/5$ of the sphere radius.

Figure 5.6 shows the effect of perturbations on the position of the centre of mass in the radial greyscale profiles. The agreement in the profiles proves the robustness of the method to possible errors in the calculation of the centre of mass of the sample.

The differences at radial distances close to centre of mass are due to the small number of pixels contained in the central bins, a different value in a small number of pixels can cause a big difference from the unperturbed profile. This effect disappears when the size of the bins increases at bigger radial distances.

The edge of the granule is found at different radial distances in each case, the granule seems to become larger the more the position of the centre of mass is shifted. This is due to the positioning of the centre of mass itself and the amount by which the granule is "enlarged" corresponding to the amount the position of the centre of mass has been shifted.

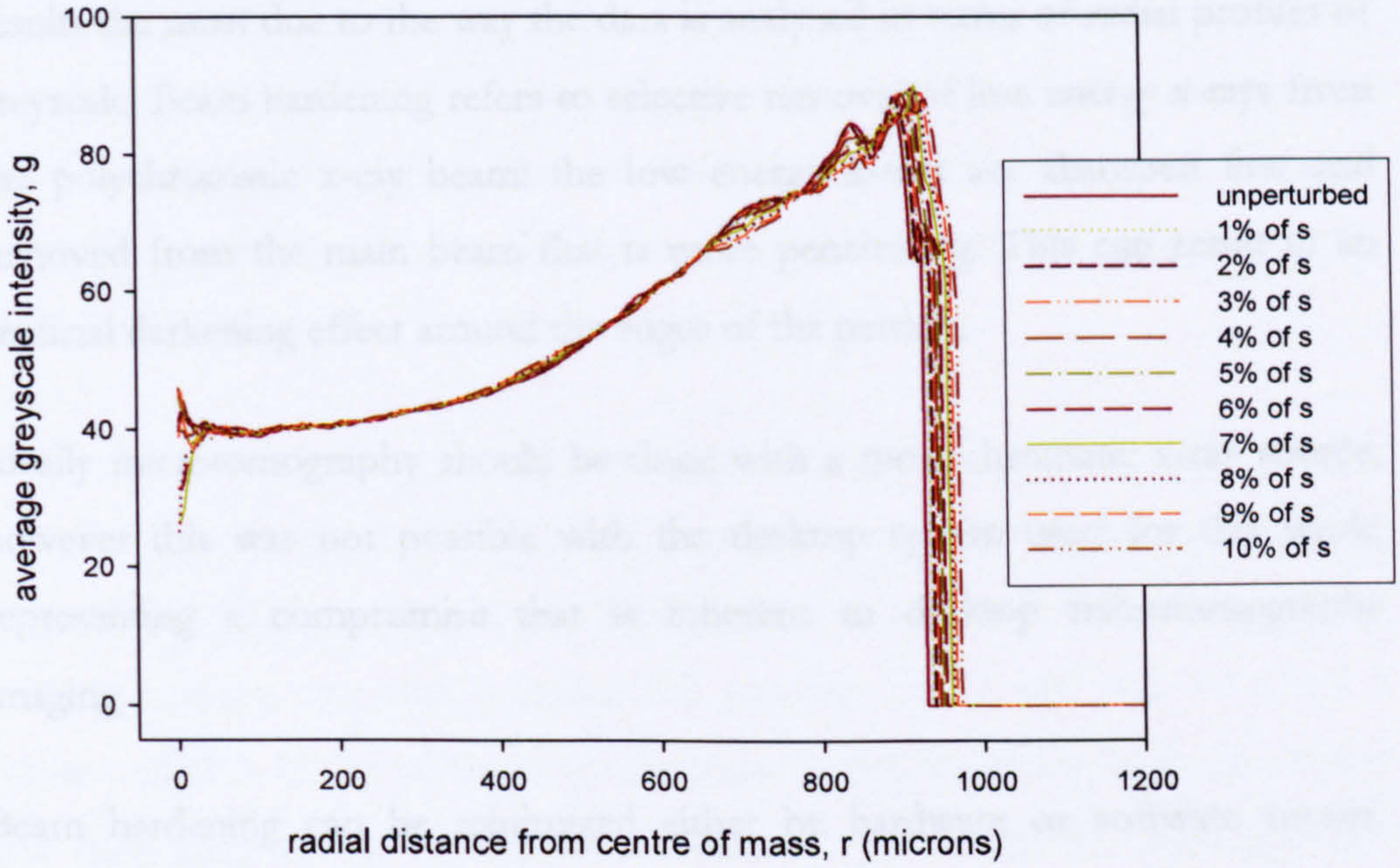

Figure 5.6. Radial profiles based on perturbations of the centre of mass. Perturbations were made in the x, y and z directions, with values ranging from 1 to 10% of the value of the radius of gyration of the sample.

5.1.4 System drawbacks: beam hardening

Possible errors can arise from artefacts related to the technique, such as ring artefacts, noise, or beam hardening.

Signal-to-noise ratio can be increased by decreasing the rotation step in the scanning procedure or by increasing the frame averaging, at the expense of increased scanning time.

Ring artefacts are due to the incremental rotation of the object-camera geometry in combination with non-uniformity of the x-ray detection performance of individual camera pixels. A background subtraction, that creates a uniform background image, is carried out to minimize this effect, referred to as "flat-field" correction.

However, it is the beam hardening the effect that could potentially affect the results the most due to the way the data is analyzed in terms of radial profiles of greyscale. Beam hardening refers to selective removal of low energy x-rays from the polychromatic x-ray beam: the low energy x-rays are absorbed first and removed from the main beam that is more penetrating. This can result in an artificial darkening effect around the edges of the particle.

Ideally microtomography should be done with a monochromatic x-ray source; however this was not possible with the desktop system used for this work, representing a compromise that is inherent to desktop microtomography imaging.

Beam hardening can be minimized either by hardware or software means. Hardware methods involve the use of metal filters on the path of the x-rays to harden the beam (remove low energy x-rays) and the use of low voltages to remove the high energy x-rays. Beam hardening makes the relationship between the attenuation and the thickness of the material non-linear; however there are software means that can correct this non-linearity by modelling the non-linear relationship. SkyScan software models this relationship with a quadratic function that has to be adjusted by the analyzer by trial and error, until the effect is no longer visible [66].

Hardware methods were tried to minimise beam hardening. Filters significantly reduced the signal to noise ratio of the results lowering the quality of the resulting images. Reducing the operational voltage can potentially also reduce the beam hardening effect, although this was not possible as at low voltages the x-ray beam was not energetic enough to completely penetrate through the sizes and materials used in the experiments.

The software beam hardening correction tool was tuned until the presence of beam hardening in the images was minimal for the samples scanned. With this correction, the effect of beam hardening was not thought to be of much importance for the size and materials used in the experiment. However a test involving scans using half (180°) and full rotations (360°) of the same samples

was devised in order to verify it. The flux of energy experienced by a sector on a sample after half and full rotations can be calculated; if the amount of x-rays that go through a given sector in a sample is not the same for a half rotation and a full rotation scan, and the effect of beam hardening is important, the radial greyscale profiles for the sample scanned with half and full rotation should be different.

Therefore the amount of energy received at a given point in the surface of the sample was calculated for full/half rotation scans (Figure 5.7). The radial greyscale profile for a sample was calculated using the method described earlier after two scans, one that included full rotation (360°) and one with half a rotation (180°). If the radiation is not uniform and the beam hardening effect was significant for the experimental conditions presented, the radial greyscale profiles should be different for full/half rotation scans, even for the same granule.

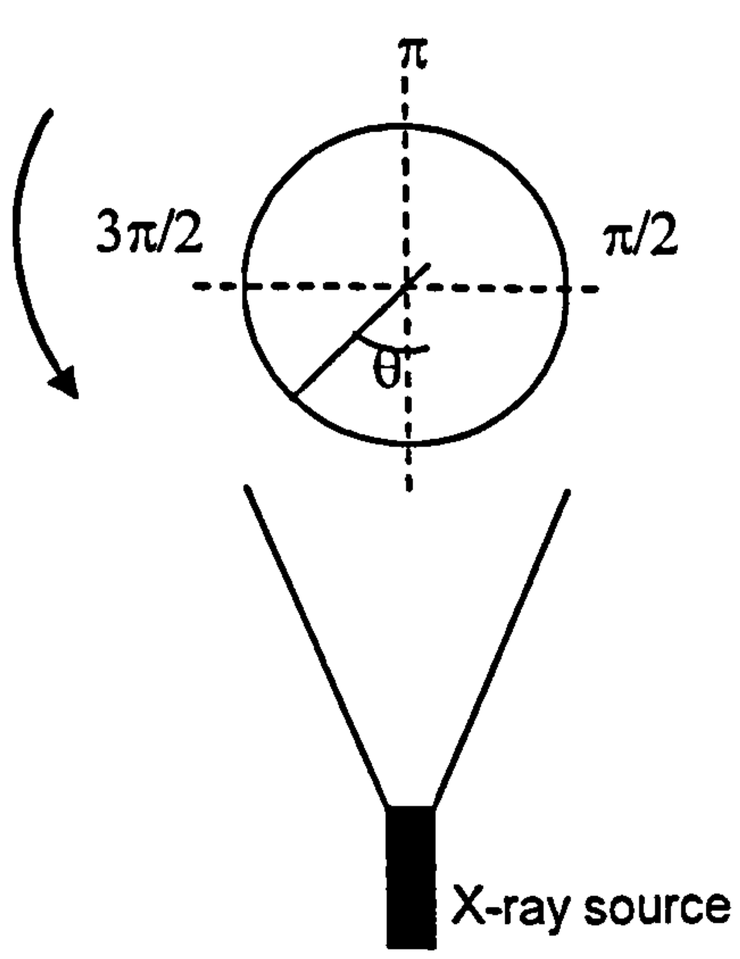

Figure 5.7. Schematic of the rotational positions of the sample during a scan.

The flux density of the x-rays normal to the surface of the sample can be expressed as:

$$\phi = \phi_0 \cos\theta; \quad -\frac{\pi}{2} \le \theta \le \frac{\pi}{2} \tag{10}$$

Let's consider now a sector on the sample starting at an angle $\theta = \alpha_0$ that rotates to $\alpha_0 + \Delta\alpha$. The possibilities are that the scan is carried out with a half rotation ($\Delta\alpha = \pi$) or with a full rotation ($\Delta\alpha = 2\pi$):

For a half rotation (180°) scan: $\Delta\alpha = \pi$.

For a sector starting in the rear half of the sample, $\pi/2 < \alpha_0 < 3\pi/2$ (hidden from incident radiation at the start of the scan) the average flux density experienced by the sector per 180° rotation can be calculated as:

$$\bar{\phi}_{(\alpha_0)} = \frac{1}{\pi}\int_{\frac{3\pi}{2}}^{\alpha_0+\pi} \phi_0 \cos\theta d\theta = \frac{\phi_0}{\pi}\left[\sin(\alpha_0+\pi) - \sin\left(\frac{3\pi}{2}\right)\right] = \frac{\phi_0}{\pi}(1-\sin(\alpha_0)) \quad (11)$$

For a sector starting in the front half of the sample, $-\pi/2 < \alpha_0 < \pi/2$ the average flux density per 180° rotation, can be calculated as:

$$\bar{\phi}_{(\alpha_0)} = \frac{1}{\pi}\int_{\alpha_0}^{\frac{\pi}{2}} \phi_0 \cos\theta d\theta = \frac{\phi_0}{\pi}\left[\sin\left(\frac{\pi}{2}\right) - \sin(\alpha_0)\right] = \frac{\phi_0}{\pi}(1-\sin(\alpha_0)) \quad (12)$$

For a full rotation (360°) scan: $\Delta\alpha = 2\pi$.

In this case it does not matter whether the sector starts at the back or the front, since every point is going to go through a full rotation. The average flux density per rotation can be calculated as:

$$\bar{\phi}_{(\alpha_0)} = \frac{1}{2\pi}\int_{-\pi}^{\pi} \phi_0 \cos\theta d\theta = \frac{\phi_0}{2\pi}[\sin(\pi) - \sin(-\pi)] = \frac{2\phi_0}{2\pi} = \frac{\phi_0}{\pi} \quad (13)$$

The resulting flux densities normal to the surface of the sample were plotted as a function of the angular position for full/half rotation scans (Figure 5.8). It can be seen that the amount of energy is non-uniform and depends on whether the scan is carried out with a full or half a rotation. Therefore, if beam hardening was of relevance in the experimental cases studies presented herein, the radial greyscale profile of the same sample, obtained from a scan carried out with a full rotation should be different than the profile of the same sample obtained after a scan with only half a rotation. If the profiles were the same it would mean that beam hardening has an insignificant effect on the resulting radial profiles, and therefore carrying out scans with a half a rotation would be the preferred method as it would half the amount of time required for the scan of the sample.

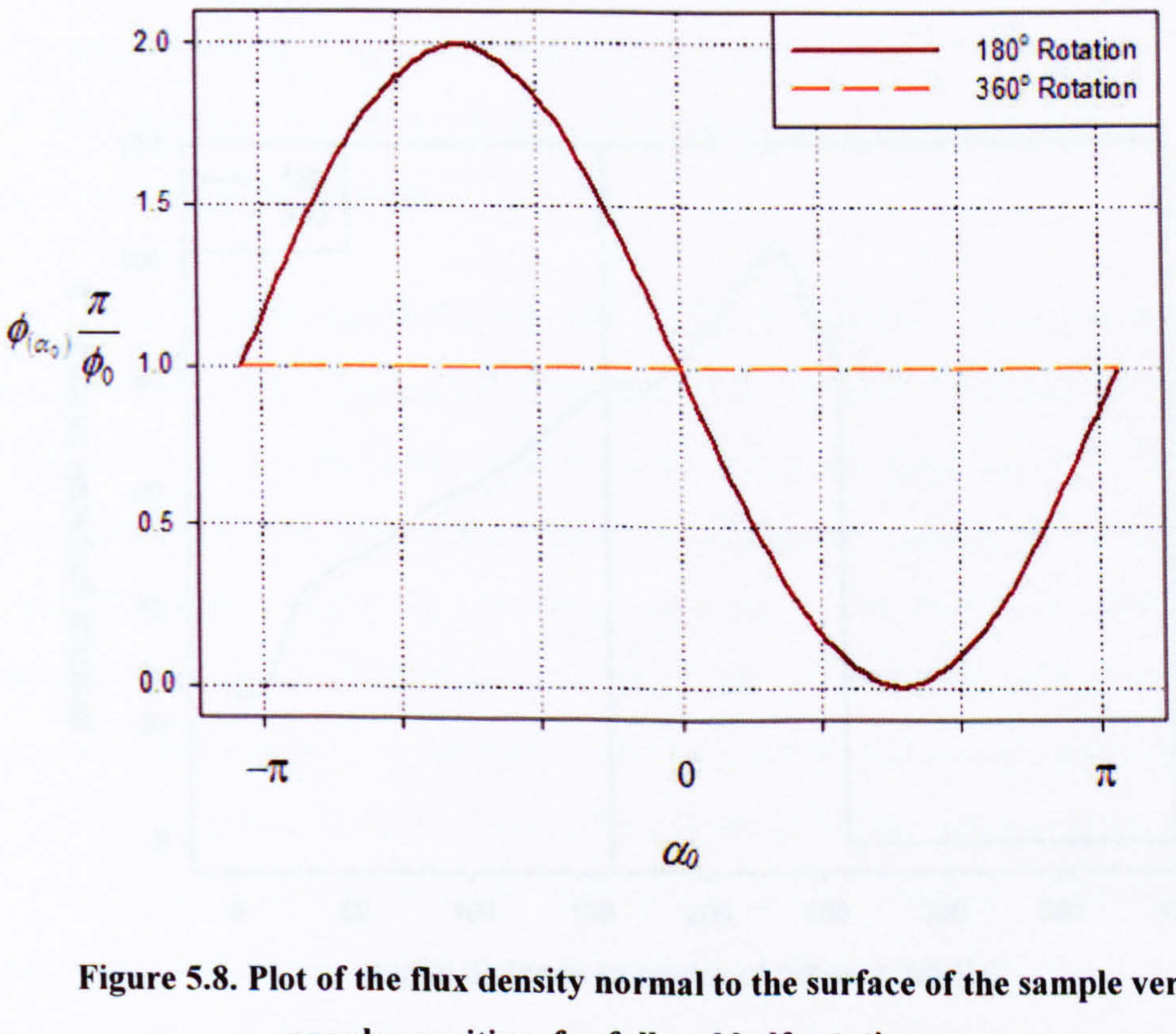

Figure 5.8. Plot of the flux density normal to the surface of the sample versus angular position, for full and half rotation scans.

In order to verify this, one sample was scanned using full and half rotation. The central cross-section of the granule can be seen in Figure 5.9 and the corresponding radial greyscale profiles, calculated according to the method explained above, and are shown in Figure 5.10.

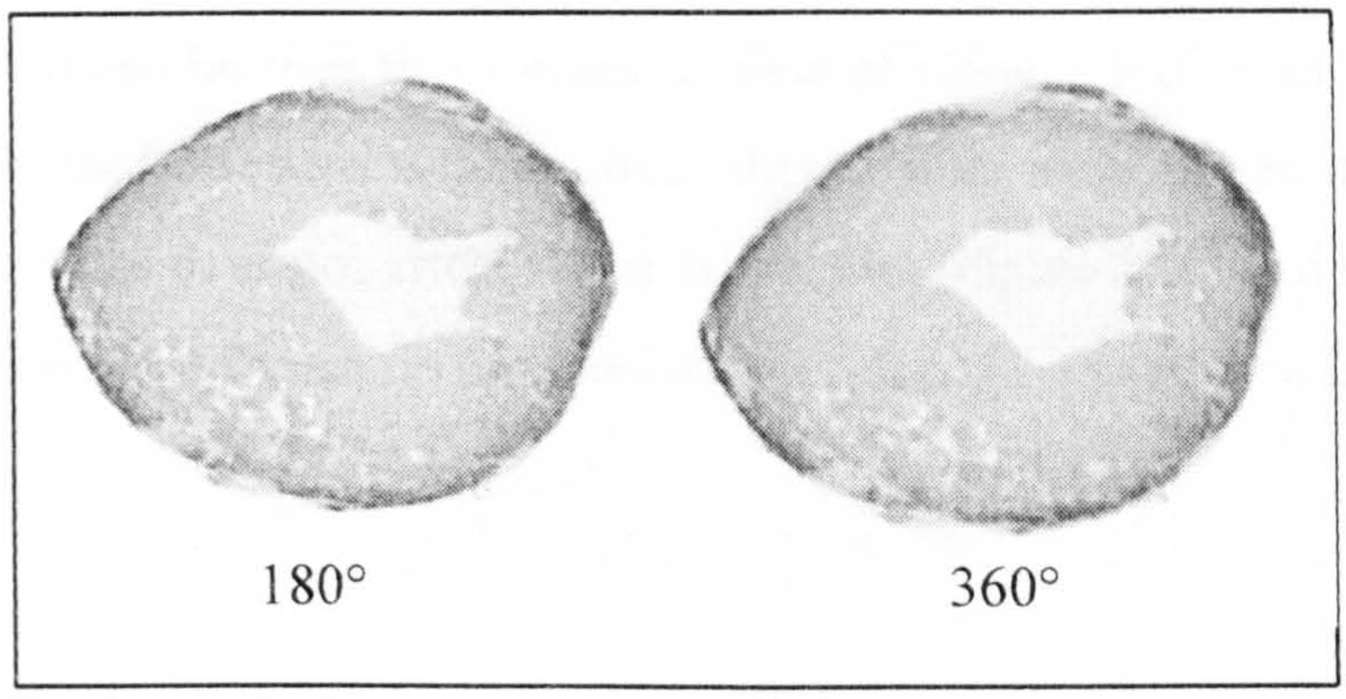

Figure 5.9. Central cross-section corresponding to the same sample after a half and a full rotation scan.

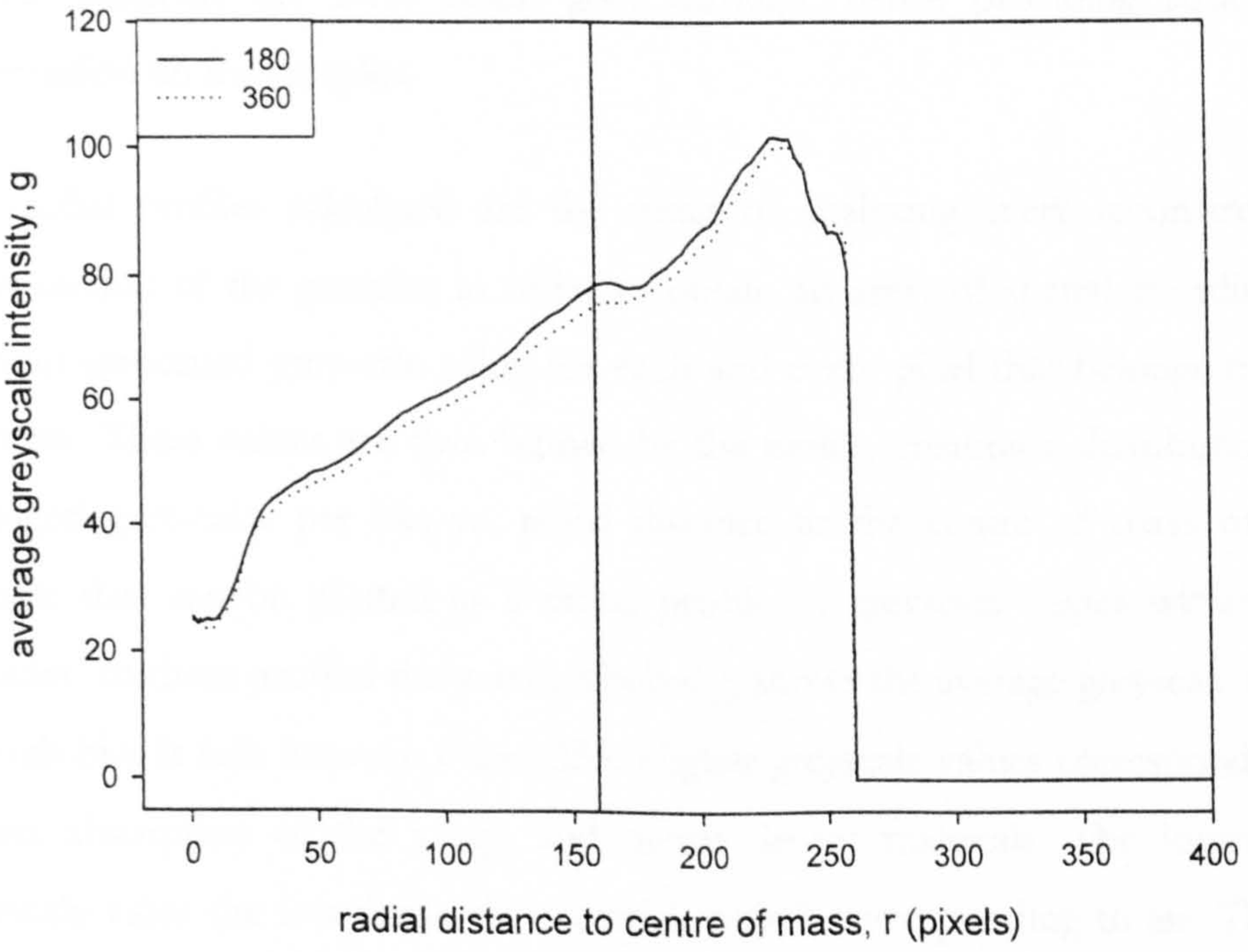

Figure 5.10. Radial greyscale profiles for the same sample after full and half rotation scans. The vertical lines identify the position of the radius of gyration of the sample.

The radial profiles do not differ for the different scans, proving that the effect of beam hardening is not affecting the results. From the cross-sections shown in Figure 5.9 it can be seen that the main effect of using a 360° scan over a 180° scan is that the noise level is diminished. On the other hand, due to the nature of the method this does not affect the radial profiles (Figure 5.10) and carrying out half rotation scans speeds up the acquisition of shadow images by a factor of 2.

5.1.5 Method summary

A method for analyzing x-ray tomography results on single granules has been developed. This method can transform raw data in a single radial profile of greyscales within the granule, avoiding the subjectivity of looking at the all the individual resulting images. These greyscale values are dependant on the density of the materials the x-ray beam goes through, hence providing structural information on the samples.

The radial profiles calculated are the result of analyzing every reconstructed cross-section of the granules in order to obtain an array of spatial coordinates with an associated greyscale value for each and every pixel that belongs to the granules. These values are then binned by the radius, creating a distribution of averaged greyscales per bin vs. radial distance to the centre of mass of the granule that can be plotted as a radial profile of greyscale values within the granules. In these profiles the y-axis, labelled g, shows the average greyscale value of each bin. It falls between 0 and 255. Higher greyscale values correspond to a higher absorption of the x-rays and hence denser materials. The lower the greyscale value the less dense the material, with 0 corresponding to air. The x-axis, labelled r, shows the radial distance from the centre of each bin to the centre of mass of the particle, hence $r = 0$ corresponds to the calculated centre of mass of the granule.

The reproducibility of the scans was tested by scanning the same sample with different orientations, obtaining matching results. The profiles indicate increasing consolidation towards the edge of the granule as expected from the granulation process.

The robustness of the method was tested by studying the influence of perturbations in the coordinates of the calculated centre of mass on the resulting radial profiles. Good agreement in the resulting profiles was found up to perturbations of 10% of the value of the radius of gyration of the sample.

6

RESULTS: QUANTITATIVE ANALYSIS

6.1 Introduction

As already discussed in Chapter 4 (Section 4.2) a series of experiments were devised in order to understand the structural changes that occur during the granulation process and how they are affected by process and formulation parameters. A group of "granulation series" experiments were carried out. Each of the series studied the effect of a process or formulation parameters. The parameters chosen were those that have a known effect on the properties of the resulting agglomerates. Calcium carbonate and polyethylene glycol were used as the granulation system

Properties are known to be linked to structure [1], so the modification of these parameters will create the bigger structural changes in the granules, visualized by means of XRT. The following "series" were carried out:

- Process parameters: granulation time (at low shear), impeller speed.
- Formulation parameters: primary particle size, binder molecular weight, binder to solid ratio.

The granulation series were discussed qualitatively in Chapter 4 (4.2). In this chapter, the method developed in Chapter 5 is applied to extract quantitative structural information as radial profiles within the granules. Information about the strength and dissolution properties of the granules will also be discussed when available.

All the granules shown here are taken from the same sieve cuts. However, this is only a size range; therefore the individual samples have slightly different sizes from each other. In order to be able to compare the profiles of granules of different sizes, the x-axis of the radial profiles has been normalized by dividing the radial distance *(r)* by the radius of gyration *(s)* of each sample. The data is analyzed up to a value of $r/s = 1$. This allows a comparison of the different sized granules and furthermore, it eradicates artefacts like beam hardening which, if present, is located at the very edge of the sample.

6.2 GRANULATION TIME AT LOW SHEAR

Figure 6.1 shows the radial profiles associated with the samples scanned. For each granulation time, an increased densification towards the edge of the granule occurs. This is consistent with the images of the cross-sections previously shown, which indicated the binder to be preferentially located towards the centre of the granules (Figure 4.15). The experimental conditions have already been given in Table 4.3 and are repeated below (Table 6.1).

The radial profiles show sudden changes in the greyscale value at low values of r/s. They can be seen for example in Figure 6.1-a for granule 1, with a sudden increase on the g value; or in Figure 6.1-c for granule 1, with a sudden decrease in g followed by a step increase before becoming more constant. These variations at low r/s happen because of the small number of pixels that are included in the bins close to the centre of mass of the granules, creating a greater uncertainty when calculating the average value of g for the bin.

Table 6.1. Experimental settings for the granulation time experiments.

Process parameters	
Binder addition method	Melt-in
Impeller speed (rpm)	200
Chopper speed (rpm)	1400
Granulation time (min)	2, 4, 6, 10, 15
Temperature (°C)	60
Granule size (μm)	1000-1180
Formulation parameters	
Primary particles (S)	Durcal40 (2000 g)
Binder (L)	PEG1500 (260 g)
Binder to solid ratio (L/S)	0.13

The profiles for 2 minutes of granulation time (Figure 6.1-a) are consistent with each other and show similar trends with starting intensity values of around 20, final intensity values between 60 and 70 with relatively constant slopes. For other granulation times examined (Figure 6.1-b, c, d and e) the starting intensity values are higher than after 2 minutes of granulation time, with different values for the different samples. However the final values all fall in the region between 60 and 80. There is a significant amount of scatter between the different profiles for a given granulation time. This is expected due to the highly heterogeneous nature of the granulation process.

The profiles were averaged for each of the granulation times and the resulting profiles are shown in Figure 6.1-f. The density of the granules increase with increasing granulation time. The profiles show a different behaviour between the 2 minutes samples and the rest of the results. Granulation times of 4, 6, 10 and 15 minutes show very similar results although unexpectedly the averaged profile for 4 minutes of granulation time shows slightly higher values of greyscale than longer granulation time granules. Looking at the x-ray cross sections corresponding to the 4 minutes granulation time (Figure 4.14-b), it can be seen that only 3 out of the 5 granules chosen at this granulation time for scanning

show an internal region of unmixed binder, whereas for higher granulation times at least 4 of the 5 granules (Figure 4.14-c, d and e) show it, explaining the observed difference in averaged greyscale.

The big difference between the samples after 2 minutes of granulation and later times seem to indicate that the major structural changes happen in the early stages of granulation (within 2 minutes)for the experimental conditions studied, with no major changes in the internal structure thereafter.

The increase in density towards the edge, indicated by the slope of the profiles, of the granule is more accentuated for the 2 minutes granules. For the rest of the granulation times, the slope remains nearly constant. Figure 6.2 shows how the radial densification is much stronger at the early stages of granulation and then stabilizes at a lower value for further times. This supports the idea that the major changes in the granule structure happen at the initial granulation period.

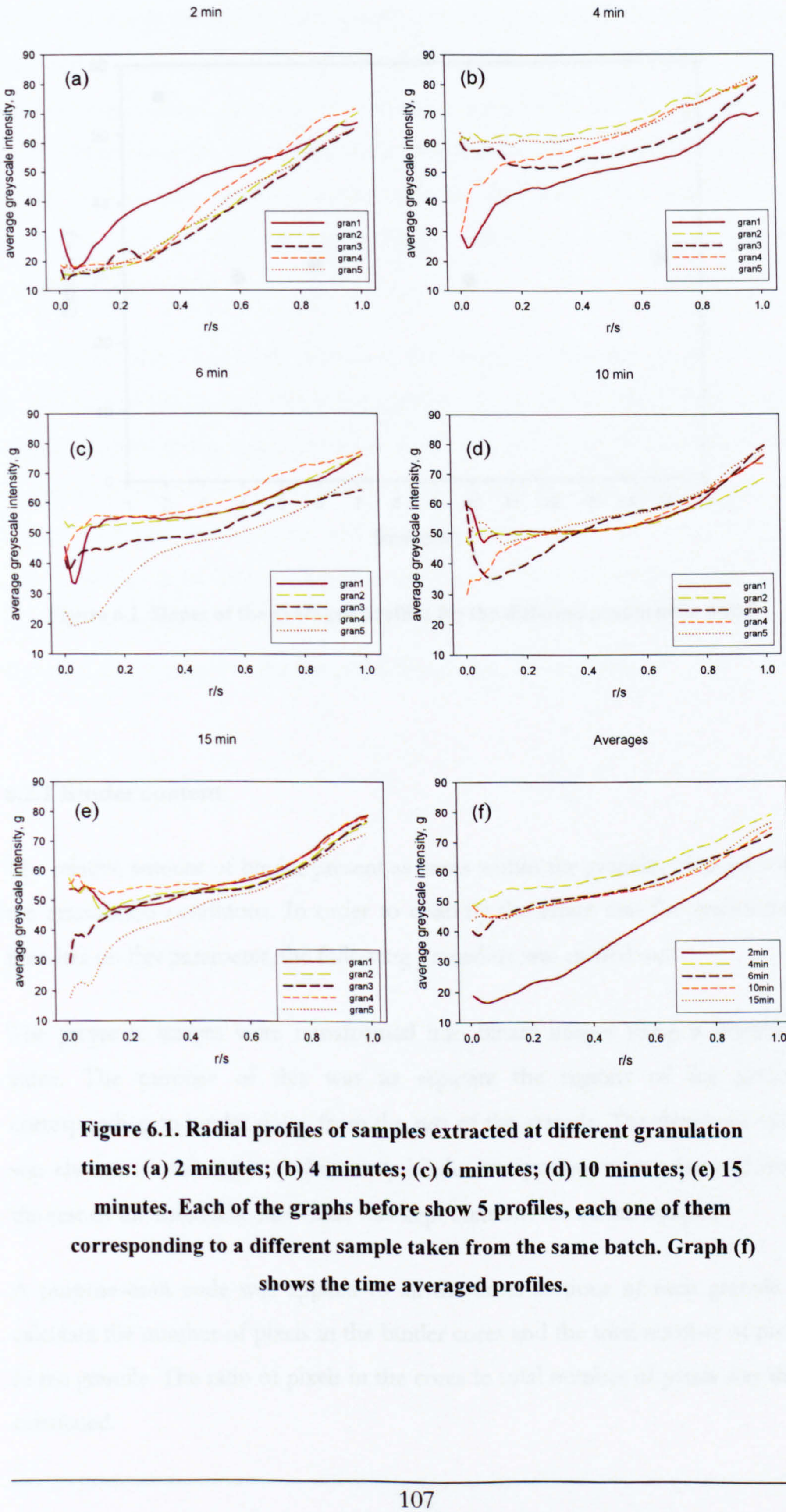

Figure 6.1. Radial profiles of samples extracted at different granulation times: (a) 2 minutes; (b) 4 minutes; (c) 6 minutes; (d) 10 minutes; (e) 15 minutes. Each of the graphs before show 5 profiles, each one of them corresponding to a different sample taken from the same batch. Graph (f) shows the time averaged profiles.

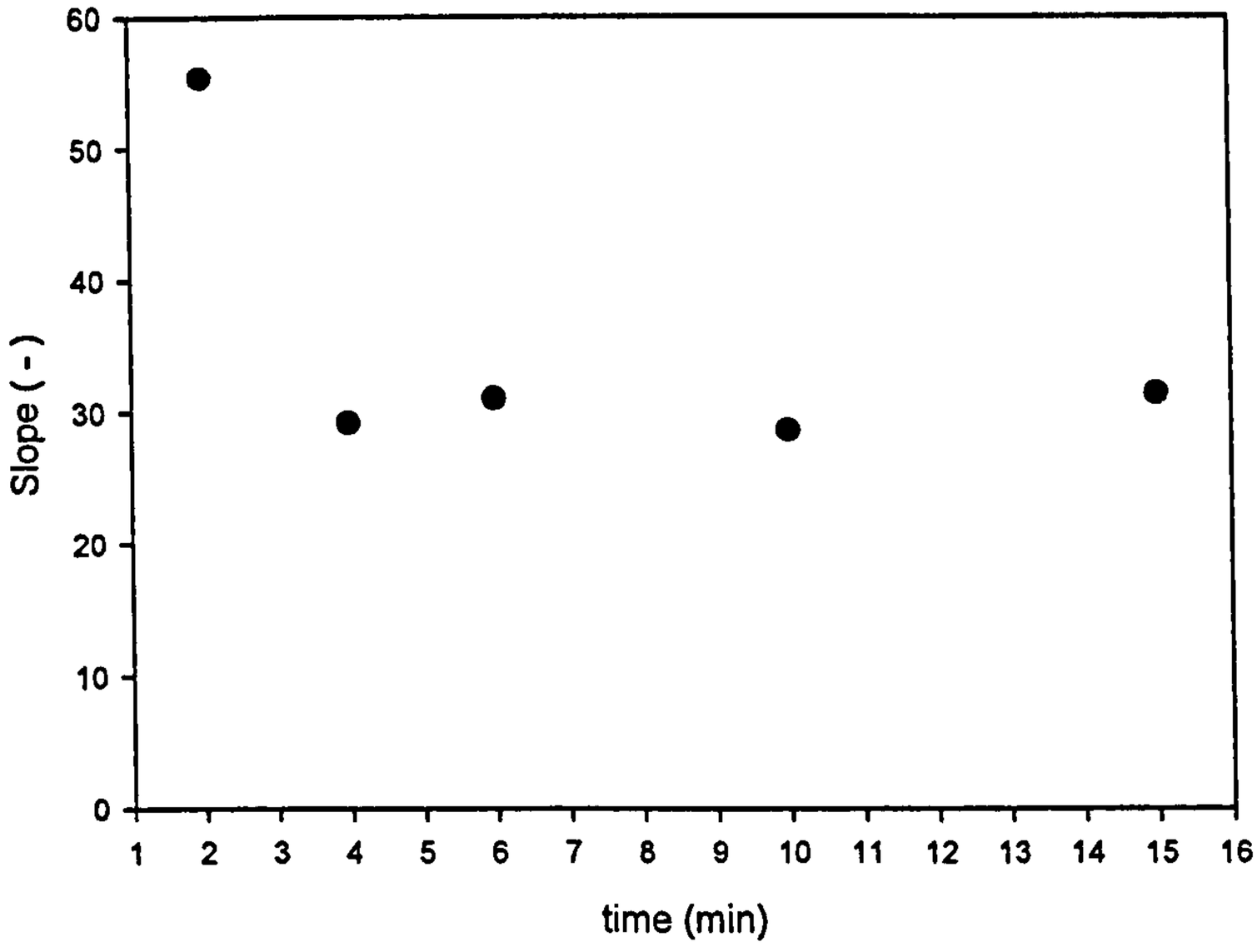

Figure 6.2. Slopes of the averaged profiles for the different granulation times

6.2.1 Binder content

The relative amount of binder present as cores within the granules changes with the granulation conditions. In order to quantify the effect that the granulation time has on this parameter, the following procedure was carried out.

The greyscale images were transformed into binary images using a threshold value. The purpose of this was to separate the regions of the granule corresponding to binder cores from the rest of the granule. The threshold value was chosen so that regions where only binder was present were separated from the rest of the materials. The value was kept constant for all the samples.

A purpose-built code was applied to all the cross-sections of each granule to calculate the number of pixels in the binder cores and the total number of pixels in the granule. The ratio of pixels in the cores to total number of pixels was then calculated.

Figure 6.3 shows the results corresponding to the granulation time series. It is evident that the amount of binder is much greater for the samples taken after 2 minutes of granulation time. For the rest of the samples the binder ratio remains practically constant for granulation times from 4 to 15 minutes. This, in addition to the images and profiles shown, indicate that under the experimental conditions used, the major structural changes within granules happen within 4 minutes of granulation.

The relative amount of binder shown in the graphs corresponds to the amount of unmixed binder present within the granule. The values lay below the amount of binder added to the batch (binder to solid ratio of 0.13) and this is due to the resolution limitations of the scanner. The resolution is not high enough to clearly identify individual components and therefore only regions in which there is enough binder to be detected are accounted for in the masking procedure used for these calculations. However, it is useful to understand how the presence of unmixed areas changes as the operation parameters are changed.

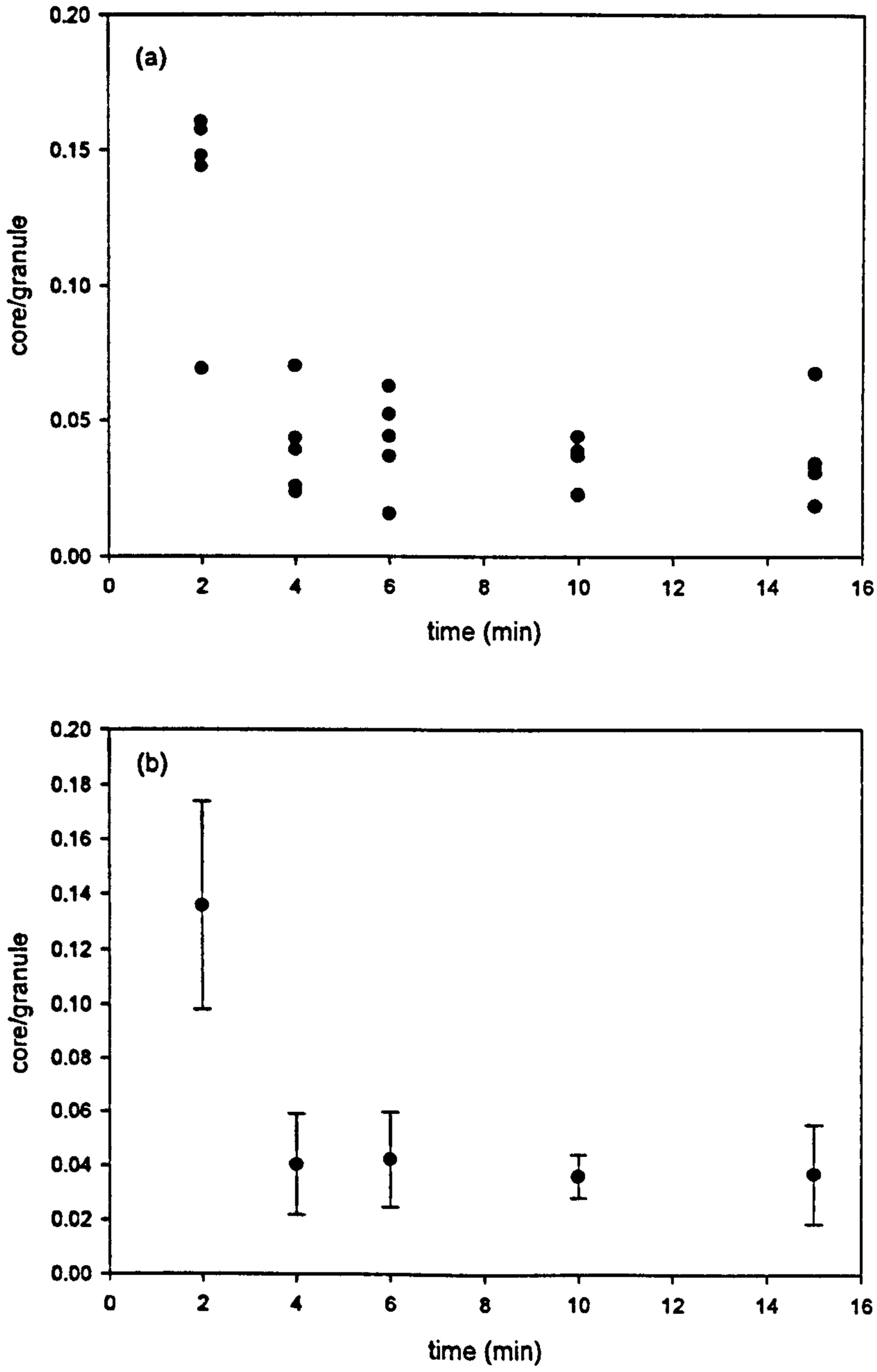

Figure 6.3. Plots of the binder ratio for the granulation time series: (a) values for the individual granules scanned; (b) time averages with standard deviation bars.

6.2.2 Summary time series - nucleation

For every sample scanned in this study increased consolidation was observed towards the surface of the granule.

The effect of the massing time was to increase consolidation of the materials. However the effect was most pronounced only for the earliest of the granulation times. There is a big change between the profiles calculated for the samples taken at 2 minutes of granulation time compared to the others, whereas the differences between the samples after 4, 6, 10 and 15 minutes of granulation time are almost negligible.

The structure of these samples is characterized by the presence of a binder core in the centre of the granule. The structure is very regular and resembles a flake of binder at 2 minutes of granulation. For granulation times from 4 minutes onwards, this core is reduced in size and the flake-like shape is lost, but even after 15 minutes of granulation time it is visible in some of the granules tested.

From these observations it is proposed that with an impeller speed of 200 rpm, the major structural changes occur mainly during the first 4 minutes of granulation.

Schaefer & Mathiesen [13] proposed two different mechanisms for nucleation. The distribution mechanism, characterised by the presence of binder-coated primary particles that coalesce to form the initial granules leading to a homogeneous distribution of the binder; and the immersion mechanism by which primary particles are engulfed by large binder droplets (Figure 6.4).

Both immersion and distribution mechanisms can coexist in the agglomeration process [8, 13, 67]. However X-ray tomography provides evidence of the immersion mechanism being prevalent under the experimental conditions applied here (Figure 6.5). This demonstrates how the application of X-ray tomography to early granulation time samples provides an insight into the mechanisms for melt granulation in a high shear mixer.

Due to the nature of the system studied here (binder added as solid flakes) it was expected that that the immersion mechanism would be prevalent. The flakes of binder act as nuclei initiators when they start to melt. Primary particles stick to the surface of the melting flakes, and then the finest of these progresses towards the centre of the flake squeezing molten material towards the surface. This makes the surface of the granules wet, allowing for further layers of primary powder or smaller nuclei to adhere.

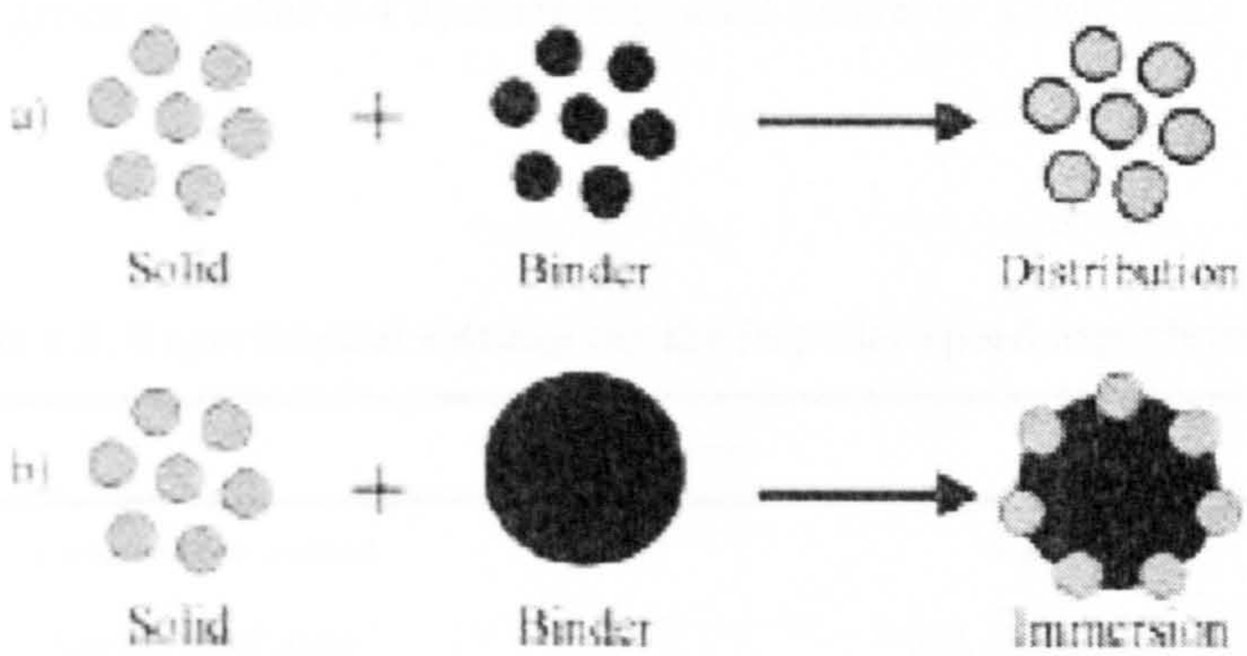

Figure 6.4. Granule formation mechanisms in melt agglomeration: (a) distribution mechanism; (b) immersion mechanism (source [13])

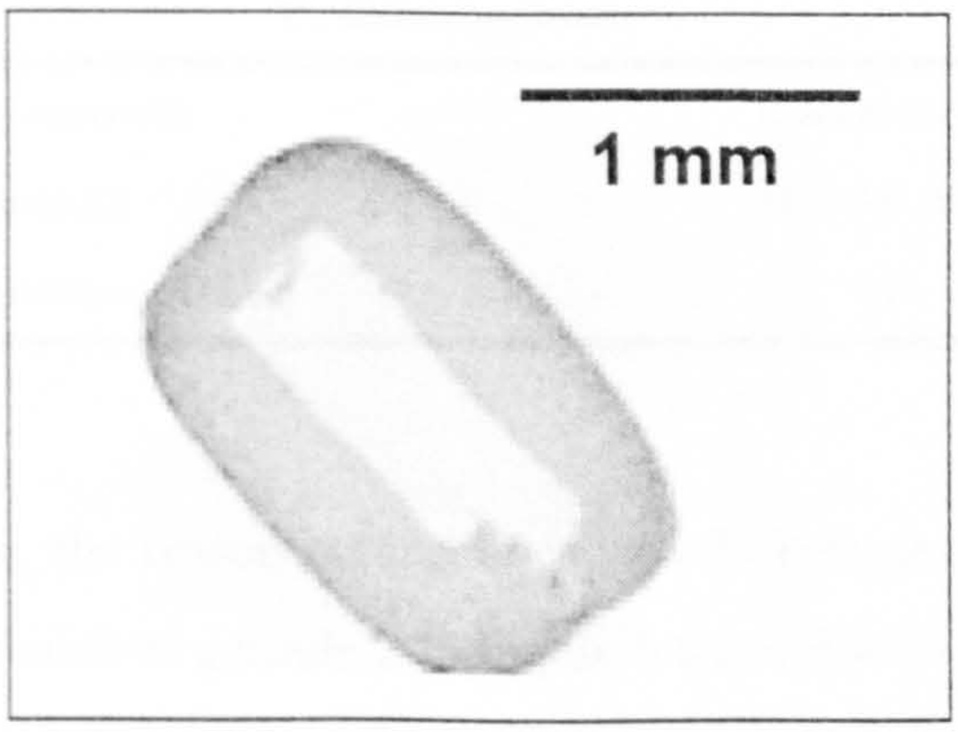

Figure 6.5. Central cross section of a 2-minute granule obtained under low shear conditions. The central core of melting binder gives visual evidence of the immersion mechanism as described by [13].

6.3 IMPELLER SPEED SERIES

Figure 6.6 shows the radial profiles associated with each of the scanned samples. For all of the granules tested they show consolidation towards the surface. This is consistent with the images of the central cross sections (Figure 4.17). It is clearer at the lower impeller speeds, when the presence of binder in the centre of the granule is easily visible, but also for the higher impeller speed the granules look less consolidated towards the centre. The experimental conditions have already been given in Table 4.4 and are repeated below in Table 6.2.

Table 6.2. Experimental settings for the impeller speed experiments.

Process parameters	
Binder addition method	Melt-in
Impeller speed (rpm)	200, 400, 600, 800
Chopper speed (rpm)	1400
Granulation time (min)	10
Temperature (°C)	60
Granule size (μm)	1000-1400
Formulation parameters	
Primary particles (S)	Durcal40 (2000 g)
Binder (L)	PEG1500 (260 g)
Binder to solid ratio (L/S)	0.13

As explained before, the reason behind unexpected decreases in the *g* values at low radial distances such as granule 2 in Figure 6.6-a is due to the small number of pixels that are included in the calculations at small values or r/s, due to the smaller size of the bins in this central regions.

The profiles for the impeller speed of 200 rpm (Figure 6.6-a) are very reproducible except towards the centre of the granule, where starting intensity values range from 20 to over 60. This large discrepancy could be due to the

effect explained above. Apart from this, the scatter between the profiles is minimal, with final intensities around 70. These profiles are consistent with the ones shown in Figure 6.1-d, which confirm granules to have the same characteristics although from different experiments.

The scatter between profiles is much greater for the rest of the impeller speeds tested (Figure 6.6-b, c and d), but the shape of the profiles is consistent for each of the impeller speeds tested. In the case of 400 rpm (Figure 6.6-b) the profiles seem to be composed of two different trends, with a fairly constant *g* value up to an *r/s* value of around 0.5, followed by a gradual increase on *g* towards the edge.

The profiles were averaged for each of the impeller speeds and the resulting profiles are given in Figure 6.6-e. A densification effect is observed for increasing impeller speeds. The profiles for impeller speeds of 400 and 600 rpm are very similar. The differences between the profiles at the lowest impeller speeds (200 rpm) and the profiles for 400 and 600 rpm are more noticeable at the lower values of r/s, towards the centre of the granule. This is consistent with the cross-sections previously shown, whereby at the lowest impeller speed, the centre of the granules is occupied by binder. The profile for 800 rpm has a slope similar to the lower impeller speeds, but the values of *g* are much higher than in the other cases.

The slopes of the averaged profiles, indication of the radial consolidation, were calculated for the different impeller speeds (Figure 6.7). As it can be seen the bigger change happens at the lower impeller speeds, when the presence of binder cores is stronger. At higher impeller speeds the value tends to stabilize.

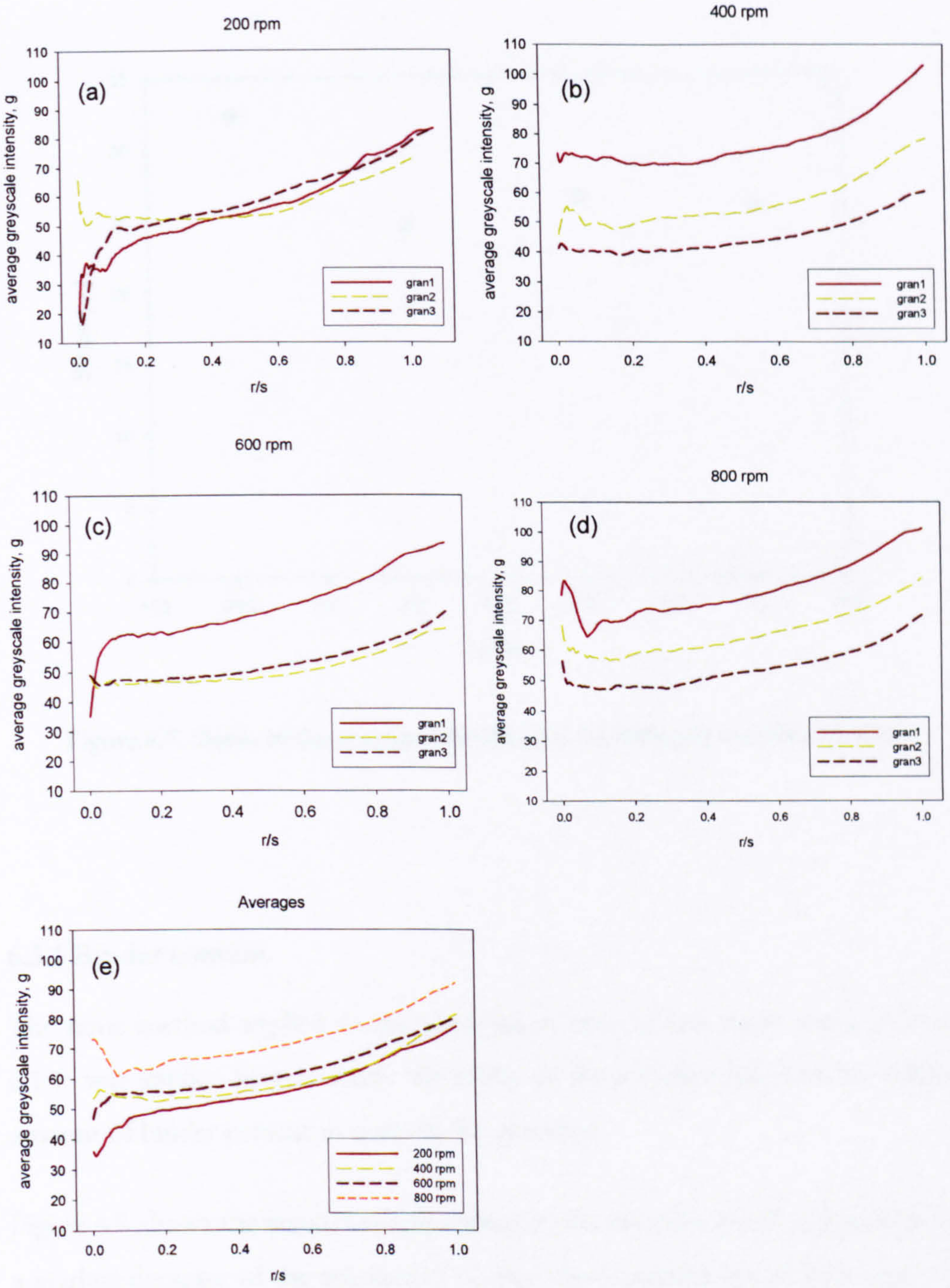

Figure 6.6. Radial profiles of samples with different impeller speeds, the granulation time is 10 minutes in all cases: (a) 200 rpm; (b) 400 rpm; (c) 600 rpm; (d) 800 rpm. Each of the graphs shows 3 profiles, each of them corresponding to a different granule taken from the same batch. Graph (e) shows the impeller averaged profiles.

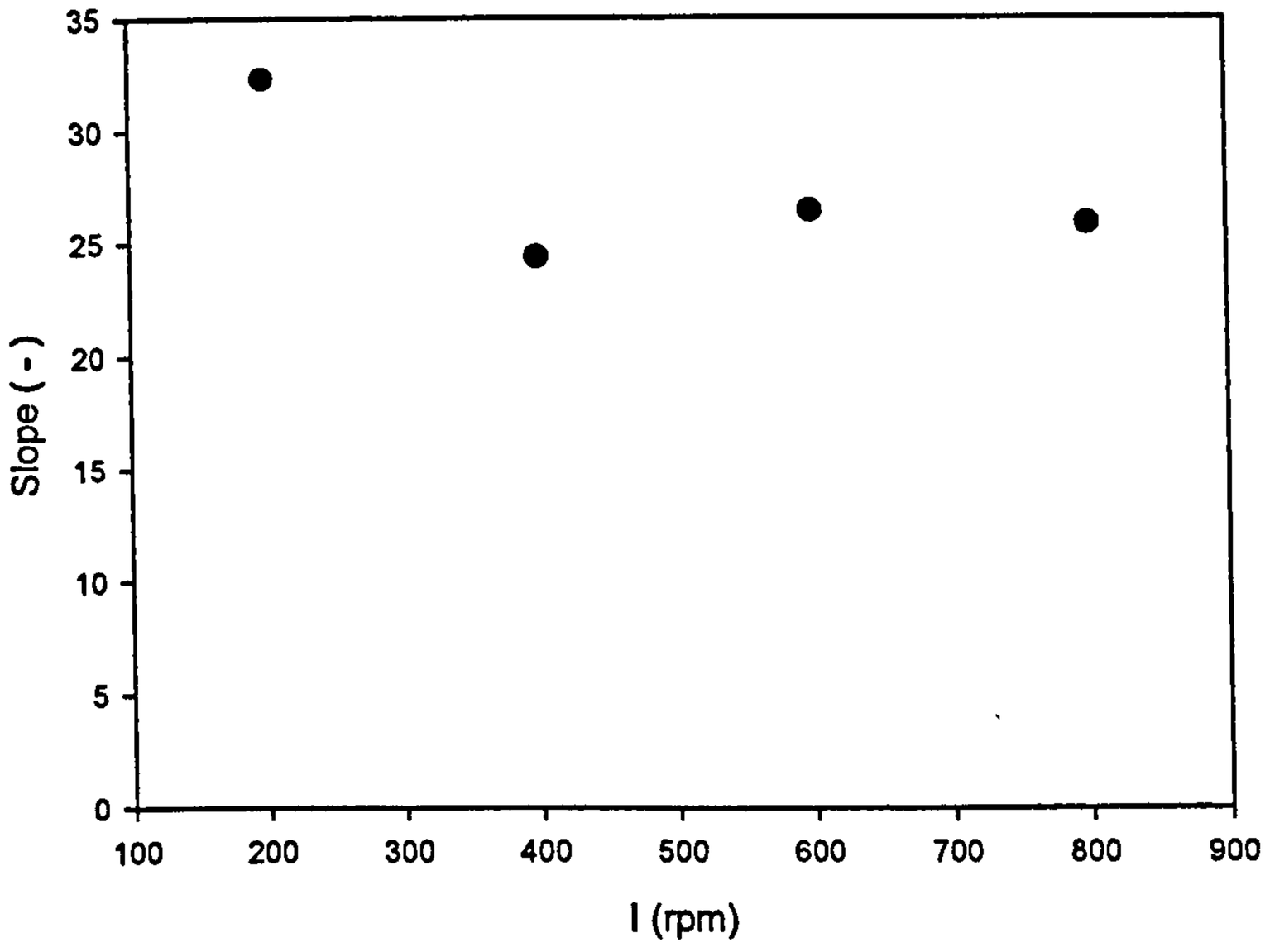

Figure 6.7. Slopes of the averaged profiles for the different impeller speeds.

6.3.1 Binder content

The same method applied to the granulation time at low shear series (Section 6.1.1) was applied here to study the effect of the impeller speed in the relative amount of binder present as cores in the granules.

Figure 6.8 shows the results corresponding to the impeller speed series. It shows a gradual decrease of the amount of binder when impeller speed increases. The open circles in Figure 6.8-a correspond to the five granules that were scanned after 10 minutes of granulation time (Figure 4.15-d). These have the same characteristics as the ones scanned as part of the impeller speed series with an impeller speed of 200 rpm even though they come from a different batch. These five extra granules were also considered for the averages (Figure 6.8-b).

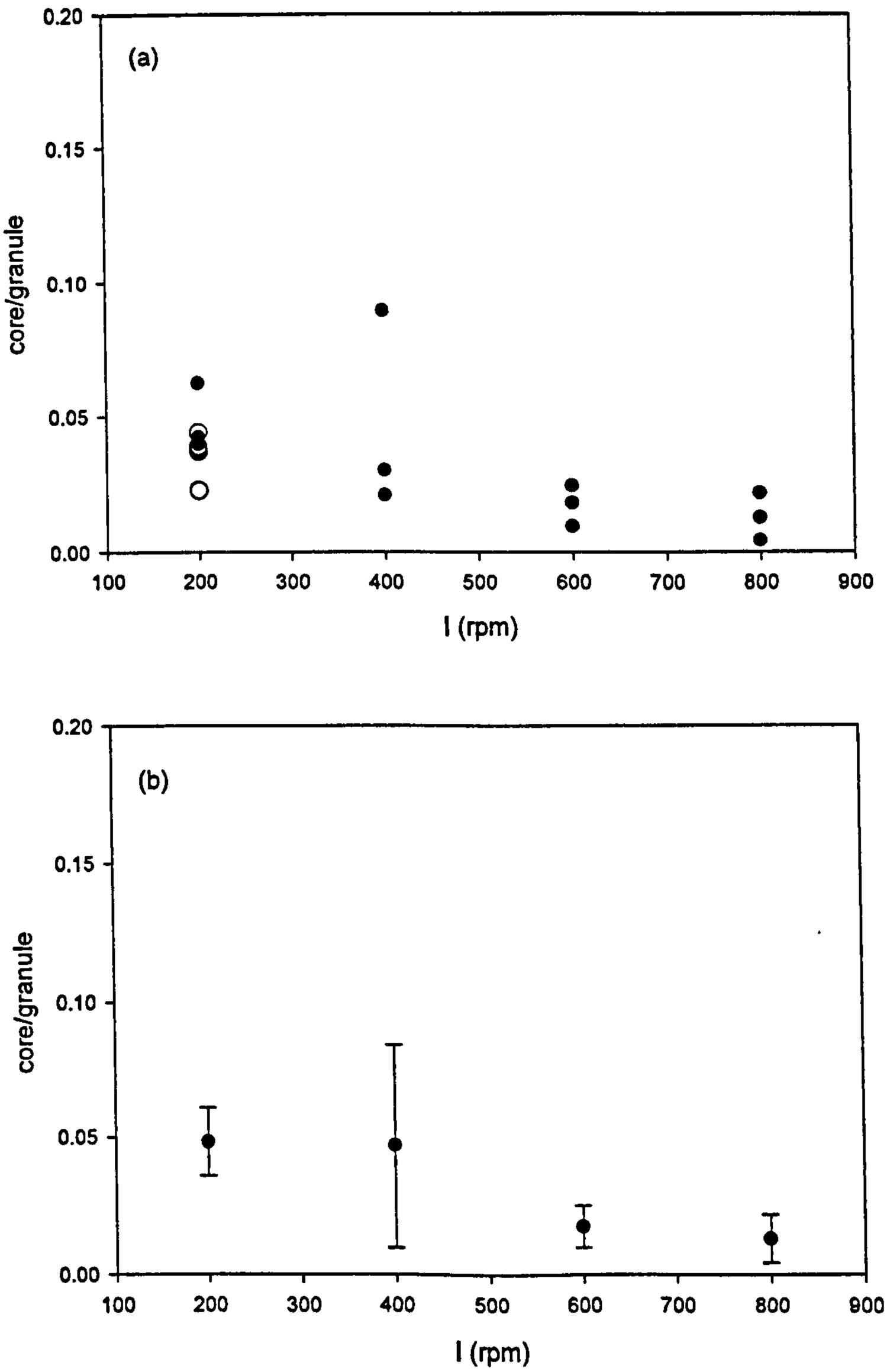

Figure 6.8. Plots of the core volume to granule volume ratio for the impeller speed series: (a) values for the individual granules scanned, the opened circles (o) correspond to the granules scanned for the time evolution series that have the same characteristics as the ones for the impeller speed of 200 rpm; (b) averages for each of the impeller speeds with standard deviation bars.

6.3.2 Strength and dissolution characteristics

The effect of the impeller speed on the dissolution (time t_{90}) and strength characteristics (failure load) of the agglomerates can be seen in Figure 6.9.

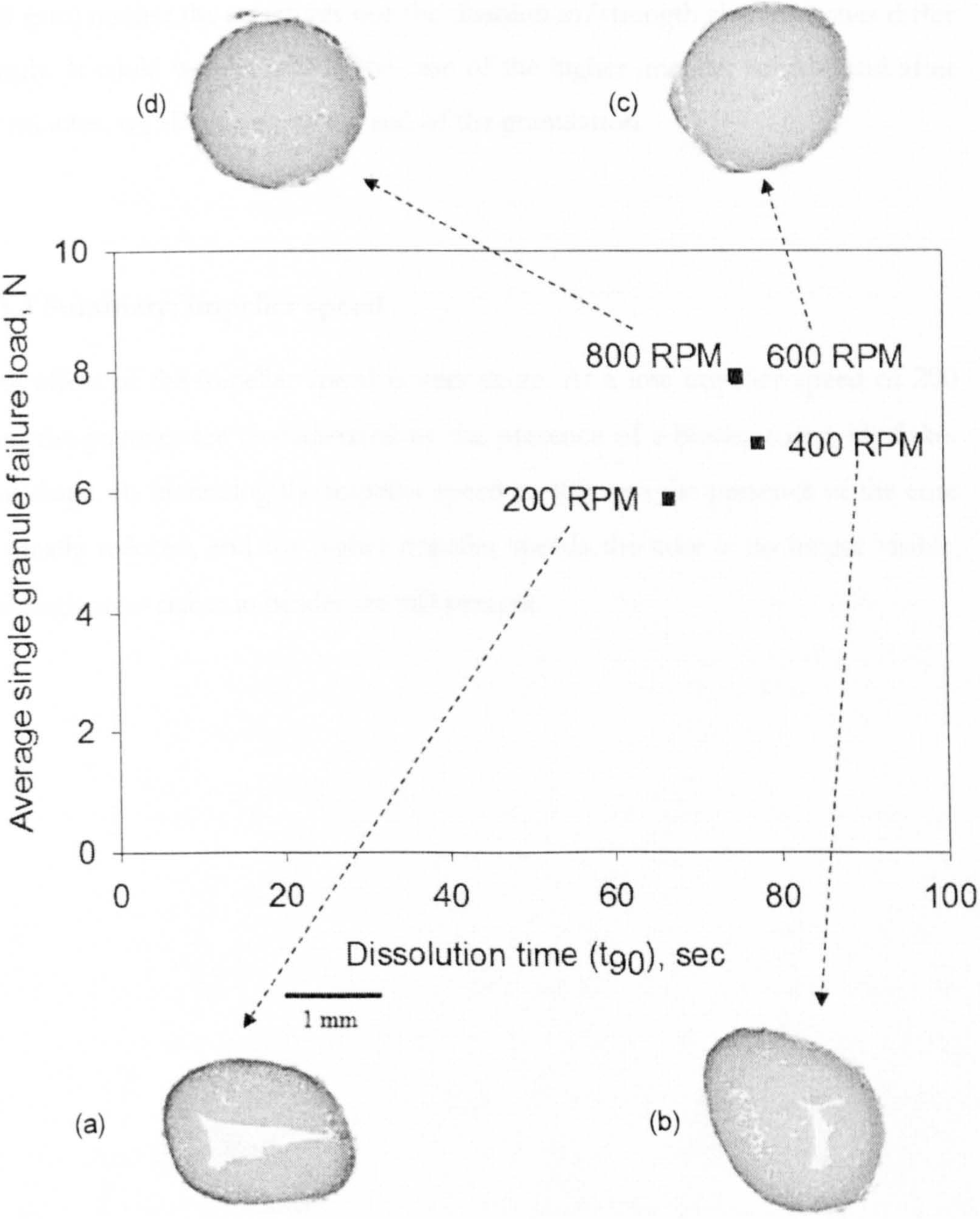

Figure 6.9. Effect on granule strength and dissolution of the impeller speed: (a) 200 rpm; (b) 400 rpm; (c) 600 rpm and (d) 800 rpm.

From these results it can be seen that increasing the impeller speed creates granules which are stronger but also dissolve more slowly. For the lower impeller speeds (200 and 400 rpm) there are big unmixed areas of binder in the centre of the granule. This could explain the lower strength and faster dissolution time, since these unmixed areas can facilitate the entrance of water inside the granule and speed up its dissolution. In the case of the higher impeller speeds (600 and 800 rpm) neither the structures nor the dissolution/strength characteristics differ greatly. It could well be that in the case of the higher impeller speeds, and after 10 minutes, we already are at the end of the granulation.

6.3.3 Summary: impeller speed

The effect of the impeller speed is very acute. At a low impeller speed of 200 rpm the granules are characterized by the presence of a binder core with flake-like shape. By increasing the impeller speed to 400 rpm the presence of the core is greatly reduced, and for higher impeller speeds the core is no longer visible, although areas richer in binder are still present.

6.4 PRIMARY PARTICLE SIZE

Figure 6.10 shows the radial profiles associated with each of the samples scanned in the primary particle size series. The profiles show a slight increase in density towards the edge of the granule. These profiles are consistent with the cross sections previously shown (Figure 4.19). The experimental conditions have already been given in Table 4.5 and are repeated below (Table 6.3).

Table 6.3. Experimental settings for the Durcal size series.

Process parameters	
Binder addition method	Melt-in
Impeller speed (rpm)	400
Chopper speed (rpm)	1400
Granulation time (min)	10
Temperature (°C)	60
Granule size (μm)	1000-1400
Formulation parameters	
Primary particles (S)	Durcal 5/15/40 (2000 g)
Binder (L)	PEG1500 (260 g)
Binder to solid ratio (L/S)	0.13

The radial profiles for the granules manufactured with the smallest primary particle size, Durcal 5, (Figure 6.10-a) show similar trends with very little radial change in the average greyscale intensity, with both initial and final (at a radial distance of $r = s$) values within the range of 40 to 50. In the case of granules manufactured with Durcal 15 and Durcal 40 this radial increase of greyscale intensity is only slightly more noticeable (Figure 6.10-b and c), with initial values at $r = 0$ falling between 40 and 50 and final values falling between 50 and 60. This is consistent with the cross sections illustrated in Figure 5.19. In the case of Durcal 15 and Durcal 40 samples, there exist small regions of unmixed binder in the centre of the granules. This explains why the radial profiles show higher

consolidation towards the outside when compared with the profiles corresponding to the Durcal 15 granules.

The profiles were averaged and the results shown in Figure 6.10-c. The profiles for the Durcal 15 and Durcal 40 granules are extremely similar, however the Durcal 5 granules, show less consolidation towards the edge of the granules.

This agrees with the dissolution/strength results shown in Figure 6.11. The behaviour of granules manufactured with Durcal 15 and Durcal 40 is very similar, although Durcal 40 granules are slightly stronger and take longer to dissolve. On the other hand, the Durcal 5 granules are very weak, this was already explained in the qualitative analysis (section 4.2.3), as they crumbled when being handled and had a very powdery consistency.

These results seem to contradict previous results showing high granule strength associated with small primary particle size and high viscosity binder and [57, 68]. It could be that since the amount of binder was kept constant for the three different sized primary particles, and due to the increased surface area in the small primary particles, there was not enough binder to create sufficiently strong agglomerates. This fact of higher requirements of binder for higher surface area is also reported in [68].

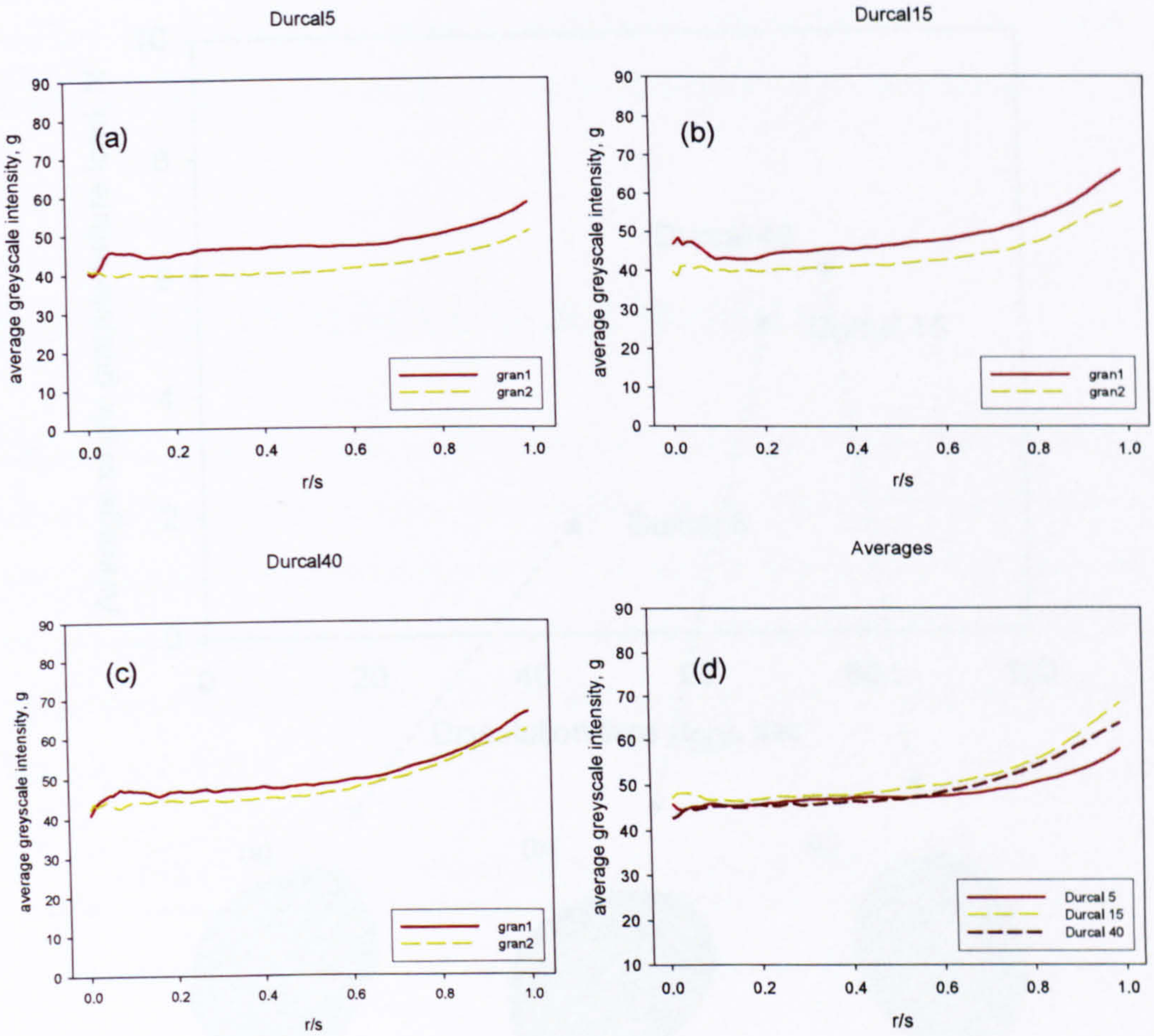

Figure 6.10. Radial profiles of sample manufactured with different grades of Durcal ($CaCO_3$): (a) Durcal5; (b) Durcal5 and (c) Durcal40; Each profile in each graph corresponds to a different granule. Graph (d) shows the averaged profiles for the different grades.

6.4.1 Strength and dissolution characteristics

The effect of the primary particle size on the dissolution (time t_{90}) and strength characteristics (failure load) of the agglomerates can be seen in (Figure 6.11). There is a clear trend showing that increasing the primary particle size results in stronger granules that take longer to dissolve.

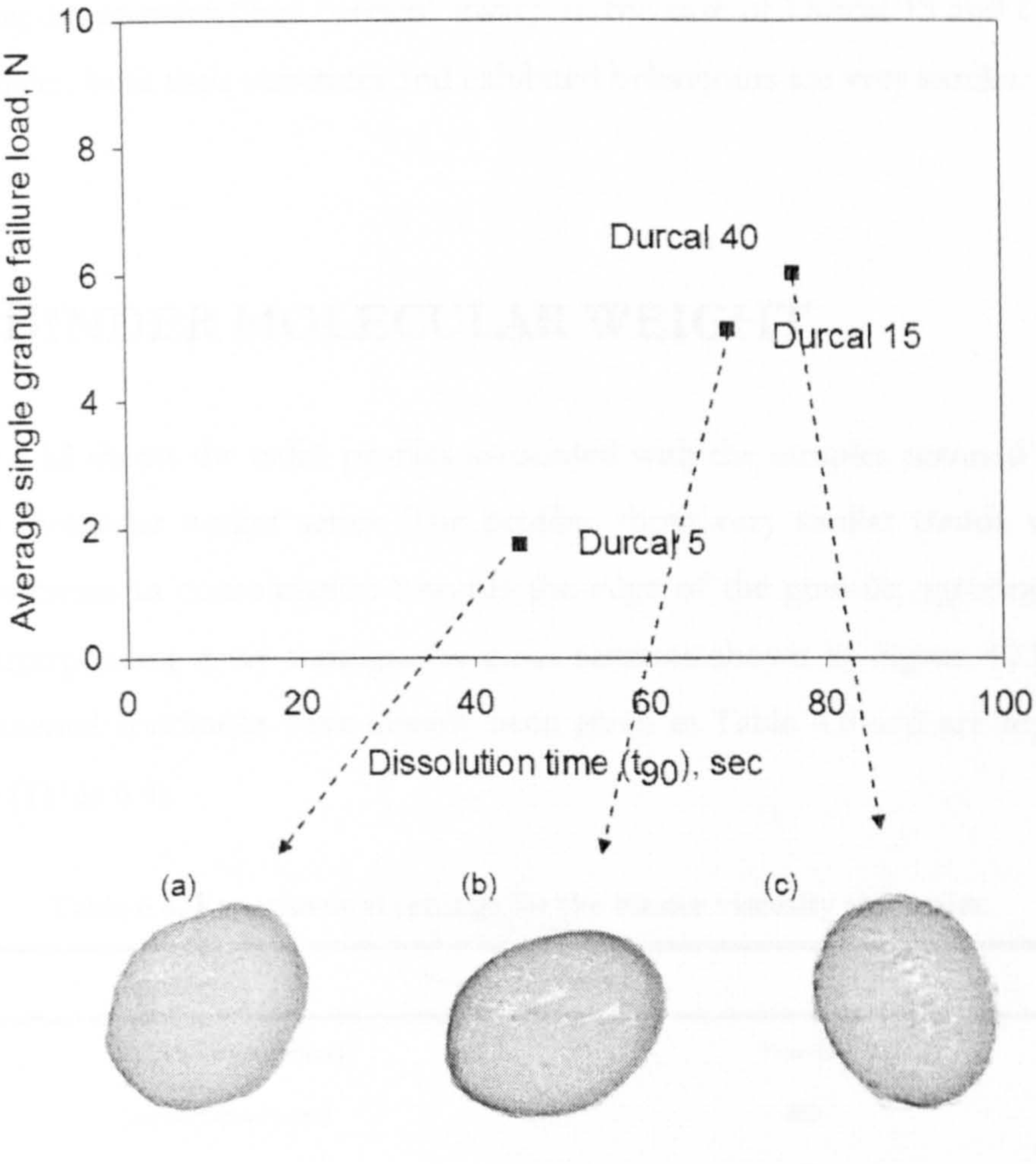

Figure 6.11. Effect on granule strength and dissolution of changing the primary particle size: (a) Durcal 5; (b) Durcal 15 and (c) Durcal 40.

6.4.2 Summary: primary particle size

For a constant binder ratio, the effect of primary particle size is most evident for the smallest primary particles. This is due to the increased surface area that the molten binder has to wet in order to create agglomerates. As a result, with 13% binder (w/w) added to the batch, the granules manufactured with Durcal 5 had a really weak and powdery consistency unlike the Durcal 15 and Durcal 40 granules. The difference could also be seen in the x-ray tomography structures, with the Durcal 5 granules showing a layered structure that was obvious when

handling the granules (they "peeled" away). In the case of Durcal 15 and Durcal 40 granules, both their structures and exhibited behaviours are very similar.

6.5 BINDER MOLECULAR WEIGHT

Figure 6.12 shows the radial profiles associated with the samples scanned in the binder molecular weight series. The profiles show very similar trends with a slight increase in consolidation towards the edge of the granule, agreeing with the corresponding x-ray tomography cross sections shown in Figure 4.21. The experimental conditions have already been given in Table 4.6 and are repeated below (Table 6.4).

Table 6.4. Experimental settings for the binder viscosity size series.

Process parameters	
Binder addition method	Pour-on
Impeller speed (rpm)	400
Chopper speed (rpm)	1400
Granulation time (min)	10
Temperature (°C)	60
Granule size (μm)	1000-1400
Formulation parameters	
Primary particles (S)	Durcal 40 (2000 g)
Binder (L)	PEG600/1500/6000/20000 (260 g)
Binder to solid ratio (L/S)	0.13

The radial profiles do not differ significantly for the different molecular weights used. In all cases, the radial increase in the average greyscale intensity ranges from 10 to 20 units, with the higher increases corresponding to the lower molecular weight binders.

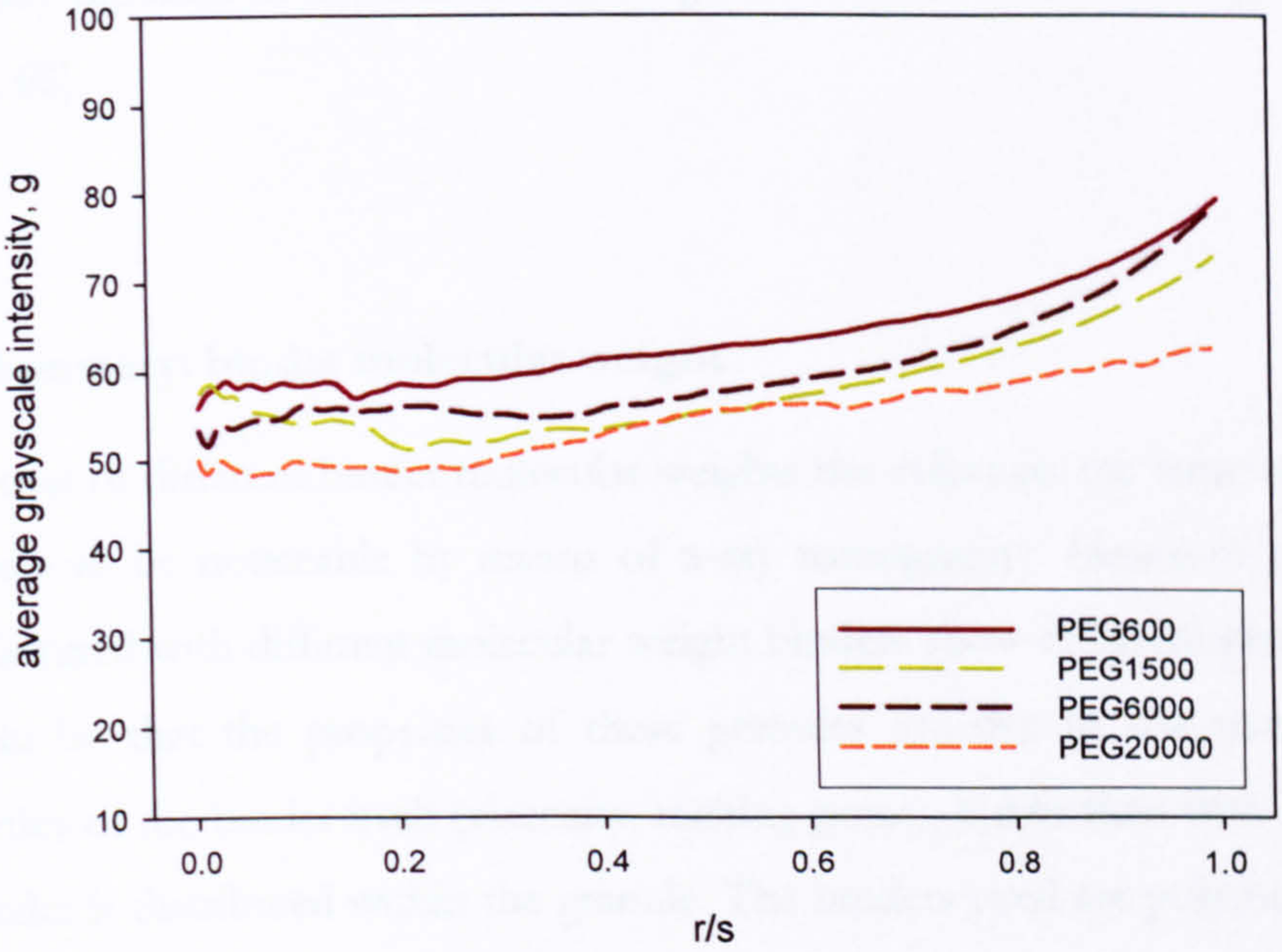

Figure 6.12. Radial profiles of samples manufactured with binders of different molecular weight.

6.5.1 Strength and dissolution characteristics

The effect of the binder molecular weight on the dissolution (time t_{90}) and strength characteristics (failure load) of the agglomerates can be seen in Figure 6.13. It shows that increasing the binder molecular weight creates stronger and less soluble granules. This trend is only broken for the granules with PEG20000, which show strength inferior to those made with PEG6000. This could be due to the high viscosity of PEG20000, which would require a longer granulation time to be on the same state of granulation as the agglomerates produced with the other binders.

A change on the shape patterns of the granules is also noticeable, with lower viscosity binders creating more spherical shapes than high viscosity binders. The effect of the binder viscosity on the granule strength and shape has been

previously reported in the literature and agrees with the results here presented [57, 67, 68].

6.5.2 Summary: binder molecular weight

In the case of different binder molecular weights the effect on the structure does not seem to be noticeable by means of x-ray tomography. However granules manufactured with different molecular weight binders show different properties. It could be that the properties of these granules are due to the nature and properties of the binder itself (viscosity, melting point), rather than with the way the binder is distributed within the granule. The binders used are polymers, with identical elemental components but different molecular weights. This would explain why the differences cannot be picked up on an x-ray tomography cross-section despite them being clearly apparent when studying the properties of the granules (the higher molecular weight binder creates stronger bonds between primary particles).

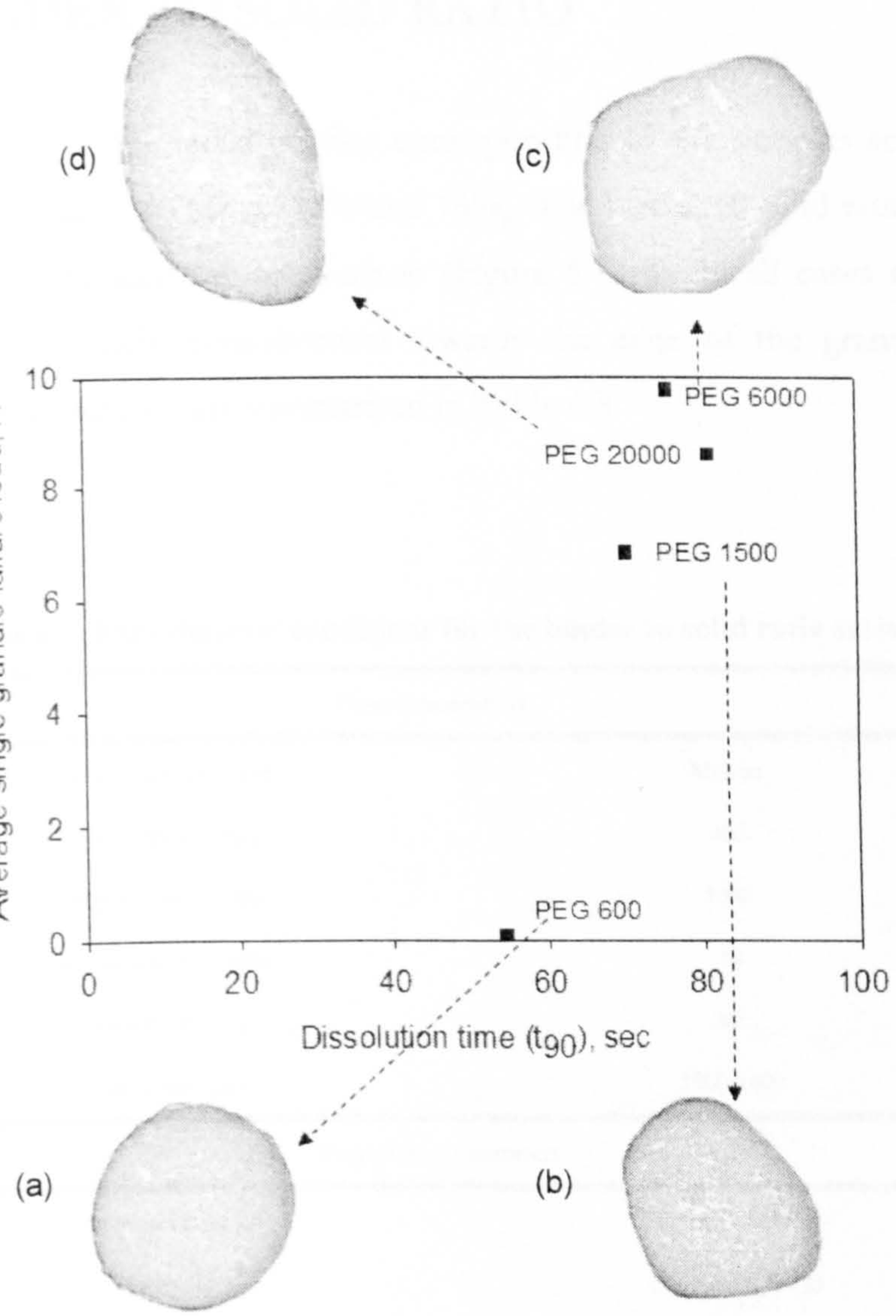

Figure 6.13. Effect on granule strength and dissolution of changing the binder molecular weight: (a) PEG 600; (b) PEG 1500; (c) PEG 6000 and (d) PEG 20000.

6.6 BINDER TO SOLID RATIO

Figure 6.14 shows the radial profiles corresponding to the samples scanned in the binder to solid ratio series (10% and 16%). The binder to solid ratio of 13% has also been included for comparison (Figure 6.14-b). In all cases the radial profiles show a slight consolidation towards the edge of the granules. The experimental conditions are summarized in Table 6.5.

Table 6.5. Experimental conditions for the binder to solid ratio series.

Process parameters	
Binder addition method	Melt-in
Impeller speed (rpm)	400
Chopper speed (rpm)	1400
Granulation time (min)	10
Temperature (°C)	60
Granule size (μm)	1000-1400
Formulation parameters	
Primary particles (S)	Durcal 40 (2000 g)
Binder (L)	PEG1500 (260 g)
Binder to solid ratio (L/S)	0.1, 0.16

For the cases of 10% and 16%, the profiles show the same trend, with approximately a 10 unit increase in radial greyscale towards the edge of the granule, but which differ in absolute values (Figure 6.14-a and c). The profiles corresponding to 13% binder to solid ratio show a greater agreement amongst themselves. The profiles for each binder to solid ratio where averaged and are shown in Figure 6.15-d. Given the great scatter the differences between the profiles are not significant, so no conclusions can be made from this graph.

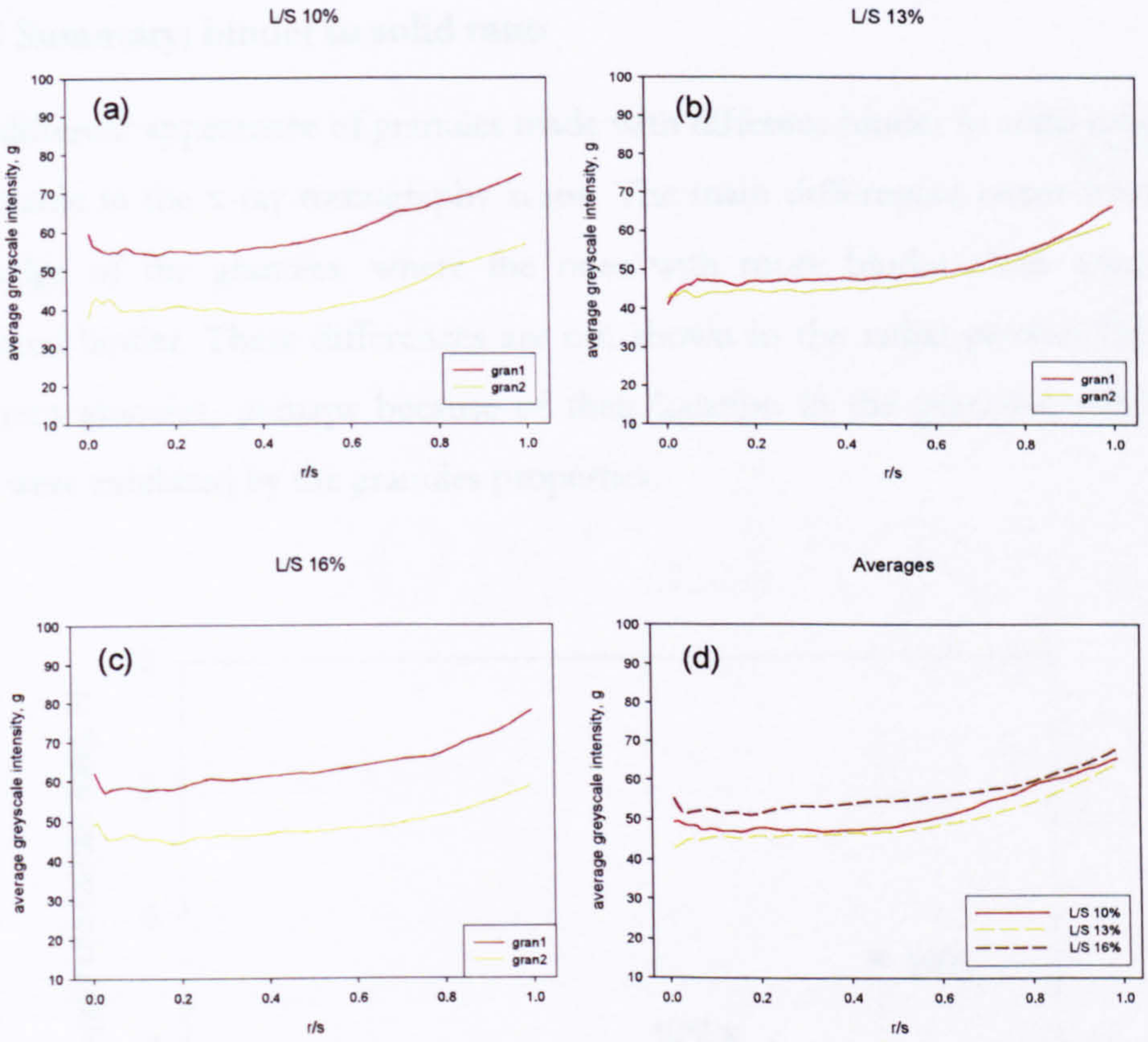

Figure 6.14. Radial profiles of sample manufactured with different binder to solid ratios: (a) 10%; (b) 13% and (c) 16%. Graph (d) shows the averaged profiles for the different ratios.

6.6.1 Strength and dissolution characteristics

Studies of dissolution/strength behaviour are available for the extreme ratios (10 and 16%) and can be seen in Figure 6.15.

The granules manufactured with the higher amount of binder are stronger. This can be explained by the higher binder concentration increasing the liquid saturation which promotes the increase in density of the granules due to a larger lubrication effect [8].

6.6.2 Summary: binder to solid ratio

The different appearance of granules made with different binder to solid ratios is noticeable in the x-ray tomography scans. The main differences occur towards the edge of the granules, where the ones with more binder show areas of unmixed binder. These differences are not shown in the radial profiles for the different granules, perhaps because of their location in the granules, although they were exhibited by the granules properties.

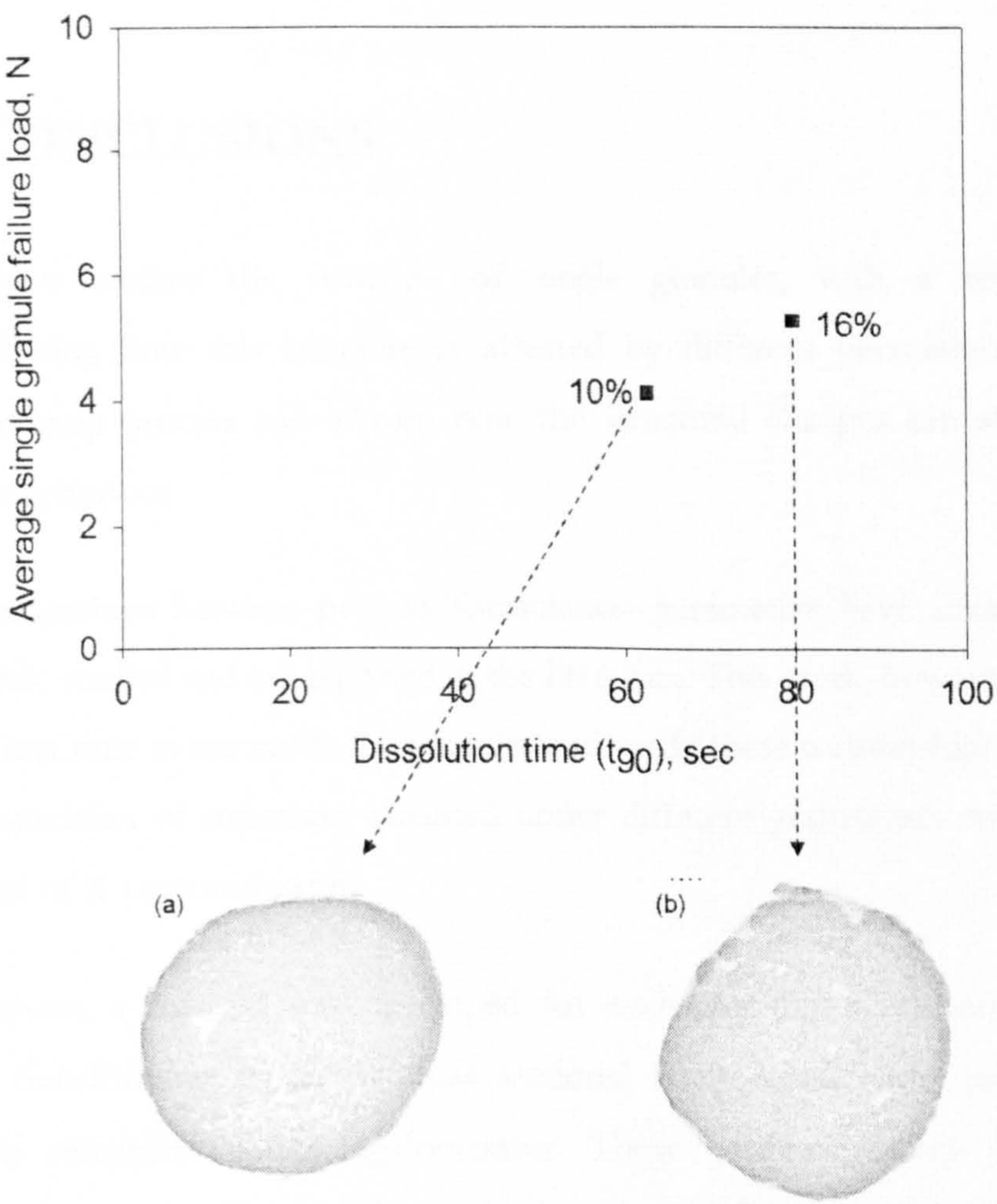

Figure 6.15. Effect on granule strength and dissolution of changing the binder to solid ratio: (a) 10% and (b) 16%.

7

CONCLUSIONS

7.1 CONCLUSIONS

This thesis studies the structure of single granules, with a review to understanding how this structure is affected by different parameters in the manufacturing process and in turn how the structural changes can affect the granules behaviour.

The relationships between process/formulation parameters have already been extensively studied and are reported in the literature. This work, however, allows for the first time to see inside the granules and verify these relationships through the visualization of structures obtained under different granulation conditions, by means of X-ray tomography.

Furthermore, a method was developed for analyzing the X-ray tomography results, transforming stacks of cross sectional images into radial profiles of greyscale intensities within agglomerates. These profiles convey structural information and complement the qualitative visual information from the XRT scans.

The following conclusions can be drawn from this project:

- Analysing single granules using XRT provided physical insight of single agglomerates structure in a non-destructive manner.

- Density distributions within the agglomerates could be qualitatively obtained as greyscale intensity maps.
- Distributions of the individual phases that make up a granule could not be obtained due to the resolution limitations of the technique.
- XRT allowed the visualization of typical structures that are expected from different granulation methods, for example compact granules from high-shear mixers and open-structure granules from fluidized bed granulation.
- XRT showed that different agglomerate structures occurred under the same granulation conditions as a result of different granulation mechanisms taking place during the agglomeration process.
- XRT identified an immersion mechanism as prevalent for nucleation in high-shear melt granulation. The flakes of binder act as nuclei initiators when they start to melt. Primary particles stick to the surface of the melting flakes, and then progress towards the centre of the flake, squeezing molten material towards the surface. This makes the surface of the granules wet, allowing further layers of primary powder or smaller nuclei to adhere.

The following conclusions can be drawn regarding the method developed for analyzing XRT results on single granules:

- This method transforms XRT raw data into a single radial profile of greyscale values within the granule, avoiding the subjectivity of looking at all of the individual resulting images from XRT.
- The greyscale values are representative of the density of the material the x-ray beam goes through, hence providing structural information on the samples.
- This method can be applied to compare different granules in terms of radial consolidation
- To evaluate the reproducibility of the scan, the same sample was scanned with different orientations. Matching results were obtained indicating the technique is reproducible.

- The robustness of the method was tested by studying the influence of perturbations in the coordinates of the calculated centre of mass on the resulting radial profiles. Good agreement in the resulting profiles was found up to perturbations of 10% of the value of the radius of gyration of the sample.

Two typical process parameters were modified in order to study their effect on the structure of single high-shear melt agglomerates: granulation time and impeller speed. The following can be concluded:

Granulation time series:

- All samples scanned showed increased consolidation towards the surface of the granule.
- Increasing the massing time, increased the consolidation of the materials. This effect was most pronounced during the earliest of the granulation time (less than 4 minutes of granulation).
- There is a significant change between the radial profiles calculated for samples taken after 2 minutes of granulation time compared to all others , whereas there is very little difference between the samples after 4, 6, 10 and 15 minutes of granulation time.
- The structure of the samples studied showed a binder core in the centre of the granule. The core is very regular and resembles a flake of binder after 2 minutes of granulation.
- For granulation times of 4 minutes onwards, this core reduces in size and the flake-like shape is lost, but even after 15 minutes of granulation time the core is still visible in the majority of granules tested.
- The ratio of core to granule volume is relatively constant after 4 minutes of granulation, however for the earliest granulation time (2 minutes) this ratio is approximately 3 times higher.

Impeller speed series:

- All samples scanned showed increasing consolidation towards the surface of the granule

- Increasing the impeller speed increases the overall consolidation of the agglomerates. This consolidation results in granules that are stronger and take longer to dissolve.
- At a low impeller speed of 200 rpm, the granules are characterized by the presence of a binder core with flake-like shape.
- Increasing the impeller speed to 400 rpm greatly reduces the presence of cores and at higher impeller speeds (600, 800 rpm) the core is no longer visible although areas richer in binder are still present.
- Increasing the impeller speed modified the shape of the agglomerates formed whereby increasing impeller speed results in rounder agglomerates.

Three typical formulation parameters - primary particle size, binder molecular weight and liquid to solid ratio were modified in order to study their effect on the structure of single high-shear melt agglomerates. The following conclusions can be drawn:

- Modification of formulation parameters did not cause noticeable changes in the cross-sectional images from XRT. This was reflected in small differences in the calculated radial profiles.
- For the primary particle size/binder molecular weight modifications the small differences in the calculated radial profiles could be due to the fact that the granules have essentially the same elemental composition and have been manufactured under the same conditions, therefore no difference can be detected with XRT unless mapping of the individual components in the granule is possible.
- For the binder to solid ratio analysis, the main difference occurs at the edges of the granule, with areas of unmixed binder stuck to the surface of the agglomerates.
- Even though no differences are obvious on the XRT images, the modification of process parameters does create differences in the strength/dissolution behaviour of the agglomerates. Increasing the primary particle size, binder molecular weight and binder to solid ratio all result in stronger/more difficult to dissolve granules.

8

FUTURE WORK

8.1 RECOMMENDATIONS FOR FUTURE WORK

This project successfully applied XRT to give an insight into how granulation conditions determine granule structure and how this will affect the properties exhibited by the final product. This work has mainly focused in high-shear melt granulation and the effect of impeller speed, granulation time, primary particle size, binder viscosity and binder to solid ratio.

Therefore it is suggested to extend this work to other granulation methods, as well as studying different materials, and the effect of different parameters. Also, a method similar to the one developed in this thesis could be designed to generate radial profiles of greyscale within single granules but from the surface towards the centre of the agglomerates, in order to maximise surface features.

In addition, this work shows how XRT can be a very useful tool to gain insight and understand the structure of agglomerates. XRT is a technique that is fast developing. New, much more powerful XRT systems are being developed. These new models have the potential of allowing faster and more accurate analysis of agglomerates. At the beginning of this work the resolution of the commercially available XRT systems was in the range of a few microns per pixel in the cross sections. This resolution is currently a few nanometres, with extremely sophisticated sample handling devices and faster scanning times. There is also the possibility of using synchrotron radiation, which can be

impractical due to beam time limitations but which can provide enough information to perfectly identify each of the components in an agglomerate giving an exact picture of its structure.

The insight achieved by tomography methods could also be used in the form of structural models that could complement current population balance models (multi-scale modelling approach). This could lead to a much more complete and accurate description of the granulation process and maybe a fully predictive model of granulation could eventually be developed from the inside knowledge of how the different components are distributed within the granules.

This work has been carried out using a laboratory scale, vertical axis, batch, high-shear mixer. These types of mixers are not very common in industry (with a few exceptions such as in the pharmaceutical industry), where bigger, continuous, horizontally mounted mixers are more common. It would also be interesting to use X-ray tomography in scale-up studies, trying to see how using different types of manufacturing methods/parameters affects the structure of the agglomerates produced.

REFERENCES

1. Knight, P.C., *Structuring agglomerated products for improved performance.* Powder Technology, 2001. **119**(1): p. 14-25.

2. Cheong, Y.S., *The production of binderless granules and their mechanical characteristics*, in *Chemical and Process Engineering, Particle Products Group*. 2006, University of Sheffield: Sheffield.

3. D. Nelson, R., *Why study particle science?* 1999, Last accessed August 2006, http://www.erpt.org/misc/whystudy.htm.

4. Iveson, S.M., Litster, J.D., Hapgood, K., and Ennis, B.J., *Nucleation, growth and breakage phenomena in agitated wet granulation processes: a review.* Powder Technology, 2001. **117**(1-2): p. 3-39.

5. Deleuil, M., *Powder Technology and Pharmaceutical Processes (preface).* Handbook of Powder Technology. Vol. 9. 1994, The Netherlands: Elsevier.

6. Ennis, B. and Litster, J., *Particle size enlargement*, in *Perry's Chemical Engineers' Handbook (seventh ed)*, R. Perry and D. Green, Editors. 1997, McGraw-Hill: New York. p. 20-89.

7. Hounslow, M.J., *Particle rate processes (course notes).* Chemical and Process Engineering, Unversity of Sheffield, 2003.

8. Schæfer, T., *Melt agglomeration with polyethylene glycols in high shear mixers*, in *Department of Pharmaceutics*. 1996, The Royal Danish School of Pharmacy: Copenhagen.

9. Knight, P.C., Instone, T., Pearson, J.M.K., and Hounslow, M.J., *An investigation into the kinetics of liquid distribution and growth in high shear mixer agglomeration.* Powder Technology, 1998. **97**(3): p. 246-257.

10. Newitt, D.M., Conway-Jones, J.M., *A contribution to the theory and practice of granulation.* Trans. I. Chem. Eng., 1958. **36**: p. 422-441.

11. Sastry, K. and Fuerstenau, D., *Mechanisms of agglomerate growth in green pelletization.* Powder Technology, 1973. **7**: p. 97-105.

12. Scott, A.C., Hounslow, M.J., and Instone, T., *Direct evidence of heterogeneity during high-shear granulation.* Powder Technology, 2000. **113**(1-2): p. 205-213.

13. Schæfer, T., C. Mathiesen,, *Melt pelletization in a high shear mixer. IX. Effects of binder particle size.* Int. J. Pharm., 1996. **139**: p. 139-148.

14. Vonk, P., CPF, G., Ramaker, J.S., Vromans, H., Kossen, N.W.F., *Growth mechanisms of high-shear pelletisation.* Int. J. Pharm., 1997. **157**: p. 93-102.

15. Iveson, S.M., J.D. Litster, *Growth regime map for liquid-bound granules.* AIChE, 1998. **44**: p. 1510-1518.

16. Pitchumani, R., Zhupanska, O., Meesters, G.M.H., and Scarlett, B., *Measurement and characterization of particle strength using a new robotic compression tester.* Powder Technology, 2004. **143-144**: p. 56-64.

17. Kohlus, R. *Quantitative descriptors for granule structure characterization.* in *4th World Congress in Particle Technology.* 2002. Sydney.

18. Fonner, D.E., Banker, G.S., and Swarbrick, J., *Physical properties of particles prepared by five different granulation methods.* J. Pharm. Sci., 1966. **55**: p. 181-186.

19. Reynolds, G.K., Biggs, C.A., Salman, A.D., and Hounslow, M.J., *Non-uniformity of binder distribution in high-shear granulation.* Powder Technology, 2004. **140**: p. 203-208.

20. Rue, P.J., Seager, H., Ryder, J., and Burt, I., *The relationship between granule structure, process of manufacture and the tabletting properties of a granulated product.* Int. J. Pharm. Tech. & Prod. Mfr., 1980. **1**: p. 2-6.

21. Seager, H., Rue, P.J., Burt, I., Ryder, J., and Warrack, J.K., *The relationship between granule structure, process of manufacture and the tabletting properties of a granulated product. Part III. Tablet structure and biopharmaceutical properties.* Int. J. Pharm. Tech. & Prod. Mfr., 1981. **2**: p. 41-50.

22. Seager, H., Burt, I., Ryder, J., Rue, P.J., Murray, S., Beal, N., and Warrack, J.K., *The relationship between granule structure, process of manufacture and the tabletting properties of a granulated product. Part I. Granule structure.* Int. J. Pharm. Tech. & Prod. Mfr., 1979. **1**: p. 36-44.

23. Seager, H., *Spray-coating bulk drugs aids dosage from production.* Manufacturing chemist & aerosol news, 1977: p. 25-35.

24. Samimi, A., Ghadiri, M., Boerefijn, R., Groot, A., and Kohlus, R., *Effect of structural characteristics on impact breakage of agglomerates.* Powder Technology, 2003. **130**: p. 428-435.

25. Bouwman, A.M., Henstra, M.J., Westerman, D., Chung, J.T., Zhang, Z., Ingram, A., Seville, J.P.K., and Frijlink, H.W., *The effect of the amount of binder liquid on the granulation mechanisms and structure of microcrystalline cellulose*

granules prepared by high shear granulation. International Journal of Pharmaceutics, 2005. **290**(1-2): p. 129-136.

26. Farber, L., Tardos, G., and Michaels, J.N., *Use of X-ray tomography to study the porosity and morphology of granules.* Powder Technology, 2003. **132**(1): p. 57-63.

27. Rubinstein, M.H. and Ridgway, K., *Solute migration during granule drying.* J. Pharm. Pharmac., 1974. **26**: p. 24-29.

28. Ridgway, K. and Rubinstein, M.H., J. Pharm. Pharmac., 1971a. **23 (suppl.)**: p. 11S-17S.

29. Ridgway, K. and Rubinstein, M.H., J. Pharm. Pharmac., 1971b. **23**: p. 587-589.

30. Aulton, M.E., Banks, M., and Davies, I., *A fluorescent technique for the observation of polyvinylpyrrolidine binder distribution in granules.* Drug Dev. Ind. Pharm., 1978. **4**: p. 537-539.

31. Gamlen, M.J., Seager, H., and Warrack, J.K., *The structure and tablet properties of paracetamol granules prepared in a fluidized bed and wet massing.* Int. J. Pharm. Tech. & Prod. Mfr., 1982. **3**: p. 108-114.

32. Sugimoto, M., Tojima, D., Yamamoto, K., and Rengakuji, S., *Continuous preparation of small composite granules by a rotating conical vessel with grinding media - observation of morphology of composite granules with electron probe microanalyzer.* J. Soc. Powder Technol., Japan, 1999. **36**: p. 685-691.

33. Sugimoto, M., Takehiko, I., Ken-Ichi, Y., and Tosihiaki, M., *On the small composite granules formed in a continuous conical vessel containing grinding media: effect of the methods of feeding powder on the size and structure of binary composite granules.* Powder Technology, 2003. **130**: p. 442-449.

34. Rodriguez, L., Cavallari, C., Passerini, N., Albertini, B., Gonzalez-Rodriguez, M.L., and Fini, A., *Preparation and characterization by morphological analysis of diclofenac/PEG4000 granules obtained using three different techniques.* Int. Journal of Pharmaceutics, 2002. **242**: p. 285-289.

35. Sochon, R., *The production of structured granular products*, in *Chemical & Process Engineering.* 2005, University of Sheffield: Sheffield.

36. Gonzalez-Ballester, M.A., Zisserman, A.P., and Brady, M., *Estimation of the partial volume effect in MRI.* Medical Image Analysis, 2002. **6**: p. 389-405.

37. Skyscan, *Skyscan micro-CT: 1072 model high-resolution microtomograph*, Last accessed June 2006, http://www.skyscan.be/next/spec_1072.htm.

38. Flannery, B.P., Deckam, H.W., Roberge, W.G., and D'Amico, K.L., *Three-dimensional X-ray microtomography.* Science, 1987. **237**: p. 1439-1444.

39. Cormack, A.M., *Representation of a function by its line integrals, with some radiological applications.* J. Appl. Phys., 1963. **34**: p. 2722-2727.

40. Cormack, A.M., *Representation of a function by its line integrals, with some radiological applications, II.* J. Appl. Phys., 1964. **35**: p. 2908-2913.

41. Hounsfield, G.N., *A method and apparatus for examination of a body by radiation such as X-ray or gamma radiation*, in *Patent specification 1283915.* 1972.

42. Ketcham, R.A. and Carlson, W.D., *Acquisition, optimization and interpretation of X-ray computed tomographic imagery: applications to the geosciences.* Computers & Geosciences, 2001. **27**: p. 381-400.

43. Macedo, A. and Crestana, S., *X-ray microtomography to investigate thin layers of soil clod.* Soil and Tillage Research, 1998. **49**: p. 249-253.

44. Salvo, L., Cloetens, P., Marie, E., Zabler, S., Blandin, J.J., Buffiere, J.Y., Ludwig, W., Boller, E., Bellet, D., and Josserong, C., *X-ray microtomography an attractive characterization technique in materials science.* Nuclear Instruments and Methods in Physics Research Section. B: Beam Interactions with Materials and Atoms., 2003. **200**: p. 273-286.

45. Butler, L.G., Owens, J.W., Cartledge, F.K., Kurtz, R.L., Byerly, P.L., Wales, A.J., Bryant, P.L., Emery, E.F., Dowd, B., and Xie, X., *Synchrotron x-ray microtomography, elcetron probe analysis and NMR of toluene waste in cement.* Environ. Sci. Technol., 2000. **34**: p. 3269-3275.

46. Feldkamp, L.A., Davis, L.C., and Kress, J.W., *Practical cone-beam algorithm.* J. Opt. Soc. Am., 1984. **1**: p. 612-619.

47. Sasov, A. *Comparison of fan-beam, cone-beam and spiral scan reconstruction for X-ray micro-CT.* in *Proceedings of SPIE International Symposium of Medical Imaging.* 2001.

48. ASTM, *E1441-00, Standard guide for computed tomography (CT) imaging.* American Society for Testing Materials, 2000.

49. Barruchel, J., Buffiere, J.Y., Maire, E., Merie, P., and Peix, F., *X-ray tomography in materials science.* 2000: Hermes Science Publications.

50. Golchert, D., Farber, L., Liu, L.X., Litster, J.D., and Page, N.W. *The use of X-ray microtomography to charcterize agglomerate structure.* in *4th World Congress in Particle Technology.* 2002. Sydney.

51. Golchert, D., Moreno, R., Ghadiri, M., and Litster, J., *Effect of granule morphology on breakage behaviour during compression.* Powder Technology, 2004. **143-144**: p. 84-96.

52. Sinka, I.C., Burch, S.F., Tweed, J.H., and Cunningham, J.C., *Measurements of density variations in tablets using X-ray computed tomography.* International Journal of Pharmaceutics, 2004. **271**: p. 215-224.

53. Yang, C.Y. and Fu, X.Y., *Development and validation of a material labelling method for powder process characterization using X-ray computed tomography.* 2004, 2004. **146**: p. 10-19.

54. Fu, J.S., Cheong, Y.S., Reynolds, G.K., Adams, M.J., Salman, A.D., and Hounslow, M.J., *An experimental study of the variability in the properties and quality of wet granules.* Powder Technology, 2004. **140**(3): p. 209-216.

55. Gabbott, I.P., Reynolds, G.K., Salman, A.D., Bonsall, J., and Hounslow, M.J. *Improvement of strength and dissolution of two-phase granules.* in *8th International Symposium on Agglomeration.* 2005. Bangkok, Thailand.

56. Bouwman, A.M., *Form, formation and deformation: the influence of material properties and process conditions on the shape of granules produced by high shear granulation*, in *Department of Industrial Pharmacyt.* 2005, Rijksuniversitei: Groningen, The Netherlands.

57. van den Dries, K., de Vegt, O.M., Girard, V., and Vromans, H., *Granule breakage phenomena in a high shear mixer; influence of process and formulation variables and consequences on granule homogeneity.* Powder Technology, 2003. **133**(1-3): p. 228-236.

58. N'Dri-Stempfer, B., Oulahna, D., Eterradossi, O., Benhassaine, A., and Dodds, J.A., *Binder granulation and compaction of coloured powders.* Powder Technology, 2003. **130**(1-3): p. 247-252.

59. Cheong, Y.S., Adams, M.J., Routh, A.F., Hounslow, M.J., and Salman, A.D., *The production of binderless granules and their mechanical characteristics.* Chemical Engineering Science, 2005. **60**(14): p. 4045-4053.

60. Le, P.K., Avontuur, P., Hounslow, M.J., and Salman, A.D. *The microscopic study of granulation mechanisms and their effect on the non-uniformity of granule properties.* in *AICheme Annual Meeting.* 2006. San Francisco, California (USA).

61. Gabbott, I.P., Barrera-Medrano, D., Reynolds, G.K., Salman, A.D., Bonsall, J., and Hounslow, M.J. *The effect of binder ratio on granule strenght, dissolution and structure.* in *World Congress on Particle Technology 5.* April 2006. Orlando (Florida).

62. Schæfer, T., Holm, P., Kristensen, H.G., *Melt granulation in a laboratory scale high shear mixer.* Drug Dev. Ind. Pharm., 1990. **16**: p. 1249-1277.

63. Saleh, K., Vialatte, L., and Guigon, P., *Wet granulation in a batch high shear mixer.* Chemical Engineering Science, 2005. **60**(14): p. 3763-3775.

64. Schaefer, T., *Growth mechanisms in melt agglomeration in high shear mixers.* Powder Technology, 2001. **117**: p. 68-82.

65. Schaefer, T., Johnsen, D., and Johansen, A., *Effects of powder particle size and binder viscosity on intergranular and intragranular particle size heterogeneity during high shear granulation.* International Journal of Pharmaceutical Sciencs, 2004. **21**: p. 525-531.

66. Casteele, E.V.d., *Personal Communication - SkyScan.* 2006.

67. Schaefer, T. and Mathiesen, C., *Melt pelletization in a high shear mixer. VIII. Effects of binder viscosity.* European Journal of Pharmaceutics, 1996. **139**(1-2): p. 125-138.

68. Johansen, A. and Schaefer, T., *Effects of interactions between powder particle size and binder viscosity on agglomerate growth mechanisms in a high shear mixer.* European Journal of Pharmaceutical Sciences, 2001. **12**(3): p. 297-309.

APPENDICES

APPENDIX A

RADIAL PROFILES PSEUDOCODE

```
% ------------------------------------------------------------------
% ------------------------------------------------------------------
% CALCULATION OF THE CENTRE OF MASS --------------------------------
% ------------------------------------------------------------------
% ------------------------------------------------------------------
```

The following need to be specified: first and last slice of series of images that make up the stack and tolerance for the masking.
For the masking the magicwand function (importer as a C+ code) needs to be loaded.
A try/catch loop is used in case there are errors reading the images.

```
for k = startslice:endslice
    sliceno = k-startslice + 1;
    fname
                                                                =
sprintf('D:/..../folder/experiment/image%d.bmp',k);
    try
        M = 255 - double(imread(fname));
        BM = magicwand1(M,1,1,tolerance);
        [rows,cols] = size(M);
        X = 0;
        Y = 0;
        Z = 0;
        Norm = 0;
        for x = 1:rows;
            for y = 1:cols;
                if BM(x,y) == 0;
                    Norm = Norm + M(x,y);
                    X = X + (M(x,y)*x);
                    Y = Y + (M(x,y)*y);
                    Z = Z + (M(x,y)*(i-1));
                end
            end
        end
        if Norm == 0;
            Norma(sliceno) = 0;
            Xa(sliceno) = 0;
            Ya(sliceno) = 0;
            Za(sliceno) = 0;
        else
            Norma(sliceno) = Norm;
            Xa(sliceno) = X/Norm;
            Ya(sliceno) = Y/Norm;
            Za(sliceno) = Z/Norm;
```

```
        end
    catch
        name = sprintf('image%d',sliceno);
        disp('the following image does not exist:');
        disp(name);
    end
end

Norm3D = sum(Norma);
X3D = sum(Xa.*Norma)/Norm3D;
Y3D = sum(Ya.*Norma)/Norm3D;
Z3D = sum(Za.*Norma)/Norm3D;

save centcoord.txt X3D Y3D Z3D -ascii -double;


% ------------------------------------------------------
% ------------------------------------------------------
% CALCULATIONS FOR THE RADIAL PROFILES AND BINNING OF THE DATA
% ------------------------------------------------------
% ------------------------------------------------------
```

All that data required for the radial profiles is calculated in this section alongside the values of the radius of gyration of the sample. Also all the data is binned by radius.
The number of bins needs to be specified in order to know the width of each of the bins (Rstep).
A try/catch loop is used in case there are errors reading the images.
After the radial binning the following quantities are calculated for each individual bin: sum of all pixel intensities, squared sum of all pixel intensities, total number of pixels, maximum intensity, minimum intensity.

```
for k = startslice:endslice
    sliceno = k-startslice + 1;
    fname =
sprintf('D:/..../folder/experiment/image%d.bmp',k);
    try
    I = 255 - double(imread(fname));
    BM = magicwand1(I,1,1,tolerance);
    for x = 1:rows;
       for y = 1:cols;
         if BM(x,y) == 0;
            r = sqrt((x-X3D)^2+(y-Y3D)^2+(sliceno-1-Z3D)^2);
            gyration(1,1) = gyration(1,1) + (I(x,y)*(r^2));
            gyration(1,2) = gyration(1,2) + I(x,y);
            binnumber = ceil(r/Rstep);
            histograms(binnumber,          I(x,y)+1)          =
histograms(binnumber, I(x,y)+1) + 1;
            data(binnumber,1) = data(binnumber,1) + I(x,y);
            data(binnumber,2)     =     data(binnumber,2)     +
(I(x,y))^2;
            data(binnumber,3) = data(binnumber,3) + 1;
            if I(x,y) > data(binnumber,4)
               data(binnumber,4) = I(x,y);
            end
```

```
                if I(x,y) < data(binnumber,5)
                   data(binnumber,5) = I(x,y);
                end
             end
          end
       end
       catch
          name = sprintf('image%d',sliceno);
          disp('the following image does not exist:');
          disp(name);
       end
end

gyrationvalue = sqrt(gyration(1,1)/gyration(1,2));

save gyration.txt gyrationvalue -ascii -double;
save histograms.txt histograms -ascii -double;
save data.txt data -ascii -double;
```

From the values already calculated the following amounts are calculated for each bin: median, mean, standard deviation, variance, coefficient of variation. The results are saved on a text file that is then imported into EXCEL for final calculations and preparation of the data for plotting.

```
for i=1:max(size(data));
    results(i,1) = (data(i,4) + data(i,5))/2;
    results(i,2) = data(i,1)/data(i,3);
    results(i,3)          =          sqrt((data(i,3)*data(i,2))-
(data(i,1)^2))/data(i,3);
    results(i,4) = results(i,3)^2;
    results(i,5) = results(i,3)/results(i,2);
end

save results.txt results -ascii -double;
```

APPENDIX B

XRT CROSS SECTIONS

The following images correspond to x-ray tomography cross sections for a granules manufactured with the experimental settings detailed below (Table B.1). Only the 1 every 20 cross sections are shown, corresponding to a distance between slices of approximately 27 microns along the z-axis. The first image of the set corresponds to an x-ray shot of the granule.

Table B.1. Experimental settings

Process parameters	
Binder addition method	Melt-in
Impeller speed (rpm)	200
Chopper speed (rpm)	1400
Granulation time (min)	10
Temperature (°C)	60
Granule size (μm)	1000-1400
Formulation parameters	
Primary particles (S)	Durcal40 (2000 g)
Binder (L)	PEG1500 (260 g)
Binder to solid ratio (L/S)	0.13

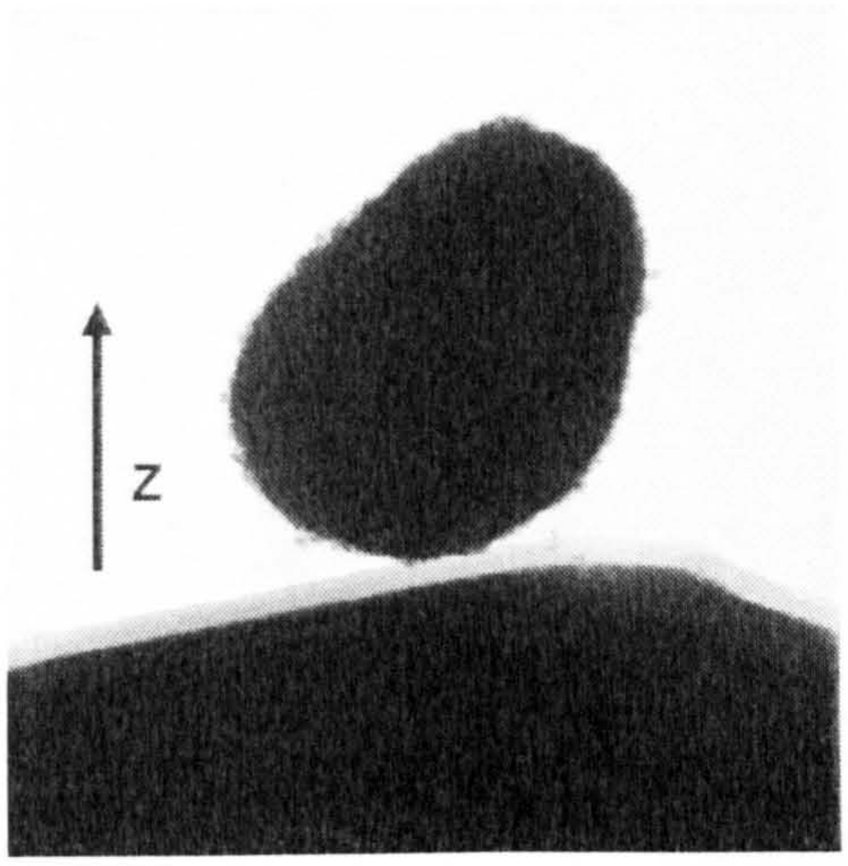
Z

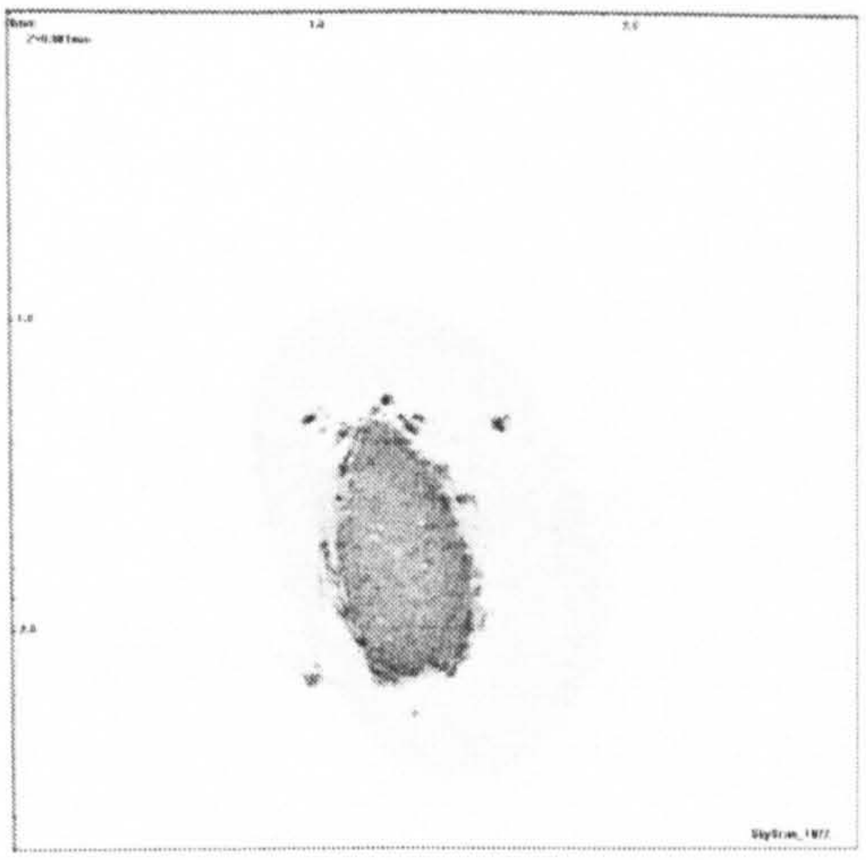

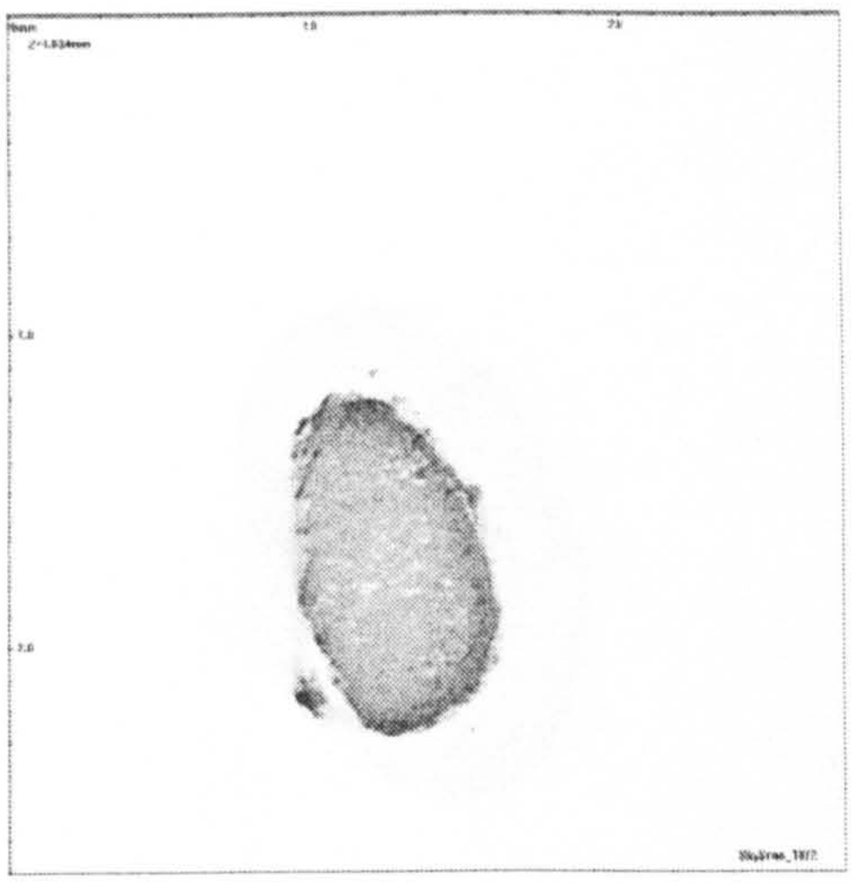

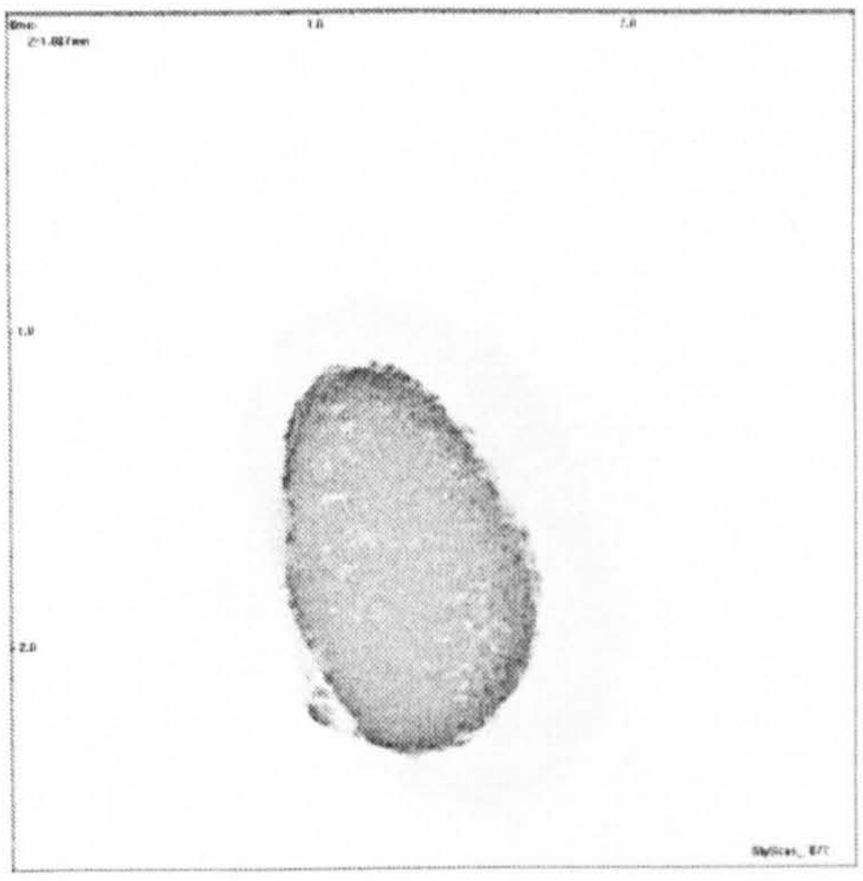

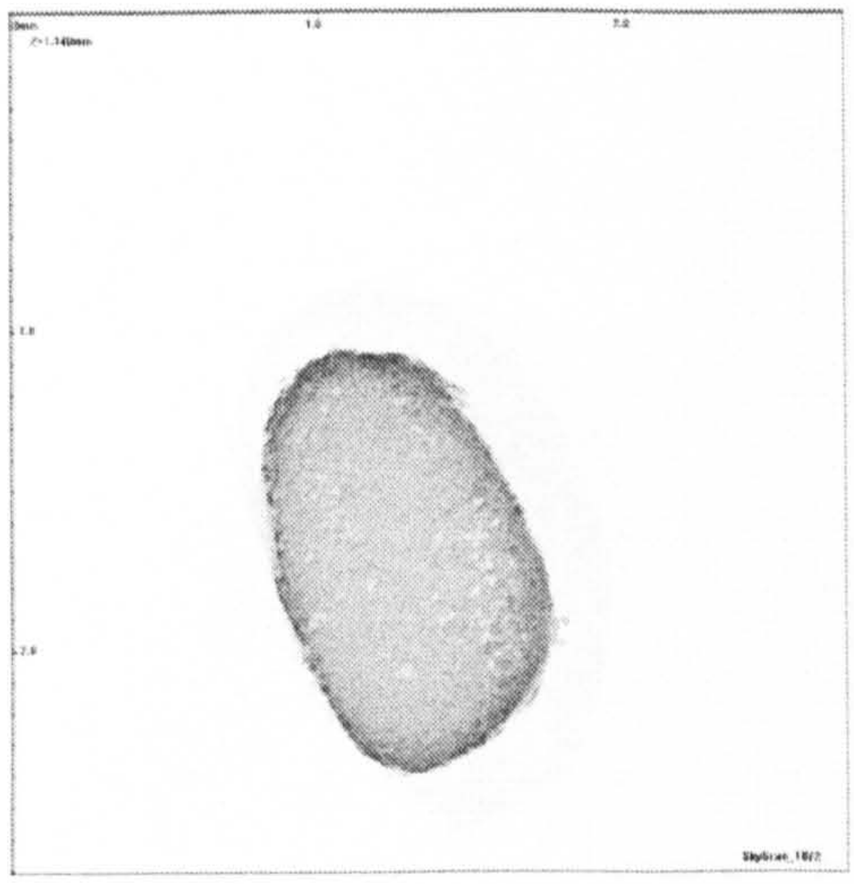

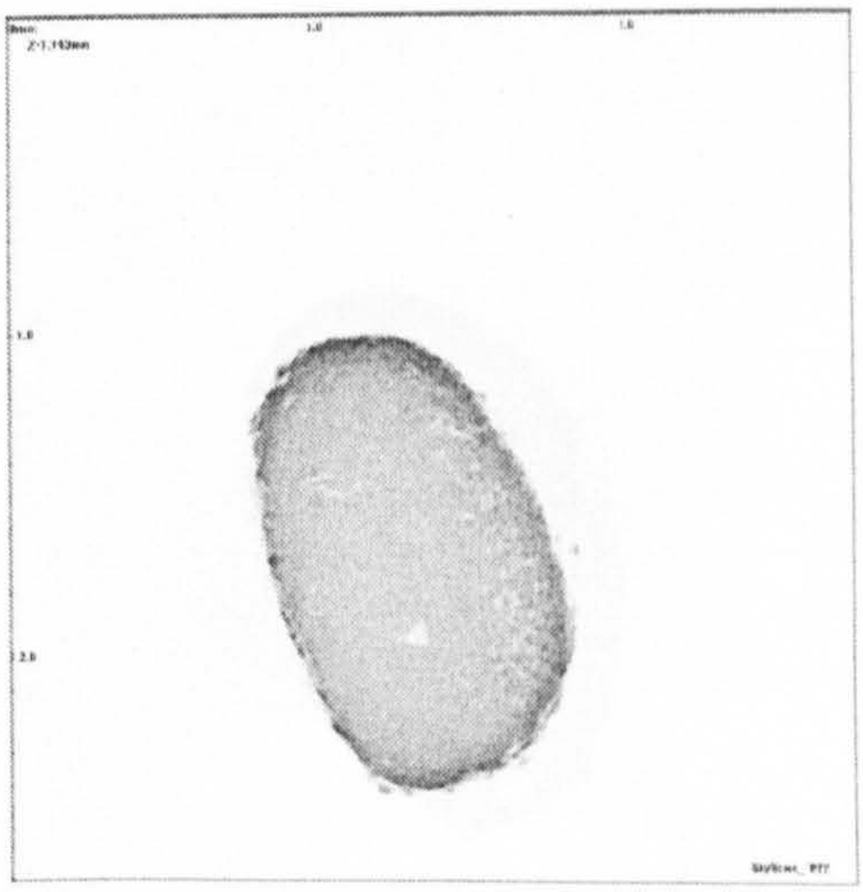

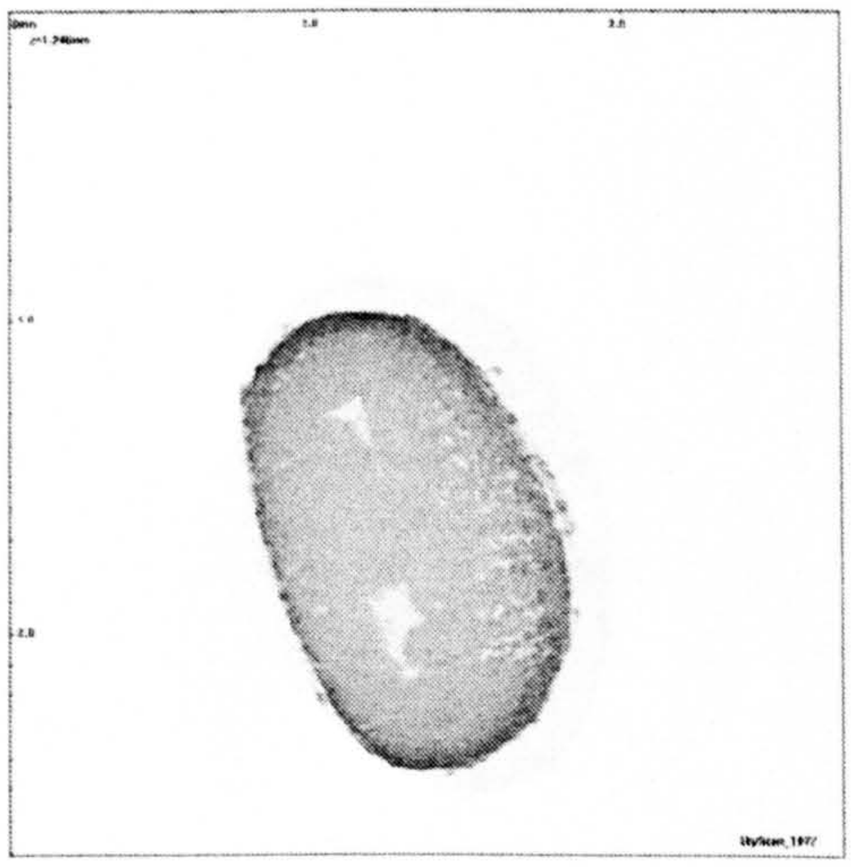

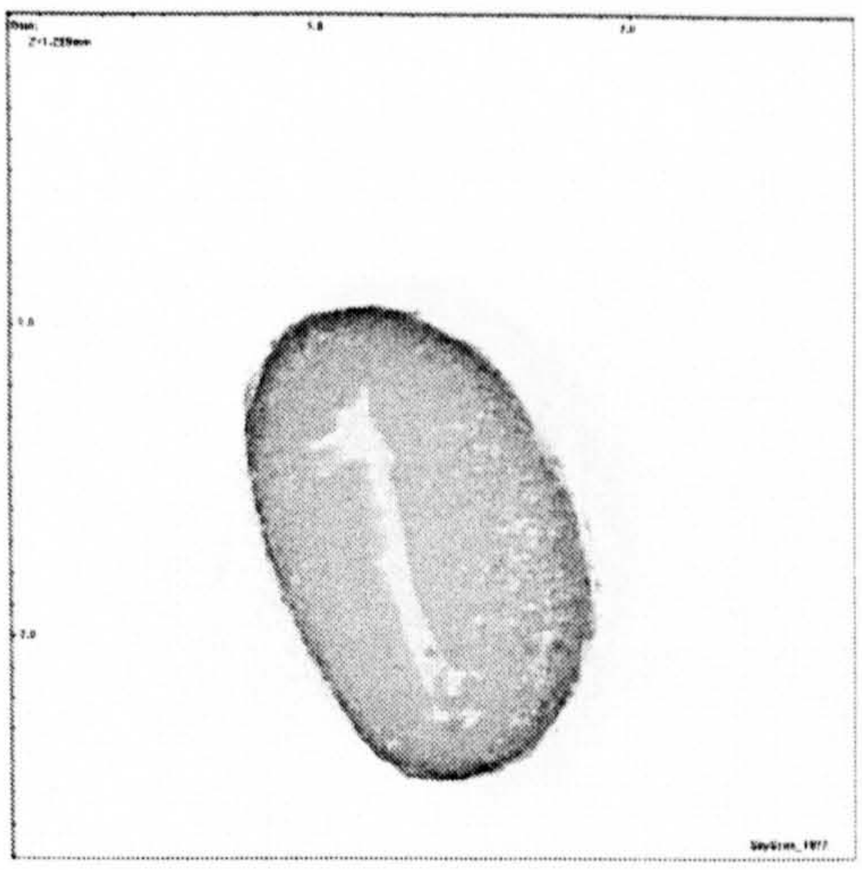

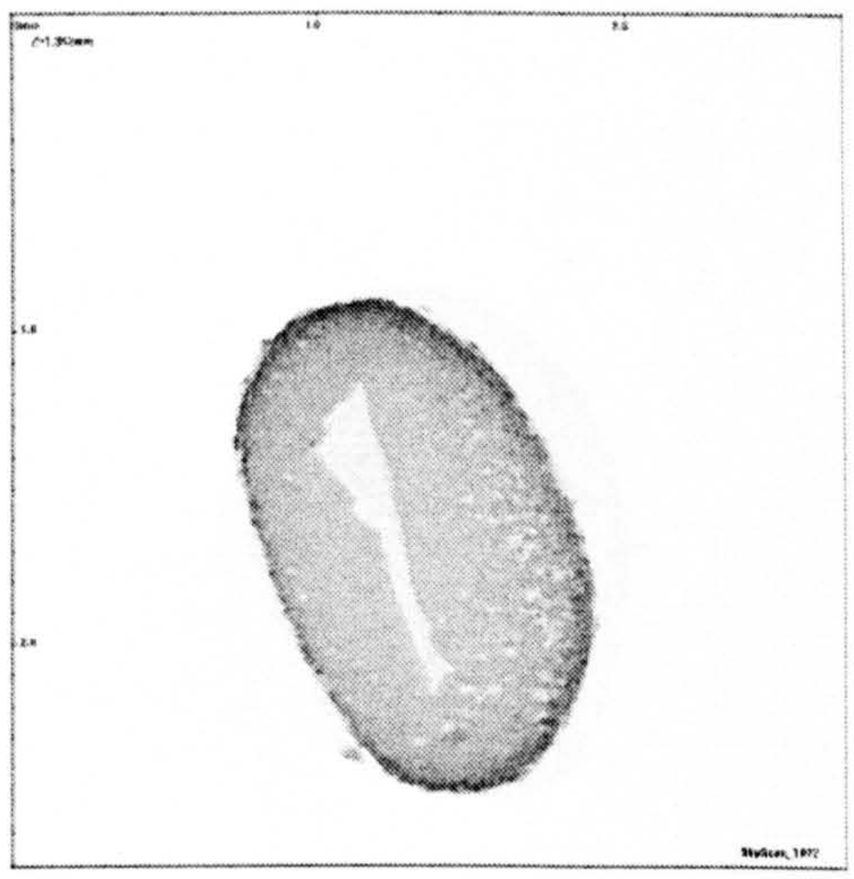

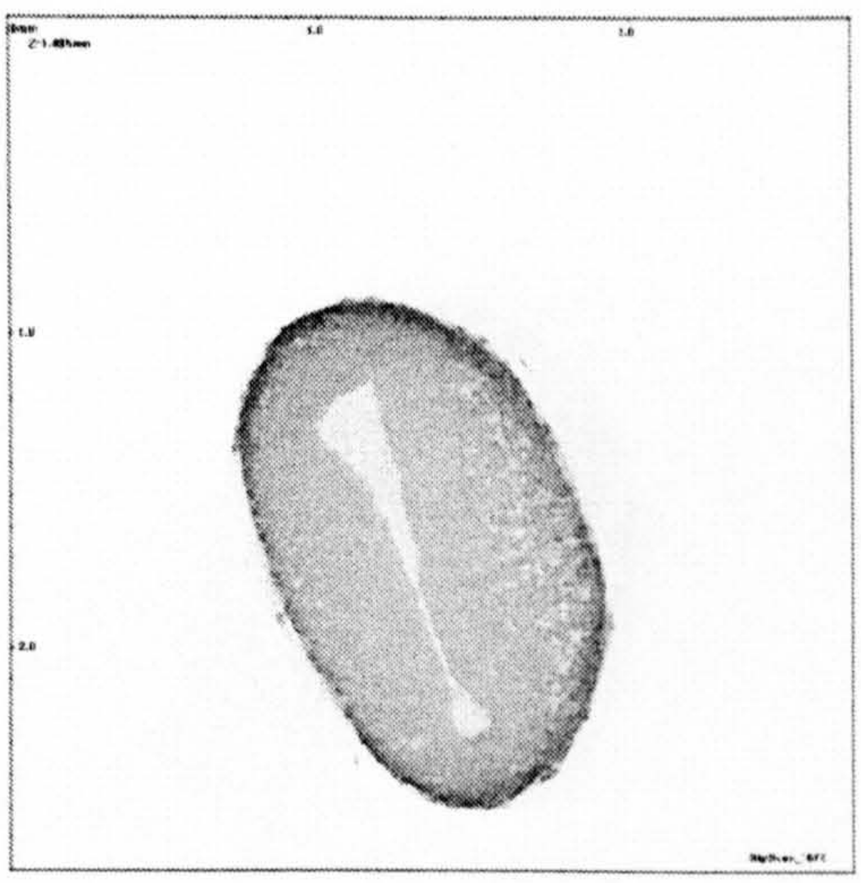

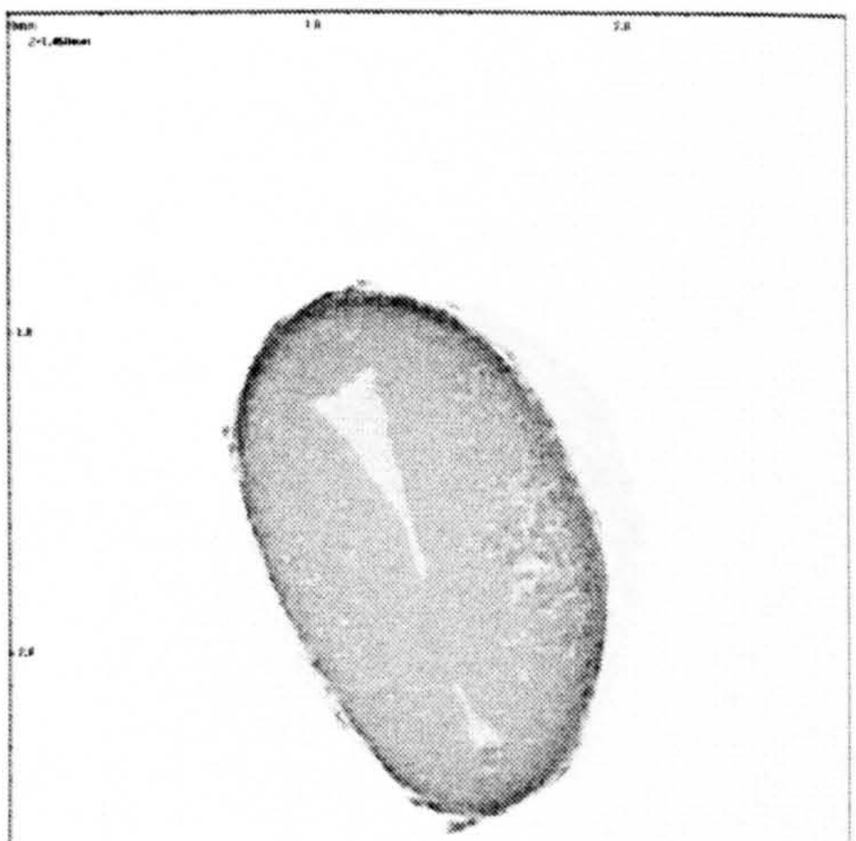

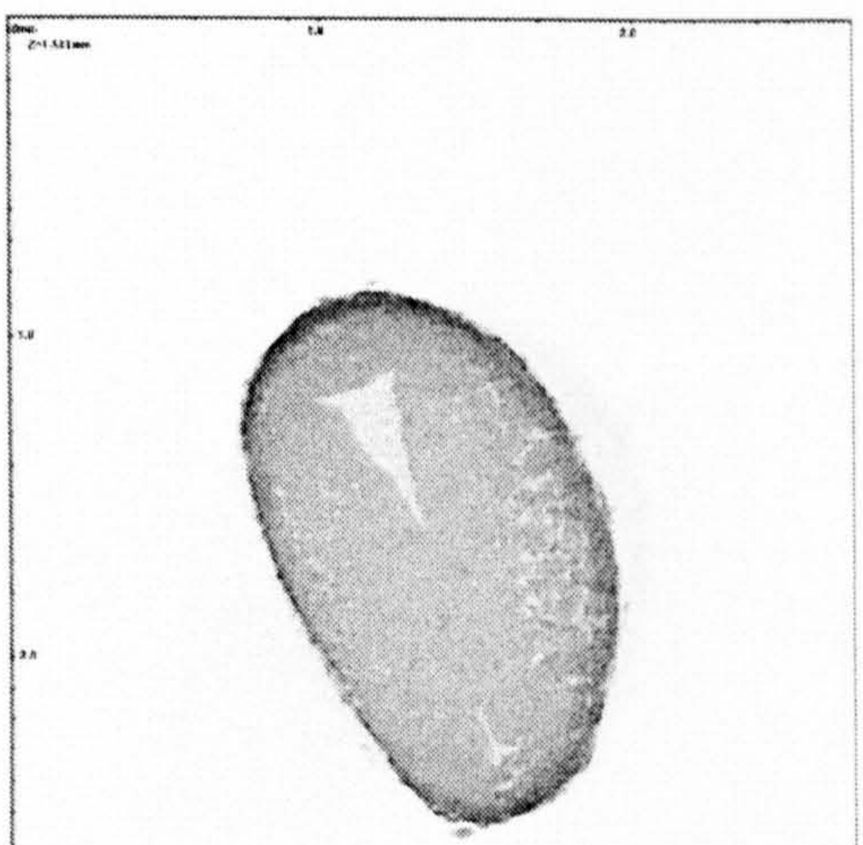

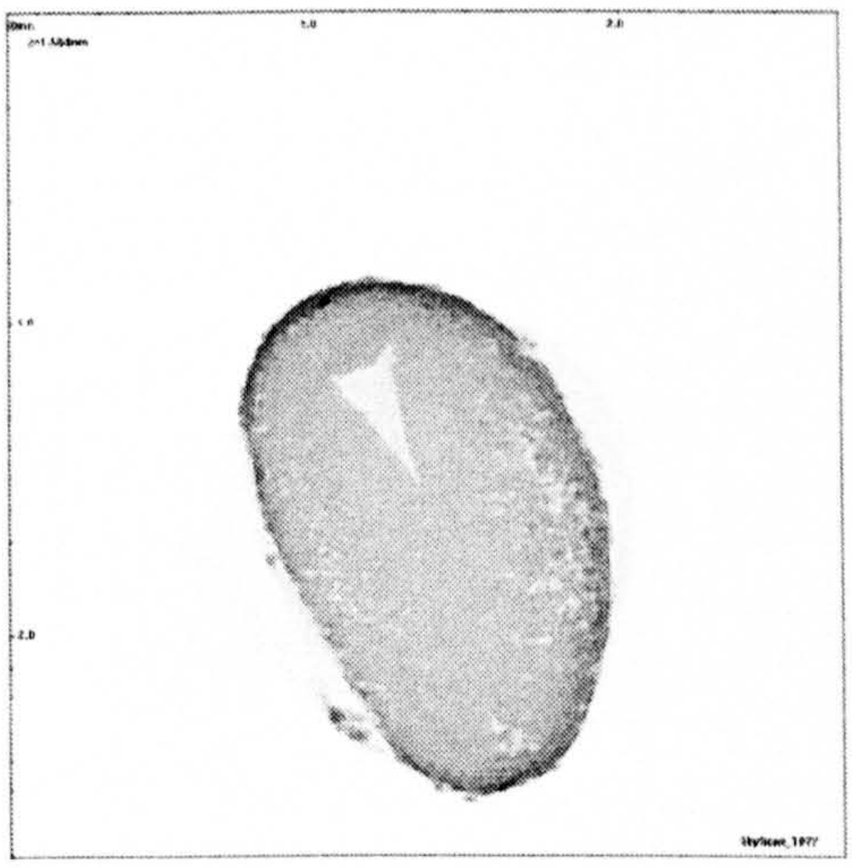

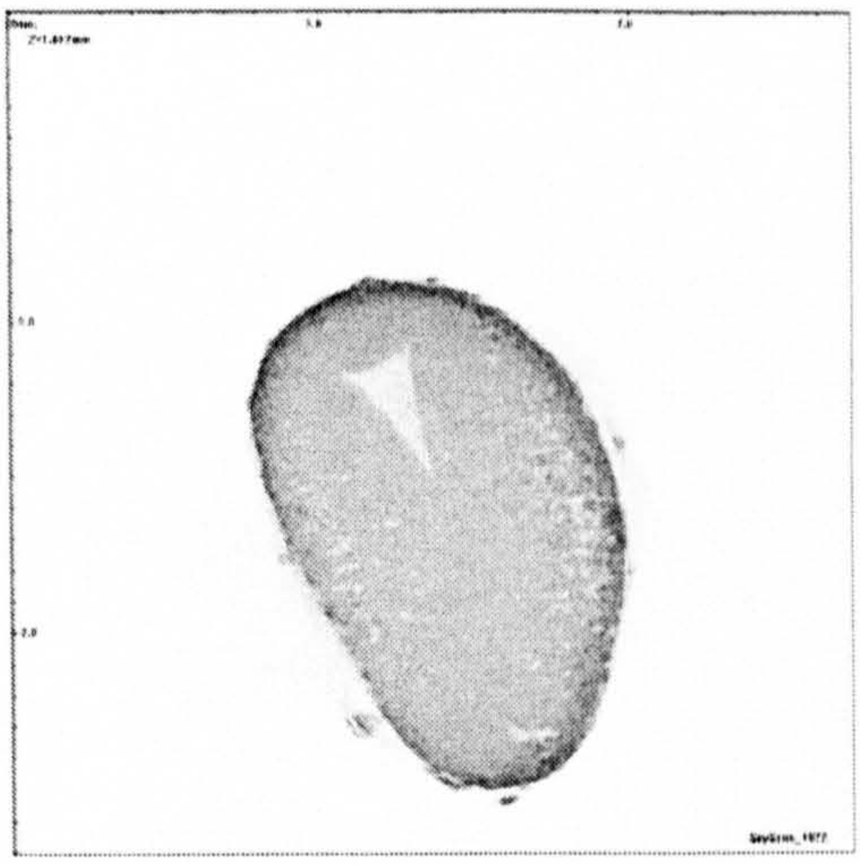

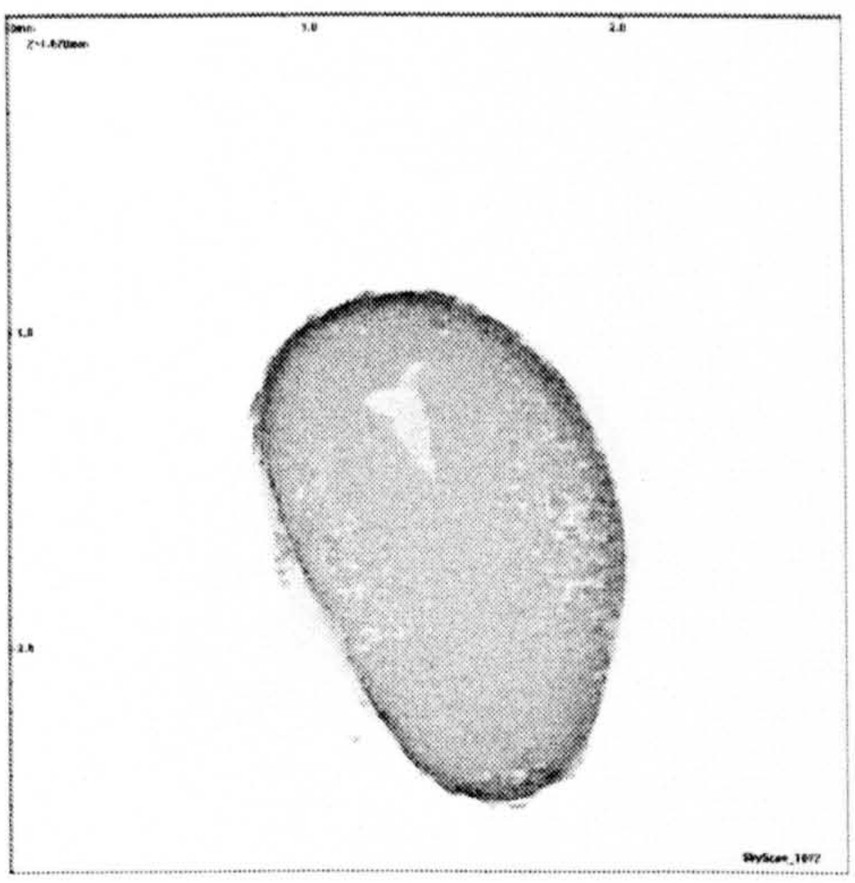

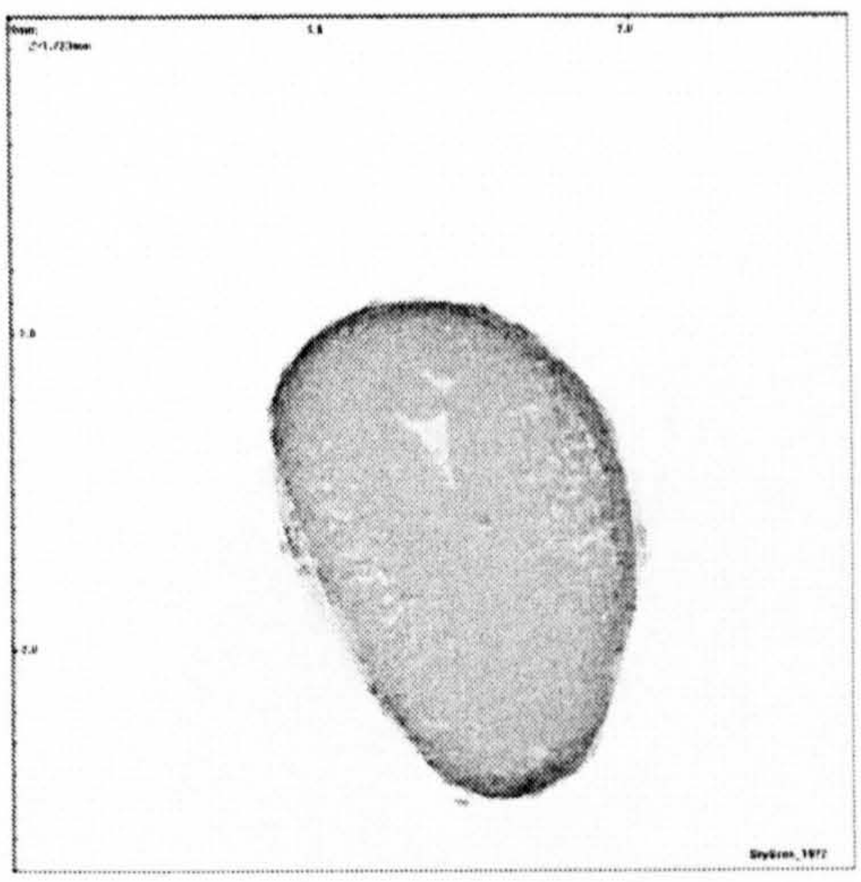

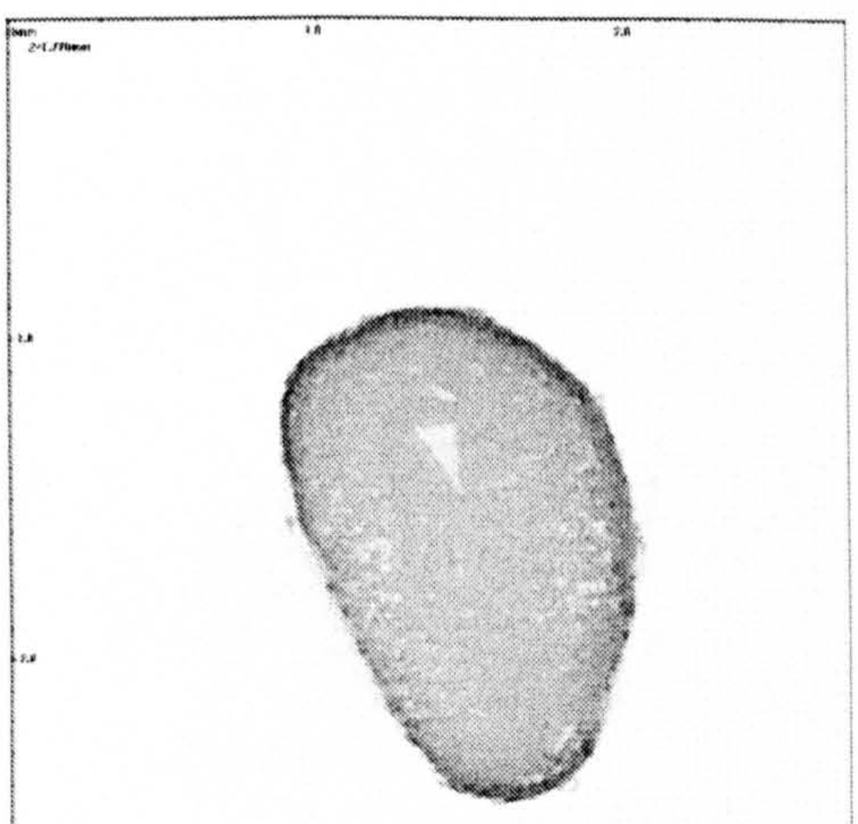

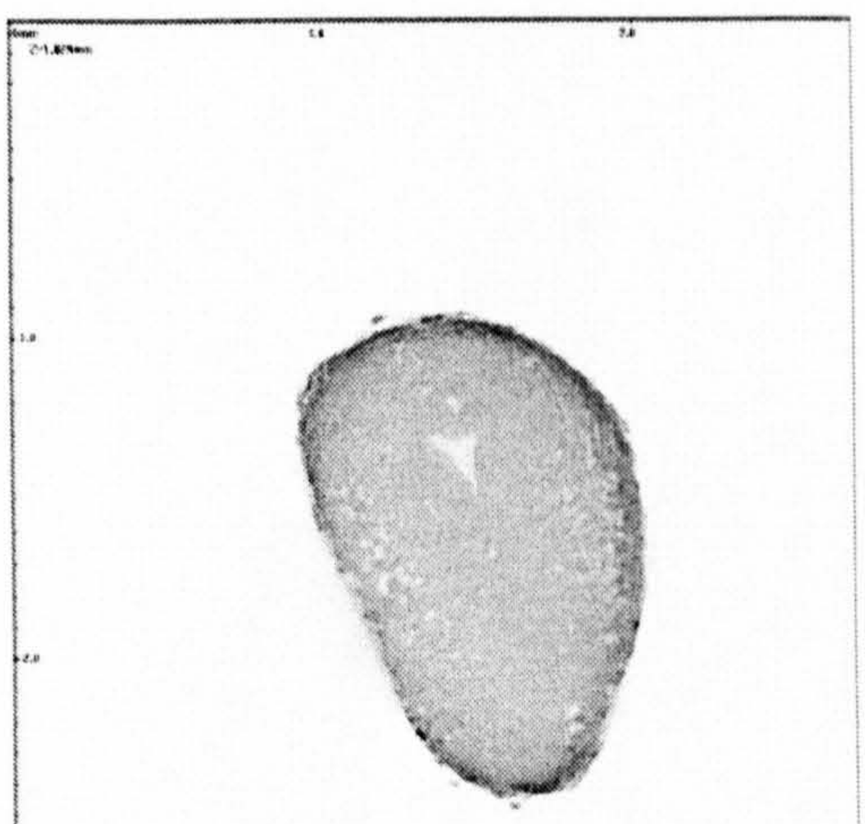

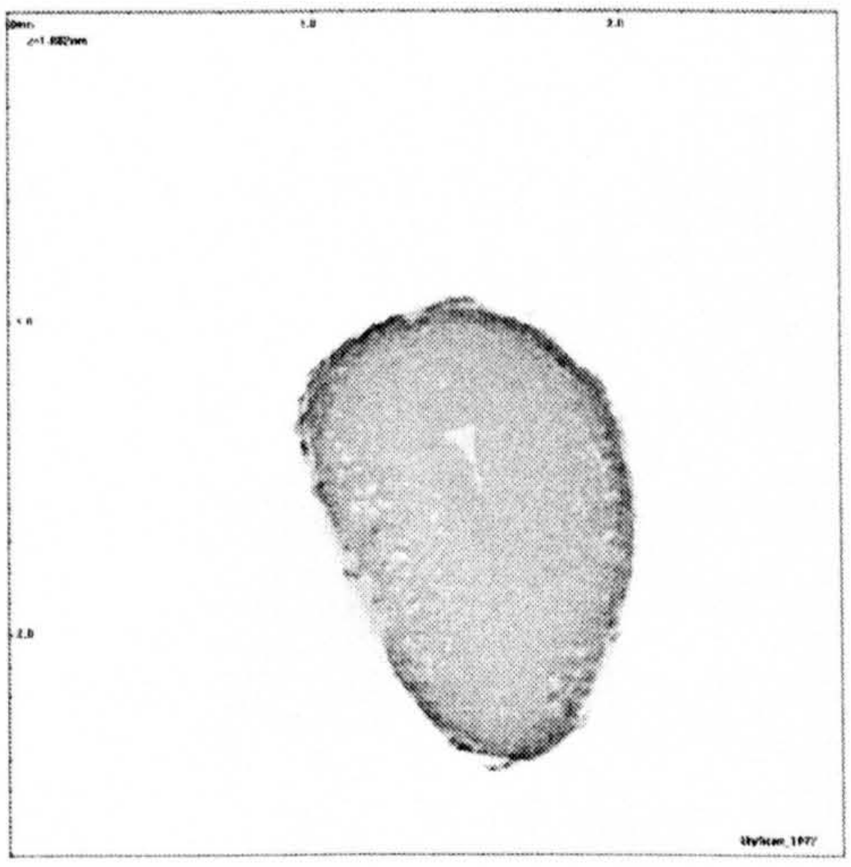

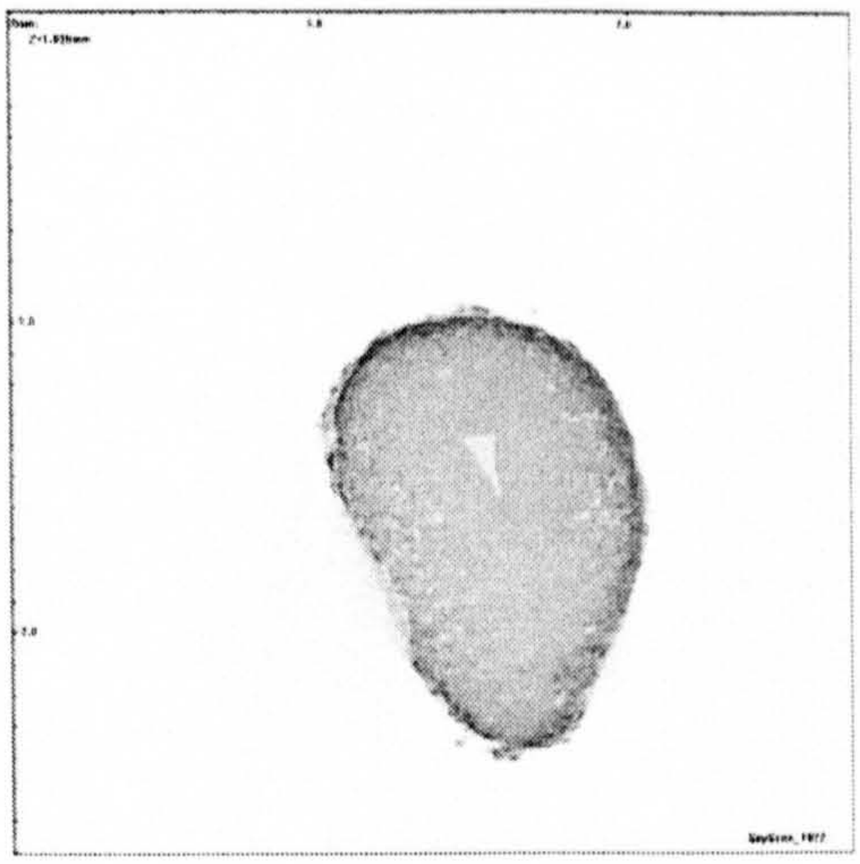

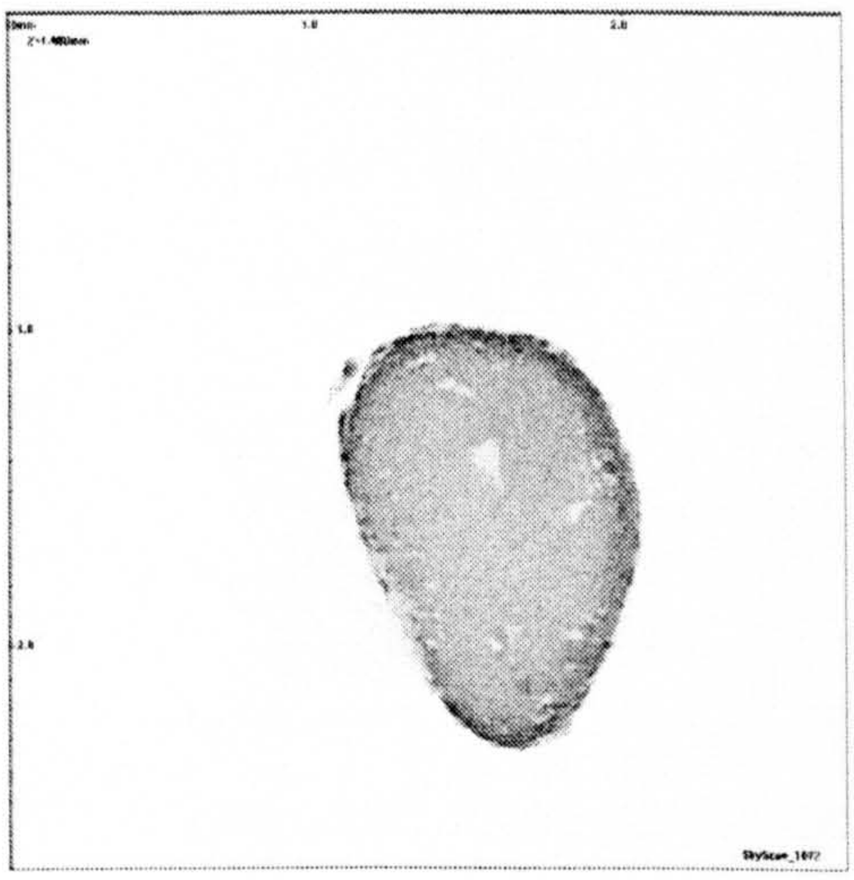

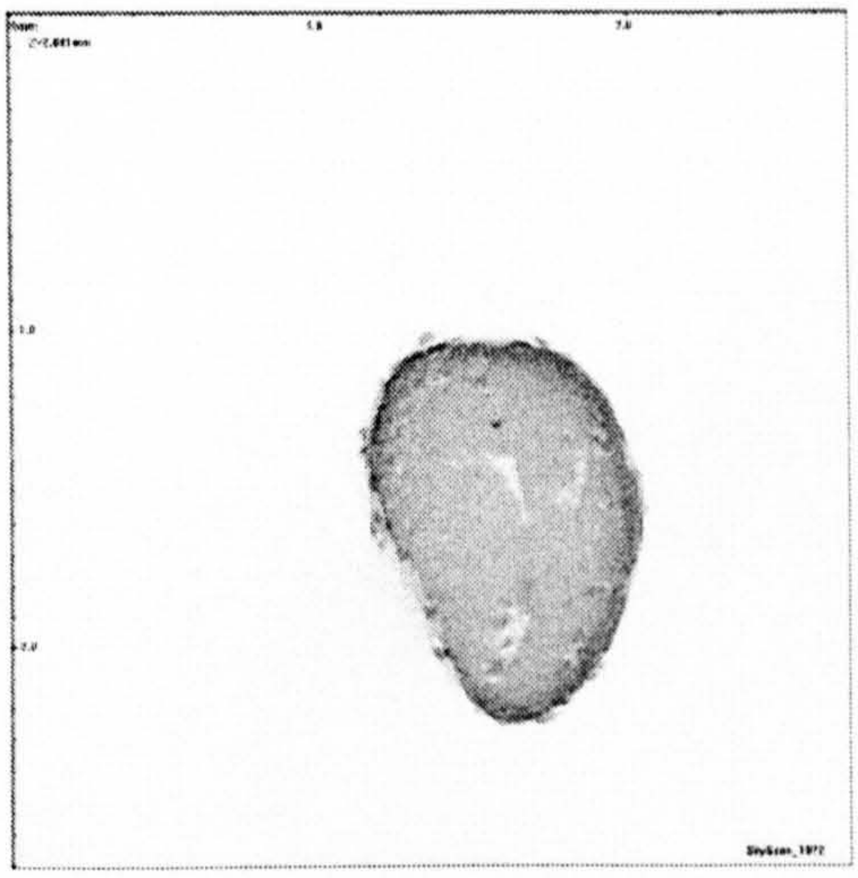

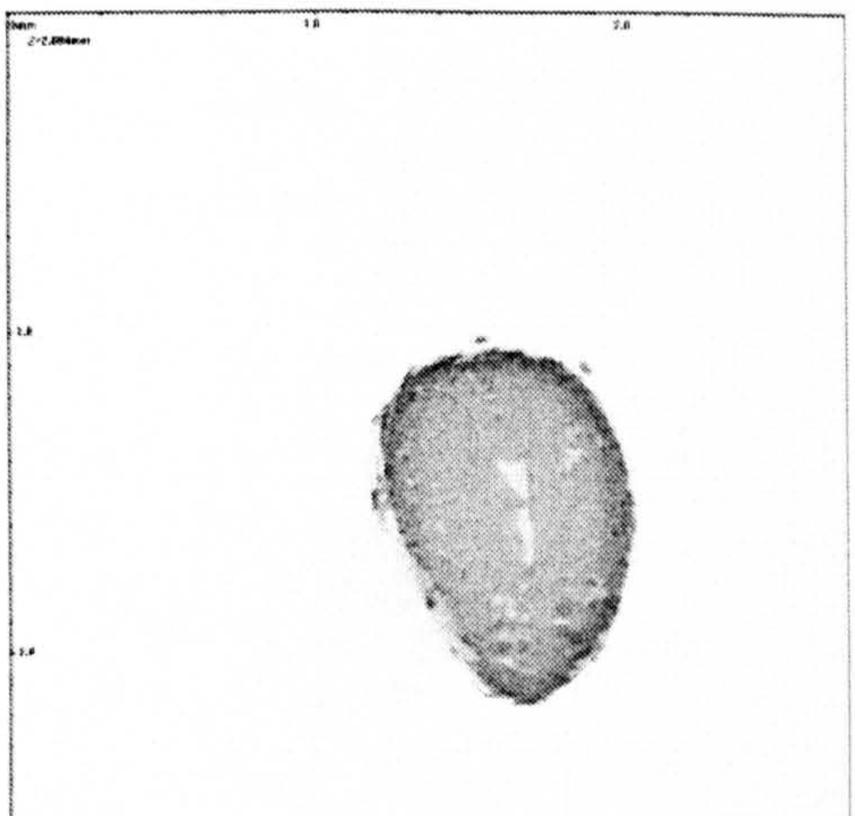

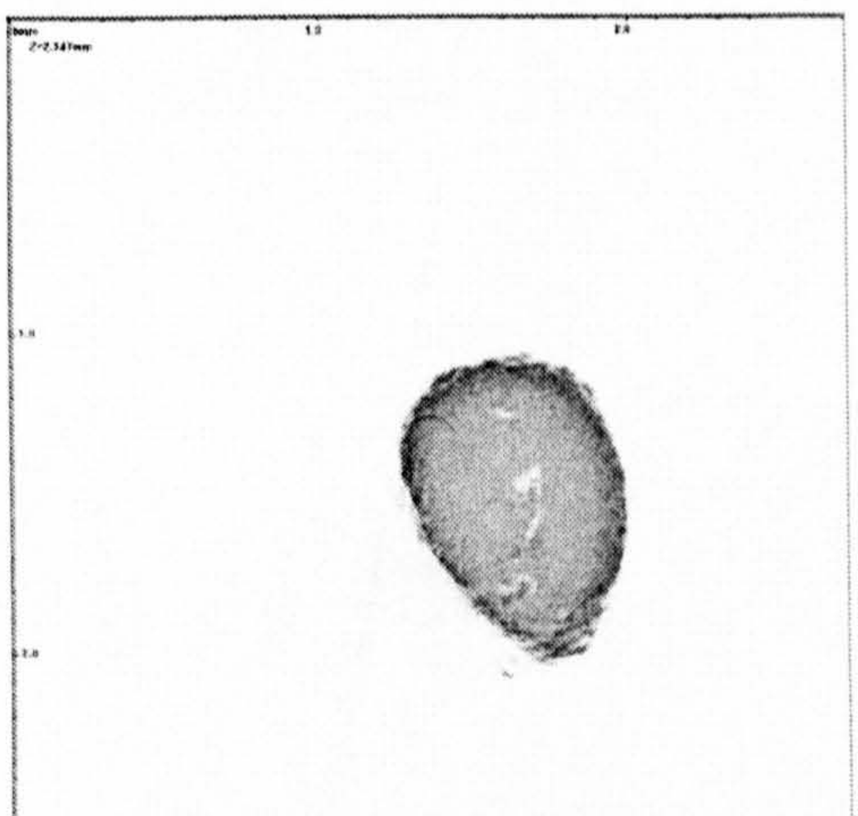

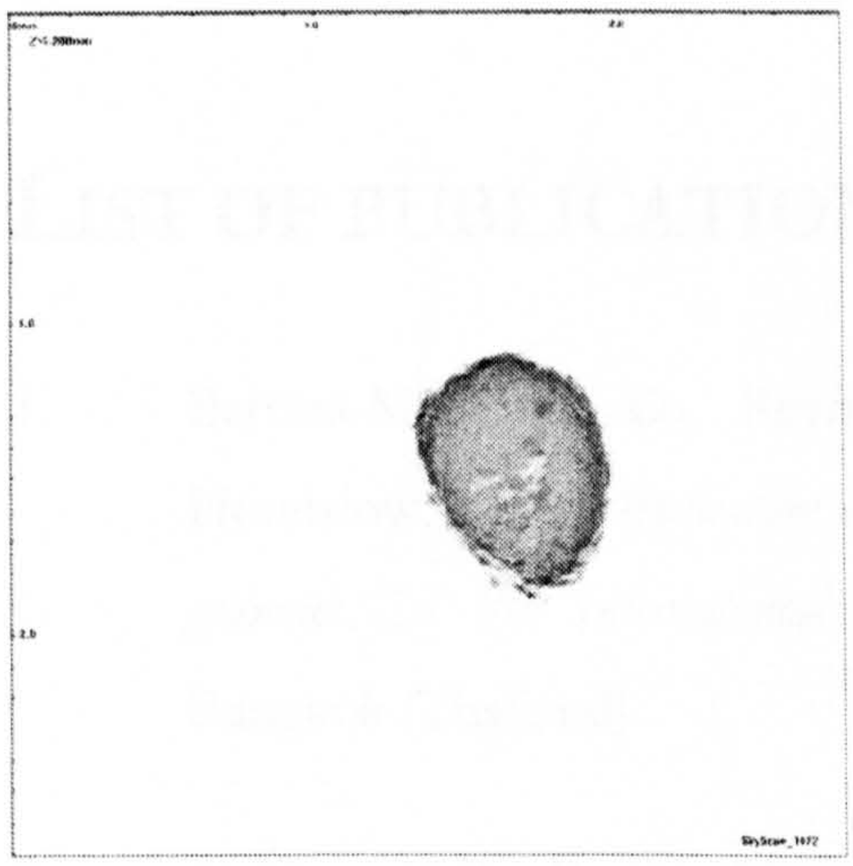

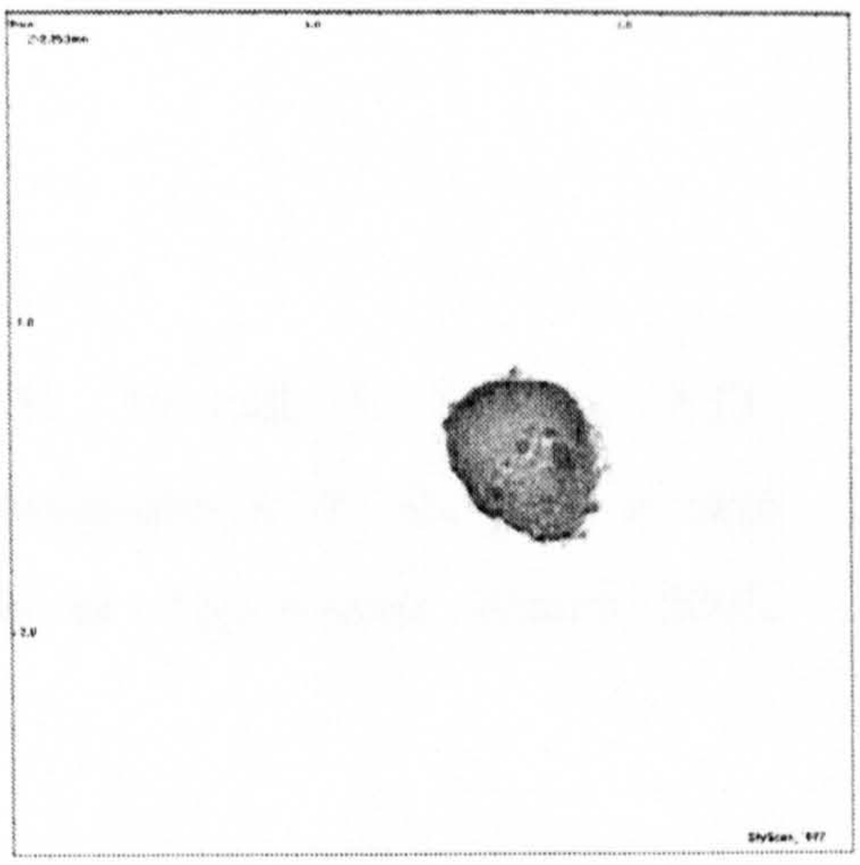

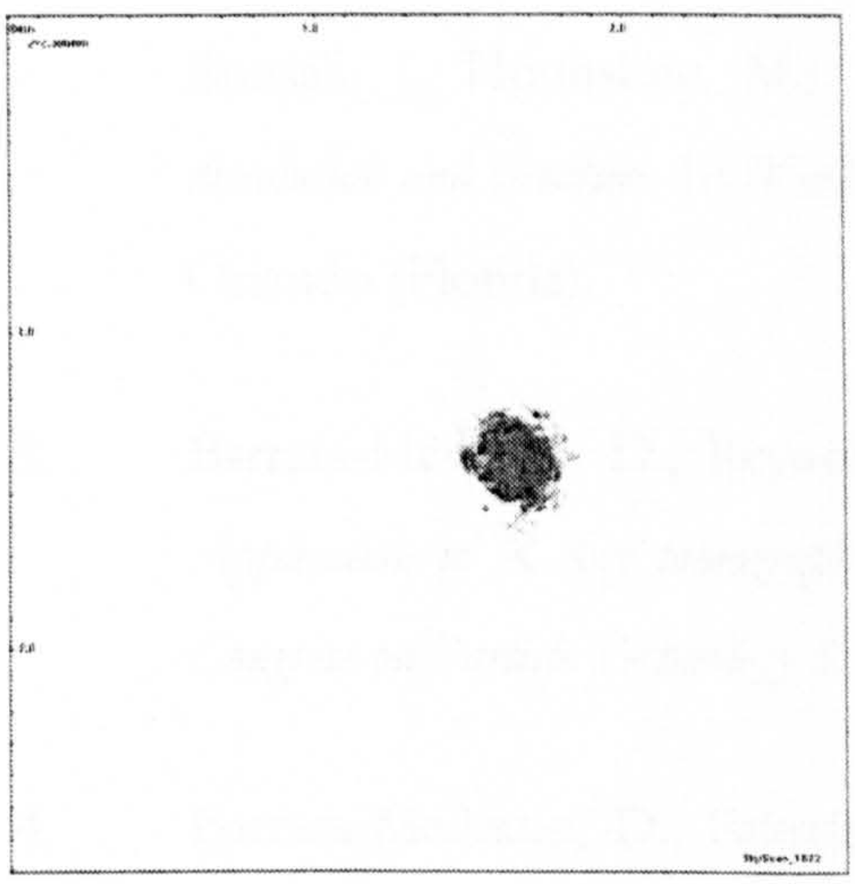

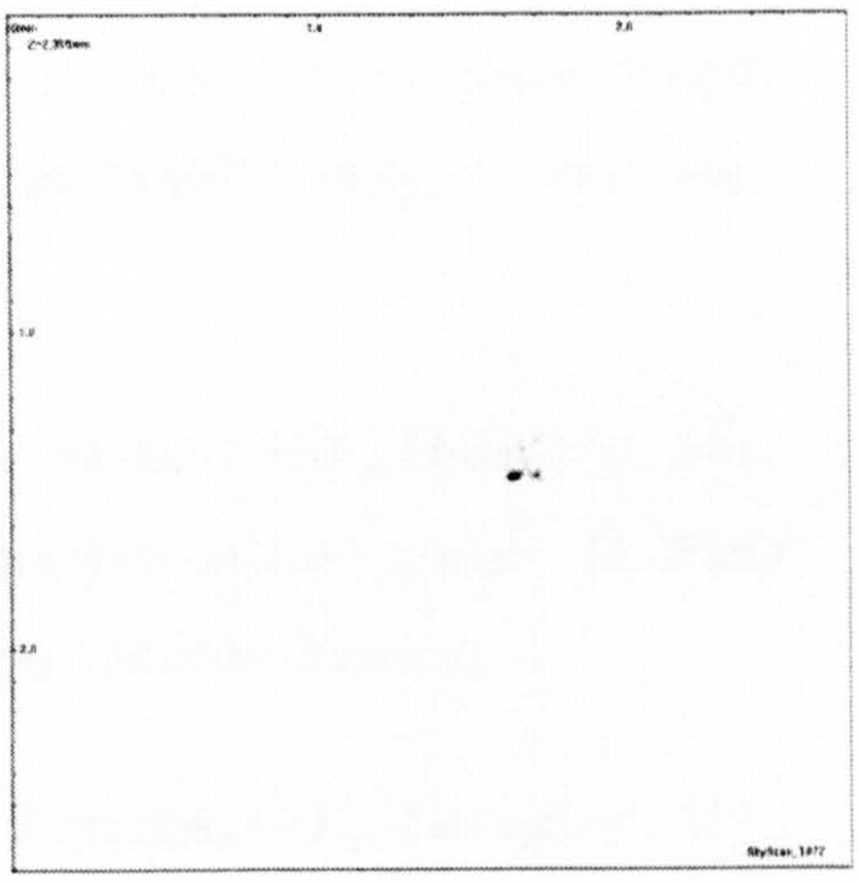

APPENDIX C

LIST OF PUBLICATIONS

1. Barrera-Medrano, D., Reynolds, G.K., Bonsall, J., Salman, A.D., Hounslow, M.J., *Application of X-ray tomography to the description of single granules.* In *8th International Symposium on Agglomeration.* March 2005. Bangkok (Thailand).

2. Gabbott, I.P., Barrera-Medrano, D., Reynolds, G.K., Salman, A.D., Bonsall, J., Hounslow, M.J. *The effect of binder ratio on granule strength, dissolution and structure.* In *World Congress on Particle Technology 5.* April 2006. Orlando (Florida).

3. Barrera-Medrano, D., Reynolds, G.K., Salman, A.D., Hounslow, M.J., *Application of X-Ray tomography to the description of single granules.* In *World Congress on Particle Technology 5.* April 2006. Orlando (Florida).

4. Barrera-Medrano, D., Salman, A.D., Reynolds, G.K., Hounslow, M.J., *Granule structure.* In *Handbook of Powder Technology* (first edition), A.D. Salman, M.J. Hounslow and J.P.K. Seville, Editors. 2007, Elsevier: The Netherlands. P.1189-1212.